Biosorption of heavy metal ions by microalgae: mechanisms and conditioning

Thesis submitted to the University of Ottawa in partial fulfillment of the requirements for the Doctorate in Philosophy degree in Chemical Engineering

uOttawa

Siwei Gu

Supervisor:

Dr. Christopher Q. Lan

Department of Chemical and Biological Engineering

Faculty of Engineering

University of Ottawa

Abstract

Wastewater contaminated with heavy metal ions (HMIs), stemming from human activities and natural disasters, poses substantial threats to both the environment and human health. The unchecked release of untreated wastewater into natural water bodies leads to severe pollution, upsetting ecological balance. To address this pressing challenge, microalgae-based biosorption technology has emerged as a promising solution for the efficient removal of HMIs from wastewater. Microalgae, with their extensive surface area and intricate cell wall structures, exhibit remarkable efficacy in HMIs biosorption. This thesis aims at elucidating the fundamental principles governing the interactions between HMI and microalgal cells to help enhance the biosorption capacity of HMI by microalgae from two perspectives: 1) conditioning of biomass by either optimizing the cultivation conditions or downstream processing; and 2) conditioning of the biosorption process for optimal performance of given algal biomass. It was demonstrated that among the tested cultivation conditions, i.e., culture pH, phosphate concentration, nitrate concentration, and dissolved inorganic carbon (DIC) conditions, which all have significant impacts on cell surface structure and therefore biosorption of HMI, DIC is the most significant factor. Furthermore, it was demonstrated that downstream processing of biomass such as lipid extraction with sonication for cell disruption could help enhance specific surface area and removal of lipids from cell wall surfaces, resulting in remarkably elevated HMI biosorption capacities. As for research on biosorption mechanisms, a correlation between HMI properties, i.e., ionic radius and electronegativity, and their biosorption capacities onto certain microalgal biomass, was established, which was validated with both experimental data and literature data. Furthermore, systematic studies on biosorption kinetics, isotherm, and thermodynamics, as well

as cell surface characterization, and determination of HMI intracellular and extracellular contents of cells after biosorption were carried out, which converged on the conclusion that biosorption was predominantly monolayer surface adsorption. A mathematical model was proposed and validated, which is a rigid model accounting for the effects of cell size and HMI radius only. Analysis of model differentiation from experimental data led to the hypothesis that the nanostructures on cells, mostly like pili, were the major locations where binding sites for HMI were housed. This research represents a significant step towards ensuring the responsible and sustainable use of microalgae for environmental engineering, promising a cleaner and healthier future.

Résumé

Les eaux usées contaminées par des ions métalliques lourds (IML), issus des activités humaines et des catastrophes naturelles, posent des menaces substantielles tant pour l'environnement que pour la santé humaine. Le rejet incontrôlé d'eaux usées non traitées dans les cours d'eau naturels entraîne une pollution sévère, perturbant l'équilibre écologique. Pour relever ce défi pressant, la technologie de biosorption basée sur les microalgues a émergé comme une solution prometteuse pour l'élimination efficace des IML des eaux usées. Les microalgues, avec leur grande surface et leurs structures de paroi cellulaire complexes, montrent une efficacité remarquable dans la biosorption des IML. Cette thèse vise à élucider les principes fondamentaux régissant les interactions entre les IML et les cellules de microalgues afin d'améliorer la capacité de biosorption des IML par les microalgues sous deux perspectives : 1) le conditionnement de la biomasse par l'optimisation des conditions de culture ou le traitement en aval ; et 2) le conditionnement du processus de biosorption pour une performance optimale de la biomasse algale donnée. Il a été démontré que parmi les conditions de culture testées, c'est-à-dire le pH de la culture, la concentration en phosphate, la concentration en nitrate et les conditions du carbone inorganique dissous (CID), qui ont toutes des impacts significatifs sur la structure de la surface cellulaire et donc la biosorption des IML, le CID est le facteur le plus significatif. De plus, il a été démontré que le traitement en aval de la biomasse, tel que l'extraction des lipides avec une sonication pour la disruption cellulaire, pouvait aider à améliorer la surface spécifique et l'élimination des lipides des surfaces des parois cellulaires, entraînant des capacités de biosorption des IML remarquablement élevées. En ce qui concerne la recherche sur les mécanismes de biosorption, une corrélation entre les propriétés des IML, c'est-à-dire le rayon ionique et l'électronegativité, et leurs capacités de biosorption sur certaines biomasses de

microalgues a été établie, ce qui a été validé à la fois avec des données expérimentales et des données de la littérature. De plus, des études systématiques sur la cinétique, l'isotherme et la thermodynamique de la biosorption, ainsi que la caractérisation de la surface cellulaire et la détermination des contenus intracellulaires et extracellulaires des IML après la biosorption, ont été réalisées, convergent vers la conclusion que la biosorption était principalement une adsorption de surface monocouche. Un modèle mathématique a été proposé et validé, qui est un modèle rigide prenant en compte les effets de la taille cellulaire et du rayon IML uniquement. L'analyse de la différenciation du modèle par rapport aux données expérimentales a conduit à l'hypothèse que les nanostructures sur les cellules, principalement comme des pili, étaient les principaux endroits où les sites de liaison pour les IML étaient logés. Cette recherche représente une avancée significative vers l'assurance de l'utilisation responsable et durable des microalgues pour le génie environnemental, promettant un avenir plus propre et plus sain.

Acknowledgement

I would like to extend my deepest appreciation to my dedicated supervisor, Dr. Christopher Q. Lan. His invaluable guidance, unwavering support, and consistently friendly demeanor have been instrumental in shaping my doctoral research into a truly inspiring and respected endeavor.

I also wish to express my gratitude to Dr. Jason Zhang for sharing essential instruments. My heartfelt thanks go out to the technical staff of the department, including Dr. Takeshi Matsuura and Dr. Dipak Rana for their invaluable advice, Mr. Gérard Nina and Mr. Franco Ziroldo for their contributions to programming, software maintenance, and their meticulous work on monitoring systems for various experimental setups. The administrative support provided by Francine Pétrin, Sylvie Saindon and Ariane Beauchamp has been indispensable.

I would like to acknowledge and appreciate the efforts of my colleagues in the research groups, including Zeqing Bao, Zitong Xu, Xinyue Wang, Aotian Li, Hongying Zhou, Vishali Gopi and Huan Wu. Special thanks to undergraduate students Emma Mary Boase, William Yuan, and Tareq Mareh, who provided valuable assistance during experiments. I am deeply grateful to Xiangchao Meng, Xiaotan Zhu, Xinglong Chen, Yuchen Chenliu, and Yuanchen Zhu for their constant encouragement and unwavering support throughout my academic journey. Furthermore, I wish to acknowledge the steadfast support of my friends Kaiyi Zhang and Junqi Ren, who have been a consistent source of encouragement throughout my doctoral journey.

I extend my sincere thanks for the financial support as research assistant provided by Dr. Christopher Lan.

Finally, I want to take this moment to express profound gratitude to my family, particularly my wife Yifan Su. Their boundless love, unwavering encouragement, steadfast support, and unshakable trust have served as the bedrock of my journey. Their support has been absolutely indispensable, and I recognize that my research experience at the University of Ottawa and the successful completion of this dissertation would have been unattainable without their unwavering presence in my life.

Table of Contents

List of figure and table

Abbreviations

ATP	Adenosine triphosphate
BDL	Below detection limit
BET	Brunauer–Emmett–Teller method
DCW	Dried cell weight
DIC	Dissolved inorganic carbon
DI	Deionized water
EPA	Environmental Protection Agency (US)
EPS	Extracellular polysaccharide substance
EDX	Energy-dispersive X-ray
EDTA	Ethylene Diamine Tetraacetic Acid
FT-IR	Fourier Transform Infrared
FAAS	Flam atomic absorption spectroscopy
HMIs	Heavy metal ions
Max	Maximum
Min	Minimum
ND	Not detected
OD	Optical density
P	p-value
PBR	Photobioreactor
R^2	Coefficient of determination
SD	Standard deviation
SEM	Scanning Electron Microscopy
WHO	Word Health Organization
XPS	X-ray Photoelectron Spectroscopy
ZP	Zeta potential

Nomenclature

A_s	Surface are of spheric cell (um^2)
A_I	Intersecting surface of heavy metal ion (um^2)
C_0	Initial heavy metal concentration (mmol/L)
C_e	Heavy metal concentration in supernatant (mmol/L)
C_s	Heavy metal concentration on cell surface (mmol/L)
C_b	Biomass concentration (g/L)
C_w	Cell weight (g/cell)
K_L	Langmuir constant (L/mmol)
K_F	Freundlich constant ($mg^{(1-1/n)}g^{-1}L^{1/n}$)
K_S	Sips constant (L/mmol)
n	Number of heavy metal ion on cell surface (ion/cell)
N	Total heavy metal ion on cell surface (ion/g)
Pb bioadsorption%	Percentage of Pb(II) adsorbed onto cell surface %
Pb bioabsorption%	Percentage of Pb(II) absorbed into the cell body %
q_e	Equilibrium biosorption (mmol/g)
$q_{e,ad}$	Equilibrium bioadsorption (mmol/g)
$q_{e,ab}$	Equilibrium bioabsorption (mmol/g)
q_m	Experimental biosorption capacity (mmol/g)
q_p	Predicted biosorption capacity (mmol/g)
r	Heavy metal ionic radius (pm)
R	Microalgal cell radius (um)

List of publications

Peer-reviewed articles

[1] S. Gu, C.Q. Lan, Mechanism of heavy metal ion biosorption by microalgal cells : A mathematic approach. J. Hazard. Mater. 463, 132875. (2023)

[2] S. Gu, C.Q. Lan, Enhanced Pb(II), Cd(II), Zn(II) biosorption by microalgae *Neochloris oleoabundans* cultivated at high culture pH. Chem. Eng. J, 468, 143579. (2023)

[3] S. Gu, C.Q. Lan, Lipid-extraction algal biomass for biosorption of bivalent lead and cadmium ions: kinetics and isotherm, Chemical Engineering Science, 118778, 0009-2509. (2023)

[4] S. Gu, Y. Su, C.Q. Lan, Effect of phosphate in medium on cell growth and Cu (II) biosorption by green alga *Neochloris oleoabundans*, Chem. Eng. Res. Des. 185, 186–197. (2022)

[5] S. Gu, E.M. Boase, C.Q. Lan, Enhanced Pb(II) removal by green alga *Neochloris oleoabundans* cultivated in high dissolved inorganic carbon cultures, Chem. Eng. J. 416, 128983. (2021)

[6] S. Gu, C.Q. Lan, Biosorption of heavy metal ions by green alga *Neochloris oleoabundans*: Effects of metal ion properties and cell wall structure, J. Hazard. Mater. 418, 126336. (2021)

[7] S. Gu, C.Q. Lan, Effect of nitrate on cell growth and biosorption of Pb(II) by green alga *Neochloris oleoabundans* (Under review at Journal of Hazardous Materials)

In addition to my thesis project, I actively participated in another project, leading to the publication of a research article.

Z. Xu, S. Gu, D. Rana, T. Matsuura, C.Q. Lan, Chemical precipitation enabled UF and MF filtration for lead removal, J. Water Process Eng. 41 (2021) 101987.

Conference presentations

[1] Biosorption of Pb(II) and Cd(II) by residual biomass of green microalgal *Chlorella vulgaris* after lipid extraction, 72nd Canadian Chemical Engineering Conference, 2022, Vancouver, Canada

[2] Enhanced Pb (II) removal by microalgae cultivated in high dissolved inorganic carbon culture, 70th Canadian Chemical Engineering Conference, 2020, Ottawa, Canada

Chapter 1 Introduction

1.1 Problem statement

According to the 2023 UN World Water Development Report, a staggering 26% of the global population, equivalent to 2 billion individuals, lacked access to safely managed drinking water services [1]. This group includes 1.2 billion people with access only to basic services, 282 million with limited services, 367 million relying on treated sources, and 122 million compelled to unsafe surface water. This alarming crisis is further compounded by the contamination of freshwater sources with heavy metal ions (HMIs), which stands as a significant contributor to this pressing issue.

HMIs have been widely used in many applications, including building, electrical, consumer durables, machinery, packaging and others [2]. They could be discharged into the ecosystem via pathways including sediments of exhaust gases and the discharge of HMI-containing industrial wastewaters that are not treated or not treated properly. Indeed, high HMI contents have been reported in the sediments of many rivers from all over the world, including 3-126 mg Cr/kg in Gorges River, Australia, 3.5-23.2 mg Pb/kg in Nile River, Egypt (Africa), 78.1-139 Cr mg/kg in Louro River, Spain (Europe); and 40.8-1347.5 mg Cu/kg in Mamut River, Malaysia (Asia) [3]. HMIs can infiltrate rivers, further exacerbating the water quality issue. For instance, levels of 12.6 µg Cu/L, 419.9 µg Zn/L, 4.1 µg Cd/L, 43.0 µg Pb/L, and 756.6 µg Cr/L have been detected in rivers in different regions around the globe, highlighting the extent of HMIs contamination in these vital water bodies [4]. The concentration in drinking water standards, as established by the World Health Organization (WHO) and the United States Environmental Protection Agency (USEPA), is set well under the parts per billion (ppb) level for most HMIs [5,6]. HMIs in the aquatic ecosystem could reach humans through bioaccumulation and biomagnification through

the food web and therefore cause serious damage to human health since they are toxic, stable and non-biodegradable [7]. Ingestion of HMIs such as lead (Pb), copper (Cu), cobalt (Co), arsenic (As), cadmium (Cd), etc., above certain threshold by humans has been known to cause serious illnesses, including respiratory, hematological, cardiac, dermal, and neurological effects [8]. Additionally, HMIs in waters have a negative impact on the aquatic ecosystem as they are toxic to microorganisms, plants and animals as well [9]. It is therefore important to develop cost-effective technologies for HMIs removal and recovery.

Up to now, there are many technologies that can be used in HMIs treatment, including chemical precipitation [10], ion exchange [11], electrokinetic [12], and membrane separation [13]. Nevertheless, the high costs of these chemical-physical methods pose a significant obstacle, especially for remediation of HMIs from contaminated waters with very low critical concentrations but nonetheless are still above the threshold to be safe for animals and humans [14].

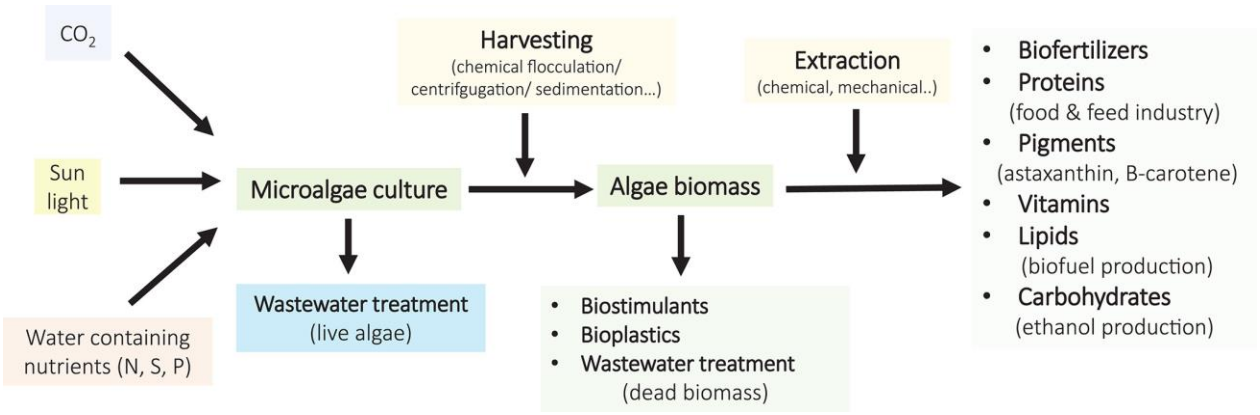

Figure 1-1 Schematic view of the product value chain of microalgae, adapted from [15].

As shown Figure 1-1, microalgae thrive on sunlight and basic nutrients like nitrogen, sulfur, phosphorous, and carbon dioxide. Remarkably, they can complete an entire growth cycle within

a matter of hours [16]. After decades of extensive research and development efforts, biosorption using unicellular or simple multicellular microalgae with or without modification has garnered significant and rapidly increasing interest both in pollution control and polluted ecosystem remediation [17–19]. These cost-effective growth demands, coupled with their versatility in serving multiple purposes, such as carbon mitigation, biofuel production, and bioremediation, have propelled microalgae into the spotlight for a wide range of biotechnological applications. Biosorption process utilizing microalgae is an ecologically safer, cheaper and more efficient method of HMIs removal in comparison with the aforementioned conventional technologies, especially when large volumes of contaminated waters such as rivers, lakes, and even regions of oceans are to be remediated [20,21]. The fundamental advantage of microalgae for such applications lays in the fact that they are self propagative. Therefore, adding a small amount of seed culture of selected non-toxic microalgae that can grow well in a target contaminated water body can effectively remove the HMIs (e.g., Pb(II)) [22], provided that cost-effective methods of microalga harvest/removal are available, e.g., in the cases with filamentous microalgae or/and attached biofilm microalgal reactor [23].

1.2 Research objectives

Extensive research efforts have been devoted to harnessing the potential of microalgae for biosorption of HMIs. Nevertheless, critical challenges persist in understanding the intricate mechanism underlying HMIs biosorption by microalgae and translating this knowledge into mechanism [24]. The complexity of the interaction between HMIs and various microalgal species, each characterized by its unique cell structures, warrants in-depth exploration to compare HMIs biosorption capacity [20]. Even within a single microalgal species, it is crucial to

explore how different cultivation conditions can impact the biosorption capacity of microalgal cells for the same HMIs [25].

To this end, I dedicated my Ph.D. thesis research to elucidating the mechanism of biosorption of HMIs, as well as the conditioning of biosorbents and biosorption process. The following are the four research studies that have been carried out:

1. Biosorption of heavy metal ions (HMI) by green alga *Neochloris oleoabundans*: effects of metal ion properties and cell wall structure
2. Effects of culture pH, nitrate concentration, phosphate concentration, and dissolved inorganic carbon concentration, on cell surface properties and biosorption of HMIs by green alga *Neochloris oleoabundans*
3. Lipid-extraction residual algal biomass for biosorption of bivalent lead and cadmium ions: kinetics and isotherm
4. Mechanism of heavy metal ion biosorption by microalgal cells, a mathematic approach

These four research endeavors collectively seek to advance our understanding of HMIs biosorption by microalgae and pave the way for more effective and practical applications in addressing HMIs contamination in water sources.

1.3 Thesis structure

The Ph.D. thesis is structured into seven chapters, each dedicated to a specific facet of the research. In Chapter 1, the problem statement and research objectives are presented. Chapter 2 furnishes a comprehensive examination of the research background, introducing essential models for HMIs biosorption, such as kinetics, isotherms, and thermodynamics. Chapter 3 details the project aimed at establishing a connection between HMI properties and biosorption capacity. Chapter 4 investigates effects of culture pH, nitrate concentration, phosphate concentration, and

dissolved inorganic carbon concentration, on cell surface properties and biosorption of HMIs. Chapter 5 compares the effectiveness of wet, dried, and lipid-free residual biomass as biosorbents for the HMIs removal. Chapter 6 proposes a mathematical model to predict the biosorption capacity of HMIs based on biomass properties and the ionic radius. In Chapter 7, the thesis concludes and suggests avenues for future research. In appendix A, B, C, the other cultivation conditions, i.e., dissolved inorganic carbon, phosphate and nitrate concentration are also investigated. Collectively, these sections provide a comprehensive exploration of the utilization of microalgal biomass as a biosorbent for HMIs removal.

Chapter 2 Research background

2.1 Introduction

Using different microorganisms such as bacteria, microalgae, yeasts, and fungi for HMIs biosorption has been established as a promising alternative to conventional methods for HMI removal/recovery from contaminated wastewaters or natural waterbodies because they are environmentally friendly and potentially cost-effective [26]. Of particular relevance, microalgae have some unique advantages in comparison to other biosorbents. They are the predominant primary producers that is ubiquitous in the aquatic ecosystem and can grow in almost all natural aquatic environments including niches of extreme salinity, pH and temperatures [27]. They have very high photosynthetic efficiency and therefore shows large growth rates in comparison to other aquatic primary producers such as macroalgae and aquatic plants [28]. There have been confirmed that many species of microalgae poses high biosorption capacities for a diversity of different toxic HMIs including lead (145 mg Pb/g biomass) [29], arsenic (57 mg As/g biomass) [30], mercury (42 mg Hg/g biomass) [31], cadmium (65 mg Cd/g biomass) [32], cobalt (52 mg Co/g biomass) etc.

While extensive studies have been carried out regarding both the fundamental principles and application of microalgal biosorption for HMI removal, there are still many knowledge gaps to be filled in this intriguing field.

2.2 Mechanisms of HMI adsorption by microalgal cells

2.2.1 Effect of biosorbents: microalgal cells

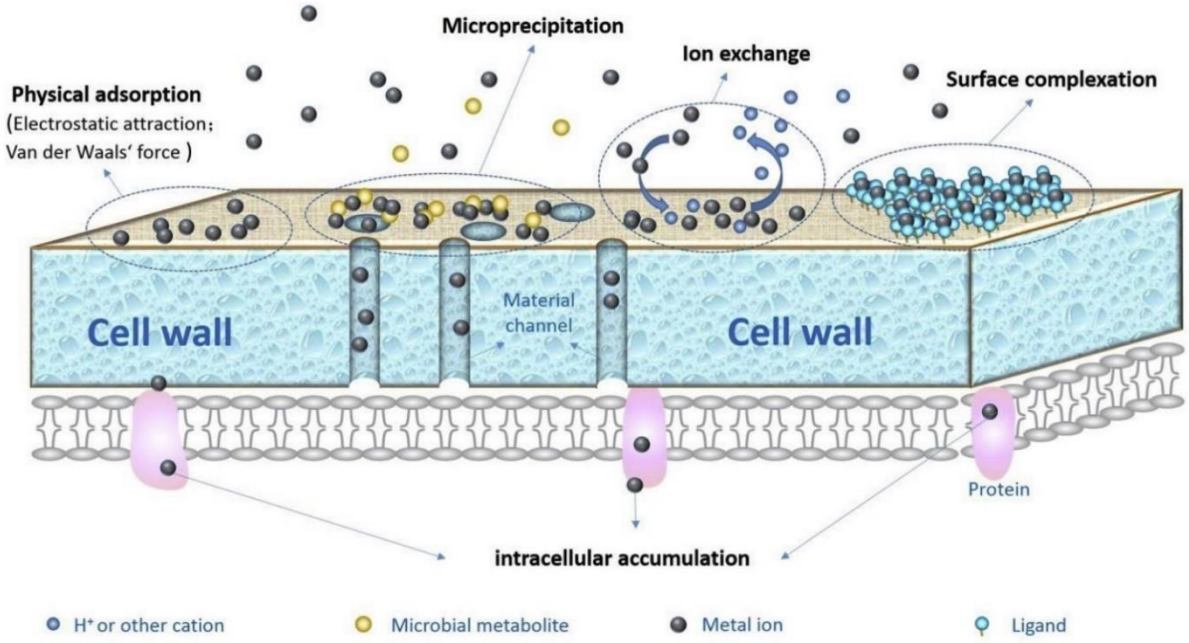

Figure 2-1 Biosorption of HMIs by microalgal cells, adapted from [33].

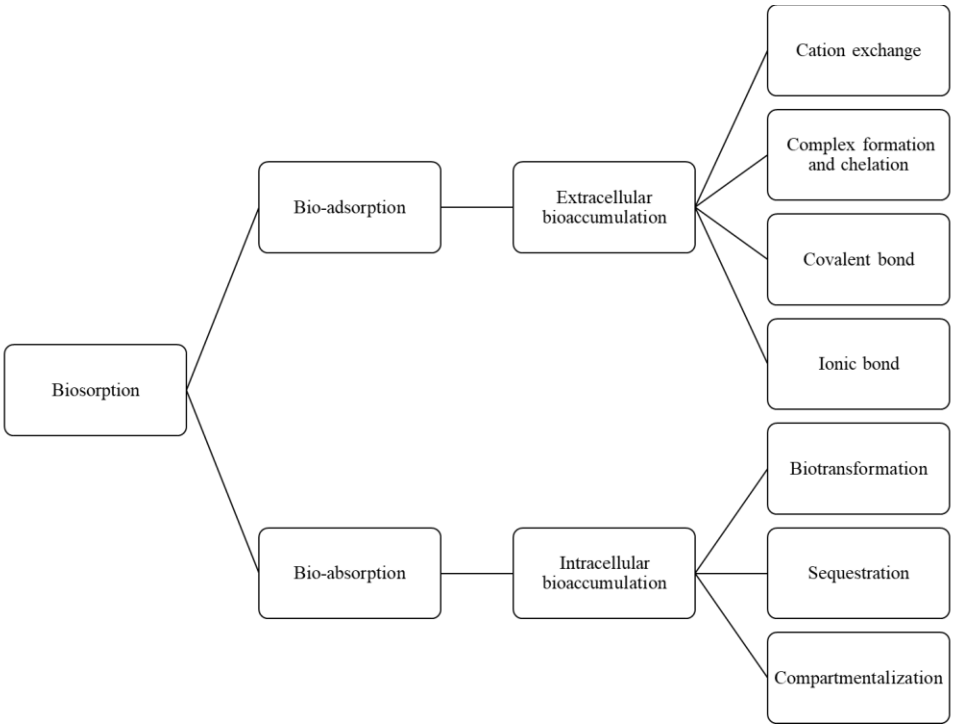

Figure 2-2 Mechanisms of HMI biosorption by microalgae.

Microalgae have complex cell wall composition and structure that are characteristic of algal species [34]. Biosorption of HMIs by microalgae can be carried out in two different ways, as shown in Figure 2-1 and Figure 2-2, i.e., bio-adsorption (adsorption) and bio-absorption (intracellular accumulation). As a surface phenomenon, biosorption by microalgae involves the surface of the sorbents only. It is independent of cellular metabolism but is greatly dependent on the cell wall structure, especially the macromolecules on cell surfaces [35]. HMIs biosorption could be carried out by growing microalgal cells, fresh but non-growing cells, dried biomass, and residue biomass after extraction of value-added products such as microalgal oils. In general, microalgal cell walls are made of a multi-layered framework consisting mainly of cellulose, which is interspersed with an amorphous matrix of glycoproteins. In addition, microalgal cell walls may contain other polymeric substances, e.g., exopolysaccharides, alginate, lipids and liposaccharides [36]. The macromolecules provide numerous functional groups, e.g., amino, carboxyl, hydroxyl, imidazole, phosphate, phosphoryl, sulfonate, thiol, amide, ether etc., which are capable of binding HMIs [37,38]. The knowledge of cell wall structure provides important insights into their affinities for HMIs. Fourier transform infrared (FTIR) and nuclear magnetic resonance spectroscopy (NMR) have been employed to determine the functional groups on microalgal cell walls that are responsible for formation of binding with HMIs. The biosorption of HMIs onto the surface of microalgae can take place through various mechanisms. These mechanisms include ion exchange, where multivalent HMIs are swapped with monovalent co-cations like Na(I) and K(I). These co-cations are linked to negatively charged functional groups found on the cell wall's macromolecules. Chelation, where HMIs form complexes with functional groups from macromolecules on the cell surface, is related with extracellular polysaccharide

substances (EPS). Physical adsorption by electrostatic attraction and van der walls' force also play a important role in HMI removal [33].

On the other hand, bio-absorption (intracellular accumulation) of HMIs by microalgal cell is a much more complex process which involves: 1) bio-adsorption of HMI onto the surface of living cells; 2) active transportation of HMIs through specialized ion channels across the cytoplasmic membrane into the cytoplasm of cells; and 3) detoxification of HMIs by mechanisms such isolating them in vacuoles inside the cells. The second and third steps are dependent and ATP-consumed on cell metabolism and has sometimes been referred to as one, i.e., intracellular ion uptake with detoxification. Therefore, bio-absorption of HMI by cells, including microalgal cells, is an energy dependent and slow process compared with bio-adsorption [39].

Zeta potential (ZP) is the electrical potential at the slipping plane adjacent to the stagnant liquid layer attached to the surface of the dispersed particles in a colloid. It depends on the net electrical charge at the particle surface and the thickness of the stagnant liquid layer. Although zeta potential does not equate to the particle surface potential, it is the only means for researchers to characterize surface charges of particles dispersed in a colloid and has recently been employed by many researchers for the characterization of the surface charges of microalgal cells [40,41]. For instance, the zeta potential of *Chlorella sp.* QB-102 was found to be dependant on adsorption pH. Within the tested pH range of 3.0 to 6.0, all the biosorbents were observed to be negatively charged and with the increase in pH, the zeta potentials became increasingly negative, which enhanced the removal of positively charged metals from aqueous solutions [42]. Similar results were found in the microalga *Neochloris oleoabundans*, where zeta potentials ranged from 50.3, 52.1, 52.9, and 59.5 mV, at pH 4.0, 5.0, 6.0, and 7.0, respectively [43]. Table 2-1 presents the

isothermal and kinetics constants for HMIs removal by microalgae, including biomass, temperature, optimal pH, state of biomass, equilibrium time and biosorption capacity.

Table 2-1 HMIs biosorption by microalgae.

Heavy metal	Species	Biomass	HMIs	T	Optimal pH	State	Kinetics	Equilibrium time	Isotherm	Biosorption capacity	Ref
		[g/L]	[mg/L]	[℃]				[min]		[mg/g]	
As	*Maugeotia genuflex*	0.4-16	10-400	20	6	Dried	Pseudo-second-order	60	Langmuir	67.48	[30]
Co	*Synechocystis pevalekii*	-	100-2000	20	7.1	Living	-	-	Langmuir	117.86	[44]
Co	*Scenedesmus bernardii*	-	100-2000	20	7.1	Living	-	-	Langmuir	11.79	
Cd	*Parachlorella sp.*	1.0	18-180	30	7	Living	Pseudo-first-order	240	Langmuir	90.72	
Cd	*Spirulina sp.*	1.0	18-180	30	7	Living	-	-	-	55.00	[45]
Cd	*Scenedesmus sp.*	1.0	18-180	30	7	Living	-	-	-	30.00	
Cd	*Nannochloropsis sp.*	1.0	18-180	30	7	Living	-	-	-	60.00	
Cd	*Coelastrum sp. PTE-15*	1.0	25-200	30	7.5	Freeze-dried	Pseudo-second-order	2	Langmuir	36.10	
Cd	*Chlorella sp. CHA-01*	1.0	25-200	30	7.5	Freeze-dried	Pseudo-second-order	2	Langmuir	25.51	[46]
Cd	*Chlamydomonas sp. TAI- 03*	1.0	25-200	30	7.5	Freeze-dried	Pseudo-second-order	2	Langmuir	23.26	
Cd	*Oedogonium sp.*	0.2-1.6	20-200	25	5	Dried	-	55	Langmuir	88.2	[47]
Pb	*Sargassum sp.*	1.0	0-2 mmol/L	22	5	Dried	-	360	Langmuir	240.35	[35]
Cu	*Sargassum sp.*	1.0	0-2 mmol/L	22	5	Dried	-	360	Langmuir	62.91	[35]
Cd	*Sargassum sp.*	1.0	0-2 mmol/L	22	5.5	Dried	-	360	Langmuir	85.43	[35]
Zn	*Sargassum sp.*	1.0	0-2 mmol/L	22	5.5	Dried	-	360	Langmuir	32.69	[35]
Ni	*Sargassum sp.*	1.0	0-2 mmol/L	22	5.5	Dried	-	360	Langmuir	35.80	[35]
Pb	*Padina sp.*	1.0	0-2 mmol/L	22	5	Dried	-	360	Langmuir	259.00	[35]
Cu	*Padina sp.*	1.0	0-2 mmol/L	22	5	Dried	-	360	Langmuir	72.44	[35]
Cd	*Padina sp.*	1.0	0-2 mmol/L	22	5.5	Dried	-	360	Langmuir	84.31	[35]
Zn	*Padina sp.*	1.0	0-2 mmol/L	22	5.5	Dried	-	360	Langmuir	52.96	[35]
Ni	*Padina sp.*	1.0	0-2 mmol/L	22	5.5	Dried	-	360	Langmuir	36.98	[35]
Pb	*Gracillaria sp.*	1.0	0-2 mmol/L	22	5	Dried	-	360	Langmuir	93.24	[35]

Cu	*Gracillaria sp.*	1.0	0-2 mmol/L	22	5	Dried	-	360	Langmuir	37.49	[35]
Cd	*Gracillaria sp.*	1.0	0-2 mmol/L	22	5.5	Dried	-	360	Langmuir	33.72	[35]
Zn	*Gracillaria sp.*	1.0	0-2 mmol/L	22	5.5	Dried	-	360	Langmuir	26.15	[35]
Ni	*Gracillaria sp.*	1.0	0-2 mmol/L	22	5.5	Dried	-	360	Langmuir	16.43	[35]
Pb	*Ulva sp.*	1.0	0-2 mmol/L	22	5	Dried	-	360	Langmuir	302.51	[35]
Cu	*Ulva sp.*	1.0	0-2 mmol/L	22	5	Dried	-	360	Langmuir	47.66	[35]
Cd	*Ulva sp.*	1.0	0-2 mmol/L	22	5.5	Dried	-	360	Langmuir	65.19	[35]
Zn	*Ulva sp.*	1.0	0-2 mmol/L	22	5.5	Dried	-	360	Langmuir	34.22	[35]
Ni	*Ulva sp.*	1.0	0-2 mmol/L	22	5.5	Dried	-	360	Langmuir	17.02	[35]
Cd	*Fucus vesiculosus*	0.5	10-150	23	6.06	Dried	Pseudo-first-order	120	Langmuir	108.21	[48]
Pb	*Fucus vesiculosus*	0.5	10-150	23	4.61	Dried	Pseudo-first-order	120	Langmuir	211.34	[48]
Cu	*Fucus vesiculosus*	0.5	10-150	23	5.4	Dried	Pseudo-first-order	120	Langmuir	105.49	[48]
Co	*Phormidium tenue*	1.0	25-200	-	6	Washed by DI	-	30	Langmuir	24.54	[49]
Co	*Chlorella vulgaris*	1.0	25-200	-	5.5	Washed by DI	-	60	Langmuir	15.73	[49]
Co	*Scenedesmus dimorphus*	0.4	4-20 mmol/L	25	5	Dried	Pseudo-second-order	60	Freundlich	39.60	[50]
Co	*Scenedesmus quadricauda*	1.0	5-40	25	6.6	Living	Pseudo-first-order	100	-	52.48	[51]
Cr	*Scenedesmus quadricauda*	1.0	5-40	25	6.6	Living	Pseudo-first-order	100	-	81.98	[51]
Pb	*Scenedesmus quadricauda*	1.0	5-40	25	6.6	Living	Pseudo-first-order	100	-	14.26	[51]
Cd	*Scenedesmus quadricauda*	1.0	5-40	25	6.6	Living	Pseudo-first-order	100	-	24.96	[51]
Ni	*Scenedesmus quadricauda*	1.0	5-40	25	6.6	Living	Pseudo-first-order	100	-	55.71	[51]
Mn	*Scenedesmus quadricauda*	1.0	5-40	25	6.6	Living	Pseudo-first-order	100	-	75.20	[51]
Cu	*Chlorella vulgaris*	0.1	5-300	25	5	Dried	-	15	Langmuir	58.82	[52]
Hg	*Chlamydomonas reinhardtii*	0.8	0-400	25	6	Living	Pseudo-second-order	60	Freundlich	72.2	[53]

Cd	*Chlamydomonas reinhardtii*	0.8	0-400	25	6	Living	Pseudo-second-order	60	Freundlich	42.6	[53]
Pb	*Chlamydomonas reinhardtii*	0.8	0-400	25	5	Living	Pseudo-second-order	60	Langmuir	96.3	[53]
Pb	*Aphanothece sp.*	0.0186	3.9-18.6	25	6	Dried	Pseudo-second-order	30	Langmuir	185.64	[54]
Cd	*Scenedesmus quadricauda*	0.2	0-10	Room temperature	5	Dried	Pseudo-second order	60	Langmuir	135.13	[55]
Pb	*Scenedesmus quadricauda*	0.2	0-50	Room temperature	5	Dried	Pseudo-second order	60	Langmuir	333.33	[55]
Cd	*Anabaena sphaerica*	0.4	50-300	25	5.5	Dried	-	60	Freundlich	111.10	[56]
Pb	*Anabaena sphaerica*	0.4	50-300	25	3	Dried	-	90	Langmuir	121.95	[56]
Zn	*Scenedesmus obliquus*	0.02	10-75	25	6	Dried	-	30	Langmuir	330.00	[57]

2.2.2 Effect of adsorbate: properties of HMIs

The characteristics of the absorbate, specifically HMIs within the scope of this thesis project, exert significant influence on their interactions with microalgal cells. Numerous research groups have investigated this subject [20,33,58,59], and there is a general consensus among researchers that certain ionic properties play a crucial role in their adsorption onto algal cell surfaces. These properties include the nature of the charges (negative or positive), the valency of charges (monovalent or multivalent), electronegativity, and ionic radius.

For instance, it has been reported that positively charged Cu(II) exhibits a much higher biosorption capacity (58.8 mg/g) than the negatively charged anionic As(II) (13.07 mg/g) when interacting with the same biosorbent, *Chlorella vulgaris* [60]. This difference arises because the negatively charged microalgal cell surface can only bind to HMIs through the formation of HMI-macromolecule complexes, e.g., through chelation, while cationic HMI with positive charges exploits an additional and more efficient mechanism, i.e., ion exchange.

Among cationic HMIs of the same charge valence, researchers are generally in the agreement that the electronegativity and the ionic radius of HMIs are two important parameters affecting their biosorption capacity by same biomass [61–63]. However, the results reported so far have been inconclusive or in some cases contradictory to each other. In an early study, Tobin et al. [64] reported that the uptake of HMIs by dried *Rhizopus arrhizus* biomass increased roughly with the ionic radius when compared among HMIs of the same charge. On the other hand, Sheng et al. [65] studied the adsorption of three HMIs, Pb(II), Cu(II), and Cd(II) from aqueous solutions by marine alga *Sargassum sp.* in single-metal and binary systems and concluded that higher electronegativity corresponded to higher adsorption capacity. In another study, Rahman and

Sathasivam [66] found the adsorption capacities of four HMIs onto *Kappaphycus sp.* biomasses followed the order of Pb(22.17 mg/g)> Cu(19.49 mg/g)> Fe(16.92 mg/g)> Zn(16.23 mg/g) and hence claimed also that the biosorption capacity of biomass to the HMIs increased with electronegativity. They, however, mistakenly used the mass capacity (mg/g) instead of mole (mmol/g) capacity. Indeed, when the unit is corrected, the order of adsorption capacity of different HMIs becomes Cu(0.307mmol/g)> Fe(0.303mmol/g)> Zn(0.248mmol/g)> Pb(0.248mmol/g). In an attempt to obtain unambiguous results about the effects of these two parameters on biosorption capacity, we strategically selected five HMIs, i.e., Pb(II), Hg(II), Zn(II), Cd(II), and Cu(II) and compared their adsorption onto *Neochloris oleoabundans*. It was shown that optimizing dissolved inorganic carbon (DIC) concentration in medium could increase the Pb(II) biosorption capacity of *N. oleoabundans* cells by up to 2.4 times, demonstrating a great potential of this unicellular green microalga for HMIs removal [67]. Among these five HMIs, the Hg(II)/Cu(II) pair and the Zn(II)/Cd(II) pair have similar electronegativity but very different radii while the Zn(II)/Cu(II) pair and the Hg(II)/Cd(II) pair have similar ionic radius but very different electronegativities. Comparison within these pairs allowed the analysis on the effects of one property, either electronegativity or ionic radius, with minimal interference of the other.

2.2.3 Engineering fundamentals

2.2.3.1 Biosorption kinetics

Kinetic information frequently finds application in the upscaling of biosorption systems [68]. Typically, the biosorption kinetics are described using either pseudo-first order or pseudo-second order kinetic model, as shown in Eqs 2.1 & 2.2. The choice of a kinetic model is made by examining curve fitting and comparing the experimental and calculated equilibrium biosorption. Additionally, the correlation coefficients (R^2 values) derived from these comparisons help in

selecting the most suitable model. A higher R^2 value suggests that the chosen kinetics model effectively captures the biosorption kinetics. Below are the mathematical equations:

$$q(t) = q_e[1 - \exp(-k_1 t)] \quad 2.1$$

$$q(t) = q_e \frac{k_2}{1 + k_2 t} \quad 2.2$$

2.2.3.2 Biosorption isotherms

Biosorption isotherms are typically described as the relationship between the residual HMI in the solution and the biosorption on biomass at equilibrium at a constant temperature. Langmuir (Eq 2.3), Freundlich (Eq 2.4), Sips (Eq.2.5) and BET (Eq 2.6) models are the often-employed isothermal models. These models help differentiate the metal biosorption behavior for various HMIs. The isotherm equations for these four models are as follows:

$$q_e = K_f C^{\frac{1}{k}} \quad 2.3$$

$$q_e = \frac{K_l C_e}{1 + K_l C_e} \quad 2.4$$

$$q_e = \frac{q_{mS} K_S C_e^{n_S}}{1 + K_S C_e^{n_S}} \quad 2.5$$

$$q_e = \frac{q_B K_{B1} C_e}{(1 - K_{B2} C_e)(1 - K_{B2} C_e + K_{B1} C_e)} \quad 2.6$$

2.2.3.3 Biosorption thermodynamics

Thermodynamics model can help us to better understand the mechanism of biosorption, which contains a lot of thermodynamics parameters, such as standard Gibb's energy change (ΔG°), standard enthalpy change (ΔH°), and standard entropy change (ΔS°) of HMIs biosorption. These equations are shown below (Eqs 2.7-2.10):

$$\Delta G^{\circ} = \Delta H^{\circ} - T\Delta S^{\circ} \quad 2.7$$

$$\Delta G^{\circ} = -RTLn(K_{eq}) \quad 2.8$$

$$lnK_{Eq}^{\circ} = -\left(\frac{\Delta H^{\circ}}{R}\right)\frac{1}{T} + \frac{\Delta S^{\circ}}{R} \quad 2.9$$

$$K_{Eq}^{\circ} = K_{Model}\frac{[Adsorbate]^{\circ}}{\gamma_{Adsorbate}} \quad 2.10$$

2.3 Influence parameters for HMIs biosorption capacity by microalgae

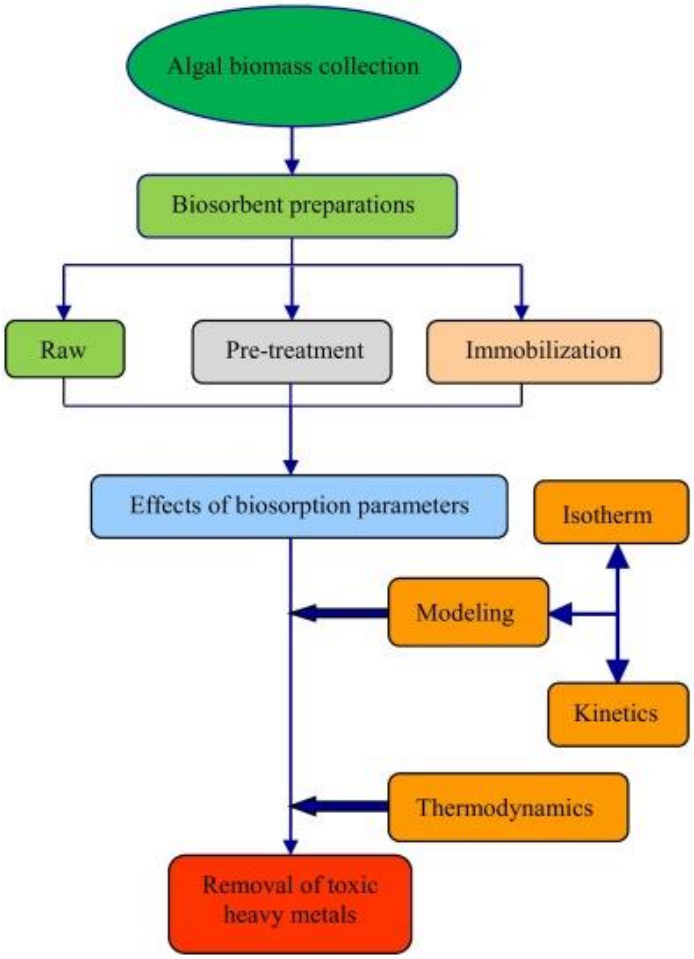

Figure 2-3 A generalized presentation of distinct stages of biosorption process using algal biomass towards the removal HMIs, adapted from [69].

Figure 2-3 illustrates a schematic diagram of the biosorption process employed for the sequestration of HMIs using algal biomass. This process involves several crucial steps and interactions that play a pivotal role in the removal of HMIs from aqueous solutions by microalgae, i.e., biosorbent preparation and effect of biosorption parameters.

2.3.1 Selection of appropriate microalgal species for HMIs biosorption

Many different species of microalgae have been demonstrated to be excellent biosorbents for HMIs removal [70]. For instance, Mohammed et al. [24] investigated the effects of HMIs, i.e., Cd(II), Ni(II), and Pb(II), on the photosynthesis of microalgae *Chlorella vulgaris, Scenedesmus quadricuda, and Spirulina platensis*, finding that they could remove Ni(II) with 95% efficiency. Additionally, microalgae were found to be able to uptake lead and Cd(II) with up to 89% and 88% removal efficacy, respectively. Zheng et al. [46] compared the biosorption of Cd(II) by three microalgal species and reported that *Coelastrum sp.* (36.10 mg/g) had the largest biosorption capacity, which was followed by *Chlorella sp*. (25.51 mg/g), and *Chlamydomonas sp*. (23.26 mg/g). This is quite understandable since microalgal cell wall is complex and different microalgal species may have very different cell wall structures [34].

Moreover, research has shown that the ability of microalgae to adsorb various HMIs is strongly dependent on the specific microalgal strain [51]. The variations in biosorption capacity of HMIs observed among different microalgal biomass can often be attributed to differences in microalgal properties such as cell size and the microstructures on cell surface. For instance, unicellular microalgal biomass, such as *Chlorella vulgaris*, *Chlorella minutissima* and *Parachlorella sp*., exhibit higher biosorption capacities than multicellular microalgal biomass, like *Scenedesmus-24* and *Spirulina platensis* [70,71]. Consequently, there appears to be a discernible preference for certain strains of microalgal cells to interact selectively with HMIs, which may differ even among closely related species. The increased selectivity of unicellular microalgal biomass is ascribed to differences in the cell wall compositions and distributions among various microalgal strains. These variations result in diverse capacities for the biosorption of HMIs.

2.3.2 Conditioning of biomass by optimizing growth medium

Currently, multiple approaches exist to enhance the biosorption capacity of microalgae through cultivation. One such approach involves manipulating various cultivation parameters to optimize biosorption capacity as it has been demonstrated that it is possible to modify structure of cell wall of microalgal cells by manipulating the composition of culture medium, thereby enhancing biosorption of HMIs using these cells. For example, 1) the stage in the life-cycle of microalgae, e.g., exponential phase, linear phase, deceleration phase, or stationary phase, could impact biosorption capacity [23], 2) phosphate levels in the medium can affect biosorption capacity, with optimal conditions varying across different strains [24,25], 3) dissolved inorganic carbon sources can improve Pb(II) biosorption capacity [26], and 4) medium pH can enhance HMIs biosorption [27]. Cultivation parameters can modify cellular growth and wall composition, particularly the negative functional groups on the cell wall, thereby affecting HMIs biosorption. Nitrate, like phosphate, is a crucial factor in microalgal cultivation, playing a significant role in regulating the growth and physiology of microalgae. Nitrate has been observed to influence the biochemical composition of microalgal cells, including protein production that potentially increasing the biosorption capacity of HMIs [28]. Numerous studies have been conducted to improve the biosorption capacity of microalgae. Li et al. developed a novel strategy for the sequential removal of phosphorus and Pb(II) by *Chlorella* species. Pb(II) biosorption capacity of 635.8 mg/g was achieved using cells grown in modified medium containing 280 mg/L phosphate, comparing very favorably to the 110.41 mg/g biosorption capacity of cells growing in 20 mg/L phosphate medium [42].

2.3.3 Processing of algal biomass for enhanced HMI biosorption

2.3.3.1. Pyrolysis

Some researchers have investigated the utilization of dehydrated microalgae for the removal of HMIs from aqueous solutions, aiming to leverage the advantages of convenient storage and transportation of dried biomass [54,72,73]. For instance, *Chlorella vulgaris* demonstrated significant potential in adsorbing Ag(I) and Nd(III) from aqueous solutions, exhibiting biosorption capacities of 174.6 mg/g and 239.7 mg/g, respectively [74]. Additionally, Cheng reported that dried *C. vulgaris* biomass exhibited a biosorption capacity of 16.65 mg/g for Cd(II) [75].

2.3.3.2. Immobilization

A number of benefits may result from using immobilized microalgal cells for HMIs biosorption. These benefits include the easy recovery or retention of immobilized cells for the reuse of the biomass and easy separation of the solid biomass from bulk liquid. Bayramoğlu et al. [17,53] investigated biosorption of Hg(II), Cd(II) and Pb(II) from aqueous system by microalgae *Chlamydomonas reinhardtii* immobilized in alginate beads, getting higher biosorption capacity of Hg(II) (116.8 mg/g), Cd(II) (88.6 mg/g) and Pb(II) (384.4 mg/g) by immobilized- algae than dried microalgae (Hg(II) (72.2 mg/g), Cd(II) (42.6 mg/g) and Pb(II) (96.3 mg/g).

2.3.3.3. Chemical modification of cell wall surface

Enhancing biosorption capacity of HMIs by microalgal biomass through chemical modification is a frequently used strategy [18,76]. Depending on the chemical modification, the biosorption capacity may be enhanced either by enhancing the specific surface area, or by functionalizing the surface [77]. Li et al. [76] compared pristine and carboxylation modified alga *Sargassum carpophyllume* and *Caulerpa lentillifera* dried biomass for removing heavy metal Pb(II) and

Mn(II) in aqueous solution. After carboxylation with butanedioic anhydride, the adsorption capacities to Pb(II) and Mn(II) were enhanced 3 to 6 times than pristine residue biomass.

2.4 Conditioning of biosorption process for optimum HMI removal

Many conditional factors may affect the biosorption of HMI by microalgae. These factors include the concentration of HMIs and microalgae biomass, pH and temperature, as well as the presence of competing ions.

2.4.1 Effects of operation pH

The pH of the adsorption mixture is an important factor in determining the biosorption capacity of HMIs by microalgal biomass. This can be explained by the interaction between HMIs and functional groups in solution, the behavior of different functional groups on algal surfaces, and the acid dissociation constant value of the functional group. However, a high pH will result in the precipitation of HMI as illustrated in the following general chemical reaction equation (Eq. 2.11):

$$HMI^{2+} + 2OH^{-} = HMI(OH)_2 \qquad 2.11$$

In order to prevent precipitation of metal ions due to high pH, research will use neutral or acidic solutions for biosorption tests. As aforementioned, there are a lot of functional groups which contribute to biosorption, such as phosphate group, carbonic group, nitric group and sulfate groups [14]. These functional groups all contain negatively charged functional groups, which may bind to positive HMI. According to Gu et al. [43], the cell wall of *N. oleoabundans* composed of 31.56% proteins, 24.3% polysaccharides, 22% lipids, 7.8% inorganics (e.g., phosphate), and 14.4% other molecules with the major constituent monomers. The pKa_1 of the constituent monomers of polysaccharides, proteins, and lipids have a large variety ranging from −1.9 of glucosamine to 15.28 of 5-methyl-3-hexanol. The fact that the effects of pH to adsorption

was significant between pH 2 and 4 but was very mild between pH 4 and 7 suggests that the residues of constituent monomers with pKa1 in the range of pH 2–4 are likely the primary sites of biosorption. These monomers include amino acids, which are commonly found in proteins (31.5% of cell wall dry weight) and hybrid macromolecules such as peptidoglycan and peptidolipids. Glucosamine (pKa_1=−1.9), galacturonic acid (pKa_1=3.24) and glucuronic acid (pKa_1=3.21), which are monomers of non-cellulosic polysaccharides, peptidoglycans, and lipoglycans, also have pKa1 in the acidic range. When pH is increased, functional groups are deprotonated, thereby leaving more space for heavy metal ions to bind to, therefore increasing biosorption capacity, as illustrated below (-OH is presented as one functional group on cell wall):

$$Functional - OH + OH^- = Functional - O^- + H_2O \quad 2.12$$

$$2Functional - O^- + HMI^{2+} = 2Functional - O^-HMI^{2+} \quad 2.13$$

Abdel-Raouf [49], in a study on two microalgal species, i.e., *Phormidium tenue* and *Chlorella vulgaris*, determined that their optimal pH for Co(II) biosorption to be pH 6.0 and pH5.5, obtaining 85% and 90% Co(II) removal, respectively. Mirghaffari et al. [55] investigated microalgae *Scenedesmus quadricauda* on heavy metal Cd(II) and Pb(II), finding optical pH for two heavy metals both are 5 and getting 66% and 82% heavy metal removal%. For green microalga *Anabaena sphaerica*, the optimal pH for Cd(II) and Pb(II) are 5.5 and 3, reaching 84.5% and 88.3% heavy metal removal%, respectively [56]. Al-rub investigated *Chlorella vulgaris* as biosorption for Cu(II), getting the highest biosorption capacity was obtained at pH 5.0 about 98.5% removal% of Cu(II) in a solution of 300 ppm Cu(II). Monteiro et al. [14] reported pH effect on Zn(II) using microalgal *Scenedesmus obliquus*, illustrated the optimal pH was 6.0 and got 112.8 mg/g equilibrium biosorption [57]. As a result, much research has confirmed that increasing pH

from 2-7 could promote HMIs removal% and equilibrium biosorption, but the optimal pH is different may be due to metal properties, such as electronegativity and ionic radius.

2.4.2 The influence of microalgal biomass concentration

The biomass concentration is another important factor influencing HMIs removal%, equilibrium biosorption, and residual HMIs concentration. It should be adjusted to an optimum level to maximize the efficiency of the process. Understandably, the HMIs removal% increases with an increase in biomass concentration while both the equilibrium biosorption and residual HMIs concentration decrease. Gupta et al. [47] reported that, when biomass concentration increased from 0.2 to 1.6 g/L, the Cd(II) removal% increased from 10% to 70%. However, equilibrium biosorption dropped from 88.2 to 12 mg/g while the residual Cd(II) decreased from 1.6 to 0.2 g/L. Abdel-raouf et al. [49] demonstrated that the removal% of Co(II) were 95% and 78% for *P. tenue* and *C. vulgaris* with 2.0 g/L biomass, respectively.

2.4.3 The influence of contact time

An important aspect of biosorption kinetics is the selection and design of reactor systems, as well as their operation. This demonstrates that biosorption of HMIs is a passive process that occurs relatively rapidly, even when algal cells are non-living. For dried microalgae, HMI biosorption is not metabolically dependent and typically rapidly, particularly when cationic metal ions are taken up [78]. For living algae, contact time has a greater effect on the biosorption capacity comparing to dried algae since bioaccumulation is metabolically dependent and slow. The majority of cationic metal uptake occurs within the first 20–60 minutes, followed by a relatively slow process [26]. Keryanti et al. [54] investigated effect of contact time with dried microalgae *Aphanothece sp*., finding that the optimal contact time range was 30-180 minutes. Similarly, one research

reported that marine green alga *Dunaliella salina* had the maximum Pb(II) removal at a contact time of 120 minutes with biosorption capacity of 3.9 mg/g [72].

In contrast to positive HMIs, the rate of the uptake of anionic HMIs (e.g., hexavalent chromium) is considerably lower than that for cationic contaminants. In most cases, equilibrium biosorption would not be reached in a few hours to a few days. In one report, the complete uptake of hexavalent chromium was achieved within 2.5 hours when *Scenedesmus sp.* was used [38].

2.4.4 The influence of initial metal ion concentration

The equilibrium biosorption of HMIs by microalgal biomass is contingent upon the concentration of initial HMIs in the solution phase. Initially, as the initial concentration of HMIs increases, there is a corresponding increase in equilibrium biosorption. However, this relationship is limited by binding site saturation, and thus, increasing the HMIs concentration beyond a certain point does not lead to a further increase in equilibrium biosorption [79]. For instance, Sarı et al. reported that the maximum monolayer biosorption capacity for As(III) by green algae *Maugeotia genuflexa* biomass was 57.48 mg/g [30]. In another study, Gupta et al. investigated the biosorption of Cd(II) by nonliving algal biomass *Oedogonium sp.* and achieved a biosorption capacity of 88.9 mg/g [47]. However, it's noteworthy that when the initial concentration of Cd(II) is 20 mg/L, the biosorption capacity is limited to 20 mg/g. This indicates that as the concentration of HMIs in the solution increases, the biosorption capacity also increases.

2.4.5 The influence of temperature

In the context of the biosorption process, temperature emerges as a critical factor that significantly impacts the biosorption of HMIs. Temperature is intricately linked to the kinetic energy of HMIs, thereby governing the diffusion process and influencing the extent of HMIs

removal or biosorption by the biomass. As biomass cell walls inherently possess porous properties, both diffusion and biosorption can be considered plausible mechanisms for the removal of metals. Remarkably, the biosorption capacity and the percentage of HMIs removal exhibit substantial variations depending on temperature conditions [80]. While temperature notably affects the ligand complexes present on the cell walls, some research suggests that elevated temperatures in algal cultures may enhance HMI biosorption capacity [29,45,80–82]. However, contrasting findings have indicated a reduction in biosorption capacity with increased temperature [47]. Various factors can contribute to these changes in HMIs biosorption, encompassing: 1) Alterations in the number of active sites participating in the uptake of HMIs. 2) Modifications in the propensity of active sites to adsorb metal ions. 3) Adjustments in mass transfer resistance within the diffusion layer due to a decrease in the thickness of the diffusion boundary layer surrounding the adsorbent groups. 4) Variations in the complex formation constant as temperature rises [39].

2.5 Knowledge gaps

Utilizing microalgae-based biosorption technology for HMIs removal from wastewater has demonstrated substantial potential. However, several notable knowledge gaps remain within the realm of its commercial applications. These knowledge gaps can be categorized as follows: 1) Understanding metal-microalgae interactions: One significant gap in our knowledge concerns unraveling the relationship between different HMI species and their interactions with the same microalgal biomass. 2) Enhancing biosorption capacity of HMIs: Another key challenge is the enhancement of biosorption capacity for HMIs using the same microalgal biomass under diverse cultivation conditions. 3) Cost reduction in wastewater treatment: A critical concern in the practical application of microalgae-based biosorption technology is the reduction of expenses,

especially those associated with biosorbents, in wastewater treatment plants. This entails the exploration of cost-effective alternatives and the efficient utilization of microalgae for biosorption to make the process economically viable. 4) Development of predictive tools for biosorption capacity: An essential aspect of advancing this technology is the investigation of whether predictive tools or models can be developed to estimate the biosorption capacity of HMIs. The goal is to create reliable predictions without the need for extensive and resource-intensive experimentation.

My thesis aims to address some of these knowledge gaps and contribute to the advancement of microalgae-based biosorption technology. I have established a correlation between HMI properties, such as ionic radius and electronegativity, and their biosorption capacity. This correlation is supported by both experimental data and existing literature. Another crucial area of focus is the intricate interactions between HMIs and microalgal cells grown under diverse cultivation conditions. Understanding these interactions is pivotal for optimizing biosorption capacity. My research findings have highlighted the significance of various factors, including nitrate and phosphate levels, culture pH, and dissolved inorganic carbon (DIC) concentration, in shaping the surface structure of microalgal cells and, consequently, their ability to absorb HMIs. Additionally, exploring downstream processing, such as the utilization of microalgal biomass post lipid extraction, has revealed the potential for further enhancing biosorption capacity. Additionally, I have proposed and validated a mathematical model that integrates cell properties and HMI radius. This model provides a valuable predictive tool for estimating HMI biosorption capacity. This research endeavors to bridge the gap between theoretical knowledge and practical application, bringing us closer to the widespread implementation of this technology in wastewater treatment.

Chapter 3 Biosorption of heavy metal ions by green alga *Neochloris oleoabundans*: effects of metal ion properties and cell wall structure[1]

Siwei Gu & Christopher Q. Lan*

Department of Chemical and Biological Engineering

University of Ottawa

* Christopher.Lan@Uottawa.ca

[1] The content of this chapter was published: S. Gu & C.Q. Lan, Biosorption of heavy metal ions by green alga *Neochloris oleoabundans*: Effects of metal ion properties and cell wall structure, J. Hazard. Mater. 418 (2021) 126336.

Highlights

- Adsorption of Cu^{2+}, Zn^{2+}, Pb^{2+}, Hg^{2+}, and Cd^{2+} on *N. oleoadundans* investigated.
- All adsorptions were quick, spontaneous, energy-independent, and Langmuir.
- Adsorption capacities showing linear relationship with impact factor of ions.
- Functional groups with pKa between pH 2-4 identified as likely sites of adsorption.

3.1 Abstract

Effects of metal ion proprieties and the cell wall structure of green alga *Neochloris oleoabundans* were investigated on five strategically selected heavy metal ions, Pb(II), Hg(II), Zn(II), Cd(II) and Cu(II). The biosorption of these ions were energy-independent and spontaneous Langmuir adsorption. The adsorption capacities of Pb(II), Hg(II), Zn(II), Cd(II) and Cu(II) were determined to be 1.03, 0.91, 1.20, 0.65 and 1.23 mmol/g, respectively. Data suggest that peptide-containing molecules and non-cellulosic polysaccharides on cell wall were the primary sites of adsorption. Ion Pb(II) showed the strongest inhibitive effects on the adsorption of other metal ions on cells in binaries, corresponding to its large affinity to the biosorbents, which was next only to that of Cu(II). A linear relation was established for the first time between the adsorption capacity and the impact factor, which is defined in this paper as the electronegativity of a metal ion normalized by its atomic radius. In other words, adsorption capacity of *N. oleoabundans* biomass to the tested two-valence metal ions is proportional to the electronegativity and inversely proportional to the radius of the metal ions. Cell aggregation was caused by the addition of Cu(II), which exhibited distinctive adsorption behaviors than other metal ions.

Key words: biosorption, heavy metal removal, green algae, *Neochloris oleoabundans*

3.2 Introduction

Heavy metals are metals or metalloids with a density of 5 g/cm^3 or above [83]. They could be discharged with domestic and industrial wastewaters as well as industrial dusts precipitations to cause pollution in rivers, lakes and oceans. Heavy metals in the aquatic ecosystem could be transmitted to humans through biomagnification moving up along the aquatic food chain, potentially causing major health problems [84]. It should be cautioned, however, that the term "heavy metals" is very imprecise and sometimes misleading as it refers to both the element and its compounds and different authors may defined the term based on different criteria [85].

Biosorption using different biomasses including plants, algae, bacteria and fungi to remove heavy metals from wastewaters has attracted extensive attention as a promising technology because they are self-propagating and environment-friendly [86]. Volume reduction of heavy metal loaded biomasses could be achieved by combustion for energy and the resulting ashes could be subjected to extraction of heavy metals for a zero-discharge cycle.

Microalgae and cyanobacteria (algae hereafter) have attracted renewed interests as effective biosorbents recently as they offer some unique advantages [87]. Bilal et al. [88] systematically surveyed Cu(II) biosorption using different biomasses and concluded that the maximum Cu(II) adsorption capacities of various biosorbents to be in the order of algae>agricultural and forest>fungal>bacterial>activated carbon>yeast.

Algae are fast growing and ubiquitous in the aquatic ecosystem and of high metal adsorption capacity. They are unicellular or simple multicellular organisms that have small cellular or colonial size and hence large adsorption surfaces and fast adsorption kinetics. Their microscale size, in combination with their close-to-water density, makes them easy to disperse in water [89].

Furthermore, algae can tolerate relatively high concentration of heavy metals and can therefore be utilized for removing metals from wastewaters as suspended cells [90] or biofilms [91].

Indeed, suspended algae or immobilized algal biofilms may prove to be the most effective agents for restoring large volumes of waters (e.g., rivers and lakes) contaminated by heavy metals at just-above-drink-water-standard level. And drinking water demands extremely low heavy metal concentration to be safe since heavy metals are toxic at very low concentration and may accumulate in human body. For instance, the drinking water standard for Lead and arsenic as recommended by WHO are both 10 μg/L [92]. At such low concentration, abiotic approaches that could treat large volumes of waters in an economically sustainable manner, e.g., chemical precipitation, are ineffective.

Understanding the effects of the properties of heavy metal ions on adsorption capacity would greatly facilitate the selection of biosorbents and optimization of adsorption processes for heavy metal removal. A few research groups have explored this topic and are in the agreement that the electronegativity and the radius of metals are two important parameters affecting their adsorption by biomasses [61–63]. However, the results reported so far have been inconclusive or in some cases contradictory to each other. In an early study, Tobin et al. [64] reported that the uptake of metal ions by dry *Rhizopus arrhizus* biomass increased roughly with the radius of metal ions when compared among ions of the same charge. On the other hand, Sheng et al. [65] studied the adsorption of three heavy metal ions, Pb(II), Cu(II), and Cd(II) from aqueous solutions by marine alga *Sargassum sp.* in single-metal and binary systems and concluded that higher electronegativity corresponded to higher adsorption capacity. In another study, Rahman and Sathasivam [66] found the adsorption capacities of four metal ions onto *Kappaphycus sp.*

biomasses followed the order of Pb(22.17 mg/g)> Cu(19.49 mg/g)>Fe(16.92 mg/g)>Zn(16.23 mg/g) and hence claimed also that the adsorption capacity of biomass to the metal ion increased with electronegativity. They, however, mistakenly used the mass capacity (mg/g) instead of mole (mmol/g) capacity. Indeed, when the unit is corrected, the order of adsorption capacity of different metal ions becomes Cu(0.307mmol/g) > Fe(0.303mmol/g) > Zn(0.248mmol/g) > Pb(0.248mmol/g). In an attempt to obtain unambiguous results about the effects of these two parameters on biosorption capacity, we strategically selected five heavy metal ions, i.e., Pb(II), Hg(II), Zn(II), Cd(II), and Cu(II) and compared their adsorption onto *Neochloris oleoabundans*. It was shown that optimizing dissolved inorganic carbon (DIC) concentration in medium could increase the lead biosorption capacity of *N. oleoabundans* cells by up to 2.4 times, demonstrating a great potential of this unicellular green alga for heavy metal removal [67]. Among these five metal ions, the Hg(II)/Cu(II) pair and the Zn(II)/Cd(II) pair have similar electronegativity but very different radii while the Zn(II)/Cu(II) pair and the Hg(II)/Cd(II) pair have similar radii but very different electronegativities. Comparison within these pairs allowed the analysis on the effects of one property, either electronegativity or ionic radius, with minimal interference of the other.

On another front, understanding the functional groups at cell surface that serve as the sites of adsorption would provide valuable information to improve our understanding on the interactions between metal ions and biosorbents. Such understanding would be particularly beneficial in the light of the recently renewed interests on the modification of algal cells to increase the efficiency of biosorption for heavy metal removal [93–95]. In this study, we identified amino acids, which are commonly found in proteins and peptide-containing hybrid macromolecules such as peptidoglycan and peptidolipid, and glucosamine, galacturonic acid and glucuronic acid, which

are monomers of non-cellulosic polysaccharides, peptidoglycans, and lipoglycans, as the most likely binding sites of metal ion adsorption according to analysis on experimental data.

3.3 Material and Method

3.3.1 Microalgal culture and media

N. oleoabundans, (UTEX# 1185) was purchased from UTEX Culture collection of Algae, the University of Texas at Austin. Algae were grown in a Modified Bristol Medium (MBM) containing (per liter): 0.35 g $NaNO_3$, 0.138 g K_2HPO_4, 0.0823 g $MgSO_4$, 0.025 g $CaCl_2$, 0.322 g KH_2PO_4, 0.025 g NaCl, and 0.0068 g $FeCl_3$ [96]. Additionally, 1 mL of A5 solution containing (per liter): 1.6423 g EDTA-Fe, 2.86 g H_3BO_3, 1.81 g $MnCl_2{\cdot}4H_2O$, 0.22 g $ZnSO_4{\cdot}7H_2O$, 0.079 g $CuSO_4{\cdot}5H_2O$, and 0.039 g $(NH_4)_6Mo_7O_2{\cdot}4H_2O$ was added. All chemicals are under analytical grade and medium was sterilized at 121℃ for 20 minutes before using.

3.3.2 Microalga cultivation

The microalga cultivation method was adapted from our previous work [67]. Briefly, *N. oleoabundans* was grown in a 3-L photobioreactor, which was converted from a stirred tank BioFlow 110 bioreactor (New Brunswick Scientific GMI Inc., Canada) by equipping it with 12 full spectrum lamps with a light intensity of 1700 μmol/(m^2·s) (Philips Plant & Aquarium T18/15, Philips Electronics Ltd. ON, Canada), which were arranged evenly around the bioreactor, and programmed to be 12 hours on and 12 hours off. Before the inoculation, the bioreactor containing 2 L of fresh medium was sterilized at 121℃ for 20 minutes. After cooling to room temperature, the sterilized medium was inoculated with 30mL of inoculant. The cultivation was then carried out at 25℃, 180 RPM, and pH 9.5 with a constant air flow of 1 LPM (i.e., 0.5 vvm). The culture pH was maintained constant by adding pure CO_2 to the air stream through a gas mixer. The air stream passed through a bottle containing distilled water to be moisturized before being filtered

through a 0.20 μm microfilter and then sparged at the bottom of the bioreactor into the culture. Algal samples were harvested when algal density reached $6*10^7$ cells /cm^3 by centrifuging at 5000 RPM (6500 ×g) for 10 minutes and washed three times by deionized water to remove medium and cell debris. Then the algae samples were kept at -80℃ until needed.

3.3.3 Adsorption studies

3.3.3.1 Stock solution preparation

Stock solutions of 1000 ppm Pb(II), Zn(II), Cu(II), Cd(II), and Hg(II) were prepared by dissolving appropriate amount of $Pb(NO_3)_2$, $Zn(NO_3)_2 \cdot 6H_2O$ (Strem Chemicals Inc., USA), $Cu(NO_3)_2 \cdot 2.5H_2O$ (Alfa Aesar, USA), $Cd(NO_3)_2$, $NaNO_3$ and $Hg(NO_3)_2$ (Fisher Scientific, USA), respectively. HNO_3 were added to stabilize the stock solution.

3.3.3.2 Adsorption kinetic study

Appropriate volumes of the stock solutions were added to the algal biomass to make the initial metal concentration 50 mg/L, and then the pH was adjusted to 6.5 by adding 0.1 N NaOH and 0.1 N HNO_3 solutions. The mixture was then incubated on a shaker oscillating at 180 RPM in dark at 25℃. Samples were taken at 1, 5, 10, 15, 20, 25 and 30 min to centrifuge at 13500 RPM (18000 ×g) for 10 minutes. The pH of the supernatant was adjusted to 2 by adding 0.1 N HNO_3 before determining the metal concentration in samples using atomic absorption spectroscopy (AAS). A control was prepared for each pH condition, in which 50 mL deionized water replaced the algal culture. The metal concentration in the solid phase, q_{eq} (mmol/g), was determined by mass balance (Eq 3.1).

$$q_{eq} = \frac{(C_i - C_{eq})}{m} \qquad 3.1$$

where C_i and C_{eq} are the metal ion concentration in the initial solution (control) and solution after adsorption, respectively (mmol); and m is the biomass concentration (g/L) in the adsorption mixture.

3.3.3.3 Adsorption isotherms

Adsorption isotherms of heavy metal Pb(II), Hg(II), Zn(II), Cd(II) and Cu(II) were carried out at pH 7 or at the pH as specified in the text. Biomass samples at concentrations as specified in the text were incubated at an initial metal ion concentration in the range of 5.0-200.0 ppm to determine the adsorption isotherm. After 30 min, the supernatant of the sample following incubation was analyzed for residual heavy metal concentration using AAS.

3.3.3.4 Thermodynamics

Thermodynamic studies were conducted using an algal biomass dosage of 0.3 g/L and pH 7 at three different temperatures, 25°C, 35°C and 45°C with 30 mins incubation. The residual lead concentration in the liquid phase following adsorption was determined using AAS. Equations 3.2 to 3.5 were used to determine thermodynamic parameters standard Gibbs energy change (ΔG°), standard enthalpy change (ΔH°), and standard entropy change (ΔS°) of adsorption [94].

$$K_{eq} = \frac{q_{eq}}{C_{eq}} \tag{3.2}$$

$$\Delta G° = -RTLn\left(K_{eq}\right) \tag{3.3}$$

$$\ln\left(K_{eq}\right) = \frac{\Delta S^{\circ}}{R} - \frac{\Delta H^{\circ}}{RT} \tag{3.4}$$

$$\Delta G° = \Delta H° - T\Delta S° \tag{3.5}$$

where, K_{eq} is the adsorption equilibrium constant, C_{eq} (mmol/L) is the equilibrium concentration, q_{eq} (mmol/g) is the observed biosorption capacity at equilibrium, T is the temperature (K), and R is the universal gas constant (8.314 J/ (mol K)).

3.3.3.5 Competition test

The competition between different heavy metal ions in binary systems was investigated with equimolar mixtures with both 0.5 mmol heavy metal under 0.3g/L biomass. The samples were incubated for 30 minutes at pH 7.0 and, at the end of incubation, the samples were centrifuged and the supernatant was analyzed for residual metal concentration using AAS. In order to better illustrate the impact of competition, introducing the % relative equilibrium adsorption, defined as Equation 3.6:

$$\%\ Relative\ equilibrium\ adsorption(REA) = \frac{q_{eq}}{q_{eq}^{o}} * 100\% \qquad 3.6$$

where q_{eq}^{0}(mmol/g) represents the equilibrium adsorption of a metal ion without competing metal ion, i.e., in a single metal ion system, and q_{eq} (mmol/g) represents the equilibrium adsorption of a metal ion in a binary system, i.e., with a competing metal ion.

3.3.4 Analytical Methods

All analyses were performed in triplicates and mean ± standard deviation values are presented.

3.3.4.1 Biomass concentration

During the growth of the microalgae, samples were taken on a daily basis to determine biomass concentration by measuring the optical density of culture using a GENESYSTM 10S UV-Vis spectrophotometer (Thermo Fisher Scientific Inc., USA) at wavelength 680 nm. The biomass was then suspended in deionized water for 2 times and centrifuged at 5000 RPM. The washed

biomass was dried overnight in an oven at 80 ℃. Then, the dried biological mass is weighed to get the dry biomass concentration. A standard curve was constructed to relate optical density to biomass concentration.

3.3.4.2 Heavy metal concentration in liquid samples

An iCETM 3300 atomic absorption spectrometer (ThermoFisher Scientific, USA) was used to analyze the heavy metal at a specific wavelength. All samples were determined after mixing with HNO_3 (68%-70%) in order to prevent precipitation and oxidization.

3.3.4.3 Zeta Potential

To measure the zeta potential of cells, Zetasizer nanometers (Malvern Panalytical, UK) were used. Samples were diluted 6 times using deionized water before testing [97].

3.3.4.4 FTIR Spectroscopy

The infrared spectra of cells without or with adsorption of heavy metals were analyzed. The microalgae were filtered with a 0.45 um membrane filter, dried at room temperature overnight, and then subjected to analysis using a Cary 630 FTIR spectrophotometer (Angellent technology, USA).

3.3.4.5 SEM-EDS

Scanning Electron Microscope (SEM) and Energy Dispersive X-Ray Spectroscopy (EDX) were used to study the morphology of microalgae before and after biosorption and presence of metals on the surface of microalgae, respectively. Algal sample (2ml) with or without being subjected to adsorption tests was mixed with 2.5% glutaraldehyde fixative solution and the coated sample was then soaked in 0.1 M phosphate buffered saline (PBS) for 48h. The coated sample was rinsed three times by soaking with 0.1 M PBS for 20 min each time, followed by rinsing twice with deionized water with 10 min soaking each time. Afterward, the sample was dehydrated in ethanol

aqueous solutions with incremental concentrations (i.e., 50, 70, 90, 95% and 100%). Finally, the samples were dried by critical point technology, coating with gold, and analysis was carried out with JSM-7500F FESEM (JEOL, USA).

3.3.4.6 Adsorption Isotherms model

In order to determine the maximum adsorption capacity of the sample, the experimental data were fitted to the Langmuir equation, i.e., Eq 3.7 [98].

$$q_{eq} = \frac{q_{max} K_L C_{eq}}{1 + K_L C_{eq}} \quad 3.7$$

Where q_{max} is adsorption capacity (mmol/g), q_{eq} the amount of metal ions adsorbed to the cell surface at equilibrium (mg/g), K_L (mg/g) the affinity coefficient of the metal ions.

For Langmuir adsorption, R_L [99] is a dimensionless separation factor defined by Equation 3.8, which is a constant measuring the favourability of adsorption.

$$R_L = \frac{1}{1 + K_L C_i} \quad 3.8$$

The Freundlich isotherm model (Equation 3.9) was also used to fit the experimental data, where $K_F(mmol^{1-\frac{1}{n}} g^{-1} L^{\frac{1}{n}})$ and n are empirical constants [100].

$$q_{eq} = K_F C_{eq}^{\frac{1}{n}} \quad 3.9$$

In order to determine the efficiency of adsorption, Equation 3.10 was used to calculate the % removal:

$$\text{Removal \%} = \frac{C_i - C_{eq}}{C_i} \; x \; 100\% \quad 3.10$$

Where C_i represents the initial concentration of heavy metal (mmol/L) and C_{eq} the concentration of heavy metal at equilibrium (mmol/L) in liquid phase.

3.4 Results and discussion

3.4.1 Characterization of biosorbents

FTIR spectra of algal biomass and algae loaded with Pb(II), Hg(II), Zn(II), Cd(II) and Cu(II) are shown in Figure 3-1. The functional groups responsible for the biosorption of heavy metal ions on *N. oleoabundans* unicellular cells were confirmed by FTIR spectroscopy, which are listed in Table 3-1.

Peaks at 1617, 1653 and 1740 cm^{-1} are caused by the stretching vibration of C=O bond in carboxyl group, which could be found in amino acids, lipids, proteins, and carbohydrates [101]. The bands at approximately 1008, 1076, 1240 cm^{-1} correspond to the P=O bond in phosphate group, which is a functional group of nucleic acids, phospholipids, phosphoprotein, and phosphosaccharides etc. Peaks at 2924 and 1149 cm^{-1} respectively represent the stretching vibration of C-H and C-O-C, which can be found in dextran functional groups on the cell wall of algae [99]. The peak at 1339 cm^{-1} is caused by the S=O group, which could be found in sulfonyl and sulfonamide groups [102].

There were significant shift of peaks at around 1008, 1339 and 1617 cm^{-1}, which correspond to P=O and C=O bonds, respectively, before and after the adsorption of all the five different heavy metal ions [103]. The common element in these three bonds is oxygen, which is partially negatively charged due to its relatively large electronegativity in comparison to that of P, S, and C. Carboxyl and phosphate are the most common functional groups containing P=O and C=O bonds that are abundant in cell walls [87]. These groups have a double-tooth complex structure and are especially suitable for ionic binding.

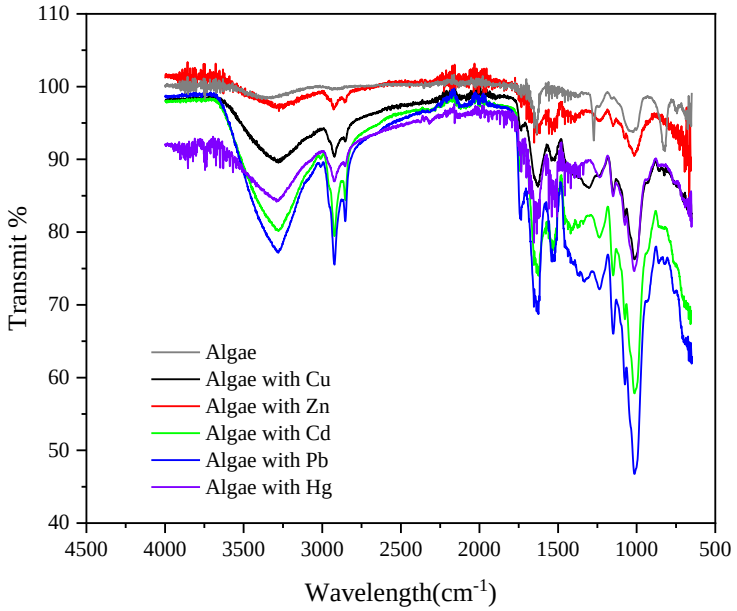

Figure 3-1 FTIR spectra of *N. oleoabundans* and loaded with Pb(II), Hg(II), Zn(II), Cd(II) and Cu(II).

Table 3-1 FTIR peaks of *N. oeloabundans* cells before and after adsorption of heavy metal ions.

Wavelength(cm^{-1})						Functional groups
Pristine Biomass	Pb-loaded	Cd-loaded	Hg-loaded	Zn-loaded	Cu-Loaded	
1008.705	1013.833	1014.572	1016.977	1016.08	1013.855	P=O(Phospholipids, carbohydrates of nucleic acids)
1076.24	1074.914	1075.303	\	1074.455	\	P=O(Phospholipids, carbohydrates of nucleic acids)
1149.311	1149.156	1149.954	1150.609	1150.941	1149.831	C–O–C(Carbohydrates as polysaccharides)
1240.256	1236.859	1237.092	1236.699	1236.825	1244.492	P=O(phosphate ester)
1339.912	1331.834	1340.164	\	\	1303.941	S=O (sulfonyl)
1542.223	1540.578	1540.473	1539.814	\	\	C–N (amide)
1617.137	1624.669	1628.06	\	\	1628.019	C=O(proteins)
1653.39	\	\	1653.306	\	\	C=O (typical amide)
1740.043	\	1740.821	\	\	1737.008	C=O (Lipids and carbonyl groups)
2923.227	2922.324	2923.026	2926.28	2857.411	2925.234	C–H (Unsaturated lipid structures)

3.4.2 Biosorption kinetics

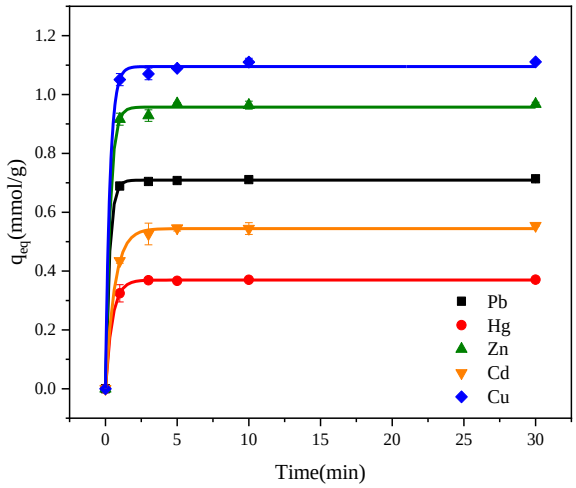

Figure 3-2 Biosorption kinetics of Pb(II), Hg(II), Zn(II), Cd(II) and Cu(II) over time using *N. oleoabundans* biomass at initial metal concentration of 50 ppm, pH 6.5 and biomass concentration 0.3 g/L.

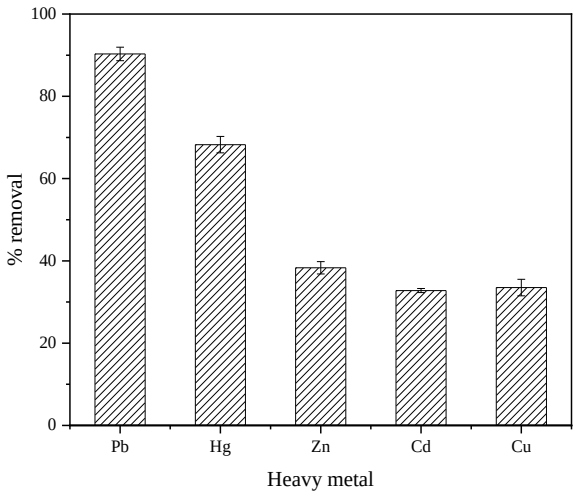

Figure 3-3 % removal of different metal ions in single-metal-ion aqueous solution of 50 ppm metal ions with 0.3 g DCW/L *N. oleoabundans* biomass at pH 7.0, 25 ℃ and 30 min. Mean values of triplets reported with standard deviations (n=3).

Figure 3-2 shows the results of the kinetics of metal ion adsorption at 50 ppm initial concentration of Pb(II), Hg(II), Zn(II), Cd(II), or Cu(II) by 0.3 g/L algal biomass. The adsorption reached plateau within 5 min for all the tested heavy metal ions. The fast kinetics suggests that metal ions were adsorbed onto the surface of the algal cells rather than absorption into cells. For the positively charged heavy metal ions to pass through the cytoplasmic membrane, energy-dependant positive transportation mechanisms through ion channels must be utilized [104], which would be a process much slower than what was observed in this study.

As shown in Figure 3-3, the % removal of Pb(II), Hg(II), Zn(II), Cu(II) and Cd(II) were 90.29%, 68.25%, 38.32%, 32.78% and 33.51%, respectively, when 50 ppm metal ions were added. The q_{eq} (mmol/g) were 0.714, 0.371, 0.968, 0.544 and 1.107 mmol/g for Pb(II), Hg(II), Zn(II), Cd(II) and Cu(II), respectively.

3.4.3 Biosorption isotherm

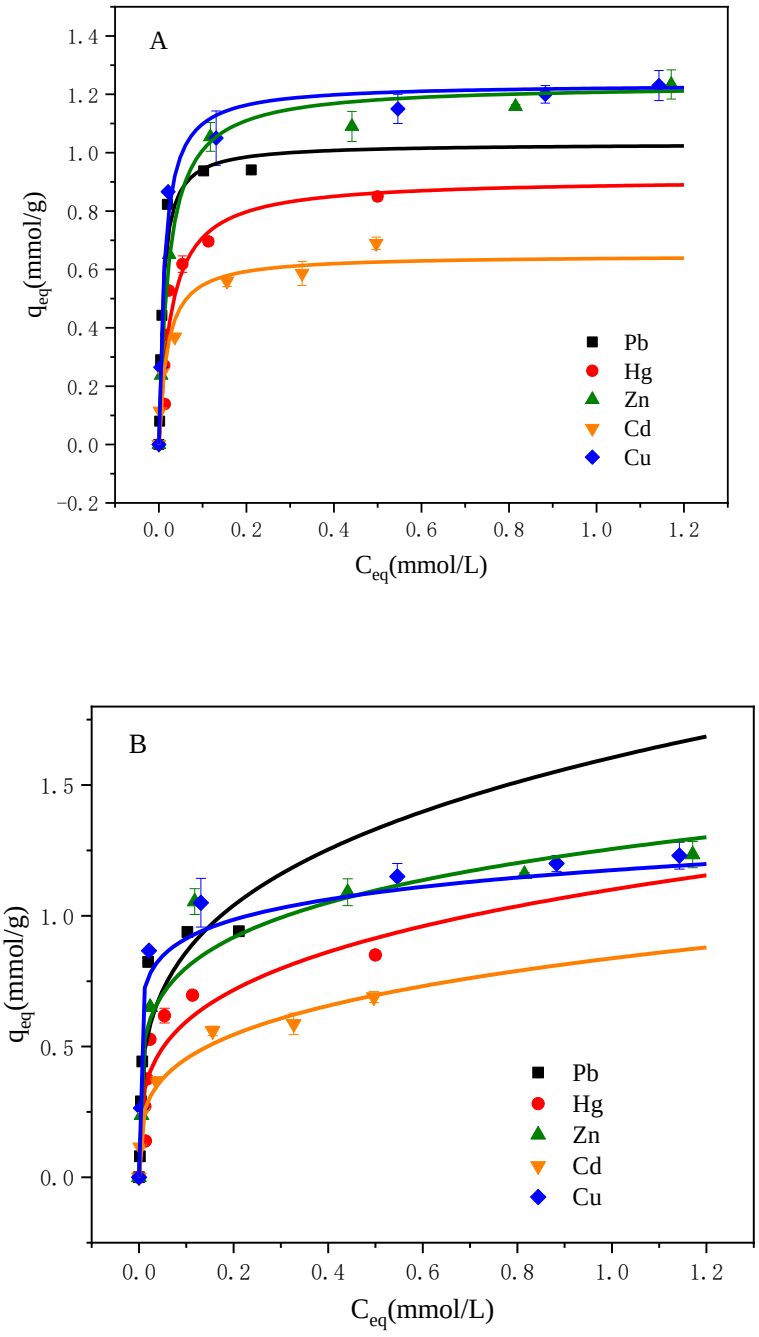

Figure 3-4 Isotherms of Pb(II), Hg(II), Zn(II), Cd(II) and Cu(II) adsorption using *N. oleoabundans* biomass by Langmuir model (A) and Freundlich model (B).

Table 3-2 Langmuir and Freundlich constants related to the biosorption isotherms of heavy metal ions by *N. oleoabundans* biomass.

	Langmuir					Freundlich	
Metal	q_{max}(mmol/g)	K_L(L/mmol)	R^2	R_L	K_F $(mmol^{1-\frac{1}{n}}g^{-1}L^{\frac{1}{n}})$	N	R^2
Pb(II)	1.03	107.53	0.9673	0.019-0.278	1.605	3.706	0.8476
Hg(II)	0.91	35.13	0.8954	0.054-0.533	1.100	3.751	0.8496
Zn(II)	1.20	44.76	0.9703	0.015-0.226	1.255	5.136	0.9255
Cd(II)	0.65	53.00	0.9833	0.021-0.297	0.838	3.751	0.9698
Cu(II)	1.23	118.34	0.9872	0.044-0.477	1.174	7.148	0.8745

The isotherms of Pb(II), Hg(II), Zn(II), Cd(II) and Cu(II) adsorption *by N. oleoabundans* biomass were established at 25 ℃ and pH7.0. The Langmuir (Figure 3-4A) and Freundlich (Figure 3-4B) models were fitted with experimental data using the nonlinear fitting tool in Origin. The isothermal parameters and R^2 obtained from the isotherm model are listed in Table 3-2. The results elucidated that the Langmuir model was better fitted than the Freundlich model with all the tested metal ions. Furthermore, the parameters of Langmuir model have well defined physical meanings. We will therefore use these parameters in the following discussions.

The favourability of a Langmuir adsorption can be characterized by R_L, which is defined by Equation 3.5. As shown in Table 3-2, all R_L was in the range from 0 to 1, implying the adsorption to be favorable. It's worthy to find that the adsorption capacity (mmol/g) of the tested metal ions follows the order of Cu (1.23) > Zn (1.20) > Pb (1.03) > Hg (0.91) > Cd (0.65). The equilibrium constant, K_L (L/mmol), which characterizes the adsorption affinity of the metal ion to the cell surface, shows the order of Cu (118.34) > Pb (107.53) > Cd (53.00) > Zn (44.76) > Hg (35.13).

3.4.4 Effects of the electronegativity and radius of metal ion on adsorption capacity

Table 3-3 Electronegativity (E), ion radius (r),, and impact factor (*I*) of different metal ions and their adsorption capacity (q_{max}(mmol/g)) on to different microalgae [105].

Metal	*E*	*r* (pm)	*I* (pm^{-1})	*N. oleoabundans*	*Sargassum sp.*		*C. vermilara*	*S. insignis*	*A. armata*	*Kappaphycus sp.*
					pH5	pH4				
Pb^{2+}	2.33	119	0.01958	1.03	1.16	1	0.3	0.25	0.31	0.107
Hg^{2+}	2	102	0.01961	0.91	\	\	\	\	\	\
Zn^{2+}	1.65	74	0.02230	1.2	\	\	0.36	0.32	0.33	0.248
Cd^{2+}	1.69	95	0.01779	0.65	0.76	0.8	0.19	0.2	0.29	\
Cu^{2+}	1.95	73	0.02671	1.23	0.99	0.92	0.27	0.30	0.33	0.307
Ref				This study	[65]	[65]	[62]	[62]	[62]	[66]

Table 3-3 summarizes the adsorption capacities of *N. oleoabundans* on the five heavy metal ions tested in this study, i.e., Pb(II), Hg(II), Zn(II), Cd(II), and Cu(II), and that of five algae, i.e., *Codium vermilara*, *Spirogyra insignis* and *Asparagpsis armata* [62], *Sargassum sp.* [65], and *Kappaphycus sp.* [66], on different metal ions. As shown in Table 3-3, the adsorption capacity of a given alga to the metal ion of larger radius was smaller when the comparison was made within metal pairs of similar electronegativities, i.e., Cd(II) (1.69) vs Zn(II) (1.65) or Hg(II) (2.00) vs Cu(II) (1.95). On the other hand, the adsorption capacity was larger for the metal ion of larger electronegativity when the comparison was made within metal pairs of similar ion sizes but of different electronegativities. For instance, the ion size of Hg(II) (102 pm) is similar to that of Cd(II) (95 pm) and the electronegativity of Hg(II) (2.00) is much larger (18.3%) than that of Cd(II) (1.69). As expected, the adsorption capacity of *N. oleoabundans* biomass on Hg(II) (0.91 mmol/g) was larger than that on Cd(II) (0.63 mmol/g). Similarly, the ion radius of Cu(II) (73 pm) is very similar to that of Zn(II) (74 pm) but the electronegativity of Cu(II) (1.95) is much larger than that of Zn(II) (1.65) and the adsorption capacity of *Kappaphycus sp*. on Cu(II), which is

0.307 mmol/g, was much larger than on Zn(II), which was 0.248 mmol/g. Significantly larger adsorption capacities on Cu(II) than on Zn(II) were reported by other researchers as well [35,63].

However, it should be noted that the adsorption capacity of *N. oleoabundans* on Cu(II) (1.23 mmol/g) was not significantly larger than that on Zn(II) ($p>0.05$) in this study. We observed that Cu(II) in the tested concentration range caused severe aggregation of *N. oleoabundans* cells while other metal ions did not (Figure 3-5).

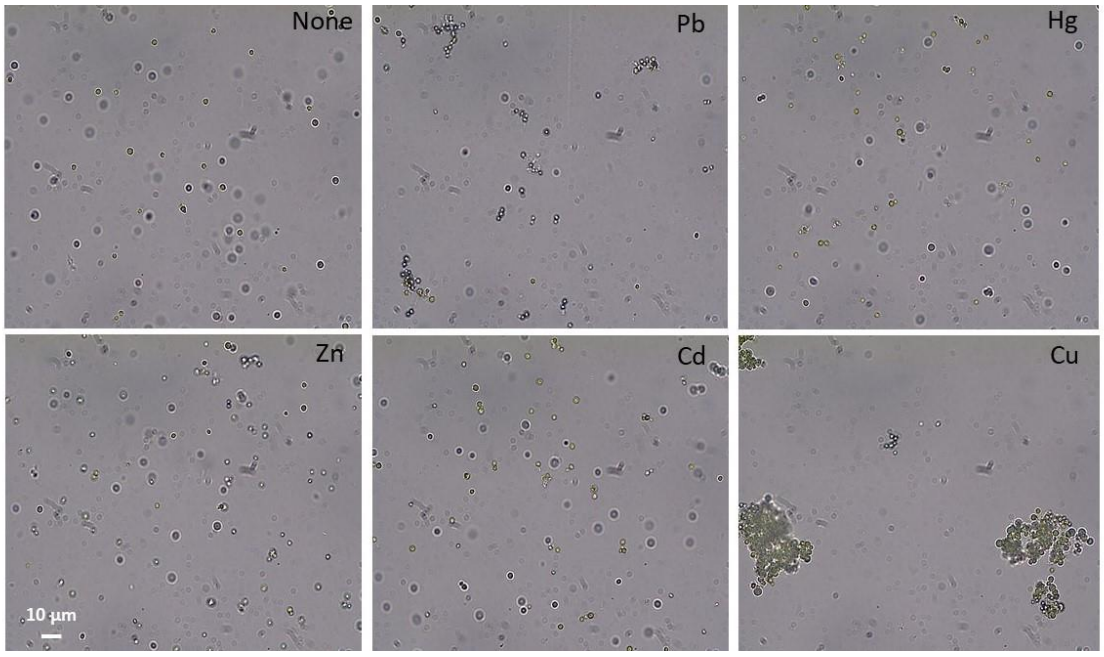

Figure 3-5 Micrographs of algal cells in culture samples containing 50 ppm of different metal ions (×200 magnification).

Formation of cell aggregates of microalgae in response to chemical (e.g., high DIC) and biological stresses (e.g., protozoa) during cell growth has been reported with other algae [106,107]. However, the aggregation of cells observed with the addition of Cu(II) in this study was unlikely a cellular response to metabolic stress since the cells were washed three times with deionized water and the cell aggregates were formed instantaneously after the addition of Cu(II).

The formation of aggregates would reduce the efficiency of mixing and mass transfer, as well as cell surface areas for the adsorption of metal ions, which could tentatively explain the "abnormal" observation that the adsorption capacity of alga on the more electronegative Cu(II) was not significantly higher than that of the less electronegative ion Zn(II). As also shown in Table 3-3, similar or even slightly smaller adsorption capacities on Cu(II) than on Zn(II) were reported by some researchers as well, although no cell aggregation was reported.

3.4.5 Definition and effects of impact factor on adsorption capacity

To further elucidate the effects of electronegativity and ion radius on adsorption capacity, a new parameter, i.e., impact factor *I*, is defined in this paper as the electronegativity of a metal ion normalized by its radius (Eq 3.11).

$$I = E/r \qquad 3.11$$

Figure 3-6 depicts the dependence of the adsorption capacity on the impact factor of heavy metal ions using the data presented in Table 3-3. Linear relationship was established between the adsorption capacity and the impact factor of metal ions, when the data of Cu(II) was excluded except for *Kappaphycus sp.*, for which the adsorption capacities on all the three metal ions tested in the study, i.e., Pb(II), Zn(II), and Cu(II), were included in the linear regression. The linear equations and the R^2 values of the regressions are listed in Table 3-4. It is of interest to note that 6 out of 7 Cu(II) adsorption capacity values presented in Table 3-3, which were excluded from the regression of the corresponding sets of data, followed the same pattern, i.e., they are all substantially smaller than the value predicted by the corresponding linear equation. It should also be noted that there are other literature data that do not fit the proposed linear relationship between the adsorption capacity and the impact factor of metal ions. Hypothetically, other factors could

have affected the adsorption capacity, just like the cell aggregation caused by the addition of Cu(II) as observed in this study, which were not noticed or were noticed but not reported.

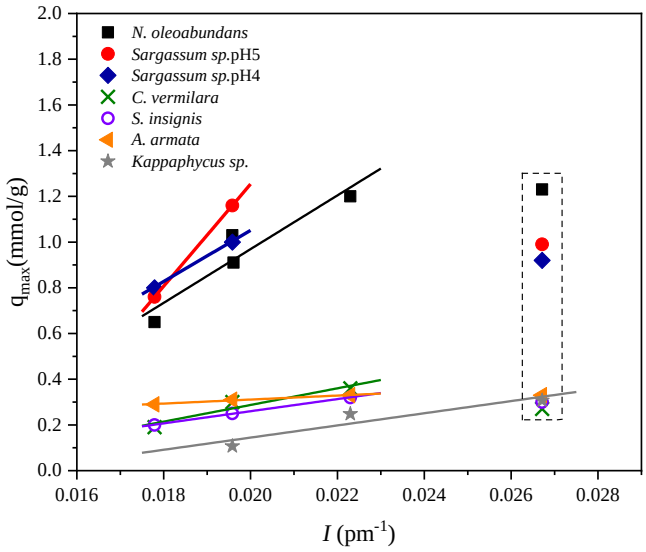

Figure 3-6 Linear relation between the impactor factor (I = E/r) of heavy metal ions, i.e., Pb(II), Hg(II), Zn(II) and Cd(II) and their adsorption capacity on four algal biomasses. (Data points in the dotted frame were derived from adsorption capacities of Cu(II).

Table 3-4 Linear relationship of adsorption capacity and impact factor of different heavy metal ions.

Bisorbent		Linear equation	R^2	Reference
N. oleoabundans		q_{max}=117.51I - 1.381	0.894	This study
Sargassum sp.	pH5	q_{max} = 223.42I - 3.214	1	[15]
	pH4	q_{max} = 111.71I - 1.183	1	
C. vermilara		q_{max} = 36.44I - 0.441	0.9202	
S. insignis		q_{max} = 26.55I - 0.271	0.9995	[12]
Asparagpsis armata		q_{max} = 8.75I + 0.136	0.9861	
Kappaphycus sp.		q_{max} = 26.63I - 0.388	0.9202	[16]

3.4.6 SEM and EDS

Figures 3-7 presents the surface morphology of cells before and after adsorption of Pb(II), Hg(II), Zn(II), Cd(II) and Cu(II). The pristine cells (Figure 3-7A) were near-spherical with smooth surface while the adsorption of different heavy metals caused the cells to deform in different manners and cell surfaces became rough with visible particles evenly distributed on them (Figure 3-7 B-F). EDX spectra of pristine algal cells and that after adsorbing different metal ions are shown in Figure 8. The peaks of elements C, O, Cl, Na, and K appeared in these spectra because they are common and abundant on cell surfaces. Au was used for fixation of cells. The peaks of heavy metal ions, which are at 10.55, 9.98, 8.63, 3.13 and 8.04 keV for Pb, Hg, Zn, Cd and Cu, respectively, were identified on cell surface subjected to adsorption of corresponding metal ions. As shown in Figure 3-7.F, the cells exposed to 200 mg/L Cu(II) had the most severe deformation with several cells stuck together. The highly irregular surface of the Cu(II)-treated cells might have contributed to the formation of cell aggregates shown in Figure 3-5.

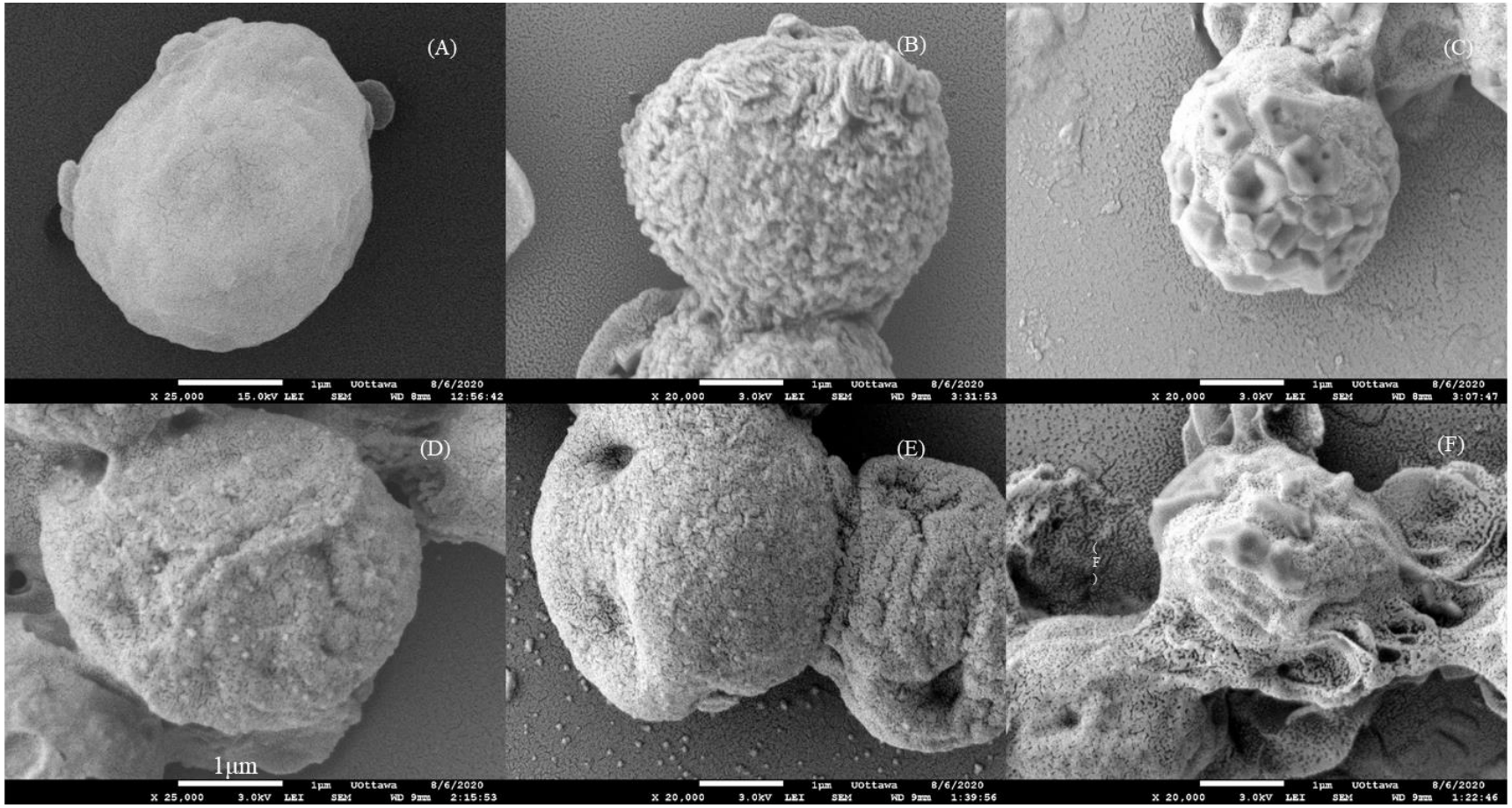

Figure 3-7 SEM micrographs of *N. oleoabundans* after incubating with: deionized water (A); and 200 mg/L Pb(II) (B); 200 mg/L Hg(II) (C); 200 mg/L Zn(II) (D); 200 mg/L Cd(II) (E); and 200 mg/L Cu(II) (F).

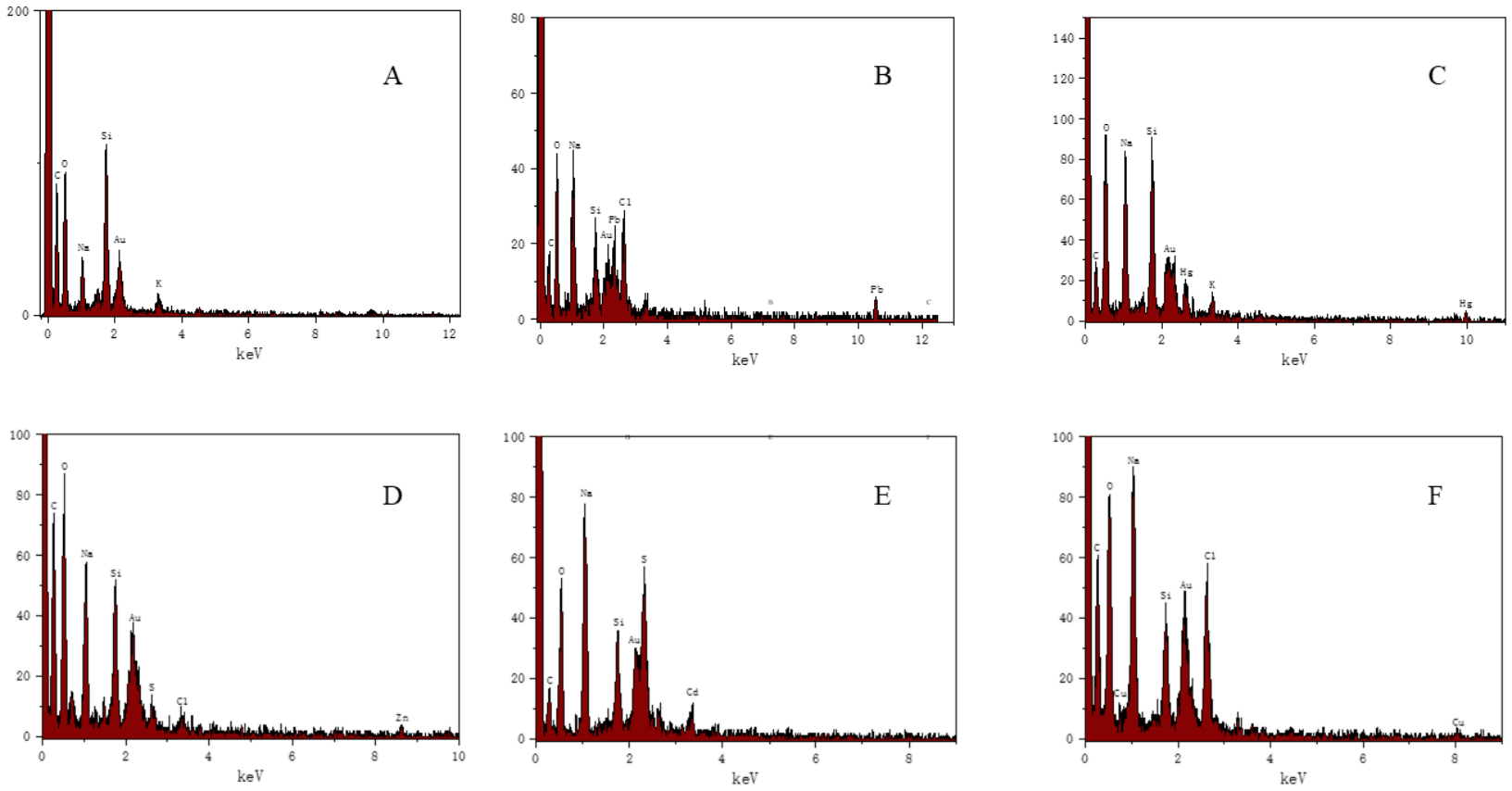

Figure 3-8 EDX analysis of the microalgal biomass: (A) before biosorption; (B) after Pb(II) biosorption; (C) after Hg(II) biosorption; (D) after Zn(II) biosorption; (E) after Cd(II) biosorption; (F) after Cu(II) biosorption.

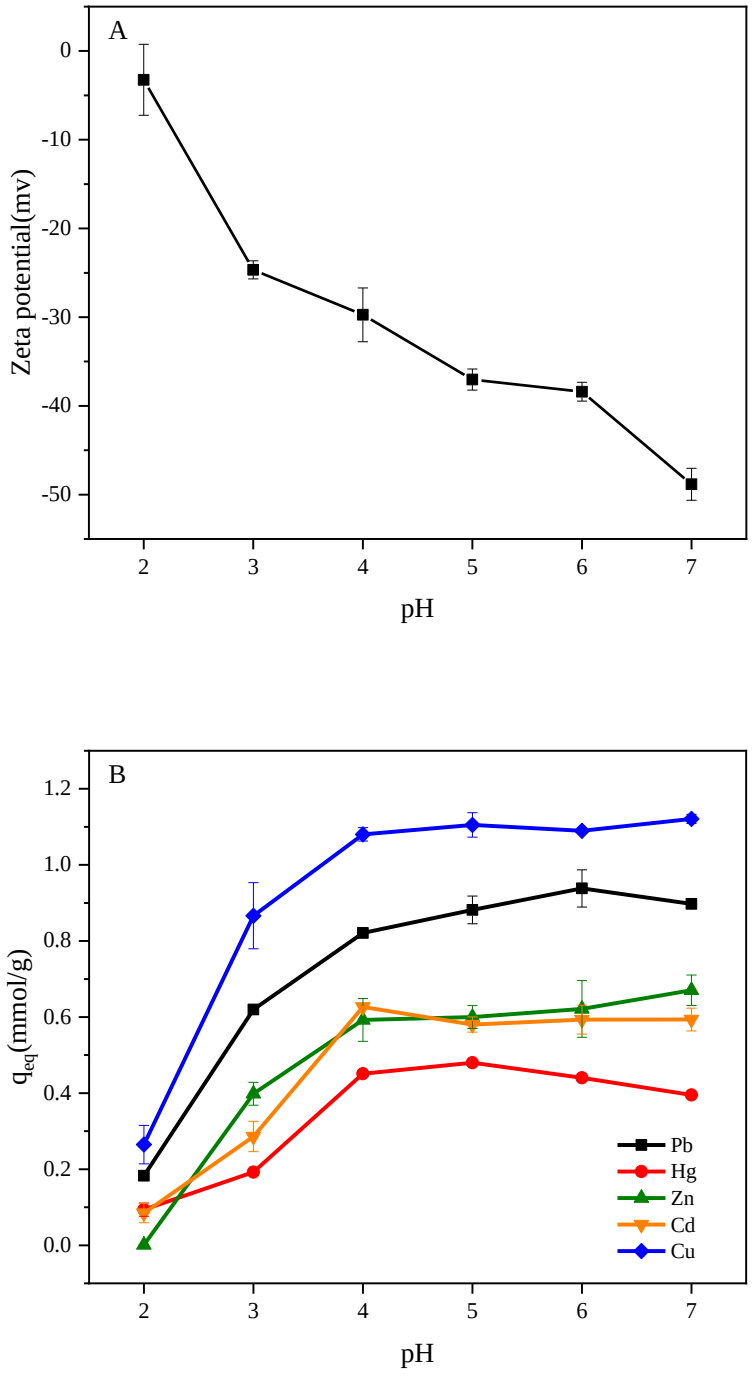

Figure 3-9 The zeta potential (A) and equilibrium adsorption (B) of Pb(II), Hg(II), Zn(II), Cd(II) and Cu(II) on *N. oleoabundans* in pH range 2.0-7.0 with initial metal concentration of 50 ppm and biomass dosage 0.30 g/L.

There is no doubt that solution pH, as an important parameter, plays a crucial role in the adsorption process of different heavy metals since it has important effects on the surface charge, functional group dissociation, adsorption chemical reaction of adsorbents. As shown in Figure 3-9A, the absolute value of the negative zeta potential of cells increased with the pH of cell suspension, which was -3.2 mv at pH 2 and -49.5 mv at pH 7. This is reasonable since the proton concentration would affect the ionization degree of ionizable groups on cell surface.

The effects of pH on biosorption of the five heavy metal ions were tested in the range of pH 2-7 at with 50 mg/L aqueous solutions and the results are shown in Figure 3-9B. The equilibrium adsorption (q_{eq}) of Pb(II), Hg(II), Zn(II), Cd(II) and Cu(II) increased 4.22, 4.33, 669.00, 6.14, 3.31 times, respectively, when pH increased from 2.0 to 7.0. This is reasonable because at low pH, proton concentration is high and the extent of ionization of functional groups was low, which is reflected by the small zeta potential at low pH (Figure 3-9A). As pH increases, ionization of functional groups would increase as well, providing more binding sites for metal ions. In other words, at low pH, high concentration protons would compete with metal ions for binding site on ligands [108]. Nevertheless, the increase of adsorption capacity occurred mostly when pH increased from 2 to 4. Indeed, the equilibrium adsorption increased only slightly despite the significant increase of the negative zeta potential in the pH range of 4 to 7.

It has been estabolished that functional groups such as amino group (-NH_2), carboxyl group(-COOH), carboxyl group(-NH_2), hydroxyl group(-OH) are the primary groups attributing to the charges of cell surfaces [109]. Of particular relevance, Rashidi and Trindade [110] studied the morphology and biochemical compostion of the cell wall of *N. oleoabundans*, observing hair like structures on the cell wall surface, which might house the adsorption sites. They further reported

that the cell wall composed of 31.56% proteins, 24.3% polysacchradies, 22% lipids, 7.8% inorganics (e.g., phosphate), and 14.4% other molecules with the major constituent monomers listed in Table 3-5. As can be seen from Table 3-5, the pKa1 of the constituent monomers of polysaccharides, proteins, and lipids have a large variety ranging from -1.9 of glucosamine to 15.28 of 5-methyl-3-hexanol. The fact that the effects of pH to adsorption was significant between pH 2 and 4 but was very mild between pH 4 and 7 suggests that the residues of constituent monomers with pKa1 in the range of pH2-4 are likely the primary sites of adsorption. These monomers include amino acids, which are commonly found in proteins (31.5% of cell wall dry weight) and hybrid macromolecules such as peptidoglycan and peptidolipids. Glucosamine (pKa1=-1.9), galacturonic acid (pKa1=3.24) and glucuronic acid (pKa1=3.21), which are monomers of non-cellulosic polysaccharides, peptidoglycans, and lipoglycans, also have pKa1 in the acidic range. Worth mentioning is that glucuronic acid and glucosamine are indeed abundant in the non-cellulosic polysaccharides of the *N. oleoabundans* cell walls according to Rashidi and Trindade [110].

Table 3-5 Components of *N. oleoabundans* cell wall and pKa1 of their constituent monomers [110].

Components of cell wall	Content	Constituent Monomers	pKa_1
Polysaccharides	24.30%	Rhamnose	11.3
		Arabinose	11.31
		Glucosamine	-1.9
		Galactose	11.3
		Glucose	12
		Mannose	12.26
		Xylose	12.34
		Galacturonic acid	3.24
		Glucuronic acid	3.21
Proteins	31.5%	Alanine	2.34
		Aspartic acid	1.88
		Cysteine	1.96
		Glutamic acid	1.96
		Glycine	2.34
		Histidine	1.82
		Isoleucine	2.36
		Leucine	2.36
		Lysine	2.18
		Phenylalanine	1.83
		Proline	1.99
		Serine	2.21
		Threonine	2.09
		Tryptophan	2.83
		Tyrosine	2.2
		Valine	2.32
Lipids		Tetrahydro-2,5-dimethyl-2H-	14.38

		pyranmethanol	
		5-methyl-3-Hexanol	15.28
		1,3-di-tert-butylbenzene	10.87
	22%	2,4-di-tert-butylphenol	11.72
		Palmitic acid	4.75
		Stearic acid	4.95
		Cis-10-Nonadecenoic acid	5.02
		10,13-Octadecadiynoic acid, methyl ester	4.77
Inorganics	7.8%	Phosphoric acid	2.16
Others	14.4%		

3.4.7 Thermodynamics of adsorption

Table 3-6 Summary of thermodynamic parameters of *N. oleoabundans*.

			ΔG^o (kJ/mol)		
Ion	ΔS^o (J/mol/K)	ΔH^o (kJ/mol)	303.15K	313.15K	323.15K
Pb(II)	105.13	16.63	-47.97	-49.02	-50.07
Hg(II)	82.67	12.08	-12.56	-13.39	-14.22
Zn(II)	35.74	3.78	-6.88	-7.24	-7.60
Cd(II)	26.88	3.06	-11.07	-11.34	-11.61
Cu(II)	85.58	21.48	-4.03	-4.89	-5.74

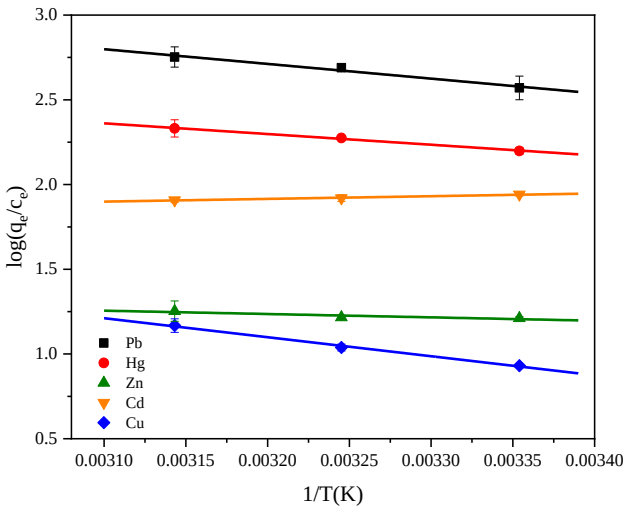

Figure 3-10 Van't Hoff plots of Pb(II), Hg(II), Zn(II), Cd(II) and Cu(II) biosorption.

Adsorption studies were carried out at different temperatures in the range of 303.15 ~ 323.15 K with 50 mg/L initial concentration of individual metal ions and the results are depicted in Figure 3-10 as $\log(q_e/C_e)$ vs 1/T linear curves. The equilibrium adsorption capacity of all metals increased with temperature. This could be due to (a) the decrease of the pKa of the organic acids with temperature; (b) the increased affinity of the adsorbent to the surface of the adsorbent, and/or (c) the increased driving force to overcome the mass transfer resistance [111]. The standard enthalpy change (ΔH^o, kJ/mol) of adsorption was determined according to the Y-intercept and the standard entropy change ΔS^o (kJ/mol/K) according to the slope of the linear curve in Figure 3-10. The standard Gibbs energy change of adsorption (ΔG^o, kJ/mol) at different temperature was determined using Eq 3.5. The thermodynamic parameters are listed in Table 3-6. The negative ΔG^o and positive ΔS^o indicate that the adsorption process was spontaneous [112]. And ΔH^o was positive and therefore the adsorption was endothermic, which is in accordance with the results of other researchers [94,113].

3.4.8 Binary metal system

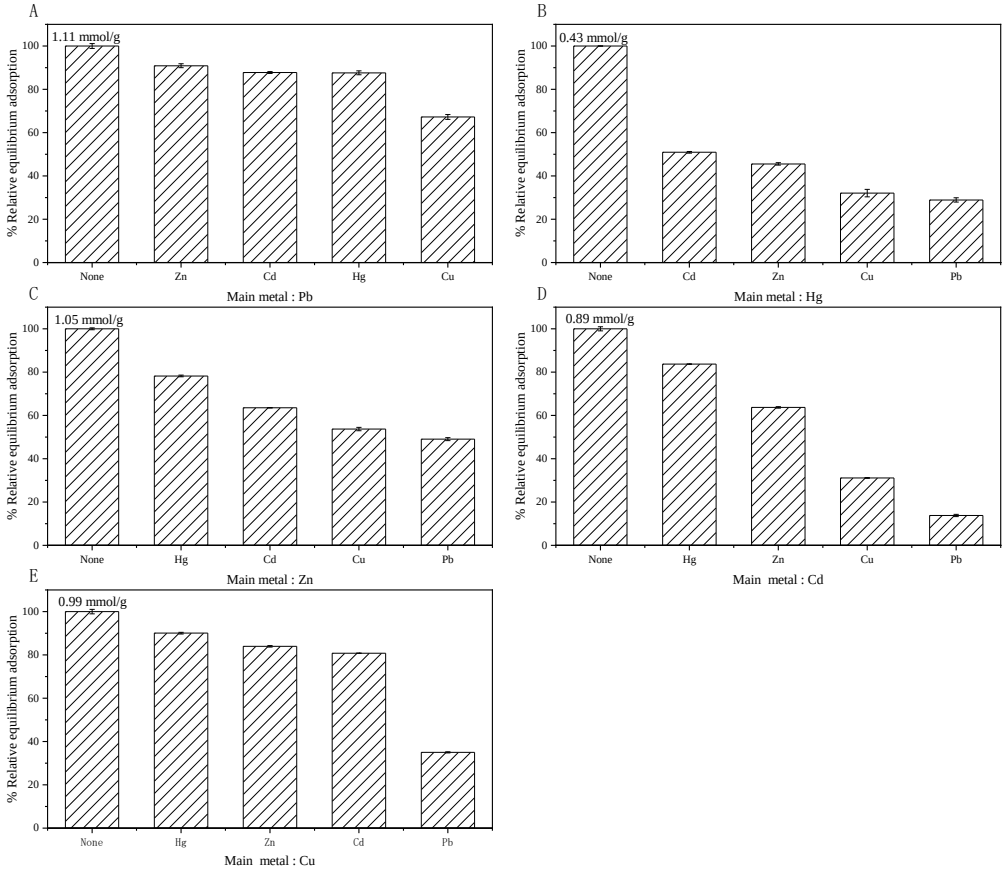

Figure 3-11 Adsorption of binary systems: the relative equilibrium adsorption (REA) at initial 0.5 mmol of both metal ions at pH7.0, room temperature (25 ℃) and 0.3 g/L biomass dosage.

Competitive adsorption was carried out in equimolar binary systems to evaluate the relative equilibrium adsorption (%REA), which is defined as the ratio of the equilibrium adsorption of a metal ion under the competition of another metal ion in a binary system over that of the same metal ion in a single-ion system. In binary system, the existence of another ion always resulted in reduction of equilibrium adsorption and therefore a REA of less than 100%. As can be seen from Figure 3-11, Pb(II), Cd(II), Hg(II), Zn(II) and Cu(II) all have a competitive relationship against each other. The lowest REA of Pb(II), Cd(II), Hg(II), Zn(II) and Cu(II) were 77.23%, 28.89%, 49.41%, 13.83%, 35.01%, respectively, which were registered with Pb(II) as the competing ion

except for Pb(II), which had the lowest REA with Cu(II) as the competing ion. It is also evident that Pb(II) and Cu(II), which have the largest values of K_L of 107.53 and 118.34 L/mmol, respectively (Table 3-3), are the two ions least sensitive to inhibition of other ions and also the two most effective ion in inhibiting the adsorption of other ions. On the other hand, Hg(II), which had the smallest K_L among all the ions (35.15 L/mmol), was sensitive to the inhibition of all other ions. As an illustrative example, the inhibition of other ions on the adsorption of Cd(II), which is reflected by the decrease of REA, increased with the K_L (L/mmol) of the competing ion in the order of Pb(II)(107.53)> Cu(II)(118.34)> Zn(II)(44.76)> Hg(II)(35.13). These results are reasonable since large K_L value correspond to high affinity of metal ions to the adsorbent, which were in this study the algal cells. It should be pointed out that the *KL* value of Cu(II) was larger than that of Pb(II) while its inhibitive effects to other ions is weaker than Pb(II). This irregularity might be linked to the fact that Cu(II) caused cell aggregation in binary systems as well.

These results are also in accordance with literature data. For instance, one research showed that the inhibitive effect of Cu(II) in binary mixtures to the adsorption of Co(II) by brown algae *Cystoseira indica* was enormous [112]. Sun et al. [114] studied the adsorption of Pb(II) and Cd(II) by *Spirulina platensis*, confirming that the inhibition of Cd(II) adsorption by Pb(II) was greater than the inhibition of Pb(II) adsorption by Cd(II) in the binary systems of the two.

3.5 Conclusions

In this study, the adsorption capacity and affinity of microalgae *Neochloris oleoabundans* to Pb(II), Hg(II), Zn(II), Cd(II) and Cu(II) in aqueous solution were investigated. Removing heavy metal can be notably influenced by biomass dosage, pH value, contact time and ion concentration. Linear relationship was established between the adsorption capacity and the impact factor of a metal ion, except for Cu(II), which caused cell aggregation and thus reduced the apparent adsorption capacity. According to SEM and EDS detection, heavy metal adsorption occurred on the cell surface and observed the Langmuir model. Each metal could inhibit adsorption capacity of another metal ion in a binary system and Pb(II) had the greatest inhibitive effect, corresponding to its largest affinity in a single metal ion system except Cu(II). The biosorption of Pb(II), Hg(II), Zn(II) Cd(II) and Cu(II) was endothermic, spontaneous and energy-independent.

3.6 Acknowledgment

Financial support of Natural Science and Engineering Research Council Canada (NSERC) to Dr. Christopher Q. Lan in the form of a Discovery Grant (RGPIN 03657) is gratefully acknowledged.

Chapter 4 Effects of culture pH, dissolved inorganic carbon concentration, phosphate concentration and nitrate concentration, on cell surface properties and biosorption of HMIs by green alga *Neochloris oleoabundans*

4.1 Effects of culture pH on cell surface properties and biosorption of Pb(II), Cd(II), Zn(II) of green alga *Neochloris oleoabundans*[1]

Siwei Gu & Christopher Q. Lan*

Department of Chemical and Biological Engineering

University of Ottawa

* Chrisotpher.Lan@Uottawa.ca

[1] The content of this paper was published and the detail: Gu, S. et Lan, C. Q. (2023). Effects of culture pH on cell surface properties and biosorption of Pb(II), Cd(II), Zn(II) of green alga *Neochloris oleoabundans*. Chemical Engineering Journal, 468(May), 143579.

Highlight

- Culture pH have strong influence on cell surface properties and metal ion adsorption capacity.
- -COOH, likely functional group for heavy metal removal, most abundant on cell surface at culture pH 9.5.
- Monolayer biosorption confirmed by the rapid kinetics and Sips isotherm.
- Linear increase of adsorption capacity with impact factor of metal ions confirmed.
- Two valence metal has larger inhibition on biosorption capacity than single valence metal.

4.1.1 Abstract

Microalgal biomass has been established as a promising approach for heavy metal removal from contaminated waters. In this study, the effects of culture pH, i.e., 7.5, 8.5, 9.5 on the cell surface properties of green alga *Neochloris oleoabundans* and the adsorption of three selected heavy metal ions, i.e., Pb(II), Cd(II) and Zn(II), using biomasses such prepared, i.e., B-7.5, B-8.5, and B-9.5, were investigated. The fast adsorption kinetics (plateau achieved within 5 minutes) in combination of the *ns* values of the Sips isotherm, indicating the adsorption was monolayer surface adsorption. Based on the Sips model, which best fits the experimental data among the three tested isotherm models, the three heavy metal biosorption capacities follows the order: B-9.5>B-8.5> B-7.5. The algal biomass obtained at culture pH 9.5, i.e., B-9.5, exhibits the highest biosorption capacities of Pb(II), Cd(II), and Zn(II) at pH 6.0, which are 100.01, 43.92, and 32.43 mg/g, respectively, corresponding to 3.0, 3.3, and 2.3 folds of the adsorption capacity to the same metal ions by biomass B-7.5. According to the FTIR spectra, the possible functional groups for biosorption include C-N, P=O, C-OH and COOH. The X-ray photoelectron spectroscopy (XPS) analysis of the biomasses revealed that a higher concentration of carboxylic acid (COOH) groups on the B-9.5 cell surface than that on the B-7.5 and B-8.5 cell surfaces, which might be responsible for the much higher biosorption capacity of heavy metal ions by B-9.5.

Key words: Biosorption, culture pH, *Neochloris oleoabundans*, Heavy metal

4.1.2 Introduction

Heavy metal contamination is a growing global issue that poses a significant threat to both human health and the environment. Heavy metals (HMs) are non-degradable, and as a result, they may accumulate at high levels through the process of bio-amplification, especially in aquatic ecosystems where there are only small traces of heavy metals [115]. Moreover, they can infiltrate the human body through food chain, leading to various adverse health effects, such as headaches, joint pain, and liver and kidney malfunction, as well as teratogenicity and cancers [116,117]. Specifically, Pb and Cd are exceptionally toxic to humans, while Zn has a relatively high level of toxicity but only at higher concentrations. The maximum contaminant limits (MCL) are set for Pb, Cd, and Zn as 15, 5, 5000 ppb by the US Environmental Protection Agency (EPA) and 10, 3, 3000 ppb according to the World Health Organization (WHO), respectively [5,6]. While a significant fraction of HMs precipitate from the waterbody over an extended period, the presence of heavy metals in sediment remains persistent and could re-enter the waterbody, causing level of HMs in contaminated waterbodies exceeding the drinking water standards in several countries if not treated properly [118]. Hence, a novel method for removing heavy metals from contaminated aquatic ecosystem, which is typically characterized by large water volumes and low HMs levels, is needed.

It has been known that microalgae can provide valuable metabolic products, such as phytoerythrin, proteins (e.g., phycocyanin), exopolysaccharides and lipids, which can be isolated from the culture biomass. *Neochloris oleoabundans,* a microalga with many uses, has recently gained much attention due to high lipid content [119]. As a spherical cells of the eukaryotic, green alga *N. oleoabundans* have a thin and smooth cell wall, single nucleus, parietal and cup-like chloroplasts, two elongate pyrenoids, ovoid zoospores with two elongate flagella and

diameter that varies between 3 and 6 um [120]. When cultivating in photobioreactor, it has been shown that microalga grows rapidly, which has a doubling time of about 1 day [121]. Further, it can grow on different kinds of media containing wastewater, in extreme conditions including pH 9.5 and 32 ℃, and tolerates toxic compounds like terpenes [96,122,123]. *N. oleoabundans* can be served as a biofuel feedstock, exhibiting a lipid content ranging from 3-34% of its dry weight under favorable growth conditions, but can surge up to 54% under unfavorable growth conditions with a dominant composition of triacylglycerols (TAGs) [96,124].

The biosorption of heavy metal ions by microalgal biomass is primarily facilitated by ion exchange occurring on the surface of the algal cell, which may involve various functional groups on the macromolecules on cell surface (i.e., the cell wall), such as OH, COOH, PO_4, C-N, etc. Microalgae are capable of adsorbing heavy metals from wastewater even when present in low concentrations. This is achieved through the functional groups on the surface of the microalgal biomass, which can bind to heavy metal ions, resulting in a final effluent that meets drinking water standards [125]. It should be noted that even when the same microalgal species is utilized as a biosorbent for the same heavy metal ion, there can be a substantial variation in the biosorption capacity. This indicates that other factors beyond the microalgal species may play a role in determining the effectiveness of the biosorption process. Indeed, studies have shown that the medium composition, e.g., dissolved inorganic carbon [43] and phosphate [126] have profound effects on cell surface properties and metal ion adsorption. Nevertheless, even when the same strain of green alga *Chlorella vulgaris* was cultivated in the same medium, significantly different biosorption capacities of Cd(II) were reported in two papers, ranging from 11.06 to 97.43 mg/g [108,127]. These data support that other cultivation factors could affect the capacity of algal biomass for HM adsorption. Form Li, the biosorption of Pb(II) can be affected by the

timing of biomass harvesting, and that the most effective biosorption capacity is observed during the stable phase as opposed to the exponential and dead phases [128]. This phenomenon may be attributed to the pH level during cultivation, which tends to increase as cultivation time.

The pH of the growth environment is one of the most important parameters influencing microalgal growth [96,129,130]. Studies have shown that cells of larger negative zeta potential tend to have greater biosorption capacity [14,43,94]. Interestingly, studies have shown that the zeta potentials of three microalgae, namely freshwater *Chlorella sp*., marine *Chlorella sp*., and marine *N. oculata,* become more negative when cultivated under higher medium pH [131]. The pH of the medium can also impact the biochemical composition of the cell wall, including C-(C,H), C-(O,N), C=O, O=C-OH. Alkaline conditions in the medium can have a significant effect on the cell wall composition, which in turn affects the biosorption of heavy metal ions [132]. However, to date, no research has examined the influence of medium pH on heavy metal ion biosorption by microalgal biomass.

This research provides a comprehensive analysis of the influence of culture-pH on the cell surface properties and the biosorption of Pb(II), Cd(II), and Zn(II) of *N. oleoabundans*. Various adsorption conditions such as initial ion concentration, pH, and contact time were examined to investigate the isotherm and kinetic behavior of the biosorption. Furthermore, some binary systems were investigated to assess the inhibitory effects of competitive metal ions. To our best knowledge, this study is the first of its kind to thoroughly examine the impact of culture-pH on heavy metal biosorption of microalgae, providing valuable insights into the field.

4.1.3 Materials and methods

4.1.3.1 Microalgal cultivation under different pH

A microalgal culture, *Neochloris oleoabundans* (UTEX 1185), was collected from the University of Texas microalgal collection. Algae were maintained in autoclaved Modified Bristol Medium (MBM), a medium suitable for freshwater microalgae. The chemical composition of medium was used in the previous paper [133]. This study involved growing microalgae in a 3-L photobioreactor (Bioflo 110, New Brunswick), which was converted from a stirred tank. Around the bioreactor chamber, spectrum lamps were arranged evenly and were programmed to operate continuously for 12 hours with light intensity of 2000 μmol/(m^2s) (Philips Plant & Aquarium T18/15, Philips Electronics Ltd. ON, Canada). Photobioreactor with fresh medium containing 2 liters was sterilized for 20 minutes at 121 ℃ before inoculation. Then, sterilized medium was inoculated with 30mL of microalgal seeds after it had cooled to room temperature to achieve 0.05 g/L initial biomass. After that, the cultivation took place at 25 ℃, 180 RPM, with a constant air flow of 1 LPM (i.e., 0.5 vvm). Additional, computer-programmed gas mixers (CO_2 and Air) maintained a constant pH of 7.5, 8.5, and 9.5 for the cultures, separately. After passing through a bottle containing distilled water, the air stream was filtered through a 0.45 um microfilter and then sparged into the culture at the bottom of the photobioreactor. Microalgae were grown for two weeks under various pH (7.5, 8.5, 9.5) to reach transition phase (cell density of $6*10^7$ cells per mL), and biomass was harvested and stored at -80 ℃ for future use. During different pH cultivation, harvested biomass under pH 7.5, 8.5, 9.5 were referred to as B-7.5, B-8.5, or B-9.5 in the following discussion.

4.1.3.2 Biosorbent preparation

Upon retrieval from the freezer, the frozen B-7.5, B-8.5, and B-9.5 biomasses were allowed to thaw at room temperature. Then, 40 mL of the thawed wet biomass was transferred to a 50 mL centrifugal tube and subjected to three rounds of washing using deionized water to eliminate any residual chemical substances and fragments present in the solution. The wet sample was then re-suspended in deionized water to prepare for the biosorption test.

4.1.3.3 Heavy metal stock solution

Lead stock solution (1000 mg/L), cadmium stock solution (1000 mg/L) and Zinc stock solution (1000 mg/L) were prepared by dissolving appropriate amount of $Pb(NO_3)_2$ (Strem Chemicals Inc., USA), $Cd(NO_3)_2$ (Fisher Scientific, USA) and $Zn(NO_3)_2$ (Fisher Scientific, USA) into deionized water using 100 mL volumetric flask. Afterward, the stock solution was stored in a 200 mL white plastic bottle at room temperature. All of the chemical reagents used in this study were of analytical grade. Sodium stock solution (20000 mg/L), potassium stock solution (20000 mg/L), calcium stock solution (20000 mg/L) were prepared by $NaNO_3$ (Fisher Scientific, USA), KNO_3 (Fisher Scientific, USA) and $Ca(NO_3)_2$ (Fisher Scientific, USA). All stock solutions were kept under room temperature.

4.1.3.4 Biosorption test

4.1.3.4.1 Effect of pH

The selection of appropriate acids, bases, or buffers for pH adjustment should be based on the properties of the metal ions involved. For instance, acids such as H_2SO_4, HCl, and HNO_3 may be used to adjust the pH as needed. Due to the fact that formation of $PbSO_4$, $PbCl_2$ precipitates, acid, such as H_2SO_4 or HCl, is not recommended to adjust pH in the biosorption of lead. In this study, pH was adjusted by HNO_3 and NaOH, which is soluble under pH 7.0. Batch biosorption experiment was carried out in a 2 mL graduated microcentrifuge tube using 1.5 mL B-7.5, B-8.5,

B-9.5 biomass, and Pb(II), Cd(II), Zn(II) stock solution were added into tube to ensure 50 mg/L Pb(II), Cd(II), Zn(II) and 0.5 g/L biomass under 25 ℃. The initial pH of the mixture was adjusted to 6.0 by adding 0.1 N HNO_3 prior to the addition of biomass. After that, the mixture was shaken at 200 RPM shaker for 10 mins contact time as specified in the text at room temperature (25 ℃). Afterwards, the sample was centrifuged for 1.5 minutes at 13000 rpm (18500 rcf). The concentration of residual Pb(II) or Cd(II) in the supernatant were extracted and determined using FAAS. The detail is shown in previous paper [14].

4.1.3.4.2 Effect of contact time

Predicting how fast heavy metals will be removed from aqueous solutions is crucial before designing an adsorption plant. To study the effect of contact time on the adsorption removal of Pb(II), Cd(II) and Zn(II), experiments were conducted under room temperature (25 ℃). The experiments of biosorption kinetics were carried out in a 15 mL glass tube. For each experiment, 10 mL of algal biomass solution at 0.5 g/L concentrations was continuously stirred at 200 rpm with 50 mg/L heavy metal ion. 1 mL sample was withdrawn at appropriate time intervals (5, 10, 15, 20, 25, 30 mins) and then centrifuged under 13000 rpm (18500 rcf) for 1.5 min. Then, 0.5 mL of solution at supernatant was determined using FAAS.

4.1.3.4.3 Effect of initial heavy metal concentration

In the present study, the biosorption of Pb(II), Cd(II) and Zn(II) by algal biomass were carried out in a batch system, which is a simple and reliable method for experimentation. 1.5 mL algal solution (0.5 g/L) in 2 mL centrifugal tube was agitated in a rotary shaker at 200 rpm and 25 ℃ and 10-mins incubation time with various initial heavy metal concentration (0-200 mg/L). Then, samples were then centrifuged in 13000 rpm (18500 rcf) for 1.5 min to separate the remaining heavy metal ion from biomass. 0.5 mL of solution at supernatant was determined using FAAS.

4.1.3.4.4 Effect of binary system

The experiments were carried out in binary systems, with a constant B-9.5 algal biomass concentration of 0.5 g/L, and varying concentrations of two other positive metal ions: Na(I), K(I), Ca(II), Pb(II), Cd(II), or Zn(II). The initial concentration of heavy metal ions, either Pb(II), Cd(II), or Zn(II), was kept at 50 mg/L, while the concentration of the other positive metal ion was varied at 25, 50, 100, and 200 mg/L in 2 mL centrifugal tubes. Subsequently, the samples were centrifuged at 13000 rpm (18500 rcf) for 1.5 min to separate the remaining heavy metal ions from the biomass. Finally, 0.5 mL of the supernatant solution was analyzed using FAAS.

4.1.3.4.5 Regeneration test

To assess the potential of microalgal biomass for repeated use, the B-9.5 biomass was subjected to multiple adsorption-desorption-regeneration cycles. In the regeneration process, 0.5 g/L B-9.5 biomass was used to adsorb 50 mg/L of initial heavy metal concentration in a 15 mL centrifugal tube. After incubating at 25℃ and 200 rpm for 10 minutes, the samples were centrifuged at 6000 rpm (8500 rcf) for 5 minutes, and 0.5 mL of the supernatant solution was extracted for heavy metal analysis. To desorb the heavy metal ions from the microalgal biomass, 0.1 M HNO_3 was added to the sample at pH 2.0 and allowed to incubate for 20 minutes. This acid was selected based on prior experiments as an effective eluent for heavy metal ions from microalgal biomass. After centrifuging and washing the samples twice with deionized water, 0.1 M NaOH was added to achieve a pH of 6.0 before the next biosorption test. The biosorption-desorption-regeneration cycle was repeated five times, and the experimental results were reported as arithmetic means with standard deviations (error bars in graphs).

The equilibrium biosorption capacity and heavy metal removal% by algae were calculated by using Eq. 4.1 and 4.2, which shows below:

$$q = \frac{C_0 - C}{x} \quad (4.1)$$

$$Removal\% = \frac{C_0 - C}{C_0} \times 100\% \quad (4.2)$$

where C_0 (mg/L) is the initial concentration of heavy metal solution, C (mg/L) the final heavy metal concentration in supernatant, x (g DCW/L) the concentration of algal biomass, q (mg/g DCW), the mass of heavy metal adsorbed by unit biomass mass, and %removal efficiency of Pb(II), Cd(II), Zn(II).

4.1.3.5 Analysis and characterization

4.1.3.5.1 Microalgal biomass

In the range of 450 to 700 nm, the concentration of dry biomass in microalgae has a direct correlation with optical density (OD). However, the photosynthetic pigments such as chlorophylls a and b, carotenoid and phycocyanin, have absorption peaks in the spectrum between 400-680 nm, where chlorophyll a has a peak at 660 nm [134]. To eliminate the interference of photosynthetic pigments, the spectrometric measurement of biomass concentration was performed at a wavelength of 700 nm. The optical density was measured using a GENESYS 10S UV-VIS spectrophotometer from Thermo Fisher Scientific Inc., USA. The linear correlation between the OD_{700} and biomass concentrations (B-7.5, B-8.5, and B-9.5) was established through Eq 4.3 to 4.5.

$$x_{B-7.5} = 0.4558 \times OD_{700} \ (R^2 = 0.998) \quad (4.3)$$

$$x_{B-8.5} = 0.4213 \times OD_{700} \ (R^2 = 0.999) \quad (4.4)$$

$$x_{B-9.5} = 0.3837 \times OD_{700} \ (R^2 = 0.997) \quad (4.5)$$

where OD_{700} denotes the measure of light absorption at a wavelength of 700 nm, while *x* (g/L) corresponds to the concentration of dried cell weight (DCW).

4.1.3.5.2 Heavy metal concentration

The flame atomic absorption spectrophotometer (Thermo Fisher Scientific, USA) was utilized to measure the concentration of lead and cadmium in solution. However, the spectrophotometer is not suitable for evaluating high lead and cadmium concentrations above 10 mg/L. Therefore, it is necessary to dilute the solution to a certain concentration using deionized water. Subsequently, the supernatant containing Pb(II) or Cd(II) was diluted with deionized water and the concentration was determined using FAAS.

4.1.3.5.3 Zeta potential

To determine the zeta potential of microalgal cells, a Zetasizer nanometer (Malvern Panalytical, UK) was employed. The samples were diluted to 0.1 optical density at 700 nm using deionized water. Then, 1 mL of the sample was placed in a DTS1070 cuvette for the analysis.

4.1.3.5.4 FTIR

The infrared spectra of the microalgal biomass, before and after biosorption of Pb(II) and Cd(II), were examined using a Cary 630 FTIR spectrophotometer (Angellent technology, USA). The microalgal samples were first filtered using a 0.45 μm membrane filter, followed by drying at 60 ℃ overnight and subsequent analysis.

4.1.3.5.5 XPS

The surface properties of microalgae, such as the elemental composition ratio, surface composition, and chemical functional groups, were quantified using X-ray photoelectron spectroscopy (XPS). The X-ray photoelectron spectroscopy (XPS) analysis of dried microalgal samples was performed using an Al X-ray source on a Kratos Axis Nova spectrometer (Kratos

Analytical, Ltd., UK). The samples were placed on an aluminum platen coated with double-sided adhesive Cu tape and kept under high vacuum in the preparation chamber overnight before analysis in the ultra-high vacuum analysis chamber. The XPS data were collected using AlKα radiation at 1486.69 eV with a delay-line detector and referenced to the C1s peak at 284.8 eV. Survey spectra were collected using a pass energy of 160 eV and an energy step size of 1 eV, and the area under each chemical peak was used for peak intensity calculation after calibration with C 1s at 284.8 eV as a blank. Data analysis was performed using CasaXPS software. (Version 2.3.25, Teignmouth, UK).

The dominant components present on the surface of microalgal cells include polysaccharides, proteins, and hydrocarbon compounds, and their composition can be correlated with the elemental ratios of [N/C] and [O/C]. Equations 4.6-4.8 can be applied to calculate the macromolecular composition [135]:

$$\left[\frac{N}{C}\right] = 0.279\left(\frac{C_{PR}}{C}\right) \tag{4.6}$$

$$\left[\frac{O}{C}\right] = 0.325\left(\frac{C_{PR}}{C}\right) + 0.833\left(\frac{C_{PS}}{C}\right) \tag{4.7}$$

$$\left[\frac{C}{C}\right] = \left(\frac{C_{PR}}{C}\right) + \left(\frac{C_{PS}}{C}\right) + \left(\frac{C_{HC}}{C}\right) = 1 \tag{4.8}$$

where [*N/C*], [*O/C*], and [*C/C*] refer to the elemental composition ratios of cell surface. (C_{PR}/C), (C_{PS}/C), (C_{HC}/C) are the ratios of carbon in proteins, polysaccharides and hydrocarbons to the total carbon, respectively.

4.1.4 Result and discussion

4.1.4.1 FTIR

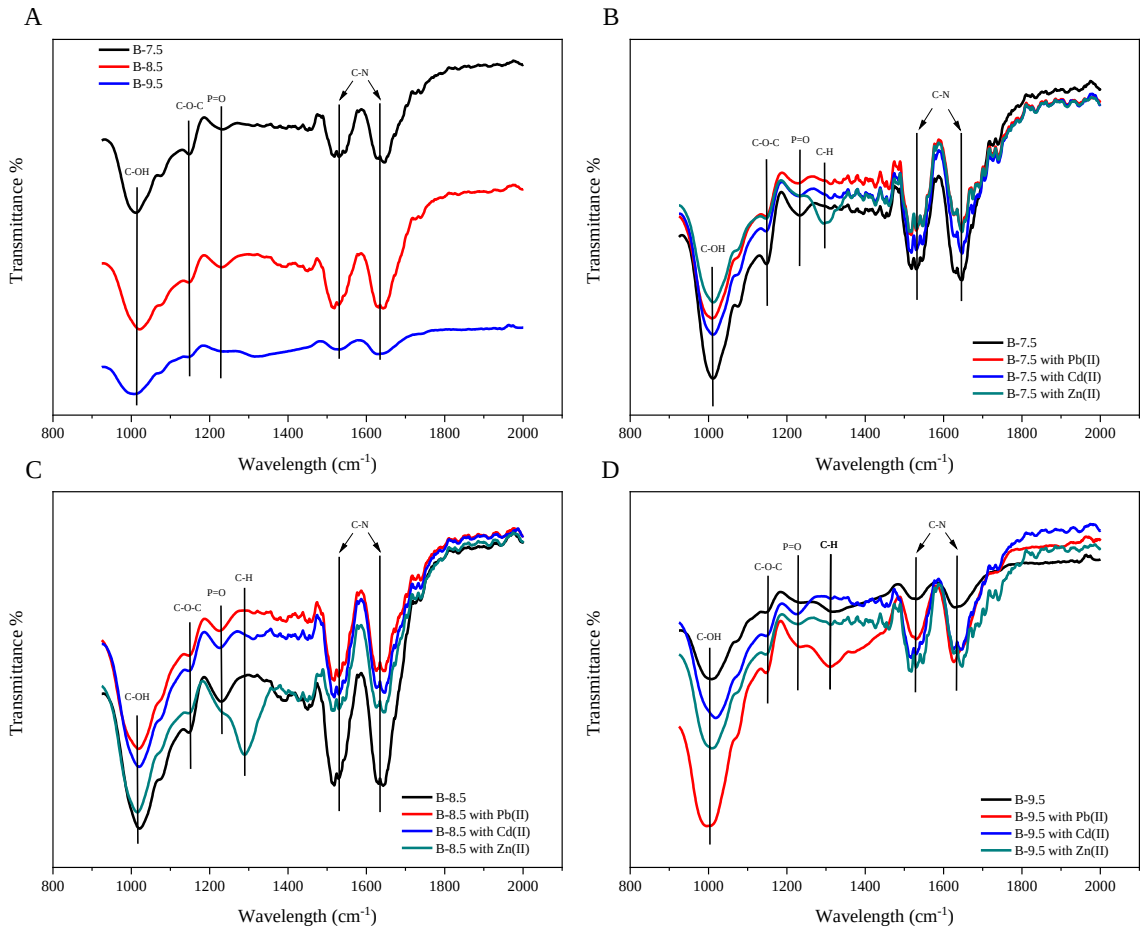

Figure 4-1 FTIR spectra of B-7.5, B-8.5, B-9.5 *N. oleoabundans* biomass (A) and pristine biomass with or without loaded 200 mg/L Pb(II), Cd(II), Zn(II) (B, C, D).

Table 4-1 FTIR peaks of B-7.5, B-8.5, B-9.5 *N. oleoabundans* before and after adsorption of heavy metal ions.

Biomass	Wavelength (cm^{-1})							
B-9.5	1017.26	1147.46	1233.00	1456.73	1506.62	1542.53	1649.15	1728.31
B-9.5 with Pb	1011.74	1148.87	1236.42	1457.41	1506.71	1541.19	1639.89	1725.52
B-9.5 with Cd	1019.83	1164.39	1237.51	1457.23	1506.24	1540.75	1652.47	1735.32
B-9.5 with Zn	1018.10	1156.54	1238.41	1457.23	1506.64	1540.94	1652.58	1734.63
B-8.5	1018.50	1148.90	1229.86	1456.70	1506.80	1542.51	1653.00	1729.23
B-8.5 with Pb	1017.82	1146.46	1221.58	1456.65	1506.64	1541.23	1652.92	1731.12
B-8.5 with Cd	1017.85	1148.31	1256.65	1456.81	1506.60	1540.63	1652.94	1734.32

B-8.5 with Zn	1017.18	1146.84	1287.92	1456.68	1506.54	1541.24	1652.96	1732.43
B-7.5	1015.23	1150.66	1232.69	1456.73	1506.68	1542.10	1653.06	1728.84
B-7.5 with Pb	1015.19	1148.89	1229.70	1456.81	1506.74	1539.56	1652.03	1724.32
B-7.5 with Cd	1017.46	1148.01	1228.24	1456.82	1506.78	1539.36	1652.03	1734.84
B-7.5 with Zn	1015.13	1148.02	1229.36	1456.80	1506.74	1539.74	1652.02	1726.53
Functional group	C-OH	C-O-C	P=O	C-H	CH_2	C-N (amid II)	C-N (amid I)	COOH
Ref.	[136]	[137]	[138]	[139]	[140]	[141]	[141]	[142]

Figure 4-1 shows the FTIR spectra of *C. vulgaris* algae with and without Pb(II), Zn(II), Cd(II) loaded in the range of 2000-900 cm^{-1}. The spectra indicates that several functional groups on *C. vulgaris* cell surfaces, which might facilitate heavy metal adsorption. The peak at 1728 cm^{-1} corresponds to the COOH group, which is abundant in macromolecules such as alginates and peptides. The peaks at 1649 and 1542 cm^{-1} are corresponded to the respective bands of amide I and amide II vibrations of C-N groups, which are related to peptides on cell surface. The absorption peak at 1456 cm^{-1} is caused by bending vibrations in the C-H aliphatic. The peak at 1233 cm^{-1} is corresponding to the phosphodiester of nucleic acids and phospholipids. Peaks at 1147 cm^{-1} are asymmetric C-O-C stretching vibrations, characteristic of ester bonds in protein such as PHA. Peak at 1017 cm^{-1} is caused by the stretching vibrations in the C-OH bond in carboxyl groups, which can be found in amino acids, lipids, proteins, and carbohydrates.

Before and after the biosorption of Pb(II), Cd(II), Zn(II), there were significant shift of peaks around 1729, 1649, 1542, 1233, 1147 and 1017 cm^{-1}, which correspond to COOH, C-N, P=O, C-O-C and C-OH bonds, respectively. Additionally, carboxyl, phosphate and amine are abundant among on cell wall, which can confirm those functional groups are contributed to biosorption. It is important to acknowledge that certain negative functional groups present on the surface of cells, such as COOH, P=O, and O-H, are capable of undergoing ion exchange to facilitate the removal

of positively charged heavy metal ions. Those functional groups, like C-N, P=O, O-H, have double-toothed structures that can make them perfect for ionic bonding. When considering the electronegativities of various functional group elements, such as C (2.55), N (3.04), O (3.44), P (2.19), and H (2.20), it can be observed that oxygen possesses a relatively high electronegativity of 3.44. The presence of a partial negative charge on oxygen atoms within functional groups, i.e., COOH, O-H, P=O, has the ability to adsorb heavy metals by ion exchange.

4.1.4.2 XPS

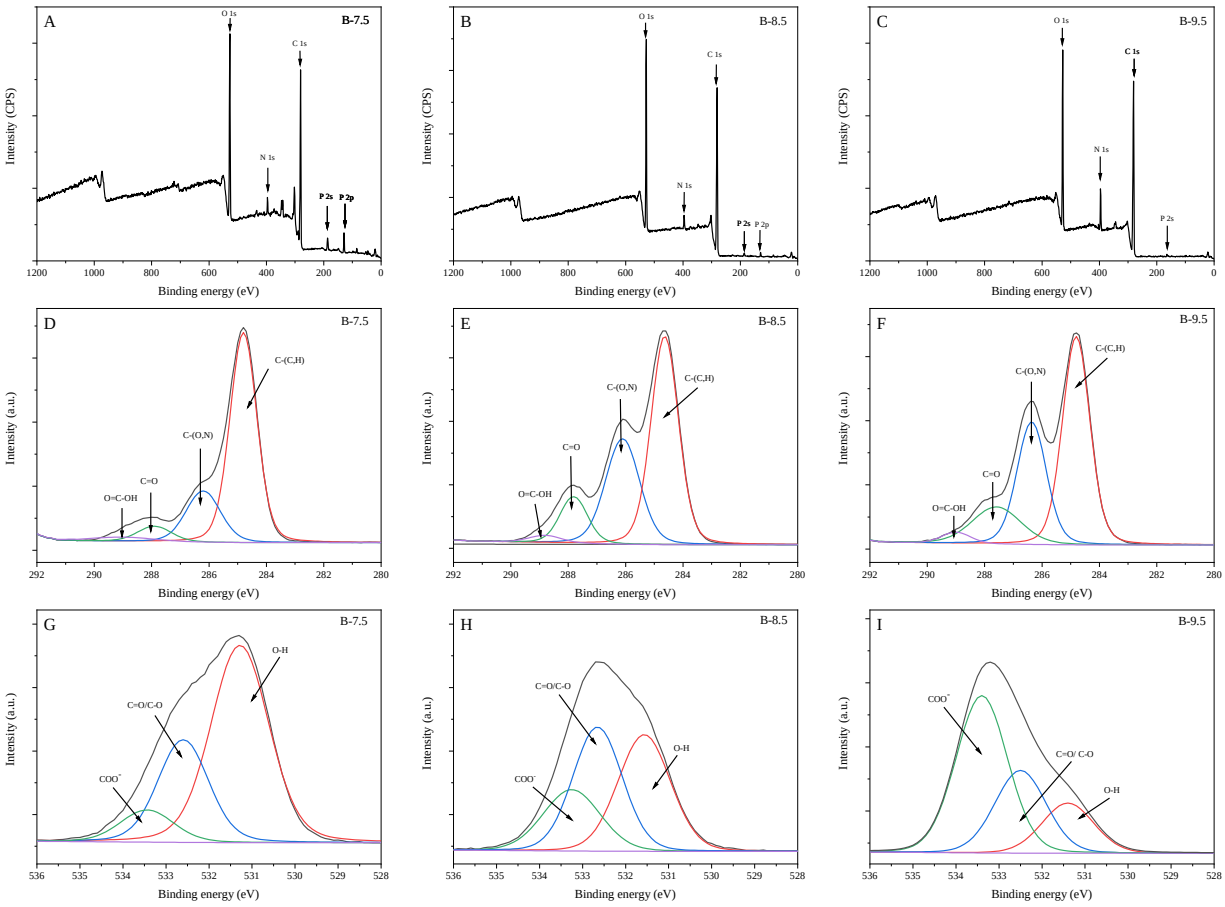

Figure 4-2 XPS whole survey spectrum, C 1s and O 1s peak of microalgal *N. oleoabundans* biomass cultured in different cultivation pH, i.e., pH=7.5 (A, D, G), pH=8.5 (B, E, H), pH=9.5 (C, F, I).

Table 4-2 Effect of medium pH on microalgal surface elemental composition, elemental ratio and surface biochemical composition.

	Elemental composition (weight %)				Elemental ratio (weight%)			Biochemical composition (weight%)		
Biosorbent	C 1s	O 1s	N 1s	P 2p	O/C	N/C	P/C	Polysaccharide	Protein	Lipid
B-7.5	64.73	27.47	2.42	5.38	42.44	3.74	8.31	45.72	13.40	40.88
B-8.5	65.75	28.12	2.35	3.78	42.77	3.57	5.75	46.34	12.81	40.85
B-9.5	71.10	24.86	2.98	1.06	34.96	4.19	1.49	36.11	15.02	48.86

Table 4-3 Composition of Functional groups related with C 1s and O 1s [143–145].

Element	Core-level	Functional groups	*Ea* (eV)	B-7.5	B-8.5	B-9.5
				Weight (%)		
C	1s	C-(C,H)	284.8	68.89	53.53	51.04
		C-(O,N)	286.2	22.56	28.73	34.13
		O-C-O, C=O	287.9	7.64	15.95	12.22
		O=C-OH, O=C-OR	289.0	1.14	1.79	2.62
O	1s	O-H	531.4	62.28	38.80	17.38
		C=O/C-O	532.5	28.35	38.97	54.22
		COO^-	533.4	9.36	22.23	28.40

XPS (X-ray photoelectron spectroscopy) is a valuable tool for investigating the elemental and functional composition of microalgal cell surfaces within a depth of approximately 10 nm. It provides information on the surface chemistry and the binding energy of electrons, enabling the identification of the elemental composition and chemical states of the surface components [146]. Figure 4-2 presents the X-ray photoelectron spectroscopy (XPS) survey spectra image of microalgal cells grown in media with pH values of 7.5, 8.5, and 9.5. Table 4-2 summarizes the elemental composition, elemental ratio, and surface biochemical composition of the microalgal cell surfaces. The main elemental composition of the biomass was determined by analyzing the C 1s, O 1s, N 1s, and P 2p peaks. Notably, the elemental composition of microalgae varies with

changes in the pH of the culture medium, with higher pH values resulting in higher carbon, nitrogen and lower oxygen, phosphorus accumulation on the cell surface. The major macromolecular components on microalgal surfaces are polysaccharides, proteins, and hydrocarbons (lipids). When the culture medium pH was raised from 7.5 to 9.5, there was an increase in protein content of the culture from 13.40% to 15.02%, and lipid content from 40.88% to 48.86%. Conversely, there is a decrease in the polysaccharide content from 45.72% to 36.11%. The protein results are in agreement with that reported by Bartley et al.[130], i.e., increasing medium pH from 6.5 to 8.5 resulted in the increase of protein content of microalga *Chlorella sorokiniana* from 15.5 to 30.7 %.

Table 4-3 displays the results of a deconvolution analysis of the carbon (1s) peak, which revealed four spectral regions. The first region corresponds to aliphatic C-C and C-H bonds (284.8 eV), which serve as carbon skeletons. The second region can be attributed to hydroxyl, ether and amines, only have one bond to oxygen or nitrogen (C-OH, C-N, 286.2 eV). The third region contains carbon with double bonds to oxygen, such as carboxyl and amides (N-C=O, O-C-O, 287.9 eV). Finally, the fourth region contains carboxyl acid or ester functional groups containing three bonds to oxygen (O=C-OH or O=C-OR, 289.0 eV). It was observed that microalgal biomass grown at pH 9.5 has a proportion of aliphatic C-C bonds (51.04%) and C-O or C-N carbons (34.13%) in amides, followed by C=O, O=C-N carbons (12.22 %) and carboxylic carbon (2.62%). Carboxylic carbons occupy a remarkable fraction (2.62 %) of the total carbon composition under medium pH 9.5 compared with pH 7.5 (1.14%) and 8.5 (1.79%).

Based on the microalgal biomass, spectral lines within the range of 531 to 534 eV were assigned and up to three oxygen-containing functional groups were expected, such as hydroxyl, esters, and

carboxyl [145]. In this study, hydroxyl (531.4 eV), esters (532.5 eV), and carboxyl (533.4 eV) groups were detected. According to the data presented in Table 4-3, there was a positive correlation between the cultivation medium pH and the content of carboxyl groups, with an observed increase from 9.36% to 28.40%. It should be noted that the primary functional groups involved in biosorption, like carboxyl groups, have a negative charge to adsorb positive heavy metal ions. Increasing protein content also enhance the biosorption of heavy metal ions. Combining the XPS results of C 1s and O 1s, the B-9.5 biosorbent, which has more protein and carboxyl groups, potentially has a higher biosorption capacity than B-7.5 or B-8.5.

4.1.4.3 Effect of adsorption pH

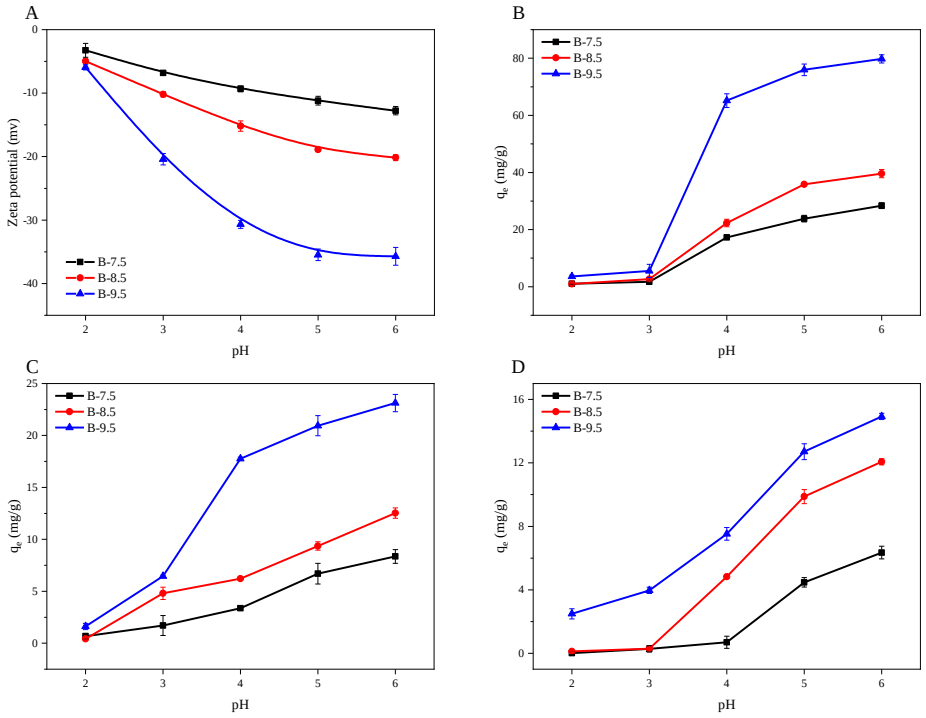

Figure 4-3 Effects of pH on the surface property and HM adsorption of B-7.5, B-8.5, and B-9.5 *N. oleoabundans* biomasses: Zeta potential (A), equilibrium biosorption of Pb(II) (B), equilibrium adsorption of Cd(II) (C), and equilibrium adsorption of Zn(II) (D). (pH range 2.0–6.0, initial metal concentration 50 mg/L, biomass concentration 0.5 g/L, contact time 10 mins, incubation temperature 25 °C).

As shown in Figure 4-3A, the absolute values of the negative zeta potentials of all three biomasses increased with the suspension pH. In the meantime, Figure 4-3B, 4-3C, and 4-3D show that the equilibrium adsorption of all cases increased with the suspension pH in the tested range. These observations are compatible with literature data [147,148] and are not surprising since increase of suspension pH would cause the increase of the extent of functional group deprotonation.

Also shown in Figure 4-3A, when comparison at the same suspension pH, the absolute value of the negative zeta potentials increased with the pH of the culture from which the biomasses were harvested, B-9.5>B-8.5>B-7.5 and the equilibrium biosorption of Pb(II), Cd(II), and Zn(II) ions as shown in Figure 4-3B, 4-3C, and 4-3C, respectively, followed the same order. These observations could be explained by the alteration of the surface properties of microalgal cells as discussed in the previous sections. Among the three biomasses, B-9.5 exhibited the highest equilibrium biosorption of Pb(II), Cd(II), and Zn(II), which were 79.75, 23.12, and 14.92 mg/g at pH 6.0, respectively.

There are two possible mechanisms that may be involved in the process of heavy metal adsorption by microalgae: 1) adsorption of positively charged HM ions onto cell surfaces that contain a range of negative functional groups, such as C-N, P=O, C-O-C, C-OH, and COOH via ion exchange and/or chelating; and 2) the transfer of HM ions into intracellular spaces through ion channels (intracellular), which is a slow and energy consuming process. Results of our previous research indicates that HM ions are primarily adsorbed by algal biomass via extracellular adsorption processes.

N. oleoabundans cell walls have a large number of macromolecules such as polysaccharides, proteins, and lipids that are abundant in carboxyl, hydroxide, amide, and phosphonyl groups. These groups become negatively charged when they are deprotonated at pH that is lower than their corresponding Pka values. The biochemicals with a pKa1 below 7.0 and are abundant on cell surfaces include galacturonic acid (3.24), glucuronic acid (3.86), aspartic acid (3.90), glycine (2.35), histidine (1.80), isoleucine (2.32), palmitic acid (4.95), and stearic acid (4.75). As the pH increases from 2.0-6.0, more and more functional groups begin to deprotonate, allowing for greater adsorption of metal ions and an increase in equilibrium biosorption. FTIR analysis confirmed the presence of these functional groups and their importance for biosorption.

Zeta potential measures the potential difference between the stagnant film attached to the surface of particles in a suspension and that of the dispersion medium and is widely used for quantification of the magnitude of the charge on particle surface. Figure 4-3A shows that the zeta potential of all the three *N. oleoabundans* biomasses, i.e., B-7.5, B-8.5, and B-9.5, increased with pH and, when compared at the same pH, following the order B-9.5>B-8.5>B-7.5. The largest zeta potential values of the three biomasses were observed at pH 6.0, with values of -35.70, -20.17, and -12.77 mV for B-7.5, B-8.5, and B-9.5, respectively. These results are compatible with the afore discussed adsorption data. It is worth mentioning that, at pH 2.0, the equilibrium biosorption values of Pb(II), Cd(II), and Zn(II) were all less than 3.0 mg/g. Regeneration tests can be performed by changing the pH from 6.0 to 2.0. For subsequent experiments, pH 6.0 was chosen as the optimal pH for biosorption.

4.1.4.4 Kinetics

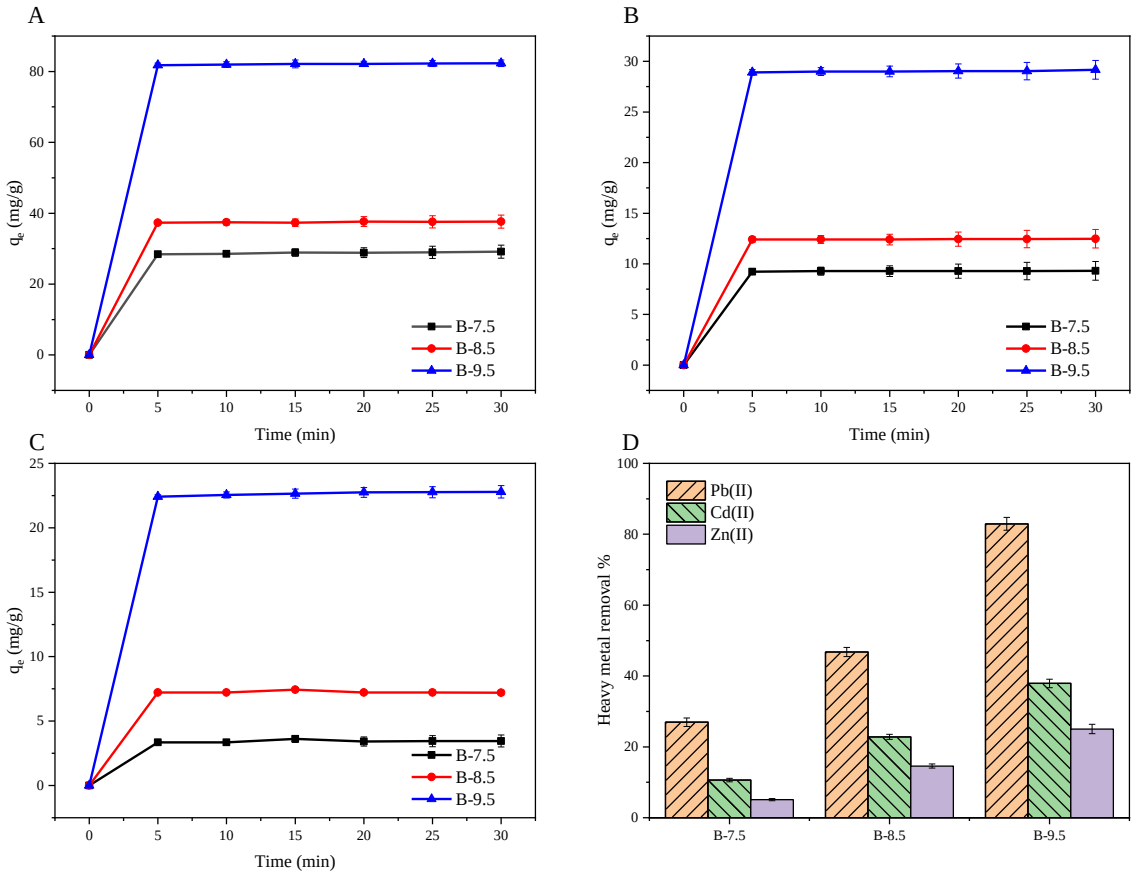

Figure 4-4 Biosorption Kinetics of Pb(II) (A), Cd(II) (B) and Zn(II) (C) by B-7.5, B-8.5, B-9.5 *N. oleoabundans* as a function of time (pH 6.0, 50 mg/L heavy metal concentration, 25 ℃). Mean values of triplets along with standard deviations (the error bars) are reported (n = 3).

The study investigates the kinetics of metal ion biosorption by 0.5 g/L algal biomass B-7.5, B-8.5, and B-9.5 in the presence of 50 mg/L Pb(II), Cd(II), and Zn(II). Figure 4-4 illustrates that the equilibrium biosorption of Pb(II), Cd(II), and Zn(II) by 0.5 g/L algal biomass was rapid, with maximum biosorption achieved within five minutes. Among the three-biomass tested, B-9.5 exhibited the highest equilibrium biosorption at 50 mg/L heavy metal concentration. The data also showed that as the pH of the cultivation medium increased, the equilibrium biosorption capacity of the biomass increased. The rapid adsorption of heavy metals by the biomass suggests

that the surface of biomass being used for adsorption has a high affinity for Pb(II), Cd(II) and Zn(II). At 30 minutes contact time, the maximum biosorption capacity was achieved for all three heavy metals with an efficiency of 26.97%, 10.63%, and 5.11% for B-7.5, 46.79%, 22.81%, and 14.58% for B-8.5, and 82.94%, 37.90%, and 25.04% for B-9.5, respectively.

Wet microalgae have been demonstrated to exhibit rapid kinetics, and other research studies have corroborated that microalgae are capable of reaching equilibrium in a relatively short period. For example, Liyanage et al. reported that live biomass of *Chlorococcum aquaticum* could achieve equilibrium in removing Pb(II) within 30 minutes [149]. Additionally, Zhang et al. noted that the self-flocculating microalga *Scenedesmus obliquus* showed efficient biosorption of cadmium with rapid kinetics, reaching equilibrium within 20 minutes [150]. Consequently, the upcoming experiment will be carried out under five-minute contact time.

4.1.4.5 Isotherm

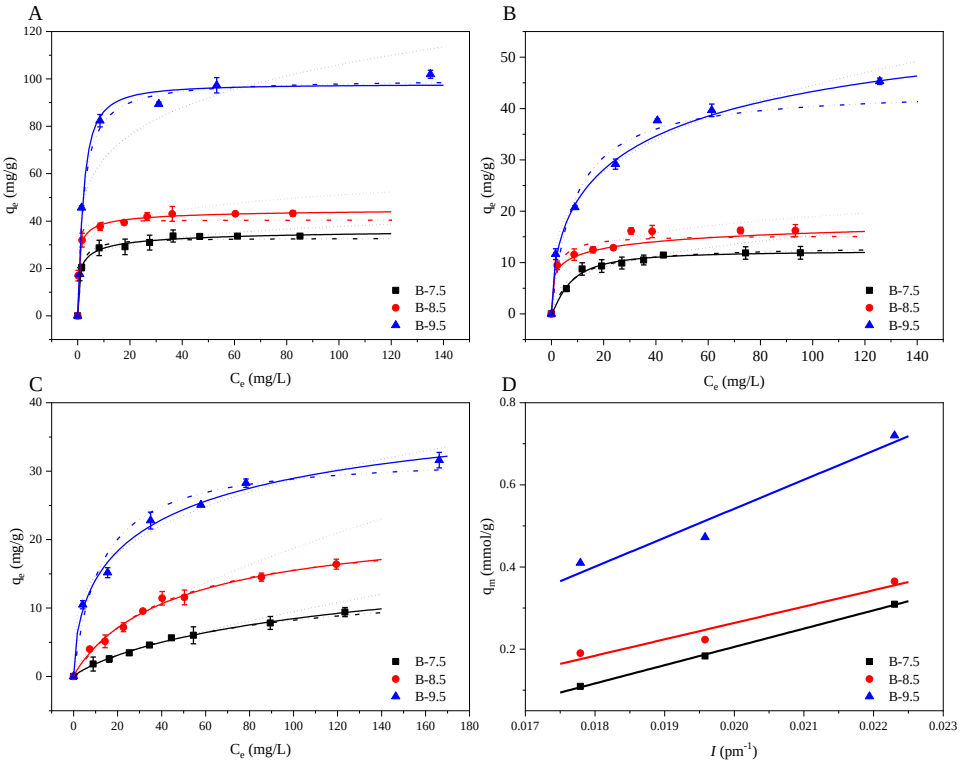

Figure 4-5 Isotherms of Pb(II) (A), Cd(II) (B), Zn(II) (C) biosorption using *N. oleoabundans* biomass by Freundlich model (dot), Langmuir model (dash-dot), Sips model (line) and relationship between impact factor *I* (electronegativity/ ionic radius) and biosorption capacity. 0.5 g/L biomass, 10-200 mg/L heavy metal concentration, pH 6.0 and 25℃. Mean values of triplets along with standard deviations (the error bars) are reported (n = 3).

Table 4-4 Freundlich, Langmuir and Sips model constants for biosorption of Pb(II), Cd(II) and Zn(II) using *N. oleoabundans* biomass.

					Freundlich			Langmuir					Sips		
Metal	Electronegativity	Ion radius (pm)	*I*	Biomass	K_F	N	R^2	q_{mL} (mg/g)	K_L (L/g)	R^2	q_{mS} (mg/g)	q_{mS} (mmol/g)	K_S (L/g)	*ns*	R^2
Pb	2.33	119	0.0196	B-7.5	20.09	7.31	0.9479	32.85	1.02	0.9138	37.93	0.18	0.96	0.50	0.9622
				B-8.5	26.54	7.05	0.9442	40.47	4.13	0.9383	46.22	0.22	1.60	0.52	0.9938
				B-9.5	41.45	4.91	0.8237	100.01	0.45	0.9677	97.85	0.47	0.42	1.24	0.9759
Cd	1.69	95	0.0178	B-7.5	3.41	3.07	0.8894	13.29	0.12	0.9455	12.29	0.11	0.08	1.27	0.9674
				B-8.5	7.58	5.03	0.8778	15.31	0.57	0.8883	22.34	0.20	0.43	0.34	0.9070
				B-9.5	11.44	3.39	0.9714	43.92	0.11	0.9417	46.32	0.41	0.13	0.53	0.9878
Zn	1.65	74	0.0223	B-7.5	0.38	1.43	0.9893	14.06	0.01	0.9870	20.22	0.31	0.01	0.85	0.9958
				B-8.5	1.10	1.62	0.9637	22.06	0.02	0.9641	23.86	0.36	0.03	0.92	0.9881
				B-9.5	7.55	3.45	0.9651	32.43	0.08	0.9471	47.08	0.72	0.12	0.57	0.9855

The Freundlich equation, which is an empirical model for describing sorption on heterogeneous surfaces, postulates that the enthalpy of adsorption decreases in a linear fashion as the fraction of occupied sites increases [151]. Freundlich's equation is based purely on empirical data from sorption on heterogeneous surfaces and can be expressed as Eq. 4.9.

$$q_e = K_F(C_e)^{\frac{1}{n}} \quad 4.9$$

The Freundlich equation involves the K_F constant, which is related to adsorption capacity, while (1/N) is linked to the adsorption intensity. The value of the exponent n determines the favourability of the adsorption process. A good adsorption is indicated by values of N between 2 and 10, whereas moderately difficult adsorption is indicated by values between 1 and 2, and poor adsorption by values less than 1. A Freundlich-type adsorption isotherm suggests surface heterogeneity of the adsorbent, whereas a Langmuir-type isotherm implies surface homogeneity [152].

The Langmuir model is a commonly utilized approach in biosorption studies. The model assumes that adsorption takes place on uniformly distributed sites within the adsorbent, and once a site is occupied by the adsorbate, it becomes unavailable for further adsorption. Furthermore, all the adsorption sites are assumed to be identical and have the same energetic properties. The Langmuir isotherm equation is typically employed to describe this adsorption phenomenon [153]. The following equation is often used to describe this isotherm:

$$q_e = \frac{q_m K_L C_e}{1 + K_L C_e} \quad 4.10$$

where there are four factors to consider when dealing with metal adsorbed in the solution: q_e the amount of metal adsorbed per gram of adsorbent (mmol/g), C_e the equilibrium concentration of

the solution (mmol/L), K_L the affinity of biosorption (L/mmol) and q_m the maximum amount of adsorption metal ions (mmol/g).

The three parametric Sips model is widely considered to be the most applicable isotherm model for monolayer adsorption [154]. Sips model can be applied to either homogeneous or heterogeneous systems and describe the monolayer adsorption of heavy metal ion molecule to the 1/ns adsorption site (functional groups), which is shown in Eq. 4.11:

$$q_e = \frac{q_{mS} K_S C_e^{ns}}{1 + K_S C_e^{ns}} \tag{4.11}$$

where q_{mS} (mg/g) is the biosorption capacity, K_S (L^{ns}/mg^{ns}) and ns are the Sips constant parameters, and C_e (mg/L) is the equilibrium heavy metal concentration in supernatant. The Sips model is reduced to the Langmuir model when ns=1.

In this study, the impact of heavy metal concentration on the biosorption of Pb(II), Cd(II), and Zn(II) by algal biomass was evaluated for a period of 5 minutes. The adsorption capacity of heavy metal ions was determined by studying the adsorption isotherms. Figure 4-5 demonstrates that the equilibrium biosorption of B-7.5, B-8.5, and B-9.5 increases with increasing initial metal ion concentrations until equilibrium is achieved. This can be attributed to the abundant functional groups available for heavy metal ion binding, which get occupied when initial heavy metal concentrations are high. As the initial heavy metal concentrations increase, the binding sites become occupied, resulting in higher equilibrium adsorption. In liquid-solid system, it is important to point that the heavy metal ion overcomes the transfer resistance so that it can be adsorbed onto the surface of the algal biomass. Based on the kinetics data, this process should take less than five minutes.

The experimental data was fitted to Freundlich, Langmuir and Sips adsorption isotherm models. The results showed that all models fit well with the adsorption of Pb(II), Cd(II), and Zn(II), but the Sips model (R^2>0.9622-0.9938) was found to be a better fit than the Freundlich and Langmuir model. This indicates that the biosorption occurs on monolayers. The Freundlich model revealed a favorable adsorption process with an N value between 1.43 and 7.31. In the Sips model, the variable *ns* denotes the quantity of active sites available for each heavy metal ion. A value of ns greater than 1 indicates that more than one binding sites is involved in adsorbing a single adsorbate (i.e., metal ions). Conversely, if *ns* is less than 1, it implies that a single binding site is responsible for adsorbing multiple adsorbates. As shown in Table 4-4, the *ns* values of all scenarios were smaller than 1 except for two occurrences, which had *ns* values slightly larger than 1, i.e., 1.24 for Pb(II) adsorption on B-9.5 and 1.27 for Cd(II) adsorption on B-7.5. These data, combining with the fast adsorption kinetics, indicating the adsorption was monolayer. Also according to the Sips model results, the biosorption capacity of B-9.5 was the highest among the three types of biosorbents, with biosorption capacities of 97.85, 46.32, and 47.08 mg/g for Pb(II), Cd(II), and Zn(II), respectively. The biosorption capacity of B-9.5 biomass for Pb(II) is 2.12 and 2.58 times higher than that of B-8.5 and B-7.5 biomass, respectively. In addition, the ratios for Cd(II) are 2.07 and 3.76 times higher, and for Zn(II), 1.98 and 2.33 times higher compared to B-8.5 and B-7.5 biomass, respectively. This can be attributed to the increase in the zeta potential of the cell surface and the number of carboxyl groups (COOH) on the cell wall when the alga was cultivated at an elevated pH in the tested range of pH7.5 to pH9.5. XPS data also showed an increase in the amount of protein on the cell surface when microalgae were cultivated under alkaline conditions, resulting in more functional groups (COOH) available for biosorption.

Metal properties are a crucial factor that relates to biosorption capacity. A previous study discovered that the same biomass could achieve a greater biosorption capacity when exposed to heavy metals with higher electronegativity and smaller metal radius [14]. Moreover, a linear relationship was established between the impact factor (I = Electronegativity/radius) and biosorption capacity (q_m, mmol/g). In the current study, we observed a similar linear relationship between the impact factor and biosorption capacity of Pb(II), Cd(II), and Zn(II) by all the three biosorbents, which is compatible with the results of our previous studies [14].

4.1.4.6 Pb(II), Cd(II) and Zn(II) biosorption in binary system

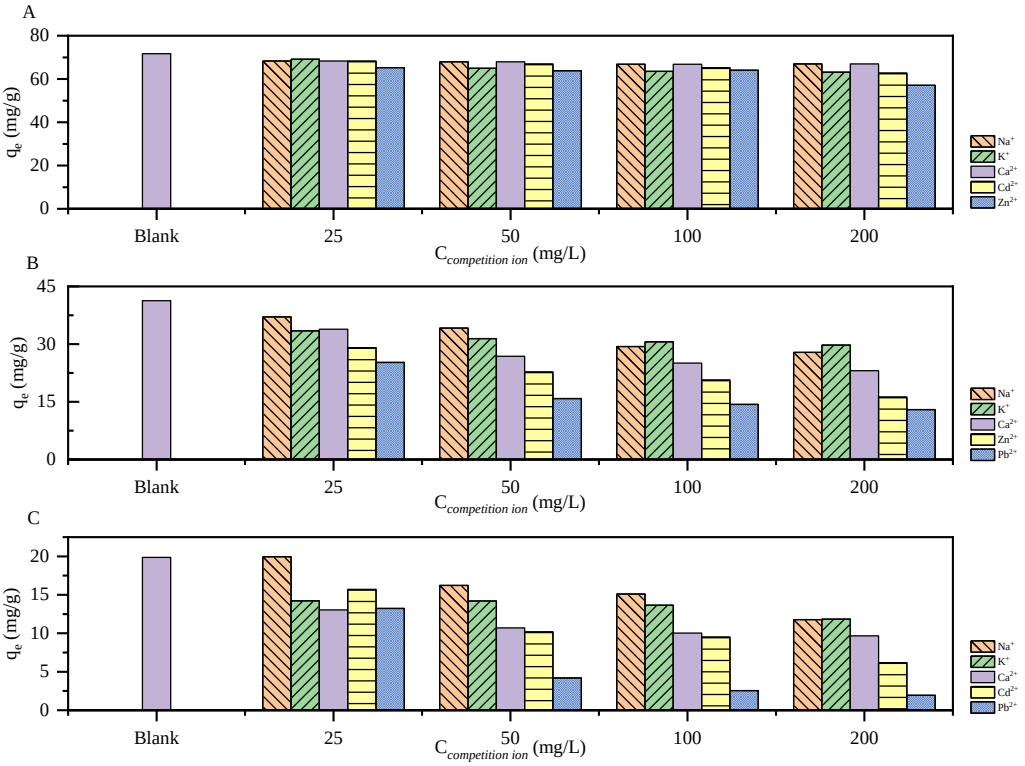

Figure 4-6 Equilibrium biosorption of Pb(II) (A), Cd(II) (B) and Zn(II) (C) by B-9.5 biomass in binary systems: 50 mg/L initial heavy metal ion concentration, competitive metal ion Na(I), K(I), Ca(II), Pb(II), Cd(II), or Zn(II) at four different concentrations, i.e., 25, 50, 100, and 200 mg/L, with 0.5 g/L B-9.5 biomass at 25 °C, pH 6. All the measurements were obtained in triplicates and the results were reported as mean values (n = 3).

The biosorption of heavy metal ions in multi-metal systems is a complex process due to the interaction between the solutes and the negative functional groups on the cell wall. In order to investigate this interaction, the equilibrium biosorption of Pb(II), Cd(II), and Zn(II) in binary systems containing one competition ion, i.e., Na(I), K(I), Ca(II), Cd(II) or Zn(II) at various competition ion concentration, i.e., 25, 50, 100 and 200 mg/L, were tested. The adsorption tests were carried out at pH 6.0 and room temperature (25 ℃) with 0.5 g/L B-9.5 biomass. As shown in Figure 4-6A, the inhibitory effects all competition ions on Pb(II) were unsubstantial except for Zn(II), which increased slightly with Zn(II) concentration in the tested range. However, all competition ions showed significant inhibitory effects on the adsorption of Cd(II) and Zn(II) at all competition ion concentrations except for Na(II) at 25 mg/L, which demonstrated negligible inhibition on the adsorption of Zn(II). In addition, Pb(II) demonstrated the strongest inhibitory effect to the adsorption of Cd(II) and Zn(II) in comparison to other tested competition ions. For the same pair of heavy metal ion and competition ion, the inhibitory effect always increases with competition ion concentration. At the highest competition ion concentration, i.e., 200 mg/L, Zn(II) exhibited the greatest inhibition on Pb(II), leading to a reduction from 71.69 mg/g to 57.08 mg/g in equilibrium biosorption (a decrease of 20.37%) and Pb(II) exhibited the strongest inhibition to both Cd(II) and Zn(II), and resulted in a 60.75% and 68.98% reduction, respectively. The inhibition by single valence metal ions, such as Na(I) and K(I), was much weaker than that of two valence metal ions, such as Ca(II), Pb(II), Cd(II), and Zn(II). Among the two valence metal ions, it was observed that a strong Lewis's metal, such as Pb(II), Cd(II), and Zn(II), had a stronger inhibitory effect than a soft heavy metal ion, such as Ca(II). Interestingly, Pb(II) had a greater influence than Cd(II) and Zn(II), possibly due to its stronger electronegativity (2.33), which may result in a higher affinity for functional groups, such as -COOH, C-OH, C-N, and P=O.

In contrast to single-component studies, experimental studies that investigate the impacts of multicomponent systems on the biosorption process provide a more accurate representation of the actual wastewater treatment process. In a multicomponent system, the biosorption capacity of a particular metal ion is expected to be lower due to the presence of other positively charged heavy metal ions that compete for active sites on the biosorbent surface. There is evidence from several research studies that metal ions compete for adsorption sites. When algae are used as biosorbents, the biosorption capacity of Pb(II), Cd(II), Cu(II), and As(II) is reduced in a binary system compared to a single-component system [61]. Additionally, the biosorption capacity decreased further under ternary systems, demonstrating an antagonistic combined effect. In a study by Li et al. [94], Pb(II) was biosorbed by microalgae *Chlorella sp.* under ternary systems, for example, Pb-K-Na, Pb-Ca-Mg, Pb-Cu-Zn. They found the competition effect of Na(I) and K(I) barely had competition effect of Pb(II) biosorption, Ca(II) and Mg(II) slightly had competition on Pb(II) biosorption, Cu(II) and Zn(II) had the strongest inhibition effect, which supports our conclusion that heavy metal ions with two valences have greater ability to form binding sites than those with one valence.

4.1.4.7 Regeneration test

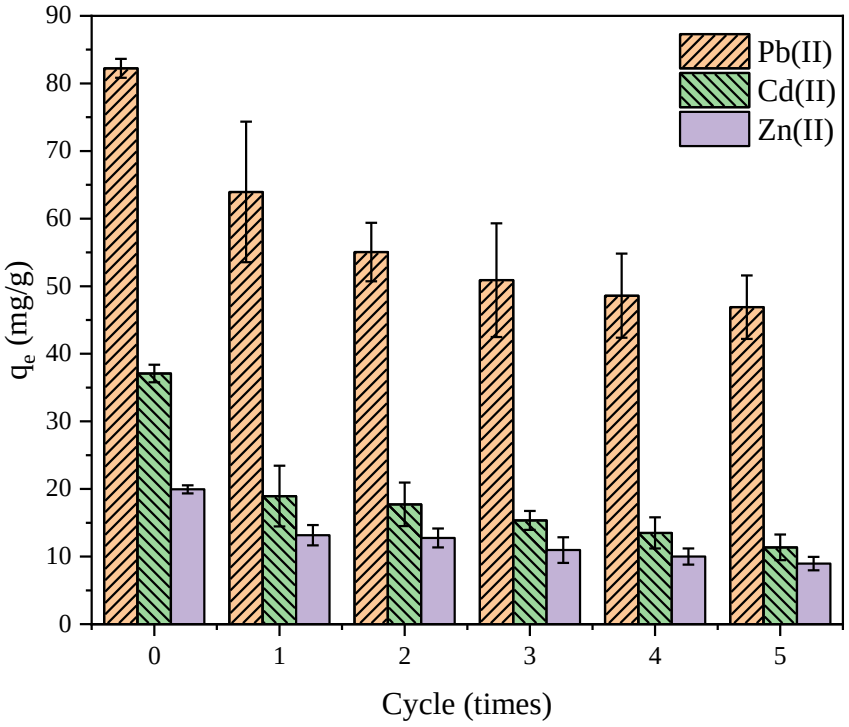

Figure 4-7 Equilibrium biosorption of Pb(II), Cd(II) and Zn(II) after biosorption-desorption cycle using 0.5 g/L B-9.5, 50 mg/L heavy metal concentration, pH 6.0, 25℃. Mean values of triplets along with standard deviations (the error bars) are reported (n = 3).

The regeneration of biosorbents can be accomplished via pH modulation, whereby heavy metal ions are eluted into the aqueous phase upon reduction of pH. Figure 4-7 depicts the uptake and desorption performance regeneration of Pb(II), Cd(II), and Zn(II) biosorption. A variety of reagents can be used for desorption of heavy metal ions, including H_2SO_4, HCl, HNO_3, EDTA, NaEDTA, $CaCl_2$, Na_2CO_3, and NaOH. According to Wang et al. [155], the highest desorption ratio can be achieved using four reagents: HCl, HNO_3, EDTA, and NA_2EDTA, with HNO_3 being the most commonly used reagent for pH modification without heavy metal precipitation. This study employed 0.1 M HNO_3 for the desorption process. Figure 4-6 shows that there was a reduction in the equilibrium biosorption of Pb(II), Cd(II), and Zn(II) with increasing cycle times.

After the fifth cycle, the equilibrium biosorption was 46.90, 11.36, and 8.96 mg/g, leading to reductions in equilibrium biosorption of 42.9%, 69.4%, and 55.1% for Pb(II), Cd(II), and Zn(II), respectively. It was observed that the biosorption reduced in the first cycle and slightly decreased in the subsequent recycle tests. Therefore, the method of desorbing heavy metal ions (changing pH) may affect the chemical and physical structure of functional groups on the surface of the cell, leading to a lower biosorption of these ions. Many studies have also shown that equilibrium biosorption decreases after biomass is recycled. For instance, the biosorption efficiency% of Pb(II), Cu(II), Cd(II), Zn(II) and Ni(II) after fifth cycle by an algal-based biosorbent (*Fucus vesiculosus*) were 73.6, 37, 5.4, 2.2 and 4.4%, respectively [87]. In the same way, after five cycles of biosorption, *Chlorella vulgaris* achieved a biosorption efficiency of 79.87% of Hg(II) [31]. According to that information, the amount of metal retained decreased significantly after five cycles.

4.1.5 Conclusions

It is noteworthy that this investigation is the first to examine the impact of pH cultivation on the biosorption of heavy metals using *N. oleoabundans*, which underscores the originality and importance of the research results. The results of the study indicated that the biosorption of heavy metals was increasing when increasing the cultivation pH. The data obtained from the isotherm experiments indicated that the biosorption of heavy metals took place on the surface of the cell and was in agreement with the Sips model. XPS analysis revealed that the cultivation of the microalgae in a higher pH medium caused an increase in the content of protein and carboxyl groups on the cell wall, leading to a higher biosorption capacity of heavy metal ions. Moreover, the study confirmed the correlation between heavy metal properties and biosorption capacity.

4.1.6 Acknowledgment

Financial support of Natural Science and Engineering Research Council of Canada (NSERC) in the form of a Discovery Grant RGPIN-2022–05242 is gratefully acknowledged.

4.2 Enhanced Pb(II) removal by green alga *Neochloris oleoabundans* cultivated in high dissolved inorganic carbon cultures[1]

Siwei Gu & Christopher Q. Lan*

Department of Chemical and Biological Engineering

University of Ottawa

* Chrisotpher.Lan@Uottawa.ca

[1]The content of this paper was published and the detail: S. Gu, E.M. Boase, C.Q. Lan, Enhanced Pb(II) removal by green alga *Neochloris oleoabundans* cultivated in high dissolved inorganic carbon cultures, Chem. Eng. J. 416 (2021) 128983.

4.2.1 Abstract

This study developed a novel strategy for Pb(II) removal from synthetic wastewater by *Neochloris oleoabundans*, in which algae was cultivated in different concentration of sodium bicarbonate and then the biomass was harvested as biosorbents for Pb(II) removal. The biosorption of lead by green alga *Neochloris oleoabundans* biomass was grown in media containing three different concentrations of sodium bicarbonate: 0 mM, 160 mM, and 320 mM, which exhibited lead adsorption capacity of 145.9, 327.26 and 494.14 mg Pb/g biomass, respectively. Isothermal data showed that the adsorption was monolayer Langmuir adsorption occurring at cell surface, which is supported by kinetic and thermodynamic evidence as well. The adsorption happens rapidly with equilibrium established within 5 minutes. The zeta potentials of these three types of biomasses increased sharply with the increase of sodium bicarbonate in medium, indicating an increase of negative charges on cell surface when increasing $NaHCO_3$ concentration in medium, which seems to be responsible for the increase of Pb(II) adsorption capacity. FTIR spectra indicated the presence of carbonyl, carboxyl, amide, and phosphate groups that might served as the sites of adsorption at cell surface. The effects of temperature and pH on lead adsorption were also studied. Finally, the inhibition of lead biosorption of *N. oleoabundans* biomass by competitive metal ions such as Na^+, K^+, Ca^{2+}, Cu^{2+} and Zn^{2+} was shown to increase with the electronegativity of these ions.

Keywords: lead removal, biosorption, microalgae, *Neochloris oleoabundans*

4.2.2 Introduction

Heavy metal contamination is a growing concern worldwide due to the increase of discharges owing to population growth, urbanization, industrialization, and modernization of agriculture [156].. Of particular relevance, Lead, one of typical toxic heavy metal, can lead to kidney failure, impaired voluntary muscle function, and damage to nerve systems, especially that of a developing baby's brain [157]. Lead (II) is released into water through industrial processes such as printing, lead smelting, mine tailings, lead batteries, and glassmaking [111]. It poses a significant risk to aquatic lives, as well as human health due to its toxicity and inability to be biodegraded, leading to bioaccumulation moving up the trophic chain [158]. It is therefore imperative to remove them from wastewaters before discharging. Conventional methods for the removal of heavy metals include chemical precipitation [159], ion exchange [160], and membrane processes [161].

Chemical precipitation is a well-known method for heavy metal removal. Under primary conditions, heavy metal ions react with lime (i.e. CaO), sodium carbonate, or sodium sulfate to form metal-hydroxide, metal-carbonate, or metal-sulfate complexes, respectively, which precipitate out of the solution to form a sludge as shown in Equations 4.12-4.15 [162].

$$CaO + H_2O \rightarrow Ca(OH)_2 \quad (4.12)$$

$$M^{2+} + Ca(OH)_2 \rightarrow M(OH)_2 + Ca^{2+} \quad (4.13)$$

$$M^{2+} + Na_2CO_3 \rightarrow MCO_3 + 2Na^{+} \quad (4.14)$$

$$M^{2+} + Na_2SO_4 \rightarrow MSO_4 + 2Na^{+} \quad (4.15)$$

Lime and sodium sulfate are used as precipitants since they are inexpensive, widely available, and easy to handle [162,163]. Chemical precipitation can effectively treat wastewater with a concentration of 1000 ppm of lead by optimizing different parameters, including pH, temperature, and chemical concentration [162]. However, this method is not suitable when metal ions are

present at low concentrations, which would require large amounts of chemicals to be used with very low efficiency. Another downside of chemical precipitation is that it produces a toxic sludge that requires further treatment, creating another environmental issue [162,163]. Moreover, this process discharges effluents into the ecosystem containing lower concentration heavy metal ions but still relatively high residual concentrations. Therefore, it is an economically viable way to mitigate the contamination of wastewaters containing a relatively high concentration of heavy metals but cannot solve the problem entirely.

Ion exchange is another commonly used process for the removal of heavy metal ions, where heavy metal ions in aqueous solution exchange with co-ions (e.g., H^+ and Na^+) on the functional groups of ion exchangers to be removed [162,164]. This method can effectively remove low concentrations of heavy metal ions in water as opposed to chemical precipitation. However, it is easily fouled when the wastewater is not properly pretreated and the regeneration of ion exchangers may consume large quantities of acid (e.g., HCl) and base (e.g., NaOH) and generate large quantities of secondary wastewaters if an economically viable heavy metal recovery process is not in place [162].

Nanofiltration (NF) and reverse osmosis (RO) are pressure-driven membrane filtration processes that can partially and completely reject heavy ions, respectively [165]. Reverse osmosis (RO) operates by applying a transmembrane pressure gradient larger than the osmotic pressure of the feed water to force water through a RO membrane that rejects all solids and solutes, including all ions. RO process requires high operational pressure and costly membranes. It an expensive and energy intensive process including relatively high operating costs, which containing labor, chemicals, membrane replacement, energy and sludge treatment costs [166].

Biosorption has gained attention over the past few decades and has been established as an attractive alternative to the conventional methods for removing heavy metal ions from contaminated waters. For example, many plants, fungal, and bacterial species have been researched as potential biosorbents [113]. And, microalgae have gained traction as novel biosorbents since they offer several advantages including low operating cost because they are self-propagating and fast growing, high selectivity, and the capacity to adsorb or absorb metal ions at low concentrations [167]. In addition, volume reduction of heavy metal loaded biomass could be achieved by combustion for heat production and heavy metals could be recovered from the ashes.

Studies have shown that medium composition such as phosphate concentration could affect the surface structure of microalgal cells and therefore their heavy metal ion adsorption capacity in a significant manner [93,94]. In the meantime, numerous studies have shown that the dissolved inorganic carbon (DIC) could affect the metabolism and cell morphology in significant manners. It has been established that DIC could serve as carbon source of some microalgal species [16], control protozoan contamination [168], and manipulate the metabolism of microalgae to increase lipid cell content and lipid productivity [96,169,170]. Of particular relevance, it was shown that DIC concentration could affect the cell morphology of microalgae [107]. It is therefore reasonable to hypothesize that DIC could affect the structure of cell surface of microalgae and hence their heavy metal adsorption/absorption behaviours. This study is the first time this hypothesis has ever been put into test and the results are affirmative and promising.

This study investigated the biosorption of Pb (II) ions using green alga *N. oleoabundans* biomass grown in media at three different sodium bicarbonate concentrations-biomass-biomass. The

effects of pH, temperature, and competitive ions on Pb(II) adsorption capacity of biomass were investigated. Adsorption mechanisms were discussed based on isothermal, kinetic, and thermodynamic data, in combination with the zeta potentials and FTIR spectra of biomasses.

4.2.3 Materials and methods

4.2.3.1 Microalgal culture and media

Neochloris oleoabundans, (UTEX# 1185) was purchased from the microalgal culture collection at the University of Texas in Austin. Biomass culture was grown in a Modified Bristol Medium containing (analytical grade, per liter): 0.35 g $NaNO_3$, 0.138 g K_2HPO_4, 0.0823 g $MgSO_4$, 0.025 g $CaCl_2$, 0.322 g H_2PO_4, 0.025 g NaCl, 0.0068 g $FeCl_3$ [96] and 1 mL of A5 solution, which was composed of (analytical grade, per liter) 1.6423 g EDTA-Fe, 2.86 g H_3BO_3, 1.81 g $MnCl_2{\cdot}4H_2O$, 0.22 g $ZnSO_4{\cdot}7H_2O$, 0.079 g $CuSO_4{\cdot}5H_2O$, and 0.039 g $(NH_4)_6Mo_7O_2{\cdot}4H_2O$ was added [96]. $NaHCO_3$ (Sigma Aldrich, USA) was added to medium at concentrations specified in the text (i.e., 0, 160, or 320mM $NaHCO_3$). Media were sterilized prior to use at 121°C for 20 minutes.

4.2.3.2 Microalgae cultivation

The procedure for the microalgae cultivation was adopted from our previous work [96]. Briefly, *N. oleoabundans* was grown in a 3-L photobioreactor, which had been converted from a stirred tank BioFlow 110 bioreactor (New Brunswick Scientific GMI Inc., Canada) by equipping it with 12 full spectrum lamps with a light density of 1700 μmol/(m^2·s). The vessel of the bioreactor was made of heat resistant transparent glass with a wall thickness of 0.5 cm and diameter of 22.9 cm. The lamps were arranged evenly around the bioreactor (Philips Plant & Aquarium T18/15, Philips Electronics Ltd. ON, Canada) and programmed to be 12 hours on and 12 hours off.

Before adding the inoculum to the medium, the medium containing vessel (working volume 2 L) was sterilized at 121°C for 20 minutes. After cooling to room temperature, the sterilized medium

was inoculated with 30 mL of inoculum to obtain 0.01g/L initial biomass concentration. Additionally, sterile sodium bicarbonate was added to the sterilized growth media at concentrations of 0 mM, 160 mM, and 320 mM, based on the experiment. The microalgal biomass grown in such media are presented as 0-biomass, 160-biomass, and 320-biomass, respectively, hereafter when applicable.

Microalga cultivation was carried out at 25°C, 180 rpm, and pH 9.5. A constant flow of air enriched with CO_2 was supplied at a rate of 1 LPM by passing the air through a bottle containing distilled water, a 0.20 μm microfiltration cartridge, and then sparging it to the culture from the bottom of the bioreactor. A stream of pure CO_2 was introduced into the air stream through a gas mixer at a flowrate that is controlled automatically to maintain the culture pH constant at the set value, i.e., pH 9.5. Cells were harvested at the beginning of stationary phase, corresponding to 6-16 days after inoculation, depending on the concentration of sodium bicarbonate present in the medium. Algal biomass was washed three times by centrifuged at 5000 rpm for 10 minutes to remove medium and cell debris. Algal samples were stored at -80°C until needed.

4.2.3.3 Adsorption studies

4.2.3.3.1 Stock solution preparation

Stock solutions of 1000 ppm Pb^{2+}, Zn^{2+}, Cu^{2+}, Ca^{2+}, Na^{+}, and K^{+} were prepared by dissolving an appropriate amount of $Pb(NO_3)_2$, $Zn(NO_3)_2 \cdot 6H_2O$ (Strem Chemicals Inc., USA), $Cu(NO_3)_2 \cdot 2.5H_2O$ (Alfa Aesar, USA), $Ca(NO_3)_2$, $NaNO_3$ and KNO_3 (Fisher Scientific, USA), respectively. 10 μL of 68% HNO_3 was added to stabilize the stock solution.

4.2.3.3.2 Adsorption kinetic study

Stock Pb(II) was added to algal biomass suspension of 320-biomass to achieve an initial lead metal concentration of 10, 50, 100 mg/L, later, pH was adjusted to 7 by 0.1 M NaOH and then

samples continuously oscillated at 180 RPM at 25℃ in darkness condition. After 1, 5, 10, 15, 20, 25 and 30 minutes shaking, the supernatant was obtained by centrifugation with 13500 rpm for 10 minutes, and the supernatant was further analyzed for Pb(II) concentration via iCE^{TM} 3300 AAS atomic absorption spectrometer. To prevent Pb(II) precipitation caused by pH and lead to errors in results, the control group was used to correct the results. In the control group, all operations were consistent except for the use material of deionized water and pH was adjusted by 0.1 M HNO_3 and NaOH. Later, subsequent experiments were also compared with a control group using same procedures. Kinetics were analyzed using the pseudo-first order model (Eq 4.16) and the pseudo-second order model (Eq 4.17).

$$\frac{dq_t}{dt} = k_1(q_e - q_t) \quad 4.16$$

$$\frac{dq_t}{dt} = k_2(q_e - q_t)^2 \quad 4.17$$

Where q_t (mg/g) is the amount of lead adsorbed per unit biomass at time t (min), q_e (mg/g) is the amount of lead adsorbed per unit biomass at equilibrium, and k_1 is a first order rate constant (min^{-1}), k_2 is a second order rate constant ($g \cdot mg^{-1} \cdot min^{-1}$).

4.2.3.3.3 Lead adsorption tests

All lead biosorption tests were carried out in 2-mL centrifugal tubes. All experiments were performed in triplicates and mean ± standard deviation values are presented. Controls, i.e., aqueous solutions of $Pb(NO_3)_2$ at given concentration and pH, were subjected to AAS analysis for all adsorption tests to provide the accurate initial Pb(II) concentration of each group of tests. 10 μl nitric acid (60-70%) was added to 1.0 mL of samples after sampling.

Adsorption kinetics was studied at three different Pb (II) concentrations, i.e., 10, 50, and 100 ppm, using 320-biomass at pH7.0 and a biomass concentration of 0.28 g/L. Samples in a series of 2-

mL centrifugal tubes were prepared and then incubated. Three centrifugal tubes were taken each time, which were centrifuged at 6000 rpm to quench adsorption and collect supernatants for AAS analysis. Sampling was carried after 1 and 5 min of incubation and at 5-min intervals thereafter until 30 min of incubation.

Adsorption isotherms of 0-biomass, 160-biomass, and 320-biomass were carried at pH 4, 5, 6, and 7. Biomass samples (0.22-0.31 g/L) were incubated with an initial lead concentration of 5-200 ppm to determine the adsorption isotherm at pH 4-7. After 30 min, the supernatant of the sample following incubation was analyzed for the residual heavy metal concentration using AAS.

Effects of temperature on lead adsorption isotherm were conducted using 320-biomass with a dosage of 0.3 g/L at pH 7 and four different temperatures, i.e., 25°C, 35°C, 45°C, and 55°C, with 30 min incubation. The residual lead concentration in the liquid phase following adsorption was determined using AAS. Eq 4.18 and 4.19 were used to determine thermodynamic parameters ΔG°, ΔH°, and ΔS° [171].

$$\Delta G° = -RTLn(K_L) \quad 4.18$$

$$ln(K_L) = \frac{\Delta S°}{R} - \frac{\Delta H°}{RT} \quad 4.19$$

Where K_L is the Langmuir constant (L/mol) [45], R the universal gas constant (J/mol·K), and T the reaction temperature (K).

Effects of competitive ions on Pb(II) adsorption isotherm were investigated with 320-biomass at biomass concentration 0.3 g/L. Each Pb(II) isotherm was obtained by increasing initial Pb(II) concentration from 5 to 200 mg/L and the competitive ions (Na^+, K^+, Ca^{2+}, Cu^{2+} and Zn^{2+}) concentration was the same, i.e., 100 mg/L. Samples were incubated for 30 mins at pH 7. At the

end of incubation, the samples were centrifuged and the supernatants were analyzed for residual lead concentration by AAS.

4.2.3.4 Analytical Methods

All analyses were performed in triplicates and mean ± standard deviation values are presented.

4.2.3.4.1 Biomass concentration

During the cultivation of microalgae, samples were taken on a daily basis to determine biomass concentration by measuring the optical density of culture using a GENESYS^{TM} 10S UV-Vis spectrophotometer (Thermo Fisher Scientific Inc., USA) at wavelength 680 nm. To determine the cell weight (DCW) of culture, 50 ml algal sample was washed with deionized water for three times, then the centrifuged sample was placed in an oven at 80℃ for over 24 hours. The dry weight was measured repeatedly until constant dry weight. A standard curve was constructed to relate the optical density at 680 nm to the biomass concentration.

4.2.3.4.2 Pb(II) concentration in liquid samples

To analyze the residual heavy metal content in the supernatant, an iCE^{TM} 3300 AAS atomic absorption spectrometer (ThermoFisher Scientific, USA) was utilized at a wavelength specific to the heavy metal being analyzed. Standard curve was constructed using Pb(II) standard (Sigma Aldrich, USA). Two drops of nitric acid (68%-70%) was added into sample upon sampling.

4.2.3.4.3 Zeta Potential

To measure the zeta potential of the cell surface, a Zetasizer Nano (Malvern Panalytical, UK) was used. Samples were diluted 6 times using deionized water prior to measurement [97].

4.2.3.4.4 FTIR Spectroscopy

Fourier transform infrared spectroscopy (FTIR) was used to investigate the interaction between functional groups at microalgal cell surface and metal ions. Samples were vacuum filtrated on a 0.45 μm filter prior to measurement and dried under room temperature overnight. The FTIR

spectra of untreated and treated biomass (i.e. after Pb(II) loading) was determined by a Cary 630 FTIR spectrophotometer (Agilent Technologies, USA).

4.2.3.4.5 Adsorption Isotherm Modelling

Experimental data were fitted to the Langmuir equation, i.e., Eq 4.20 [87]

$$q_{eq} = \frac{q_m K_L C_{eq}}{1+K_L C_{eq}} \qquad 4.20$$

Where q_m is the maximum amount of metal ions adsorbed to the surface of the cells per gram of biomass (mg/g), q_{eq} is the amount of metal ions adsorbed to the cell surface at equilibrium (mg/g), K is an affinity coefficient of the metal ions to the biomass (L/mg), and C_{eq} is the concentration of metal ions at equilibrium (mg/L).

For Langmuir adsorption, R_L [171] is a dimensionless separation factor defined by Equation 12, which measures the favourability of adsorption. Adsorption is favorable with $0<R_L<1$, unfavorable with $R_L>1$, linear with $R_L=1$ and irreversible with $R_L=0$. It is defined by Eq 4.21.

$$R_L = \frac{1}{1 + K_L C_o} \qquad 4.21$$

Additionally, the Freundlich isotherm model (Eq 4.22) was also used to fit the experimental data, where K_F ($mg^{1-n}g^{-1}1^n$)and n are empirical constants [172].

$$q_{eq} = K_F C_{eq}^{1/n} \qquad 4.22$$

Furthermore, in order to determine the efficiency of adsorption, Eq 4.23 was used to find the lead removal %:

$$\text{Removal } \% = \frac{C_i - C_{eq}}{C_i} \; x \; 100\% \qquad 4.23$$

Where C_i represents the initial concentration of heavy metal (mg/L) and C_{eq} the concentration of heavy metal at equilibrium (mg/L) in liquid phase.

4.2.3.4.6 Regeneration experiments

Regeneration experiments were carried out with 50 mL 0.3 g/L 320-biomass with initial Pb(II) concentration of 50 mg/L and pH of 6.0 at 298 K. The mixture was oscillated at 160 rpm for 30 min before being centrifuged at 5000 RPM. After washing with 50 mL deionized water for once, the Pb(II) loaded biomass slurry was transferred to 50 mL 0.1 N HNO_3, incubated for 20 min by oscillating at 298 K and 160 RPM. The biomass was then separated by centrifugation at 5000 RPM, for 10 min, washing three times with deionized water. The regenerated biomass was then subjected to the next cycle of adsorption. The adsorption-regeneration cycle was repeated 5 times. The regeneration efficiency of algae biomass was calculated using the following formula:

$$\%\text{Regeneration} = \frac{q_e}{q_m} \times 100\% \qquad 4.24$$

where q_e and q_m (mg/L) are the equilibrium biosorption of regenerated biomass or pristine biomass under the adsorption conditions of the regeneration tests and the adsorption capacity of pristine biomass, respectively.

4.2.4 Results and discussion

4.2.4.1 FTIR spectra

In order to determine the functional groups contributing to the biosorption, the FTIR spectra of cells from cultures containing 0 mM, 160 mM, and 320 mM $NaHCO_3$ were compared before and after Pb(II) adsorption. The wavelengths where a shift occurred after lead adsorption are summarized in Figures 4-8 A-C and Table 4-5.

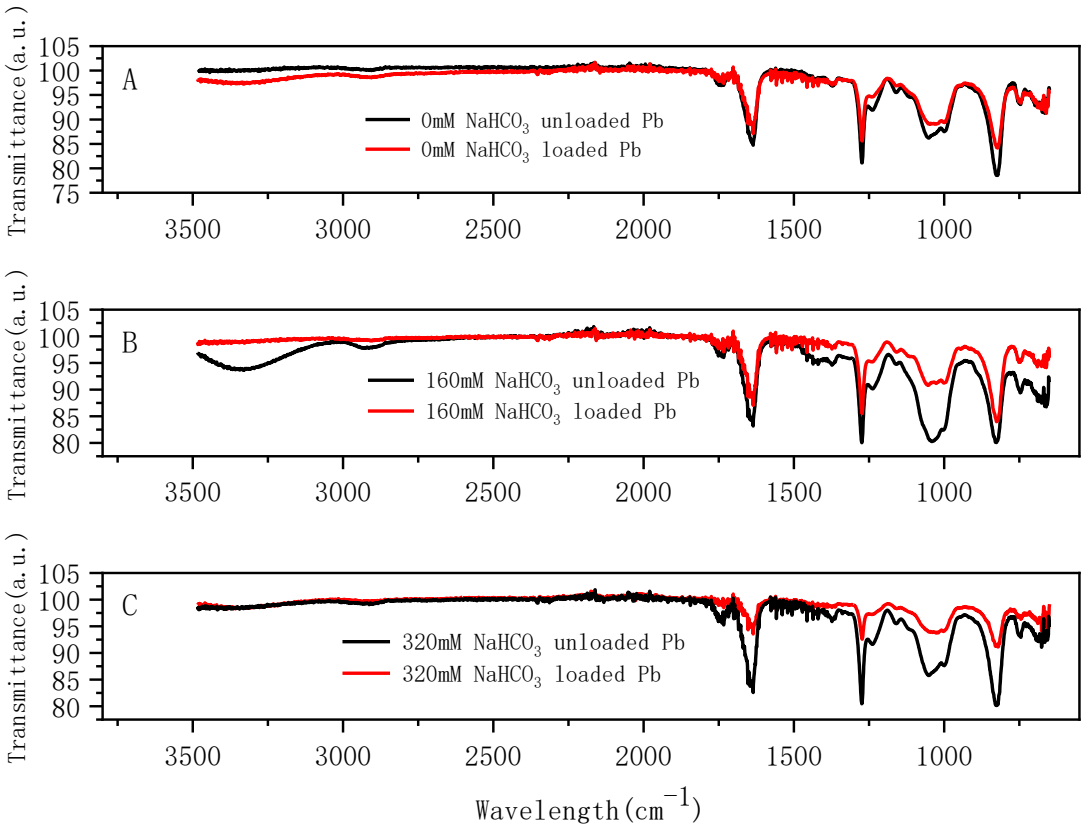

Figure 4-8 FTIR spectra of *N. oleoabundans* cells grown in media containing 0 mM $NaHCO_3$ (A), 160 mM $NaHCO_3$ (B), and 320 mM $NaHCO_3$ (C) before and after treatment with 100 ppm Pb(II) solution.

Table 4-5 Summary of change in FTIR of biomass before and after Pb(II) treatment.

Biomass	Before Pb(II) loading (cm^{-1})	After Pb(II) loading (cm^{-1})	Wavelength Shift (cm^{-1})	Bond
0 mM $NaHCO_3$	826.1	821.86	4.24	C-N
	999.65	999.58	0.07	C-O-C, C-OH
	1239.99	1240.54	-0.55	P=O
	1273.47	1273.40	0.07	P=O
	1635.74	1637.42	-1.68	C=O
160 mM $NaHCO_3$	826.22	825.64	0.58	C-N
	1040.87	1052.81	-11.94	C-O-C, C-OH
	1237.25	1243.25	-6.00	P=O
	1274.20	1273.41	0.79	P=O
	1635.52	NP	UD	C=O
320 mM $NaHCO_3$	820.47	825.22	-4.75	C-N
	1002.93	999.96	2.97	C-O-C, C-OH
	1159.15	1159.88	-0.73	C-O-C, C-OH
	1241.80	1240.28	1.52	P=O
	1273.10	1273.91	-0.81	P=O
	1646.14	NP	UD	C=O

Note: NP - no peak
UD – wavelength shift undeterminable

The FTIR spectra provided evidence of ionisable groups including hydroxyl, carboxyl, amide, and phosphate, which are presented on the algal cell wall and can directly contribute to the binding of heavy metal ions. As shown in Table 4-5, banding at 1000 cm^{-1}, 1040 cm^{-1} and 1159 cm^{-1} are representative of the C-O-C bond in glycosidic linkages and the hydroxyl C-OH group [173–175]. The existence of the phosphate P=O bond is evident through bands present at 1237-1274 cm^{-1} [173]. There are a large variety of phosphate containing compounds in cells, including nucleic acids, phospholipids, glycerophospholipids including phosphatidylglycerols, vitamins (e.g., pyridoxal phosphate), and others. It is possible that the P=O group present is due to phosphatidylglycerols secreted by the algae to its cell surface as an lipid, as seen in other microalgal species [176]. An ionisable protein amide bond is shown through the carboxyl C=O stretching at 1640 cm^{-1} [173]. Finally, C-N bonds are shown through the band at 820 cm^{-1}[177].

The C-N band at 820 nm^{-1} experienced the largest wavelength shift before and after adsorption of lead onto the 0-biomass. These results suggest that the C-N group, which could be found in molecules such as proteins and/or peptidoglycan, could served as the major adsorption sites on the surface of the 0-biomass. It is worth noting that there are C=O group peaks (1635 cm^{-1}) with all three untreated biomasses, which, however, disappeared from the 160-biomass and 320-biomass after lead adsorption. This phenomenon might happen due to the shielding of the C=O bond by lead ions bound to it after lead adsorption. If this is indeed the case, then C=O is likely one of the major functional groups involved in lead adsorption. It was worth noting that the significantly larger lead adsorption capacities of the 160-biomass and the 320-biomass ($p<0.05$) could be at least partially attributed to enhanced abundances of C=O containing groups on the cell surfaces of these biomasses.

Algal functional groups play an important role in the binding of heavy metal ions in adsorption process, which contains complexation, chelation and electron attraction. In surface adsorption, heavy metal ions are simply attached to the surface of algal cells [157]. The cell walls of microalgae *N. oleoabundans* has carbohydrate content, and the three most abundant components are rhamnose, galactose and glucuronic acid, which includes carboxyl group [178]. Changes in carboxyl functional groups were highlighted in this study to explain the higher Pb(II) removal of algae biobsorbent obtained from high-bicarbonate cultures.

4.2.4.2 Adsorption of heavy metals

4.2.4.2.1 Kinetics

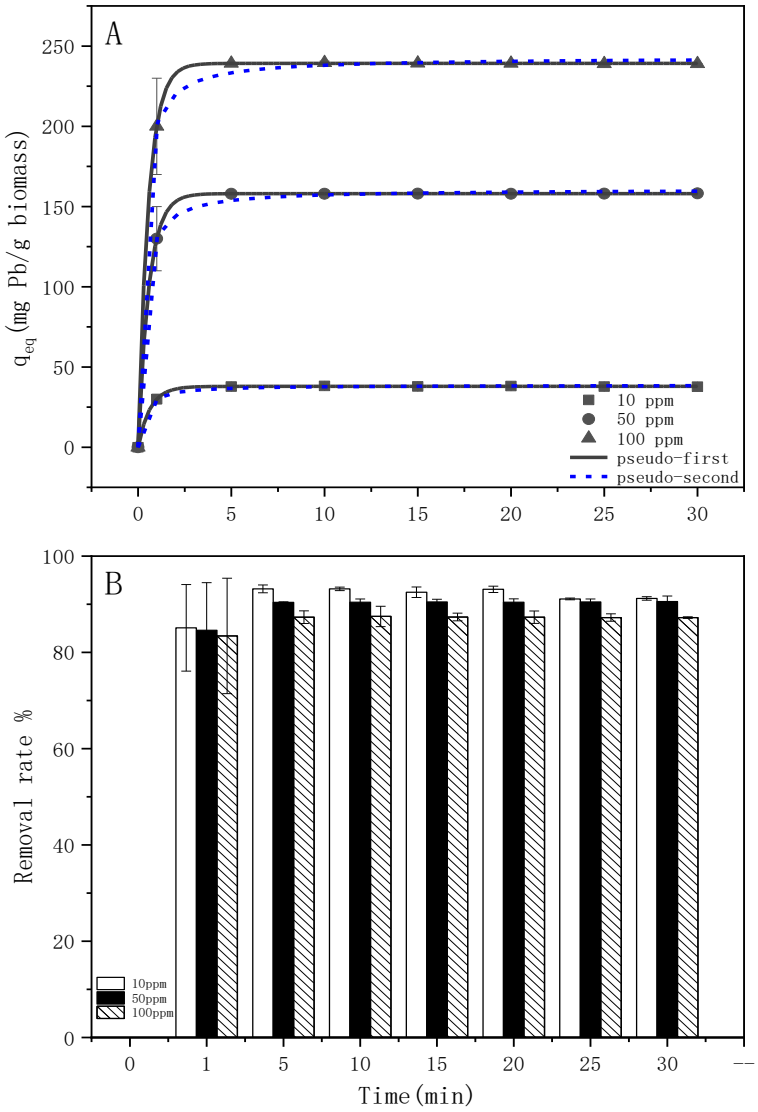

Figure 4-9 Biosorption of lead over time using *N. oleoabundans* biomass at initial lead concentration of 10, 50, or 100 ppm at pH 7 A) lead adsorption per unit biomass vs time; B) lead % removal from aqueous solution vs time.

Table 4-6 Kinetic parameters of pseudo-first order and pseudo-second order models.

Kinetic model	Parameters	Concentration of Pb(II) ion solution (mg/L)		
		10	50	75
Pseudo-first	$k_1(min^{-1})$	1.567	1.729	1.808
	q_e(mg/g)	37.91	158.04	239.22
	R^2	0.9998	0.9999	0.9999
	$SSE(mg^2/g^2)$	0.198	0.038	0.308
	RMSE(mg/g)	0.033	0.006	0.051
Pseudo-second	$k_2(g \cdot mg^{-1} \cdot min^{-1})$	0.074	0.037	0.020
	q_e(mg/g)	38.70	160.77	242.98
	R^2	0.9980	0.9989	0.9990
	$SSE(mg^2/g^2)$	2.422	23.344	50.219
	RMSE(mg/g)	0.404	3.891	8.370

SSE : residual sum of squares
RMSE : root mean square error

Figure 4-9 shows the adsorption within a 30-min time course. In fact, the plateaus were established within 5 minutes of adsorption. These results are compatible with literal data using different microalgae, e.g., those by Vilar *et al.*[80], where the equilibria were established rapidly at or before the first sampling, which were 10 minutes. Similarly, Roy *et al*. [179] reported that the adsorption equilibrium of Pb (II) by green alga *Chlorella minutissima* was established within 15 minutes. The fast establishment of adsorption equilibria implies that the adsorption occurred at cell surface since absorption of lead ions across the cytoplasmic membrane of green alga into the cytoplasm of cells would take much longer time to reach equilibrium [108]. The rapid metal adsorption indicated that *N. oleoabundans* has the potential for practical applications from the kinetic perspective.

The R^2 values of fitting experimental data with the pseudo-first-order kinetic model in the range of 0.9998-0.9999, which were only slightly higher than that of the pseudo-second-order kinetic model, i.e., in the range of 0.9980-0.9990. This small difference is not sufficient to determine

with certainty one way or another. The ambiguity was due to the fast kinetics that allowed precise measurement of only two points before the plateau of adsorption was reached. It is worth noting that many researchers reported pseudo-second-order kinetics of Pb(II) adsorption by microalgae [36,94]. In the microstructure, biosorption mechanism including ion exchange, chelation and electrostatic attraction is investigated gradually by the advanced instruments. Ion exchange takes place between the positive charge on the surface of the algae(such as H^+) and heavy metals. When the algae adsorb heavy metal ions, the elements that previously bound to the functional groups are released. The functional groups of algae(such as Polysaccharides, Proteins and Lipids) play important roles in chelation process and electrostatic attraction [157].

4.2.4.2.2 Adsorption isotherms of *N. oleoabundans* cells grown in media of varied DIC

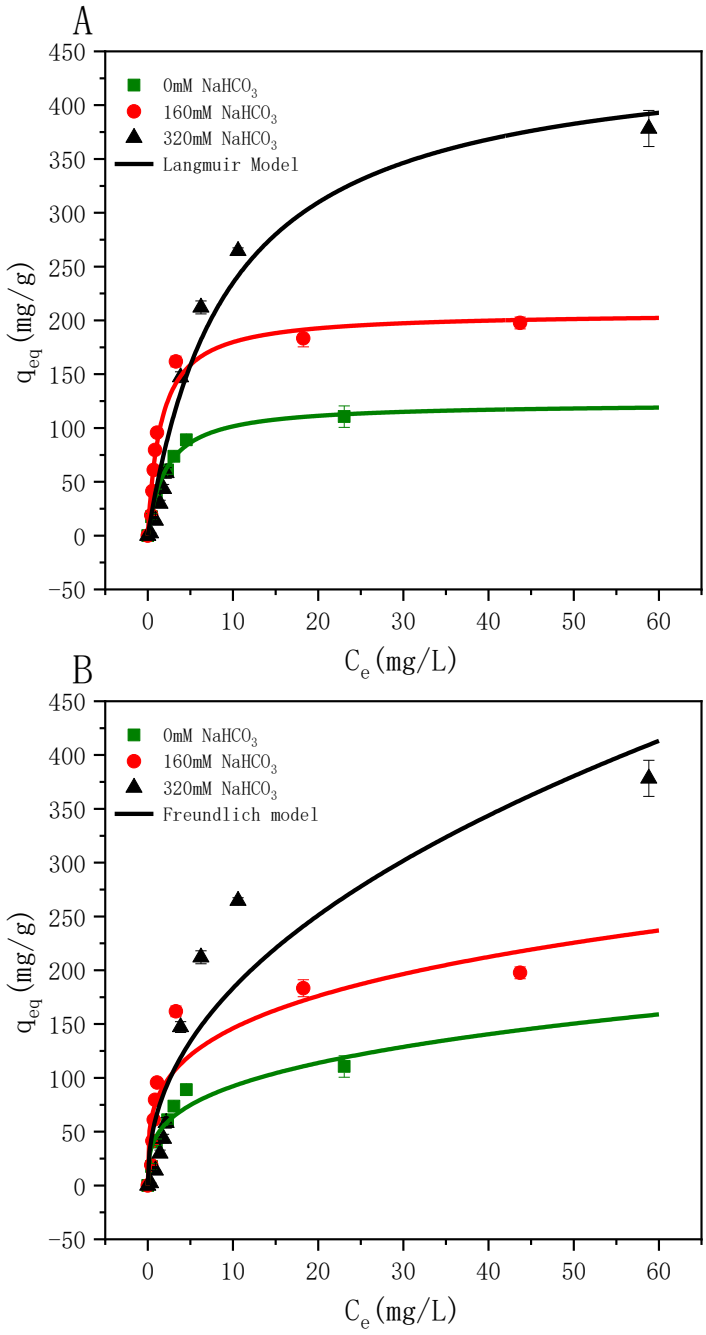

Figure 4-10 Isotherms of Pb(II) adsorption using *N. oleoabundans* biomass grown in media containing 0, 160, or 320 mM at pH7.0 and fitted with: A) Langmuir model; and B) Freundlich model.

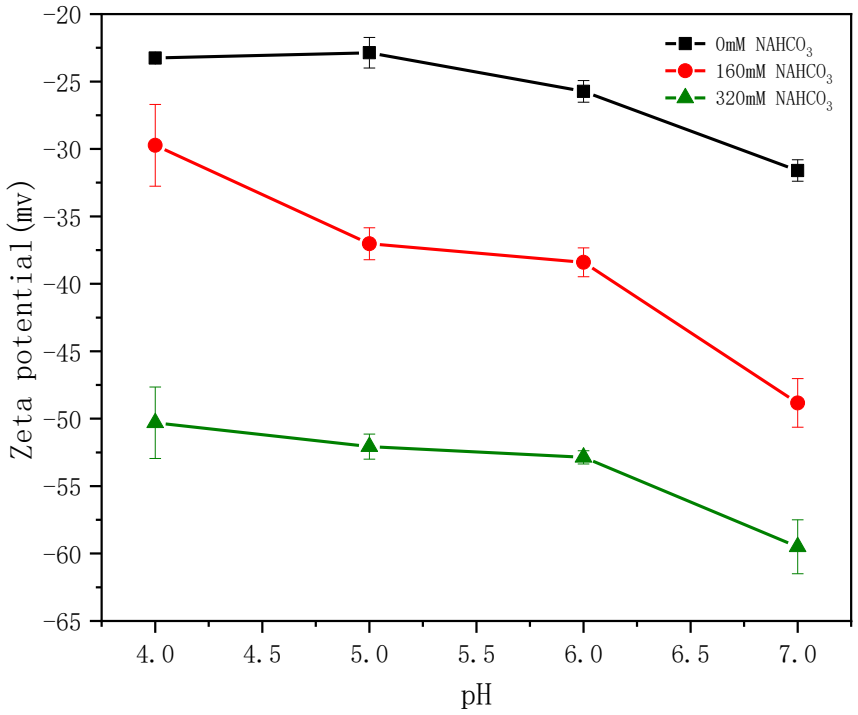

Figure 4-11 Effect of pH on zeta potential of living *N. oleoabundans* biomass.

Table 4-7 Correlation of sodium bicarbonate concentration and adsorption values. Initial lead concentration = 5-200 ppm, biomass concentration = 0.27, 0.28, and 0.30 g/L, corresponding to 0 mM, 160 mM and 320 mM, respectively, pH 4-7.

			Langmuir			Freundlich			
	pH	Zeta Potential (mV)	q_m (mg/g)	K_L (L/mg)	R^2	K_F ($mg^{1-n}g^{-1}1^n$)	1/n	R^2	R_L
0 mM $NaHCO_3$	4	-23.3	139.14	0.413	0.9974	41.31	0.529	0.9870	0.012-0.326
	5	-22.9	141.61	0.382	0.9996	39.91	0.543	0.9814	0.013-0.344
	6	-25.7	142.52	0.443	0.9970	44.50	0.503	0.9750	0.111-0.311
	7	-31.6	145.90	0.319	0.9934	36.54	0.603	0.9869	0.015-0.385
160 mM $NaHCO_3$	4	-29.7	278.75	0.343	0.9742	70.36	0.536	0.9132	0.060-0.391
	5	-37.0	287.61	0.311	0.9668	72.75	0.518	0.9185	0.055-0.368
	6	-38.4	317.36	0.319	0.9878	76.95	0.576	0.9555	0.065-0.411
	7	-48.8	327.26	0.287	0.9786	73.69	0.591	0.9422	0.059-0.385
320 mM $NaHCO_3$	4	-50.3	482.99	0.087	0.9758	60.36	0.533	0.9132	0.319-0.701
	5	-52.1	487.47	0.086	0.9780	62.66	0.525	0.9128	0.324-0.705
	6	-52.9	491.54	0.084	0.9791	58.93	0.541	0.9209	0.324-0.705
	7	-59.5	494.14	0.084	0.9791	59.25	0.541	0.9209	0.288-0.700

Figure 4-10 shows the isotherms of Pb(II) ions adsorption at 25 ^{o}C and pH 7 on the *N. oleoabundans* biomasses grown in media containing 0 mM, 160 mM or 320 mM $NaHCO_3$. As shown in Figures A and B it is evident the experimental isotherms fit well with the Langmuir model but poorly with the Freundlich model. These observations are further confirmed by the data summarized in Table 4-7, which lists isothermal parameters of 0, 160, and 320-biomasses at different pH levels. The R^2 values show that the Langmuir model ($0.9668< R^2 <0.9996$) is much higher than the Freundlich model ($0.9128< R^2 <0.987$) when fitted with the experimental isotherms at all tested pH levels. Considering this piece of evidence, in combination with the observation of fast kinetics as discussed previously, we conclude that the biosorption of Pb(II) by *N. oleoabundance* cells as observed in this study is Langmuir adsorption, which involves adsorption of a monolayer of adsorbates (i.e. lead ions) onto the surface of absorbents (i.e. *N. oleoabundans* cells). As also shown in Table 4-7, R_L values for all types of cells were calculated to be between 0.012-0.700, indicating favorable adsorption processes ($0 < R_L < 1$). The Pb(II) adsorption capacities determined with the Langmuir model of the biomasses grown under three DIC concentrations followed the order of 0 mM<160 mM<320 mM. With the increase of DIC in medium, the functional binding group(hydroxyl, carboxyl, amide, and phosphate) increases, which may be one reason for improving the adsorption capacity of Pb(II) metal ions using *N. oleoabundans* [180]. As shown in Table 4-7, q_m of the three different biomasses as determined by the Langmuir model, when compared at the same pH, followed the following same order, i.e., $q_{m,0}<q_{m,160}<q_{m,320}$, and the differences are quite significant. Using q_m at pH 7.0 as examples, the q_m values were 145.9, 327.26, and 494.14 mg/g for 0-biomass, 160-biomass, and 320-biomass, respectively. The significant difference of q_m among the three different types of biomasses could be tentatively explained by the zeta potential differences.

In Figure 4-11, when compared at the same pH, the absolute value of the zeta potential of different biomasses differs from each other significantly according to the following order: ζ-potential,0 < ζ-potential,160 < ζ-potential,320. Zeta potential is the electrical potential at the slipping plane adjacent to the stagnant liquid layer attached to the surface of the dispersed particles in a colloid. It depends on the net electrical charge at the particle surface and the thickness of the stagnant liquid layer. Although zeta potential does not equal to the particle surface potential, it is the only means for researchers to characterize surface charges of particles dispersed in a colloid and has recently been employed by many researchers for the characterization of the surface charges of microalgal cells [40,41]. On the other hand, the q_m of all three types of biomasses exhibited a trend of slight increase when pH increased in the range of 4-7, while the K_L in general decreased slightly. These results are accordance with literature data [55,65,80], confirming a significant effects of pH when it was 4 or below but only small impacts at pH levels between 4 and 7. As shown in Figure 4-11, the zeta potential of cells demonstrated significant increase with the DIC concentration in media. For the same biomass, the absolute value of zeta potential increased significantly with pH increase from 4 to 7 but at increments much smaller than that of the three different biomasses. For instance, at pH pH 7, the zeta potentials of 0-biomass, 160-biomass or 320-biomass at -31.6, -48.8 and -59.5 mv, respectively, while for 320-biomass, the zeta potentials were -50.3, -52.1, -52.9, and -59.5 mv at pH 4, 5, 6, and 7, respectively.

4.2.4.2.3 Effect of Pb concentration

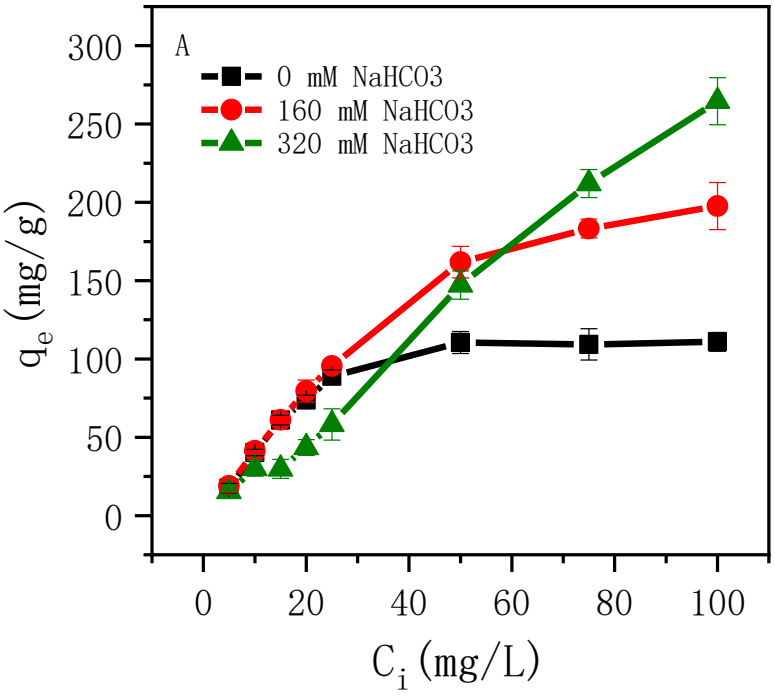

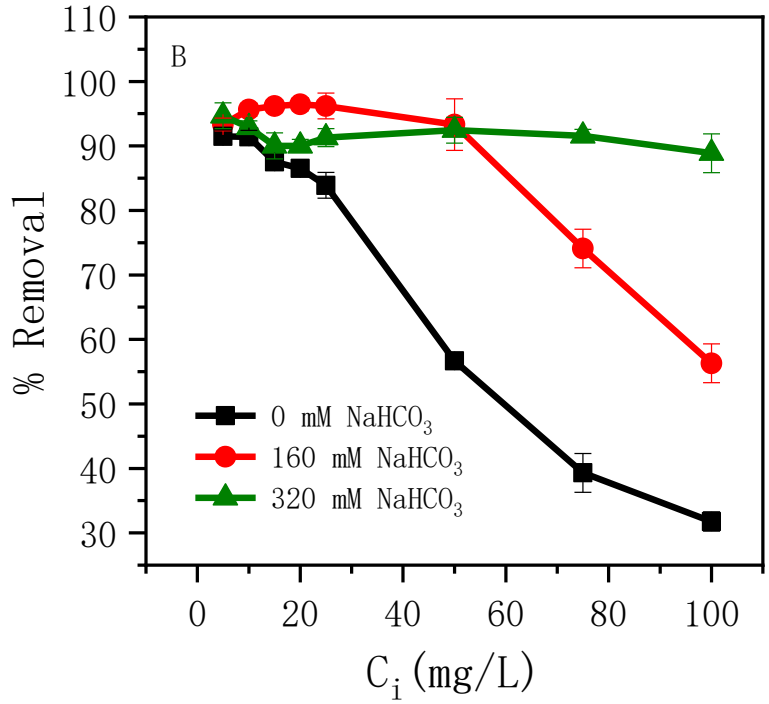

Figure 4-12 Equilibrium adsorption (A) and % removal (B) at different initial Pb(II) concentration (in the range of 5-100 ppm) at pH 7 and 25 ℃.

Initial ion concentration is an important factor determining the driving force of mass transfer between the bulk solution and the surface of solid adsorbent. Figure 4-12 shows the q_e (mg/g) and the % removal of Pb (II) at the same adsorbent (biomass) dose (0.3 g/L) at different lead concentrations ranging from 5 to 100 mg/L at 303.15 K. The equilibrium lead adsorption on unit biomass (q_e) increased while the lead % removal decreased when the initial lead concentration increased with all the three different types of biomasses. The lead % removal of 0 mM $NaHCO_3$ biomass decreased about three times from 91.5% to 31.8%and that the 160 mM $NaHCO_3$ biomass decreased nearly two times from 95.6% to 56.3%, when the initial lead concentration increased 20 times from 5 ppm to 100 ppm. For the same range of initial lead concentration change, the lead removal of the 320 mM $NaHCO_3$ biomass decreased only slightly from 94.7% to 88.9%. The different impacts of initial lead concentration on % lead removal can be explained by the aforementioned drastically different lead adsorption capacities of the three different biomasses.

It is reasonable to hypothesize that at low metal ion concentration, the removal of metal ions is relatively high due to the abundant active sites on the surface of the adsorbent (i.e., biomass in this study) in relevance to the available metal ions, which lead to a relatively small ions/sites ratio [69]. With the increase of the initial metal ion concentration, the ratio would increase and eventually approach and then exceed 1, at which point the ions in solution would exceed adsorption capacity of the biomass. Since the 320-biomass had the largest number of adsorption ligands (corresponding to the largest q_m) among the three, it is logical that the decrease of its lead %

removal with the increase of initial lead ion concentration was the slowest among the three types of biomasses.

4.2.4.2.4 Thermodynamics of biosorption

Experiments were performed to determine the adsorption capacities of 0, 160, and 320-biomasses in a temperature range of 25°C-55°C. A negligible difference in the adsorption capacity was observed over the four temperatures tested, as seen in Table 4-8. This is quite reasonable because the number of binding sites on the cell surface, which determines the adsorption capacity, is independent of adsorption temperature. For the thermodynamic parameters, a negative Gibbs free energy is seen across all four temperatures. A negative standard heat of adsorption (i.e., $\Delta H°$) was obtained, indicating an exothermic adsorption. Furthermore, positive $\Delta S°$ values were seen across the temperatures tested, showing an increase in the randomness at the solid-solution interface during biosorption, which is likely caused by the replacement of Pb(II) ions for some of the water molecules on the adsorbent surface [94]. Since the adsorption has a positive entropy value, it is spontaneous over the temperature range tested. As shown in Figure 4-13 and Table 4-8, the standard Gibbs energy change, the standard entropy change, and the standard enthalpy change of lead adsorption by the three types of *N. oleoabundans* are all independent of temperature in the tested range.

The standard enthalpy changes of adsorption showed an evident trend of decreasing when cells were grown in medium containing an increasing amount of DIC while both standard Gibbs energy change and standard entropy change did not exhibit significant variation among the three different types of biomass cultures. The negative $\Delta G°$ and positive $\Delta S°$ indicate the adsorption was an energy-independent spontaneous process and therefore surface adsorption since internal diffusion (alias absorption) by living cells would be an energy dependant process involving

positive transfer of lead ions across the cytoplasmic membrane of cells [38]. This observation is in accordance with the afore discussed kinetic and isothermal data. The negative value of ΔH° indicates the adsorption was an exothermal process.

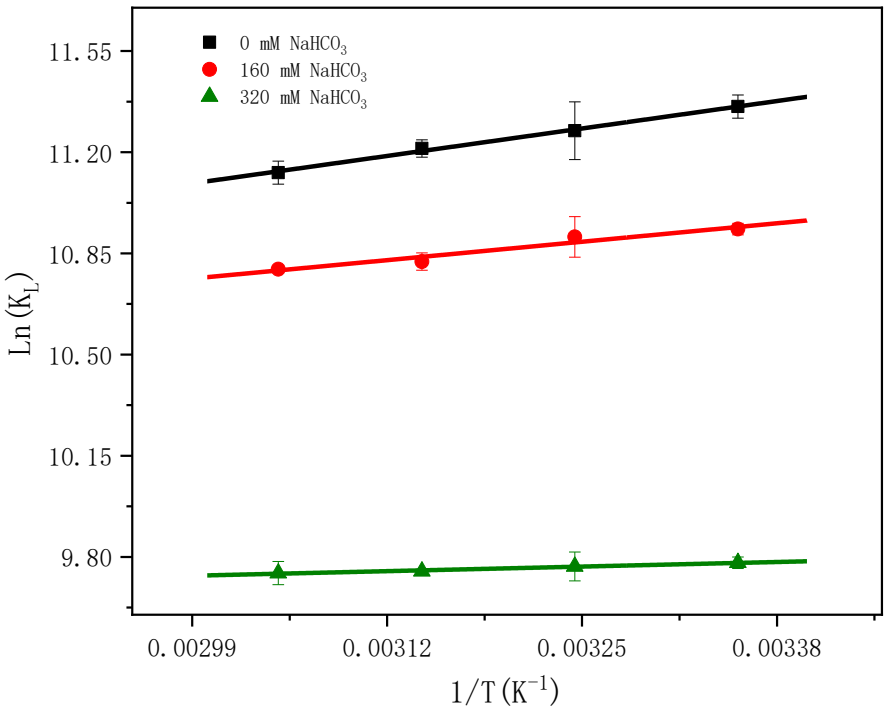

Figure 4-13 Adsorption of Pb(II) onto 0, 160, and 320-biomasses at temperature in the range of 25°C-55°C with biomass dosage 0.30 g/L, initial lead ion concentration between 5.0 and 200.0 ppm and pH 7.

Table 4-8 Summary of thermodynamic parameters of lead ions adsorption by three biomasses with initial [Pb] = 5-200 ppm, [biomass] = 0.30 g/L, pH 7 in temperature range 25-55 °C.

	T (K)	q_m (mg/g)	K_L (L/mol)	ΔG° (kJ/mol)	ΔS° (J/K·mol)	ΔH° (kJ/mol)	R^2
320 mM $NaHCO_3$	298	490.47	85656.48	-28.16	74.06	-6.07	0.996
	308	492.56	78777.44	-27.95			
	318	486.21	74094.72	-27.80			
	328	487.32	68148.08	-27.58			

160 mM $NaHCO_3$	298	313.28	56057.96	-27.10	77.29	-4.08	0.943
	308	304.68	54559.90	-27.04			
	318	307.73	50094.74	-26.83			
	328	305.83	48795.60	-26.76			
0 mM $NaHCO_3$	298	139.14	17674.16	-24.24	77.91	-1.32	0.978
	308	141.87	17446.24	-24.21			
	318	138.77	17156.16	-24.17			
	328	136.81	17052.56	-24.15			

4.2.4.3 Effects of competitive metal ions on lead biosorption

Effects of 100 ppm Na^+, K^+, Ca^{2+}, Zn^{2+}, and Cu^{2+} on the adsorption of lead by *N. oleoabundans* biomass grown in culture containing 320 mM $NaHCO_3$ (i.e., the 320-biomass) were tested at pH 7 and 25ºC and the results are shown in Figure 4-14. Experimental data were fitted to Langmuir model and the corresponding parameters are listed in Table 4-9.

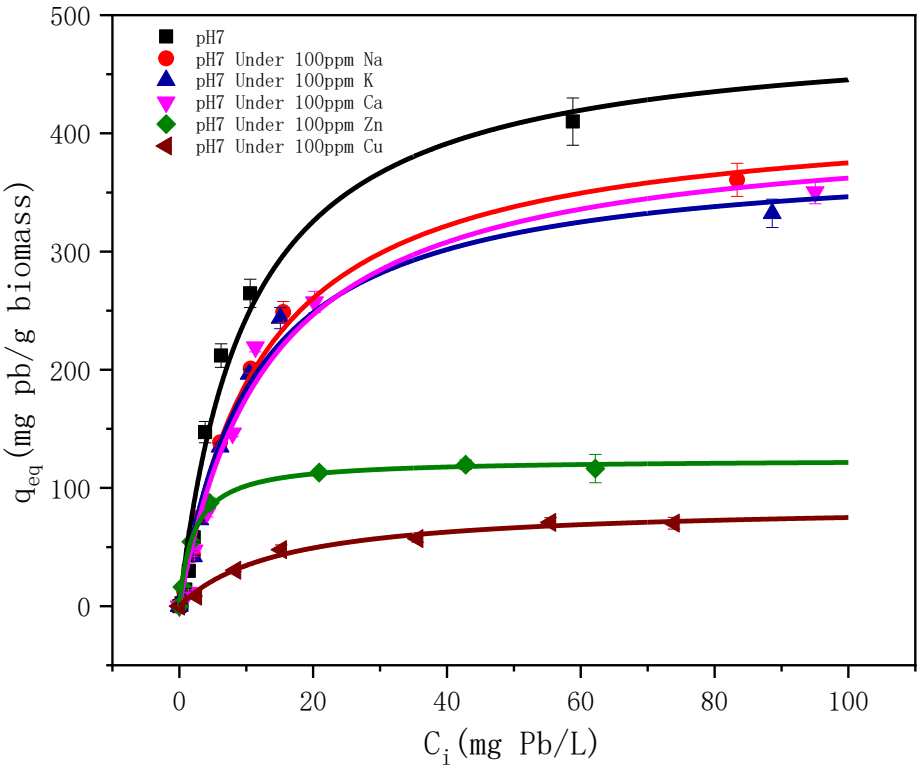

Figure 4-14 Pb(II) adsorption by 320-biomass at pH 7 and 25oC in binaries with the presence of 100 ppm competitive metal ion (K+, Na+, Cu2+, Ca2+ or Cu2+) with a biomass dosage of 0.3 g/L. Experimental data points (symbols) are fitted with Langmuir model (solid line)

Table 4-9 Langmuir isotherm parameters of Pb(II) adsorption by 320-biomass at pH 7 and 25oC in binaries with the presence of 100 ppm competitive metal ions (K+, Na+, Cu2+, Ca2+ or Cu2+) with a biomass dosage of 0.3 g/L.

			Langmuir Parameters		
Competition metal ions	Concentration of competing ion (mM)	Electronegativity [181]	q_m (mg/g)	K_L (L/mg)	R^2
None	0	2.33*	490.41	0.099	0.968
Ca^{2+}	2.50	0.82	410.35	0.075	0.975
Na^{+}	4.35	0.93	421.46	0.081	0.992
K^{+}	2.56	1.00	384.34	0.091	0.983
Zn^{2+}	1.53	1.65	124.21	0.453	0.994
Cu^{2+}	1.57	1.95	86.27	0.066	0.980

*Electronegativity of Pb^{2+}

As shown in Table 4-9, the highest Pb(II) adsorption capacity, 490.4 mg/g, was achieved in the absence of any competing metal ions. An inhibitory effect on the adsorption of Pb(II) was observed in binaries with the presence of 100 ppm of any of the five tested competitive ions, i.e., K^{+}, Na^{+}, Cu^{2+}, Ca^{2+} and Cu^{2+}. Copper presented the largest inhibitive effect on the adsorption of Pb(II) with lead adsorption capacity of 86.27 mg/g, which was only 17.6% of that of the pure lead solution (490.4 mg/g). On the other hand, sodium exhibits the smallest inhibitive effect with an adsorption capacity 85.9% of the pure lead solution. When the Langmuir model was used to fit the data to obtain the K_L value, we found that the addition of 100 ppm zinc ions significantly increased the adsorption affinity (alias equilibrium constant) while the addition of all other four tested ions resulted in the decrease of equilibrium constant. Li *et al.*[94] investigated the performance of *Chlorella sp*. biomass for adsorption of Pb(II) in tertiary systems including Pb^{2+}-K^{+}-Na, Pb^{2+}-Ca^{2+}-Mg^{2+} and Pb^{2+}-Cu^{2+}-Zn^{2+} systems and found that K^{+} and Na^{+} have a little competitive effect, Ca^{2+} and Mg^{2+} had a mild inhibitive effect, Cu^{2+} and Zn^{2+} exhibited the strongest inhibitive effect on Pb(II) adsorption, which are in accordance with our findings in this study.

A summary of the tested metal ions' electronegativities is presented in Table 5, together with their inhibitive effects. It is clear that as the electronegativity increased, a higher competitive effect to lead adsorption was observed. These results are compatible with a study by Rahman and Sathasivam Faculty[66] using *Kappaphycus sp.* cells for adsorption of a series of single metal ion systems, which reported that the adsorption capacity and affinity both increased with the electronegativity of metal ions. It is reasonably hypothesized that the metal ion with the lowest electronegativity would exhibit the least competitive effect on lead adsorption in a binary system due to its small affinity to adsorption sites on cell surface. Sodium exhibited a very small inhibitive effect, which corresponds to its small electronegativity in comparison to that of lead. On the other hand, copper had the largest electronegativity among the five competitive ions, which was close to that of lead. Consequently, Cu^{2+} showed the strongest inhibitive effect and adsorption capacity of lead at the presence of 100 ppm Cu^{2+} (86.3 mg/g) was only 17.6% of that of pure lead solution (490.4 mg/g). However, when compared calcium and sodium, it seems to have an opposite result. Ca^{2+}, which had a smaller electronegativity than Na^{+}, exhibited a stronger inhibitive effect than Na^{+}. This could be explained by the fact that, although both metal ions were present at 100 ppm, the molar concentration of Ca^{2+} (2.50 mM) was only 57.4% of Na^{+} (4.35 mM). The effects of a competitive ion is also related to its molar concentration.

4.2.4.4 Regeneration efficiency

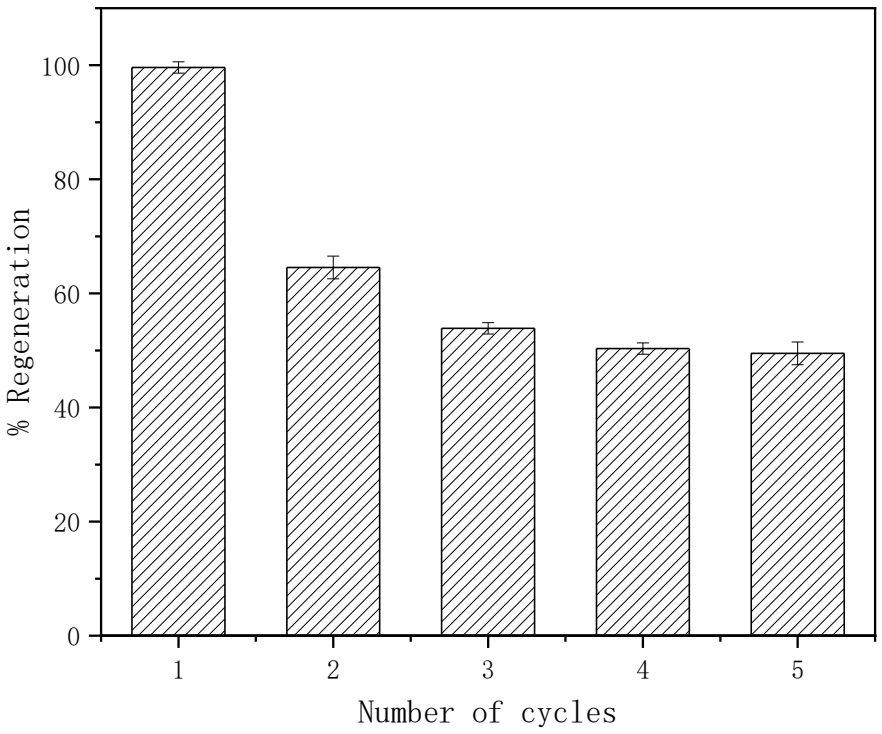

Figure 4-15 Regeneration efficiency of 320-biomass in 5 adsorption/regeneration cycles at 298 K with initial Pb(II) concentration 50mg/L and pH 6.0

As shown in Figure 4-15, equilibrium adsorption of the pristine biomass was 99.6% of the adsorption capacity of pristine biomass. However, the second cycle f adsorption, which involved biomass of one regeneration, had 64% of the adsorption capacity of the pristine biomass (i.e., 64% regeneration efficiency). After 3 cycles, the equilibrium adsorption of regenerated biomass was reduced to 49.5% (the 4^{th} cycle). There was no significant difference (P>0.05) between the q_e of the regenerated biomass after 4 regenerations (the 5^{th} cycle) and 3 regenerations (the 4^{th} cycle). The stabilized biomass (i.e., after three cycles) maintained an equilibrium adsorption of 103.94 mg/L and a Pb(II) %removal of 54% at the tested conditions.

4.2.5 Conclusion

Results of this study indicate that it is possible to remarkably increase the Pb(II) adsorption capacity of *N. oleaabundans* biomass by manipulating the composition of the growth medium, which in this study is to add an appropriate amount of DIC into the medium. The highest Pb(II) adsorption capacity of the biomass grown in media containing 320 mM $NaHCO_3$ (494.14 mg Pb/g biomass) was 3.4 times of that of biomass grown in medium containing 0 mM $NaHCO_3$ (145.9 mg Pb/g biomass). The increase of adsorption capacity with DIC concentration in the tested range, i.e., 0 to 320 mM, corresponded to the increase of the zeta potentials of cells. The changes in FTIR spectra of biomasses indicate that ionizable functional groups, including carbonyl, carboxyl, amide, and phosphate. The kinetics of adsorption equilibrium was completely established after 5min. The adsorption isotherm was fitted to Langmuir and characterized as monolayer surface adsorption. Thermodynamic data shows that adsorption is a spontaneous exothermic process. Results of studies on the effects of competitive ions in binary metal ions systems show that metal ions with larger electronegativity had a more severe inhibitory effect on the adsorption of lead ion.

4.2.6 Acknowledgment

Financial support of Natural Science and Engineering Research Council of Canada (NSERC) in the form of a Discovery Grant RGPIN03657 is gratefully acknowledged.

4.3 Effect of phosphate in medium on cell growth and Cu (II) biosorption by green alga *Neochloris oleoabundans* [1]

Siwei Gu & Christopher Q. Lan*

Department of Chemical and Biological Engineering

University of Ottawa

* Chrisotpher.Lan@Uottawa.ca

[1]The content of this chapter was published and the detail: S. Gu, Y. Su, C.Q. Lan, Effect of phosphate in medium on cell growth and Cu (II) biosorption by green alga *Neochloris oleoabundans*, Chem. Eng. Res. Des. 185 (2022) 186–197.

4.3.1Abstract

Green microalga *Neochloris oleoabundans* cultivated in media containing varied phosphate (K_2HPO_4) concentration was investigated as the biosorbent for Cu(II) removal from aqueous solutions. The highest adsorption capacity of 180.16 mg-Cu/g-biomass was achieved with biomass grown in media containing 300 mg/L K_2HPO_4, which was 2.4 and 2.3 times of that with the biomass obtained with medium containing 100 and 500 mg/L K_2HPO_4, respectively. A semi-empirical isotherm model is proposed to account for the inhibition of Cu(II) adsorption by the cell aggregation induced by Cu(II). Furthermore, it was shown that the Cu(II) induced cell aggregation could be explored to enhance the sedimentation of biomasses to facilitate biomass separation. The Cu(II) adsorption was fast with equilibrium established within 10 minutes of contact time and adsorption kinetics was characterized as pseudo-second order.

Key words: Copper removal, Biosorption, Microalgae, Flocculation, *Neochloris oleoabundans*

4.3.2 Introduction

Copper is a heavy metal that has been exploited extensively since the ancient time of human history. In 2020, 23.4 million tons of copper were consumed worldwide [182]. Copper, like other heavy metals, could be discharged into the ecosystem via pathways including exhaust gases, sediment of dusts, industrial wastewaters without appropriate treatment and runoffs of contaminated soils [183]. Untreated industrial wastewaters containing high concentration of copper ions may also be discharged directly into rivers or lakes accidentally or in natural disasters. High concentration of copper in the aquatic ecosystem, which can ultimately reach humans via water consumption or biomagnification moving up along the food chain, may cause serious diseases such as cancer, nervous system damage and kidney failure [183]. Indeed, the copper concentration in the sediments of some polluted rivers could exceed hundreds of milligrams per kilogram sediment [3], indicating severe copper pollution in these waters, while the drinking water standards set by WHO and USEPA are 2.0 mg-Cu/L and 1.3 mg-Cu/L, respectively [5,6]. Therefore, it is important to develop cost-effective technologies for the removal of Cu(II) from contaminated waters or, even better, the recycle of copper as a valuable resource.

Various technologies have been developed for the removal of cooper from aqueous systems, which include chemical precipitation [13], nanofiltration [184], solvent extraction [185], ion exchange [186], reverse osmosis [187] and adsorption [188]. Among these methods, adsorption is one of the most effective due to their simplicity, cost effectiveness, and eco-friendliness [14]. Biosorption is a special type of adsorption using biomasses as the adsorbents [189], and a wide variety of different biomasses, including yeasts, bacteria, plants and algae, have been investigated for this purpose[190]. Of particular relevance, the adsorption of heavy metals, including copper, from polluted water by aquatic plants and algae has received extensive attention [191].

Microalgae have a number of advantages over other adsorbent technology, including their highly efficient capacity to adsorb metal ions from polluted water, the ability to reuse adsorbent material, low energy costs, and their ability to multiply quickly, therefore removing heavy metal ions from water at relatively low costs [192]. It is possible to use abiotic or dried microalgae for wastewater treatment, which has a high value and development potential [97].

However, low adsorption capacity is one of the major challenges in the application of biosorption to copper (II) recovery at large scale in wastewaters. To this end, researchers have successfully improved the heavy metal adsorption capacity of algal cells by modifying the culture medium. For instance, Gu et al. [67] investigated the effect of dissolved inorganic carbon (DIC) to green microalgae *N. oleoabundans* for biosorption of lead (II), showing that DIC could significantly influence biomass growth and biosorption of the cells. Joo et al. [18] found that algae growing in a phosphate rich medium could adsorb heavy metals significantly more than conventional growth medium, improving performance by 1.6-9.4 folds. Li et al. [42] proposed a method for the removal of lead (II) from water using *Chlorella sp.* QB-102 cultured in media containing different concentrations of phosphate (20, 40, 120, 280 and 580 mg/L) and found that the algal biomass grown in 280 mg/L phosphate medium had the highest adsorption capacity for Lead (II) (635.8 mg/g).

On a related note, in a previous study, copper was found to cause the unicellular cells of *N. oleoabundans* to aggregate [14]. While the aggregation reduced the adsorption capacity, we hypothesize that copper may be employed to enhance the sedimentation of cells, leading to higher biomass recovery efficiency%.

In this study, we investigated for the first time the concentration of phosphate in medium on cell growth, cell surface structure, and Cu(II) adsorption of green microalgae *N. oleoabundans*. Flocculation of biomass was also investigated at different concentrations of Cu(II) to verify the feasibility of exploiting the cell aggregation accompanying Cu(II) for enhanced biomass recovery.

4.3.3 Materials and methods

4.3.3.1 Preparation of algal biomass and copper solution

Neochloris oleoabundans, (UTEX# 1185) was purchased from the microalgal culture collection at the University of Texas in Austin. Modified Bristol Medium was using for biomass cultivation, which contained (analytical grade, per liter): 0.35 g $NaNO_3$, 0.0823 g $MgSO_4$, 0.025 g $CaCl_2$, 0.025 g NaCl, 0.0068 g $FeCl_3$ [96] and 1 mL of A5 solution, which was composed of (analytical grade, per liter) 1.6423 g EDTA-Fe, 2.86 g H_3BO_3, 1.81 g $MnCl_2{\cdot}4H_2O$, 0.22 g $ZnSO_4{\cdot}7H_2O$, 0.079 g $CuSO_4{\cdot}5H_2O$, and 0.039 g $(NH_4)_6Mo_7O_2{\cdot}4H_2O$ was added [96]. K_2HPO_4 (Sigma Aldrich, USA) was added to medium at concentrations as 100, 200, 300, 400 or 500 mg/L. The media were sterilized at 121°C for 20 minutes prior to use. The microalgae were cultivated for 15 days until reaching transition phase, and then the biomass was harvested by centrifugation, which was washed twice using deionized water before being stored at -80 °C in a freezer for future use. Media containing five different phosphate concentrations, i.e., 100, 200, 300, 400 and 500 mg/L K_2HPO_4 (17.8, 35.6, 53.3, 71.1 and 88.9 mg/L phosphorus) were tested for alga cultivation and the algal biomasses grown in these media are reported as 100-P, 200-P, 300-P, 400-P and 500-P, respectively.

Copper stock solution (1000 mg/L) was prepared by dissolving appropriate amount of $Cu(NO_3)_2 \cdot 3H_2O$ into deionized water. The chemical reagents used in this study were all of analytical grade and purchased from Sigma, USA.

4.3.3.2 Batch biosorption experiments

Batch biosorption experiment was carried out in a 2 mL centrifuge tube using deionized water, biomass, and Cu(II) stock solution to ensure a concentration of 5-50 mg/L Cu(II) and 0.3 g/L biomass under 25℃. The initial pH 7 of the mixture was adjusted to the desired value by adding 0.1 N HCl or 0.1 NaOH prior to the addition of biomass. The biomass was taken out of the freezer and thawed at room temperature (25 ℃) in advance. Then the mixture was shaken at 180 RPM for a period of contact time as specified in the text at room temperature, which was then centrifuged 13000 rpm(18500 rcf) for 10 min. The concentration of residue Cu(II) in the supernatant was determined using AAS. The detail is shown in previous paper [14].

There is an evaluation of the effect of initial pH (2-7), adsorbent dosage (0.05-0.3 g/L), initial copper concentration (5-50 mg/L) and contact times (1, 5, 15, 30, 45 minutes) under room temperature.

All experiments were performed in triplets and the reported values are the arithmetic means with standard deviation (as errors bars in graphs).

$$q = \frac{C_0 - C}{C_b} \tag{4.25}$$

$$Copper\ removal\% = \frac{C_0 - C}{C_0} \times 100\% \tag{4.26}$$

where C_0 (mg/L) is the initial concentration of copper solution, C (mg/L) the final concentration of supernatant, C_b the concentration of biosorbents, i.e, algal biomass (g DCW/L), q (mg/g

DCW), the mass of Cu(II) adsorbed by unit mass of biosorbents, and %removal the efficiency of Cu(II) removal.

4.3.3.3 Microalgal flocculation

To ensure consistency of algae, 300-P biomass was used as the biosorbent in this experiment. The initial concentration of microalgal biomass in suspension was estimated from the optical density measured at 700 nm during the flocculation test. For each 10 mL 0.5 g/L algal sample in a 15 mL centrifuge tube, appropriate volume of the Cu(II) stock solution was added to reach a predetermined concentration of Cu(II), i.e., 0, 10, 20, 30, 40, 50, 100 and 200 mg/L, which is followed by rapid mixing using a vortexer for 30 seconds and then place on a test tube rocket upright. Sample of 1 mL was extracted from the supernatant without disturbing the settling cells at pre-determined time intervals, i.e., 5, 10, 30, 60 min, to measure the biomass concentration using UV-Vis spectrophotometer at 700 nm. The control group was obtained by centrifugation at 4000rpm (5700 crf) for 10 minutes.

The percentage of the microalgal biomass remaining in tube was estimated using Eq 4.27:

$$Residual\ biomass\% = \frac{C_f}{C_i} \times 100\% \quad 4.27$$

Harvest efficiency% is an intuitive way to express the efficiency of microalgae harvest by sedimentation, which can be expressed as Eq 4.28:

$$Harvest\ efficiency\% = \frac{C_i - C_f}{C_i} \times 100\% \quad 4.28$$

where C_i (mg/L) and C_f (mg/L) are represent as the initial concentration of biomass and after the settlement of biomass at the end of Cu(II) adsorption.

4.3.3.4 Analyses and characterization

For biomass concentration, 1 mL of the sample was extracted from the cultivation bottle and the optical density was determined by a GENESYS^{TM} 10S UV-VIS spectrophotometer (Thermo Fisher Scientific Inc., USA). To avoid the interference of photosynthetic pigments, the wavelength of 700 nm was selected for spectrometric measurement of biomass concentration in this study. The biomass was centrifuged twice in deionized water under 5000 RPM to remove chemicals and debris remaining in the supernatant. The washed biomass was dried overnight in an oven at 60 ℃. Then, the dried biomass is weighed to get the dry biomass concentration. The linear relationship between OD_{700} and *N. oleoabundans* biomass concentration of was determined showing in following Eq 4.29.

$$X = 0.4332 \times OD_{700} - 0.1051 \quad (4.29)$$

where OD_{700} is the optical density under 700 nm wavelength and X (g/L) refers to the dry cell weight (DCW) concentration of algal concentration.

The following method was used to determine chlorophyll cell content [193]. Each 2 ml sample was centrifuged at 13,000 rpm (18500 crf) for five minutes. Afterwards, the supernatant was discarded leaving the algal pellet on the bottom, and 2 mL of 99.9% methanol was added to the pellet, mixed properly, and left in 4°C refrigerator overnight at in the dark. The following day, sample was centrifuged at 13,000 rpm (18500 crf) for five minutes, and the supernatant was used to estimate chlorophyll cell content. 1 mL sample was discharged into 2 mL cuvette and optical densities at 645 and 663 nm were determined using a spectrophotometer. Chlorophyll cell content (mg/g) in supernatant was determined and calculated according to the Eq 4.30 below:

$$Chl\left(\frac{mg}{g}\right) = \frac{8.02 * OD_{663} + 20.21 * OD_{645}}{X} \quad (4.30)$$

The concentration of copper in solution was determined by flame atomic absorption spectrophotometer (Thermo Fisher Scientific, USA). Since AAS cannot evaluate high copper concentrations beyond detection line, diluting the solution to a certain concentration using deionized water is necessary. The supernatant containing Cu(II) was diluted 10 times with deionized water within standard concentration and then the concentration was determined using AAS.

To measure the zeta potential of cells, Zetasizer nanometers (Malvern Panalytical, UK) were used. Samples were diluted to 0.1 OD_{700} using deionized water before testing.

The infrared spectra of cells with or without adsorption of Cu(II) were analyzed using a Cary 630 FTIR spectrophotometer (Angellent technology, USA). Microalgae samples were prepared by filtering the culture using a 0.45 um membrane filter, dried at 60 ℃ in oven overnight, and then subjected to analysis.

To measure phosphate concentration in medium, the molybdenum blue colorimetric method (Sigma Aldrich, USA) was used [194]. To determine the concentration of phosphate in the supernatant, centrifuge a 40mL sample for 10 minutes at 6000 rpm. After extract 1mL supernatant to 2 mL centrifuge tube, ammonium molybdate [(NH4)6Mo7O24·4H2O] was added into the mixed solutions and pH was adjusted to 5.5 by adding with 0.1 M HNO3 into the mixed solutions. The samples were incubated for 20 minutes before analyzing for color. GENESYS™ 10S UV-VIS spectrophotometer (Thermo Fisher Scientific Inc., USA) was used to measure the absorbance of solutions at 880 nm.

For the determination of phosphate concentration in biomass, 20 ml of algae sediment were digested by adding 20 mL of 5% HNO_3 solution in 1 hour. After that, 1 mL sample was extracted and measured using the molybdenum blue colorimetric method described before.

4.3.4 Results and discussion

4.3.4.1 Effects of phosphate concentration on algal cell growth

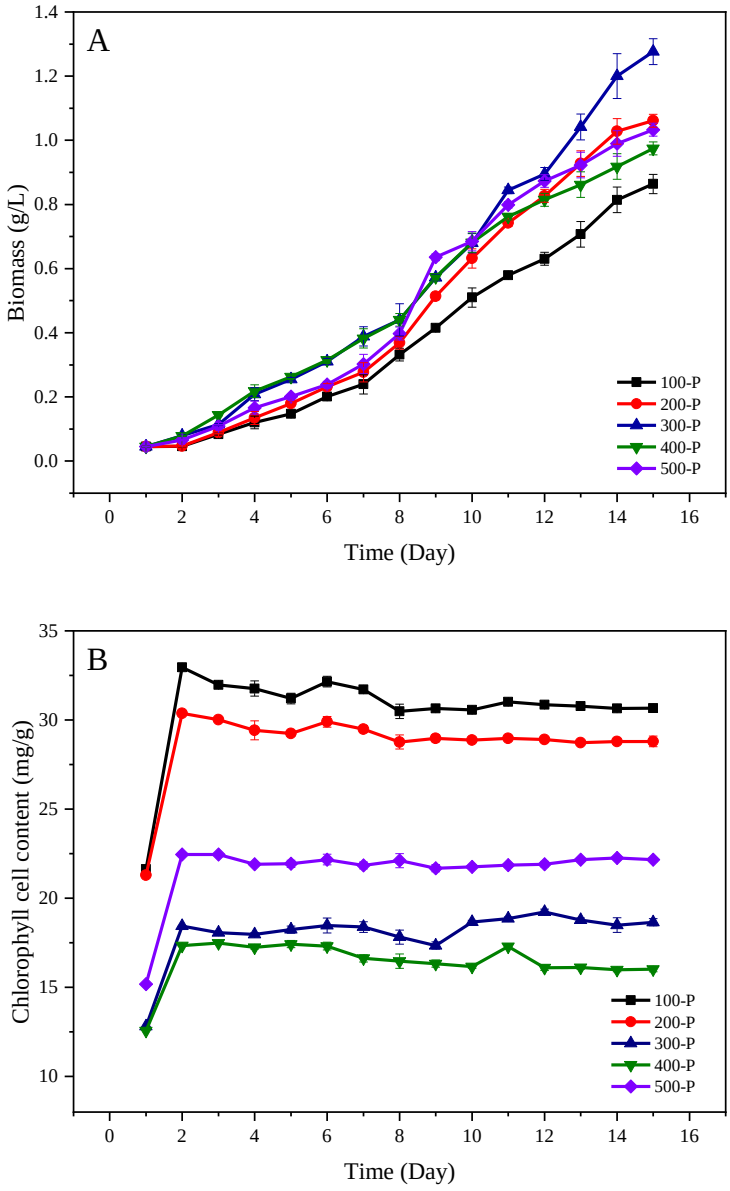

Figure 4-16 Growth curve biomass concentration (A) and chlorophyll cell content (B) for *N. oleoabundans* under different phosphate concentrations (initial biomass concentration 0.05g/L).

Table 4-10 Effects of different phosphate concentration on biomass, cell density, phosphate removal% of *N. oleoabundans* cultured for 15 days.

K_2HPO_4 (mg/L)	N/P mass ratio	Biomass (g/L)	Cell density (10^6 cell/ml)	Cell Mass (μg/cell)	μ_{max} (day^{-1})	Cell P-content (mg/g)	Residual phosphate (mg/L)	Phosphate removal (%)
100	3.24	0.86	1.53	0.56	0.20	15.32	39.51	60.49
200	1.62	1.06	1.28	0.83	0.21	19.42	37.38	81.31
300	1.08	1.28	2.59	0.49	0.29	34.21	54.92	86.27
400	0.81	0.97	1.20	0.81	0.24	24.23	42.46	85.85
500	0.65	1.03	1.41	0.73	0.19	21.24	75.33	84.93

Green alga *N. oleoabundans* was cultivated with initial concentration 0.05 g/L in medium containing varied initial phosphate concentration, i.e., 100, 200, 300, 400 and 500 mg/L K_2HPO_4, and the growth curves are shown in Figure 4-16A. Based on the data, there was a conventional microalgal growth pattern, with an exponential phase lasting from day 1 to 7. With the light limiting, microalgae entered the linear phase after 7 days of cultivation, and the highest biomass was harvested for all the cultures. 300 mg/L K_2HPO_4 was the optimal concentration for *N. oleoabundans* growth. Cell growth was significantly reduced when phosphate concentrations in medium increased to 400, 500 mg/L K_2HPO_4 or decreased to 100, 200 mg/L K_2HPO_4. The maximum biomass concentrations (achieved at the 15th day) were 0.86, 1.06, 1.28, 0.97 and 1.03 g/L for 100, 200, 300, 400 and 500 mg/L K_2HPO_4, respectively. Those data are in general in agreement with that reported by Kim et al. [195] on three different microalgae, i.e., *Chlorella sp.*, *Dunaliella salina DCCBC2* and *Dunaliella sp*. It was found that increasing phosphate concentration from 4.4 to 69.68 mg/L K_2HPO_4 led to an increase in biomass concentration in culture but a reduction in biomass concentration when phosphate concentration further increased

to 348.4 mg/L K_2HPO_4. Similarly, Feng et al. [196] found that increasing phosphate concentration (0 to 40 mg/L K_2HPO_4) in the medium could result in the increase of biomass productivity of another green algae *Chlorella zofingiensi*. Also, Li et al. [42] investigated effect of phosphate concentration (0 to 580 mg/L) for *Chlorella sp*. QB- 102, getting highest biomass under 280 mg/L K_2HPO_4.

As shown in Figure 4-16B, the chlorophyll cell content (mg/g) at different phosphate concentrations had very similar patterns, i.e., increasing in the first two days to reach a plateau of 30.65, 28.79, 18.49, 15.99, and 22.25 ug/g for 100-P, 200-P, 300-P, 400-P, and 500-P biomass, respectively. These data point to a trend of decreasing that chlorophyll cell content with the increase of phosphate concentration with that of the 500-P biomass being seemingly an outlier. It has been well established that chlorophyll cell content can be modulated by culture conditions, which is dependent on both species and cultivation mode, such as light, phosphate concentration, temperature, nitrogen, agitation, and N/P mass ratio etc. [197]. Of particular relevance, our previous results [193] demonstrated that chlorophyll cell content would decrease under nitrogen limiting conditions since the N-rich chlorophyll molecules might be used as part of the intracellular nitrogen reservoir. The stable chlorophyll content of cells as shown in Figure 4-16B can thus be viewed as an indication that nitrogen limitation did not happen in the course of the 15-day cultivation of *N. oleoabundans* under the tested conditions. Figure 4-16B also shows that the chlorophyll cell content in general decreased with the increase of phosphate concentration in medium with the 500-P as an exception. Since nitrogen source (i.e., $NaNO_3$) concentration was the same in all the media used in this study, these results indicate a trend of decreasing cell chlorophyll content with the decrease of N/P mass ratio, which is compatible to many reports in literature. For instance, Song et al. [198] investigated the cultivation of marine microalga

Dunaliella tertiolecta under different N/P mass ratios and found that the chlorophyll cell content continued to increase when the N/P mass ratio increased from 8.8:1 to 35.4:1. Zhang et al.[199] reported in a study on nutrient (N and P) removal from synthetic municipal wastewater using *C. vulgaris* that, when increasing N/P mass ratio from 3.9 to 4.9, average chlorophyll-a increased from 27.01 mg/g to 32.58 mg/g.

The biomass concentration, cell density, and phosphate removal efficiency% of *N. oleoabundans* cultured for 15 days are shown in Table 4-10. The tested N/P mass ratio was in the range of 0.65-3.24, which is quite low comparing with commonly tested N/P mass ratio range in literature. This is because the primary objective of this research was to investigate the effects of phosphate in medium on the adsorption capacity of algal cells to remove Cu(II). The experimental results also provide an opportunity for us to evaluate the potential of *N. oleoabundans* for phosphate removal from high phosphate wastewaters, which is an important environmental challenge [200,201]. When the phosphate concentration was 100, 200, 300, 400, and 500 mg/L, the phosphate removal% were 60.5%, 81.3%, 86.3%, 85.8%, and 84.9%, respectively. It is interesting to notice that the phosphate removal increased with its concentration in medium in the range of 100-300 mg/L K_2HPO_4. These somewhat counterintuitive results could be explained by the increase of both biomass concentration and the P-contents of biomass (Table 4-10) in this range.

While the results of the current study show that *N. oleoabundans* could achieve 60.49-86.27% P-removal under the tested conditions, it is worth mentioning that the same alga has been demonstrated to be able to consume nitrogen and phosphate completely from wastewater containing high concentrations of phosphate (47.1 mg/L) and high sodium nitrate (850 mg/L) while achieving high biomass production (2.1 g/L) under optimal conditions [122]. In other

words, while there is a potential of using *N. oleoabundans* (and other microalgae) for simultaneous removal of nutrients (i.e., N and P) and heavy metal ions such as Cu(II) from contaminated wastewaters, certain tradeoffs may have to be made between the different objectives, which should be based on specific wastewaters to be treated.

4.3.4.2 Characterization of the biosorbent

4.3.4.2.1 FTIR spectra

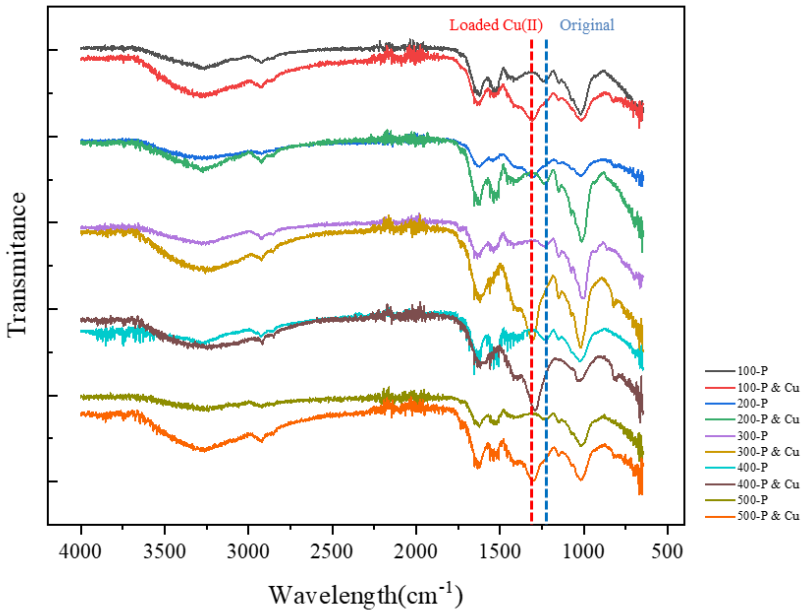

Figure 4-17 FTIR spectra of *N. oleoabundans* 300-P biomass before and after Cu(II) adsorption with 50 mg/L Cu(II) aqueous solution at pH 7.0.

Table 4-11 FTIR peaks and redshift of 300-P biomass before and after Cu(II) adsorption.

	Before (cm^{-1})	After (cm^{-1})	Redshift (cm^{-1})	Redshift (%)
100-P	1148.17	1149.35	-1.18	0.10
	1241.15	1236.11	5.04	0.41
	1623.60	1622.51	1.09	0.07
200-P	1071.74	1075.25	-3.51	0.33
	1238.53	1308.06	-69.53	5.61
	1623.44	1636.43	-12.99	0.80

300-P	1150.80	1150.62	0.18	0.02
	1236.77	1308.19	-71.42	5.77
	1653.20	1623.87	29.33	1.77
400-P	1150.87	1150.50	0.37	0.03
	1230.60	1289.69	-59.09	4.80
	2924.18	2930.55	-6.38	0.22
500-P	1243.27	1246.28	-3.01	0.24
	1623.58	1623.66	-0.09	0.01

In FTIR analysis, the main bands corresponding to the functional groups of the sorbents before and after Cu(II) adsorption were identified within the range of 500~4000 cm^{-1} (Figure 4-17). The absorbance in the range of 3400~3600 cm^{-1}represents the O-H groups, that in the 1590~1620 cm^{-1} range is attributed to the asymmetrical stretching of C=O bond, which is commonly found in carboxylic (COOH) and acyl groups (C=O); the stretching of C-H bond absorb light in the range of 2880~2910 cm^{-1}, and C-O-C stretching in the range of 1010~1034 cm^{-1}; the peak at 1623 cm^{-1} can be assigned to S=O stretching. The peaks representing phosphorus-oxy bonds, e.g., P=O stretch in organic phosphates, P-O-C stretch of aliphatic phosphates, P-O-C stretch of aromatic phosphates are 1350–1250, 1050–990 and 1240–1190/995–850 cm^{-1}, respectively [202]. For methyl phosphonic acid, peaks for $P\text{-}O^{-}$, P=O, P-OH were reported as 800-1050 cm^{-1}, 1100-1300 cm^{-1} and 2100-2220 cm^{-1}, respectively [203]. As shown in Table 4-11, our results indicate that there is a peak in the range of 1350-1250 cm^{-1}, which corresponds to the phosphorus bond (P=O) in organic phosphate at the surface of all pristine cells. This peak had substantial redshift from 1238 cm^{-1} to 1308 cm^{-1} after Cu(II) adsorption (loading Cu(II)) with the exception of 500-P. Furthermore, as highlighted in Figure 2, the intensity of the peak on Cu(II) loaded biomass was vastly larger than that on the corresponding pristine biomass except 200-P. These data suggest that the P=O bond in organic phosphates in association with macromolecules on the surface of *N.*

oleoabundans likely served as one of the primary binding sites for Cu(II) adsorption. The binding of Cu(II) onto the partially negative O atom in the P=O bond might be responsible for both the redshift and increase of absorbance intensity as Cu(II) might attract the electron cloud of the P=O bond to it, causing redistribution of electron cloud within the bond. It has been demonstrated that both the spectrum shift of absorbance peak [204] and the change of peak intensity [205] might be associated with the change of the hybridization state or electron distribution within a molecular bond. According to FTIR, *N. oleoabundans* cell wall has a bunch of carboxyl, phosphate and hydroxy group, which contributes to biosorption of Cu(II).

4.3.4.2.2 Zeta potential of cells

Zeta potential refers to the electrical potential developed at solid-liquid interfaces due to relative motion between solids and liquids. And the value of zeta potential could be used to describe ionic strength on cell surface [206,207]. The zeta potentials of different biomasses are shown in Figure 4-18A as a function of pH. As data indicated, zeta potential data suggest that the surfaces of algae were all negatively charged in the pH range of 2 to 7. Since the highest adsorption capacity of Cu(II) was at pH 7 in the tested range, the following biosorption experiments were performed at pH 7. Furthermore, the absolute value of the negative zeta potential of biomass increased with increasing buffer pH. It is worth noting that the absolute value of zeta potential increased from 100-P to 300-P and decreased from 300-P to 500-P, which is consistent with the pattern of the cell P-content (Table 1) and the equilibrium Cu(II) adsorption of corresponding biomasses (Figure 4-18B).

4.3.4.3 Adsorption of Cu(II)

4.3.4.3.1 Effect of pH on Cu(II) adsorption

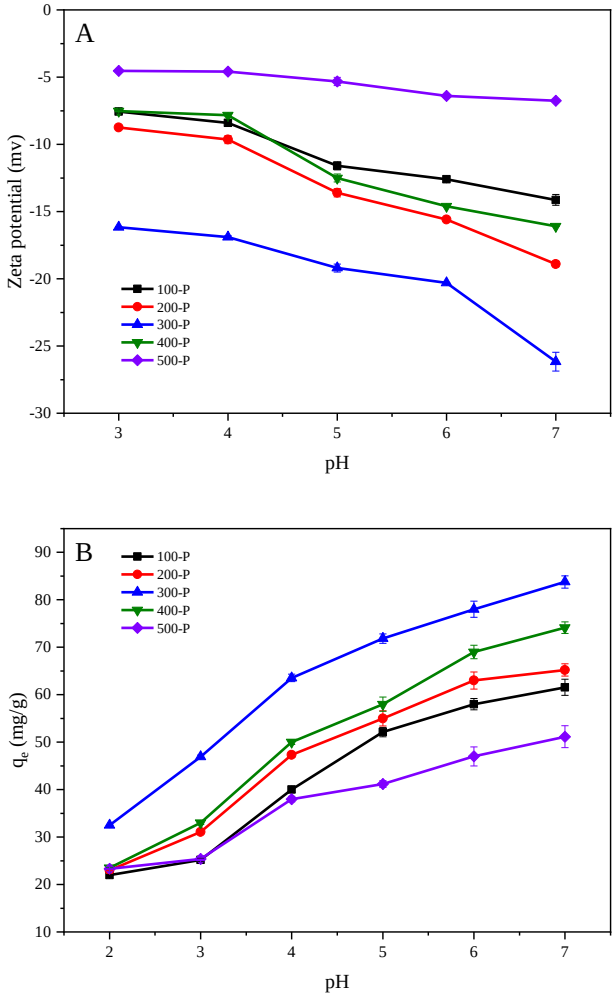

Figure 4-18 Effect of pH value and phosphate concentration on Zeta potential (A) and equilibrium adsorption(B) of Cu(II) from pH 2-7 under 0.3 g/L biomass, 50mg/L Cu(II).

The equilibrium adsorption of Cu(II) by different biomasses at different pH (2-7) was investigated at room temperature. The results are shown in Figure 3B. The equilibrium Cu(II) biosorption of all biomasses increased with increasing pH from 2 to 7. It should be noted that increasing of equilibrium adsorption with pH was more rapid in the pH range of 2-4 than in the range of 5-7, which are consistent with our previous results for lead adsorption using the same

type of algal species [14]. The effect of pH on equilibrium adsorption is relative with functional groups (carboxyl, phosphate and hydroxy) on cell surfaces. There is a competition between H(I) and Cu(II) for occupancy of the binding sites due to protonation of the active biosorption sites. As pH increases, equilibrium biosorption increases due to a decrease in competition between protons and metal ions for the same functional groups on the cell surface, resulting in a stronger electrostatic attraction between Cu(II) and functional groups. These results are in agreement with literature data as well. For instance, Wanta et al. [208] reported a similar result, in which they investigated the biosorption of Cu(II) using *Chlorella sp.* in which copper removal% increased from 35.2% to 96.1% when pH is increased from 2 to 5. Similarly, Fraile et al.[73] found that the equilibrium adsorption of Cu(II) by *Chlorella sp.* increased from 2.98 mg/L to 16.00 mg/L when pH increased from 1.5 to 5.

With increasing pH, equilibrium adsorption increases, which is consistent with an increase in the absolute negative zeta potential. Moreover, the highest equilibrium Cu(II) adsorption was obtained by 300-P at the same pH. There may be some significance in the fact that this pattern agrees with that of the absolute value of the negative zeta potential, which also increased from 100-P to 300-P, but decreased from 300-P to 500-P. Following the same pattern, the 300-P showed the highest zeta potential (Figure 4-18A), the highest cell P content (Table 4-10) and the greatest redshift (5.77% change) in FTIR spectrum (Table 4-11). It would seem that this observation confirms the hypothesis that the phosphoryl groups may be one of the primary functional groups in Cu(II) adsorption. With 300-P biosorbent at pH 7, the highest equilibrium biosorption could be obtained. Following experiments will be carried out under pH 7.

4.3.4.3.2 Biosorption kinetics

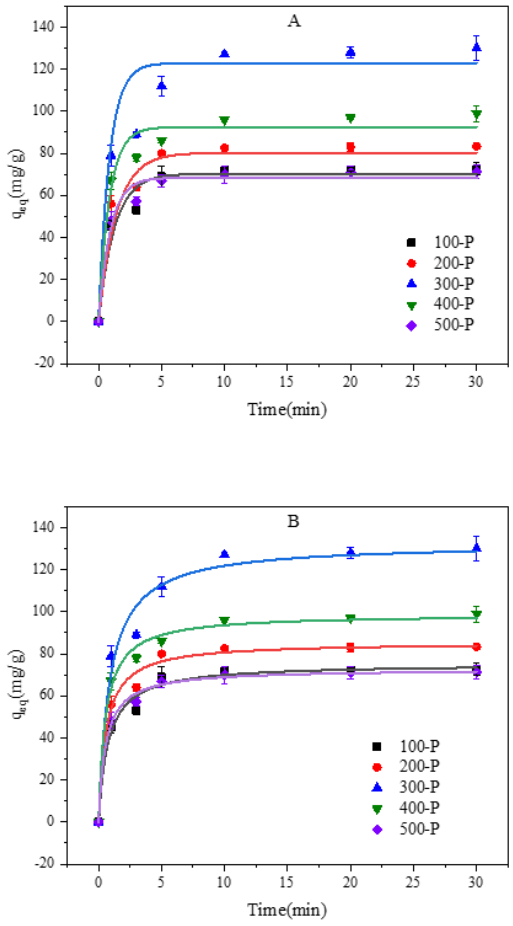

Figure 4-19 Effect of contact time for the removal of Cu(II) ions onto *N. oleoabundans* using pseudo-first (A) and pseudo-second (B) model, 0.3 g/L biomass, 50ppm Cu(II) and pH7.

Table 4-12 Kinetic parameters for the adsorption of Cu(II) on *N. oleoabundans*.

Kinetic model	Parameters	Concentration of Pb(II) ion solution (mg/L)				
		100	200	300	400	500
Pseudo-first	K_1(min^{-1})	0.79	1.02	0.72	1.15	1.07
	$q_{e,cal}$ (mg/g)	70.26	80.15	122.89	92.41	68.34
	R^2	0.9515	0.9563	0.9265	0.9573	0.969
	SSE	170.63	200.01	793.11	260.13	102.41
Pseudo-second	K_2(g/min^{-2})	0.017	0.02	0.009	0.018	0.024

$q_{e,cal}$(mg/g)	75.25	85.46	132.47	98.82	72.77
R^2	0.9792	0.9989	0.9737	0.9902	0.9927
SSE	73.16	23.34	283.68	59.58	24.18

The pseudo-first order model, i.e., Eq. 4.31, considers the rate of adsorption to be proportional to the number of unoccupied sites [209]:

$$Q = Q_e[1 - \exp(-k_1 t)] \quad 4.31$$

where k_1 (min^{-1}) is the rate constant of pseudo-first order, Q_e (mg/g) and Q (mg/g) are the equilibrium Cu(II) adsorption and the Cu(II) adsorption at time *t*, respectively.

The pseudo-second-order kinetic model, i.e., Eq. 4.32, assumes that the rate-controlling step of the biosorption process is the interaction between the unoccupied sites of the biosorbent and heavy metal ions [210].

$$\frac{t}{Q} = \frac{1}{k_2 Q_e^2} + \frac{t}{Q_e} \quad 4.32$$

where k_2 ($g \cdot mg^{-1} \cdot min^{-1}$) is the rate of constant of pseudo-second order.

Kinetic parameters provide important information regarding the control mechanisms of biosorption processes, including mass transfer (i.e., diffusion) or ionic reaction, which is vital for the design and modeling of biosorption processes. As shown in Figure 4-19, that the Cu(II) equilibrium adsorption increased rapidly with time within the first 5 minutes and approached plateau at 10 minutes of incubation for all biosorbents. The Cu(II) adsorption increased only slightly between 10 and 30 minutes of incubation.

The kinetic data were fitted with the pseudo-first-order model and the pseudo-second-order model, and the relevant parameters are summarized in Table 4-12. The results indicate that the adsorption was the pseudo-second order ($0.97<R^2<1.00$) not pseudo-first order ($0.92<R^2<0.97$). This is compatible with studies by other researchers. For instance, Lucaci et al. reported pseudo-second order adsorption of Cu(II) from aqueous solutions by marine Red Algae *Callithamnion corymbosum sp.*, finding that based on the correlation coefficient (R^2), the sorption kinetics was fitted by the pseudo-second-order kinetic model [190]. Among the different cultures, 300-P had the highest Cu(II) adsorption at any time.

The removal of Cu(II) by microalgal cells could be achieved via two different processes, i.e., adsorption and absorption. The adsorption of heavy metal ions is a surface phenomenon which can be divided into three stages: 1) metal ions in the bulk solution migrate to the vicinity of a cell by convection; 2) metal ions diffuse to cell surface; 3) metal ions bind onto negatively charged functional groups at cell surface. The absorbance of Cu(II) and other metal ions involves the aforementioned adsorption plus the transportation of charged metal ions across a double-layer cytoplasmic membrane into the cell via specialized Cu transport [59].This process requires the consumption of bioenergy in the form of ATP and is a slow process comparing to adsorption. Since the removal of Cu(II) is quite fast in this study, it appears that adsorption, rather than absorption, is the main mechanism.

4.3.4.3.3 Biosorption isotherm

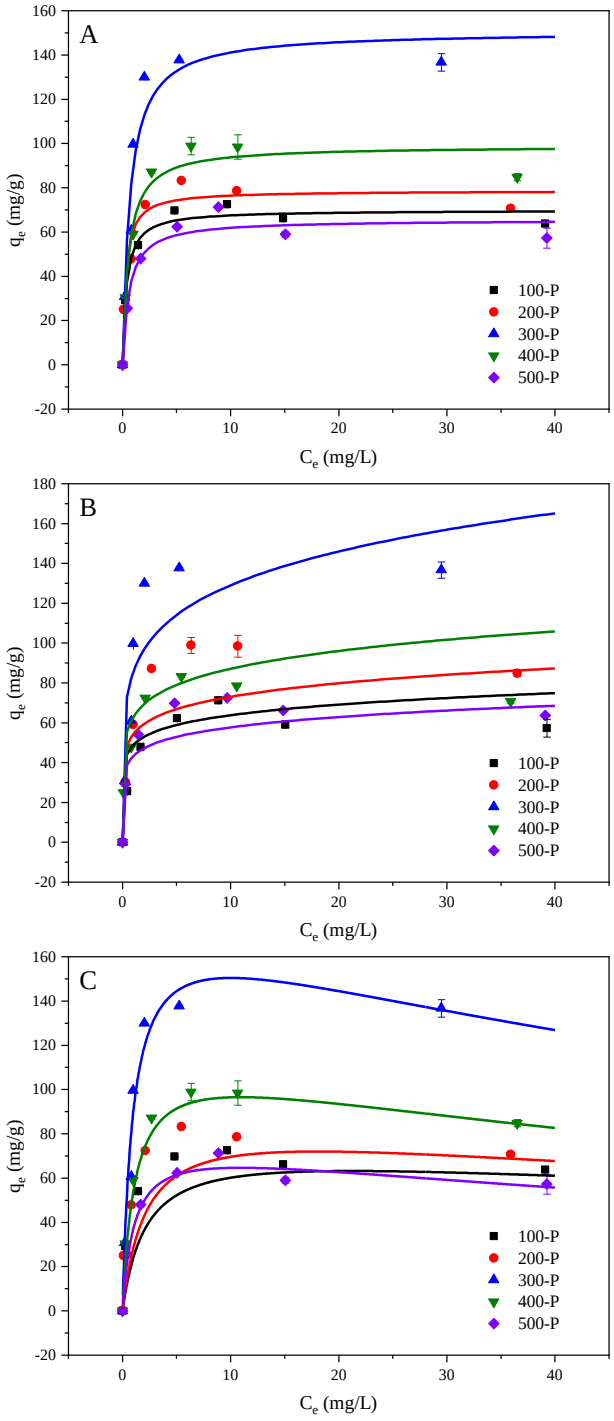

Figure 4-20 Representation of equilibrium data fitted to the Langmuir (A), Freundlich (B) and semi-empirical isotherm (C) models for Cu(II) adsorption by *N. oleoabundans*, 0.3 g/L biomass, pH 7, and 5-50mg/L Cu(II).

Table 4-13 The isotherm model parameters for the adsorption of Cu(II) ions onto *N. oleoabundans* at various concentrations (5–50 mg/L).

Biosorbent	Langmuir			Freundlich			Semi-empirical			
	q_{max} (mg/g)	K_L (L/mg)	R^2	K_F	n	R^2	q_{max} (mg/g)	K_M (mg/L)	K_I (mg/L)	R^2
100-P	69.91	2.82	0.9799	48.9	8.66	0.8856	76.11	2.17	208.81	0.9921
200-P	78.68	3.44	0.9514	54.41	7.81	0.8446	88.98	2.13	153.24	0.9655
300-P	150.66	1.48	0.9468	85.67	5.62	0.7954	180.16	0.99	101.24	0.9643
400-P	98.88	1.83	0.9667	62.94	7.09	0.826	117.01	1.16	103.39	0.9973
500-P	65.55	1.69	0.9511	43.35	8.05	0.8384	77.47	1.08	109.96	0.9813

The capacity of an adsorbent can be described by equilibrium adsorption isotherm, which is characterized by certain constants whose values express the surface properties and affinity of the adsorbent. The Langmuir isotherm is probably the most widely applied adsorption isotherm [211]. A basic assumption of this model is that adsorption takes place at specific homogeneous sites within the adsorbent. The saturated monolayer isotherm is represented as below:

$$q_e = \frac{q_m K_L C_e}{1 + K_L C_e} \quad 4.33$$

where q_m(mg/g) is the adsorption capacity and K_L(L/mg) is an affinity constant related to the energy of adsorption. The value of K_L indicates the strength or affinity of the Cu(II) from synthetic wastewater [212].

The Freundlich isotherm is an empirical isotherm that can be used for non-ideal adsorption and expressed as follows [213]:

$$q_e = K_F C_e^{1/n} \quad 4.34$$

where K_F and n are the Freundlich constants parameter related to the adsorption capacity and adsorption intensity of the adsorbent, respectively.

It is obvious that a model accounting for the effect of Cu(II) on cell aggregation during adsorption is needed to accurately simulating the adsorption process. However, it is difficult to establish a theoretical model to describe this complex effect. Hence, we propose three parameters semi-empirical isotherm model for the system based on non-competitive inhibition, showing in Eq. 4.35. This model assumes that, as the initial heavy metal concentrations increase, biosorbents aggregate then reduce the amount of functional groups on the cell surface and specific surface area, reducing equilibrium adsorption.

$$q_e = \frac{q_m}{1 + \frac{K_M}{C_e} + \frac{C_e}{K_I}} \qquad 4.35$$

Where q_m is the maximum equilibrium adsorption (a.k.a. adsorption capacity), K_M (mg/L) is the modified-Langmuir constant, and K_I (mg/L) is the inhibition constant accounting for the reduction of Cu(II) adsorption caused by cell aggregation due to the addition of Cu(II) in samples.

The experimental data were fitted to the Langmuir, Freundlich and semi-empirical isotherm models as shown in Figure 4-20. For all biosorbents, equilibrium adsorption increases with increasing Cu(II) concentration. The Langmuir (Figure 4-20A), Freundlich (Figure 4-20B), and semi-empirical isotherm (Figure 4-20C) models were fitted with experimental data using the nonlinear fitting tool in Origin. The isothermal parameters and R^2 obtained from the isothermal model are listed in Table 4-13. The results showed that the R^2 value of semi-empirical isotherm model ($0.96<R^2<1.00$) was higher than Langmuir model ($0.94<R^2<0.98$) and Freundlich model

($0.82<R^2<0.89$) for all the different biomasses obtained with media containing different phosphate concentrations.

According to the semi-empirical isotherm, the q_{max} is in the order of 300-P (180.16 mg/g)>400-P (117.01 mg/g)>200-P(88.98 mg/g)>500-P(77.47 mg/g)>100-P (76.11 mg/g). The adsorption capacity of 300-P is 2.36 times higher that of 100-P. It can be intuitively stated that the phosphate content had somehow influenced the surface structure of algal cells, which in turn had enormous impact on the adsorption of Cu(II). A table listing some of the biosorption properties (biosorption capacity, pH and contact time) of algal biomass as biosorbents can be found in Table 5. Comparatively, *N. oleoabundans* biomass was a very good biosorbent to remove Cu(II) due to its higher biosoprtion capacity (180.16 mg/g) and shorter reaction time (10 mins). Furthermore, Biosorbent 300-P showed the highest biosorption capacity compared to other phosphate-based biosorbents. It was suggested that the biomass could be enhanced by changing cultivation conditions to act as biosorbents for Cu(II) removal.

4.3.4.3.4 Effect of biomass dosage

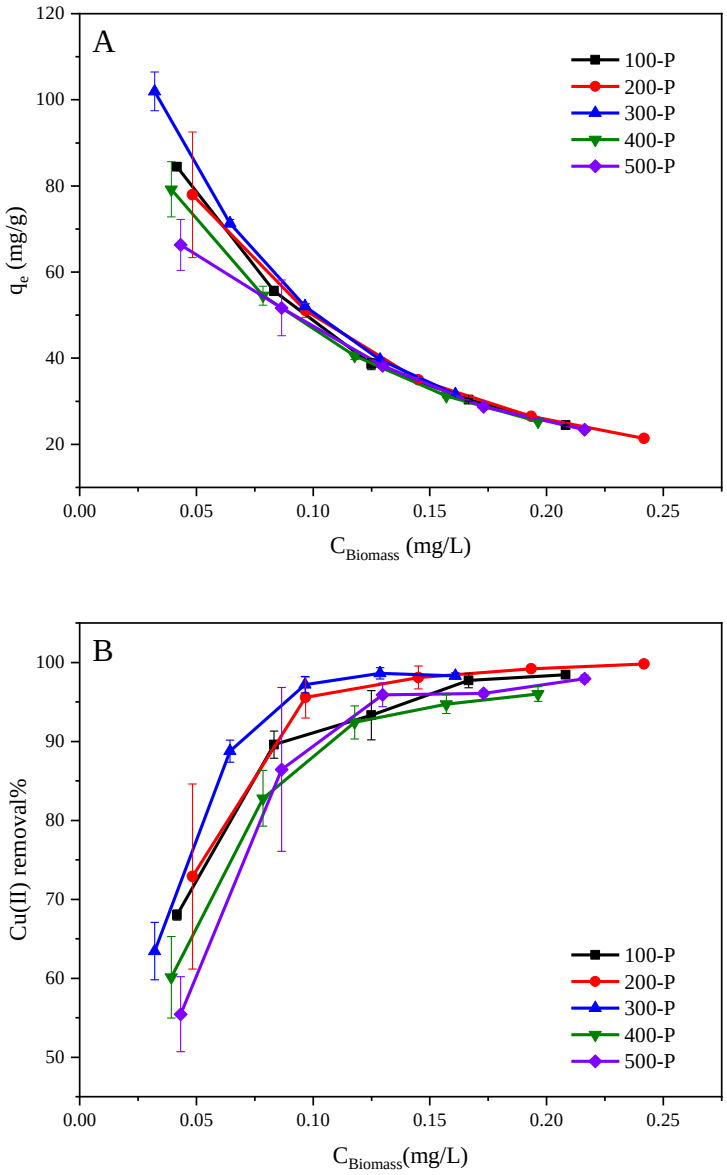

Figure 4-21 Effect of adsorbent dosage for equilibrium adsorption (A) and Cu(II) removal% (B) of Cu(II) ions onto *N. oleoabundans*, pH 7, 5 ppm Cu(II) initial concentration.

Effect of biomass dosage in the range of 0.05-0.3 g/L was studied at pH 7, contact time 30 min, room temperature, and initial Cu(II) concentration 5 ppm and the results are shown in Figure 6. The equilibrium adsorption (Figure 4-21A) decreased with the increase of the dosage of all five

different biomasses, i.e., 100-P, 200-P, 300-P, 400-P, and 500-P. It is of interest to note that the equilibrium adsorptions of different biomasses exhibited relatively large differences at low biomass dosages but converged at a dosage of 0.125 g/L and beyond. These results may be explained by the fact that all tests were carried out at the same Cu(II) concentration of 5 ppm, which was apparently not sufficient to saturate the biomass even at the lowest dosage of 0.05 g/L since the equilibrium adsorption was lower than the q_{max} of corresponding biomass as listed in Table 4 with that of 100-P being an outlier. As a result, when the biomass dosage increased, the equilibrium adsorption would decrease as Cu(II) ions available per unit biomass would decrease. The converge of equilibrium adsorption of different biomasses at large dosages occurred when the binding sites on different biomasses were all in excess that their differences only had marginal effects on adsorption. According to Figure 4-21B, when biomass dosage increased from 0.05 to 0.3 g/L, Cu(II) %removal increased at the same initial 5 ppm Cu(II) concentration and 90% Cu(II) %removal was achieved when the biomass dosage was 0.105 g/L and beyond.

4.3.4.4 Microalgal Flocculation

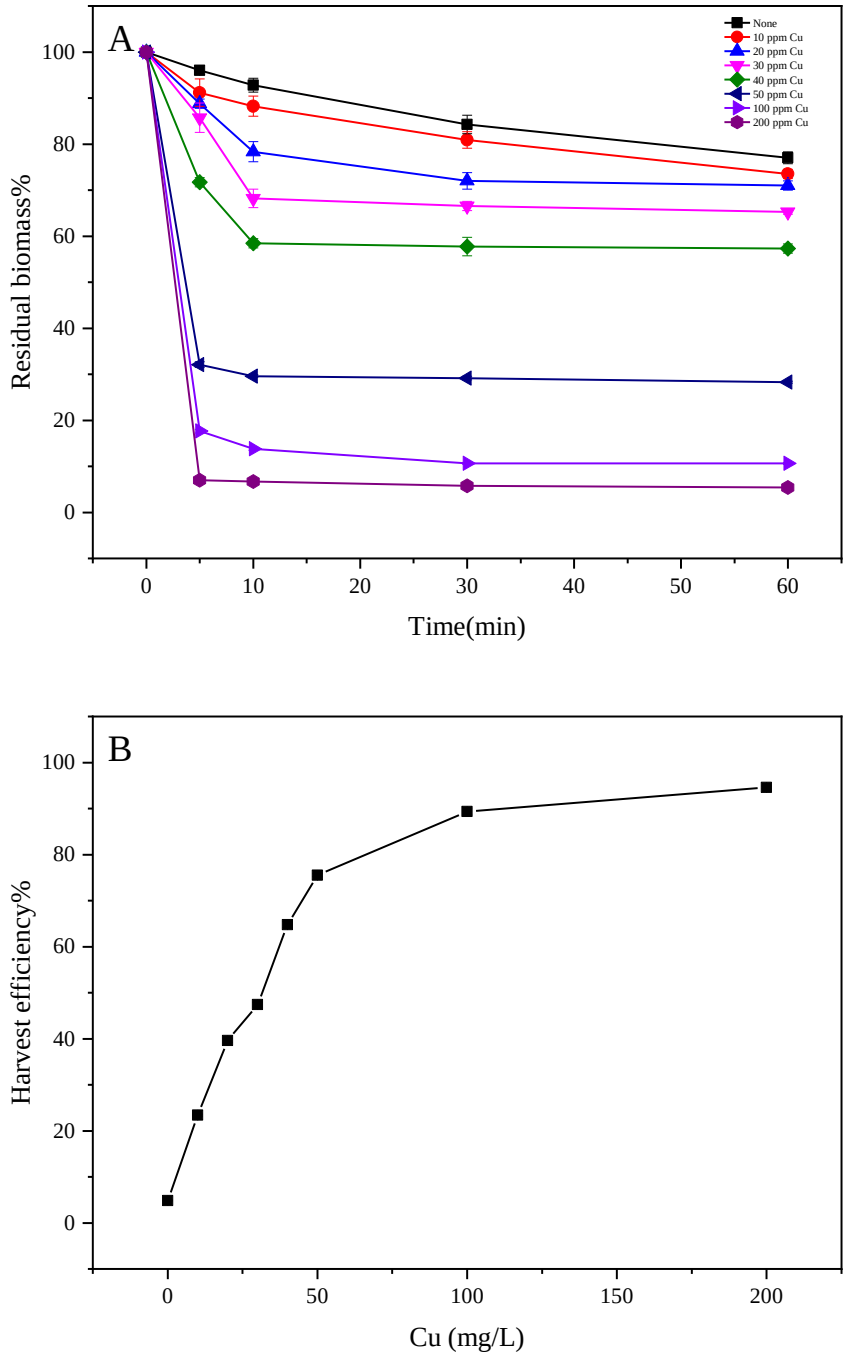

Figure 4-22 The change of *N. oleoabundans* biomass in cell suspension at different time (0-60 min) (A) and biomass harvest efficiency% (B) using Cu(II) as the flocculant with 0.5 g/L 300-P biomass.

Table 4-14 Comparison of different inorganic chemical flocculants on biomass harvesting efficiency%.

Chemical flocculants	Optimal dosage(g/L)	Microalgae Species	Biomass (g/L)	Harvesting efficiency%	Settle time(mins)	Ref.
$Al_2(SO4)_3$	2.5	*Chlorella vulgaris*	1.2	92.4	10	[214]
$Al_2(SO4)_3$	1.5	*Scenedesmus sp.*	0.4	99.4	10	[215]
$FeCl_3$	0.2	*Chlorella zofingiensis*	0.5	>90%	60	[216]
$FeCl_3$	7.0	*Scenedesmus sp.*	0.4	98.4	10	[215]
$FeSO_4$	1.5	*Scenedesmus sp.*	0.4	69.0	10	[215]
$Fe_2(SO4)_3$	1	*Chlorella minutissima*	0.5	>99.0	60	[217]
$CuSO_4$ (Cu 0.2g/L)	0.5	*N. oleoabundans*	0.5	94.6	10	This study

Sedimentation is a low-cost and energy-saving approach for biomass recovery. However, microalgae have a density similar to water and have a cell size of 2-20 mm, resulting in a slow sedimentation process that is time consuming and of low efficiency. The driving force of sedimentation is the buoyance force of cells in suspension, which is proportional to the density difference of the cells and water and the cell volume. Flocculation, which is based on the principle of adding flocculants to induce cell aggregation, would cause the formation of cell aggregates magnitudes larger than individual cells and therefore drastically increase the speed of sedimentation. In our previous studies [14], it was observed that Cu(II) could result in the

aggregation of *N. oleoabundans* cells. The effectiveness of Cu(II) as a flocculant was tested in the concentration range of 0-200 ppm and the results are shown in Figure 4-22.

As shown in Figures 4-22B, harvest efficiency% increased with Cu(II) dosage in the range of 0-200 ppm. Figure 4-22A illustrates residual biomass% at different times during sedimentation. During the time period 0-60 minutes, biomass in suspension decreased quickly in the first 10 minutes and with very little changes occurred afterward except for Cu(II) of 20 ppm or below. Figure 4-22B shows that the biomass harvest efficiency% increased with Cu(II) concentration and the highest biomass recovery efficiency% of 94.6% was achieved with 200 ppm Cu(II). Results indicate that 90% biomass harvest was achieved at 100 mg/L. It is also obvious that enhanced sedimentation of *N. oleoabundans* could be obtained when it is applied for Cu(II) removal from wastewaters of relatively low Cu(II) concentration.

Table 4-15 provides a comparison of the different inorganic chemical flocculants commonly used in microalgae harvesting. Those result shows that copper sulfate could be employed as good inorganic flocculants for microalgae harvesting, due to low dosage (0.2 g/L Cu), high harvesting efficiency% (94.6%) and short settle time (10 mins).

Table 4-15 Comparative study of the biosorption capacity of Cu(II) with other biosorbents.

Biosorbent	Optimal pH	adsorption capacity (mg/g)	Contact time (min)	Reference
Callithamnion corymbosum sp. (Red algae)	4.4	47.62	60	[190]
Spirulina platensis	7	26.24	120	[218]
Modified *Padina sanctae crucis* (brown algae)	6	14.00	80	[113]
Cystoseira indica	6	103.09	240	[112]

Arthrospira platensis	5	40.65	15	[219]
Durvillaea antarctica	5	91.51	120	[220]
Neochloris oleoabundans	7	180.16	10	This study

4.3.5 Conclusions

Results indicate that varying phosphate concentration of medium could cause the change of properties including zeta potential of the cell surface of green alga *N. oleoabundans*, leading to varied adsorption behaviours of the biomass. Indeed, the cells grown in medium containing 300 mg/L K_2HPO_4 showed the highest biomass yield (1.28 g/L), the highest cell phosphate content concentration (34.21 mg/g), the largest negative zeta potential, and the highest Cu(II) adsorption capacity (180.16 mg/g). According to the FTIR results, while carboxyl, hydroxyl, and phosphate-based functional groups may have contributed to Cu(II) biosorption, phosphate-based functional groups, most likely phoshoxel groups, are the most important. Furthermore, copper (II) has been found to be an effective flocculant for algal recovery. In other words, cell aggregation induced by Cu(II) might enhance biomass harvest although the cell aggregation caused the decrease of Cu(II) adsorption. A semi-empirical isotherm model is proposed to account for the inhibitive effect of Cu(II) on the adsorption of biomass on itself.

4.3.6 Acknowledgment

Financial support of the Natural Science and Engineering Research Council of Canada (NSERC) in a Discovery Grant RGPIN-2022–05242 is gratefully acknowledged.

4.4 Effect of nitrate on cell growth and biosorption of Pb(II) by green alga *Neochloris oleoabundans* [1]

Siwei Gu & Christopher Q. Lan*

Department of Chemical and Biological Engineering

University of Ottawa

* Chrisotpher.Lan@Uottawa.ca

[1] This paper is under review on Journal of hazardous material.

4.4.1 Abstract

This study presents an innovative approach to enhance the biosorption capacity of Pb(II) from synthetic wastewater by cultivating *Neochloris oleoabundans* using various sodium nitrate concentration (125, 250, 500, 650, 800 mg $NaNO_3$/L) as biosorbents. The cultivation condition with 800 mg/L $NaNO_3$ exhibited the highest levels of biomass production (2.41 g/L), pigment content (Chlorophyll a 29.19 mg/g, Chlorophyll b 16.78 mg/g, and Carotenoid 5.02 mg/g), and zeta potential (-23.41 mV). Furthermore, the biosorption of Pb(II) demonstrated an increasing trend as the pH rose from 2.0 to 6.0. The Sips model was employed to fit the biosorbent isotherm, and the culture cultivated under 800 mg/L $NaNO_3$ exhibited the highest biosorption capacity (60.26 mg/g) for Pb(II), which was 3.40 times greater than that of the culture with 125 mg/L $NaNO_3$ (17.72 mg/g). X-ray photoelectron spectroscopy (XPS) analysis revealed that the microalgae surface cultivated in the high medium-nitrate condition exhibited elevated protein content (95.28%) and carboxyl groups (52.88%), contributing to the enhanced biosorption capacity. For the competition test, Cu(II) has the highest inhibition effect of biosorption capacity of Pb(II) compared with other metal ions. The findings suggest that the biosorption of Pb(II) can be substantially enhanced by cultivating the microalgae in a higher sodium nitrate condition.

Key words: Biosorption, Sodium nitrate, Pb(II), *Neochloris oleoabundans*

4.4.2 Introduction

The contamination of aquatic ecosystems by heavy metal ions (HMIs) has emerged as a critical global environmental issue [221]. HMIs presence in wastewater poses a significant threat to the environment due to their non-biodegradable nature and potential harm to aquatic microorganisms and humans. Moreover, HMIs can be accumulated in higher levels through the food chain, amplifying their impact on ecosystems [222]. Lead (Pb), for instance, is highly toxic to humans, causing severe damage to the skin, nervous system, stomach, kidneys, and digestive system [223–225]. Consequently, lead is subject to stringent drinking water standards, with limits set at parts per billion (ppb) by health jurisdictions such as the World Health Organization (WHO) and the U.S. Environmental Protection Agency (USEPA) [5,6]. However, the prevalence of excessive lead pollution in various regions worldwide, surpassing these established standards, has become a concerning issue, as observed in locations such as Ross Barnett Reservoir, American [226], Nova Scotia, Canada [227], Zijiang River, China [228], Bartin River, Turkey [229] etc. Conventional techniques including ion exchange, chemical precipitation, membrane filtration, and electrolysis have been employed to remove Pb(II) from wastewater [230]. Nevertheless, these conventional methods often suffer from drawbacks such as high costs, limited feasibility, reduced efficiency, and negative environmental impact [231]. One major drawback is their high expense, energy requirements, and the generation of substantial amounts of sludge or other waste products that necessitate proper disposal [232]. Conversely, microalgae-based biosorption of HMIs offers several advantages, including enhanced efficiency, reduced costs, and the ability to selectively remove specific HMIs [125,155]. Microalgae also possess the capability to accumulate HMIs from dilute solutions, enabling them to meet drinking water standards and making them ideal for treating natural water bodies. Furthermore, the biomass produced during microalgae biosorption

can be further processed into value-added products such as biofuels or fertilizers, which can offset the treatment process's costs [20].

The process of HMIs removal by microalgae is complex and involves two mechanisms: bio-adsorption (extracellular) and bio-absorption (intracellular) [36]. The extracellular bio-adsorption of HMIs by microalgal biomass is a primary mechanism responsible for their removal from aquatic environments. This conclusion is supported by studies analyzing the biosorption of HMIs (such as Zn(II) and Cu(II)) using *Chlorella pyrenoidosa* and *Scenedesmus obliquus* [233], as well as the biosorption of Zn(II) and Cd(II) by *Chlorella vulgaris* [234]. These studies found that the primary contribution to HMIs removal occurs through the extracellular process, which involves the negative functional groups on the microalgal surface. Extracellular polymeric substances (EPS), composed of a diverse range of biomolecules such as carbohydrates, lipids, proteins, and negative functional groups like COOH, OH, SO_4, and PO_4, play a crucial role in HMIs removal [235,236].

Currently, multiple approaches exist to enhance the biosorption capacity of microalgae through cultivation. One such approach involves manipulating various cultivation parameters to optimize biosorption capacity. For example, 1) the cultivation stage can impact biosorption capacity [128], 2) phosphate levels in the medium can affect biosorption capacity, with optimal conditions varying across different strains [126,237], 3) dissolved inorganic carbon sources can improve Pb(II) biosorption capacity [43], and 4) medium pH can enhance HMIs biosorption [238]. Cultivation parameters can modify cellular growth and wall composition, particularly the negative functional groups on the cell wall, thereby affecting HMIs biosorption.

Nitrate, like phosphate, is a crucial factor in microalgal cultivation, playing a significant role in regulating the growth and physiology of microalgae. Nitrate has been observed to influence the biochemical composition of microalgal cells, including protein production [239]. Furthermore, nitrate availability can also modulate the biochemical composition of the cell surface, which, in turn, affects HMIs biosorption by microalgae. A study demonstrated that medium-nitrate levels affect the biochemical composition (protein, lipid, and carbohydrate) of *C. pyrenoidosa* and *S. obliquus* [240]. Considering the alterations that occur in the biochemical composition of microalgae, it is reasonable to assume that the concentration of sodium nitrate could also impact the functional groups on the cell surface involved in HMIs removal. Hence, optimizing the nitrate concentration in microalgae cultivation is necessary to improve biomass production and its efficiency in HMIs removal.

This study systematically examines the impact of varying concentrations of sodium nitrate (ranging from 125 to 800 mg/L $NaNO_3$) on the cultivation of the microalga *Neochloris oleoabundans* and its ability to remove Pb(II). Pb(II) removal was investigated in terms of kinetics, isotherm, and thermodynamics by assessing the effects of contact time, initial heavy metal ion concentration, and temperature. Additionally, the study evaluates the biosorption isotherm of Pb(II) in a binary system with competing metals such as Na(I), K(I), Ca(II), Zn(II), Cd(II), Ni(II), Co(II), and Cu(II). X-ray photoelectron spectroscopy (XPS) is employed to determine the possible functional groups and biochemical composition on the cell surface. An analysis of cultivation conditions is conducted to underscore the impact of these conditions on the biosorption capacity of HMIs.

4.4.3 Material and methods

All experiments and determinations were conducted in triplicate.

4.4.3.1 Microalgal cultivation and biosorbent preparation

The microalgae strain *Neochloris oleoabundans* (UTEX#1185) was acquired from the University of Texas and cultivated in a Modified Bristol Medium (MBM) supplemented with varying concentrations of sodium nitrate ($NaNO_3$) [14]. The concentrations used were 125, 250, 500, 650, and 800 mg $NaNO_3$/L, corresponding to nitrogen concentrations of 20.60, 41.20, 82.40, 107.12, and 131.84 mg N/L, respectively. The medium was sterilized by autoclaving at 121°C for 20 min. After cooling to room temperature (25°C), 0.5 L of the sterilized medium was added to a 1 L cultivation flask bottle. The bottle was then inoculated with 20 mL of microalgal incubation seeds (10^7 cells/mL), and the pH was maintained at 7.5 using a programmed aeration system with a mixture of 5% CO_2 and air. The microalgal culture was cultivated for 11 days, and the resulting biomass was harvested and stored at -80 ℃ for further use.

To prepare the biosorbent, the frozen microalgal biomass was thawed overnight in a refrigerator at 4 ℃ and subsequently washed three times with deionized water to remove any residual chemicals or debris. The biomass was then suspended in an appropriate volume of deionized water. In the subsequent sections of the study, the microalgal biomass obtained from the different sodium nitrate concentrations of 125, 250, 500, 650, and 800 mg $NaNO_3$/L were denoted as 125-N, 250-N, 500-N, 650-N, and 800-N, respectively.

4.4.3.2 Biosorption

To prepare the stock solution of Pb(II), 1.60 g of $Pb(NO_3)_2$ (Strem Chemicals Inc., USA) was dissolved in deionized water using a 1.0 L graduated cylinder to obtain a concentration of 1000

mg/L Pb(II). The stock solution was stored in a 1.0 L white plastic bottle, protected from direct light, and kept at room temperature.

4.4.3.2.1 Experimental design

The study investigated several parameters, including contact time (5 to 60 min), initial Pb(II) concentration (10 to 200 mg/L), pH (2 to 6), and temperature (20 to 60 ℃), using a biomass dosage of 0.5 g/L. These parameters were analyzed to understand the kinetics, isotherm, and thermodynamics models of biosorption comprehensively. The experiments were conducted in 2.0 mL microcentrifuge tubes with a 1.5 mL mixture. Prior to incubation, the pH of the mixture was adjusted to the desired value using 0.1 M HNO_3. The mixture was agitated using a shaker device (Multitron-Pro, Infors HT, Switzerland) at 200 r/min. After reaching the desired contact time, the sample was centrifuged for 1.5 min at 13,500 r/min to obtain a supernatant of the mixture solution. The concentration of Pb(II) in the aqueous solution was determined using Flame Absorption Atom Spectrometer (FAAS). Control groups without biomass were also included for comparison during the experiment.

4.4.3.2.2 Binary system

The influence of competitive metal ions, including Na(I), K(I), Ca(II), Zn(II), Cd(II), Ni(II), Co(II), and Cu(II), on the biosorption of Pb(II) in a binary system was investigated. The experiments were conducted at room temperature (25 ℃) with an optimal pH of 6.0, using a constant biomass concentration of 0.5 g/L. Isotherm experiments were carried out using a 1 mmol/L concentration of competitive metal ions and Pb(II) concentrations ranging from 10 to 200 mg/L. After a 10-minute incubation, the mixture was centrifuged for 1.5 min at 13,500 r/min to obtain the supernatant. The remaining Pb(II) concentration in the supernatant was determined using FAAS.

4.4.3.3 Measurements and analysis

4.4.3.3.1 Biomass concentration

The growth of each microalgal culture was monitored for 11 days using a UV/Vis spectrophotometer (GENESYS™ 10S, Thermo Fisher Scientific Inc., USA) at a wavelength of 700 nm, which serves as an indicator of the living cell concentration. The dry cell weight (DCW) of the microalgal biomass was determined by drying the biomass overnight at 60 ℃. A linear relationship was observed between the microalgal dry weight and the optical density (OD_{700}), with high correlation coefficients (R^2) close to 1.0 (0.9994-0.9999). This allowed for the monitoring of microalgal growth using the spectrophotometric method. The results are presented below:

$$x = C * OD_{700} \tag{4.36}$$

where the *x* (g/L) is the biomass concentration, *C* (g/(L*OD)) is the convert factor and OD_{700} is the optical density under 700 nm wavelength. The convert factor exhibits variations among various culture biomass and has been presented in Table 1.

The microalgal growth curve, biomass doubling time, changes in specific growth rate during the exponential phase (days 2-5), and biomass dosage after 10 days of cultivation were determined by analyzing the correlation curves between OD_{700} and dry weight. The specific growth rate and doubling time were calculated using the Eq 4.37&4.38.

$$\mu = \frac{(Lnx_1) - (Lnx_2)}{t} \tag{4.37}$$

$$dt = \frac{Ln(2)}{\mu} \tag{4.38}$$

where μ is the specific growth rate (day^{-1}), and x_1 (g/L) and x_2 (g/L) are the biomass at day 5 and day 2, respectively. And *dt* is compounding to doubling time (day).

4.4.3.3.2 Nitrate concentration

The concentration of nitrate was determined using an Agilent 1200 series High-Performance Liquid Chromatography (HPLC) system (Agilent Instruments, Stockport, U.K) equipped with an Anion IC-PAKTM column (50 × 4.6 mm, 10 µm particle size, Waters, Millipore, USA), as previously described [241]. The mobile phase consisted of a borate buffer/gluconate concentrate, methanol, acetonitrile, and deionized water in a ratio of 2:12:12:74 (v/v/v/v) at a flow rate of 1 mL/min. The UV detector was set at 220 nm, and the pH of the mobile phase was adjusted to 8.5. The borate buffer/gluconate concentrate was prepared by dissolving 0.07 M sodium gluconate, 0.3 M H_3BO_3, 0.1 M $Na_2B_4O_7$, and 3.8 M glycerol in deionized water. The analysis was conducted at 50 ℃ with an injection volume of 30 µL and a retention time of approximately 5 min. Sample concentrations were determined by dilution according to a pre-determined standard curve.

The cellular nitrate concentration (mg N/g biomass) was calculated using the following equation:

$$C_N = \frac{N_i - N_f}{x} \tag{4.39}$$

where C_N is the cellular nitrate concentration (mg N/g biomass), N_i and N_f are the nitrate concentration (mg N/L) on day 0 and day 11, respectively, and x is the biomass concentration (g/L) on day 11.

4.4.3.3.3 Pigment concentration

The determination of pigment content in *N. oleoabundans* culture was performed using a sampling method after washing the biomass [242]. Briefly, 1 mL of the culture suspension was centrifuged for 1.5 min, and the supernatant was carefully removed with a pipette. The pellet biomass was then treated with 1 mL of 100% methanol to extract Chlorophyll a, Chlorophyll b, and Carotenoid pigments. The samples were stored overnight at 4 ℃. Methanol was used as the

diluent instead of water to prevent any redshift in determination. The pigment extracts were subjected to spectral measurements on a spectrophotometer within the wavelength range of 400 to 800 nm using a 0.1 cm cuvette. The concentration of pigments in the aqueous extract was determined using the optical density corresponding to the respective wavelengths, according to the method described by Wellburn [242]:

$$Chlorophyll_{\ a} = \frac{16.72A_{665.2} - 9.16A_{652.4}}{x} \quad 4.40$$

$$Chlorophyll_{\ b} = \frac{34.09A_{652.4} - 15.28A_{665.2}}{x} \quad 4.41$$

$$Carotenoid = \frac{(1000A_{470} - 1.63C_a - 104.96C_b)}{221x} \quad 4.42$$

Where *x* (g/L) is the biomass concentration. *Chlorophyll a*, *Chlorophyll b* and *Carotenoid* (mg/g) are the pigment concentration in biomass. $A_{665.2}$, $A_{652.4}$ and A_{470} are the optical density of wavelength under 665.2, 652.4 and 470 nm.

4.4.3.3.4 Pb(II) concentration

Pb(II) concentration was determined using Flame Absorption Atom Spectrometer (FAAS). The supernatant solutions obtained after centrifugation were diluted with deionized water to achieve a concentration range of 0.1 to 10 mg/L. To stabilize the solutions, 10 µL of 68% HNO_3 was added to each sample. Calibration curves were constructed using standard Pb(II) solutions (Sigma-Aldrich, Canada) at concentrations of 2, 4, 6, 8, and 10 mg/L. 2 mL sample was injected into the sample collector, and the Pb(II) concentration was determined at a wavelength of 217 nm.

4.4.3.3.5 Zeta potential

Zeta potential, which assesses the electrostatic repulsion between charged particles in microalgal biomass, was measured using a zeta potential analyzer (Mastersizer 2000, UK) over a pH range of 2 to 6. The measurements were conducted at a standard temperature of 20 ℃. Triplicate

cultures were measured to ensure result reliability, with each sample providing 10-20 readings per dataset.

4.4.3.3.6 XPS

To analyze the functional groups on the cell surface, 2 mL of microalgal biomass suspension was filtered using a cellulose acetate filter (0.45 µm, Satorius). The filtrate was then resuspended in 1 mL of distilled water. The cells were subjected to centrifugation (5000g, 4 min, 5417C, Eppendorf, Germany), washed with 1 mL of distilled water, and centrifugation was repeated. The resulting pellets were resuspended in 100-200 µL of distilled water, depending on the cell density. Subsequently, 1 mL volumes of the resuspended samples (containing approximately <105 cells) were placed in a cabinet dryer and dried for 5 min at 60 ℃. Infrared spectra were recorded in transmission mode using 32 scans co-added to improve the signal-to-noise ratio, in the spectral range of 4000-700 cm^{-1}. The freeze-dried samples were fully ground using an agate mortar for X-ray photoelectron spectroscopy (XPS) analysis. The resulting data was sorted, and the corresponding spectra were obtained through peak processing using the Casa software. The carbon spectra were characterized by binding energies at 284.8, 286.4, 287.8, and 289.2 eV, while oxygen scanning was performed at binding energies of 531.4, 532.6, and 533.4 eV. Nitrogen spectra exhibited two peaks at 399.8 and 402.5 eV.

The dominant components on the surface of microalgal cells, including polysaccharides, proteins, and hydrocarbons, were determined based on the elemental ratios of [N/C] and [O/C]. The macromolecular composition was calculated using Eqs 4.43-4.45 [135]:

$$\left[\frac{N}{C}\right] = 0.279\left(\frac{C_{PR}}{C}\right) \quad 4.43$$

$$\left[\frac{O}{C}\right] = 0.325\left(\frac{C_{PR}}{C}\right) + 0.833\left(\frac{C_{PS}}{C}\right) \quad 4.44$$

$$\left[\frac{C}{C}\right] = \left(\frac{C_{PR}}{C}\right) + \left(\frac{C_{PS}}{C}\right) + \left(\frac{C_{HC}}{C}\right) = 1 \qquad 4.45$$

the symbols [*N/C*], [*O/C*], and [*C/C*] represent the elemental composition ratios of the cell surface. Additionally, (C_{PR}/C), (C_{PS}/C), (C_{HC}/C) denote the ratios of carbon in proteins, polysaccharides, and hydrocarbons to the total carbon, respectively.

4.4.4 Results and discussions

4.4.4.1 Effect of nitrate on microalgal cultivation

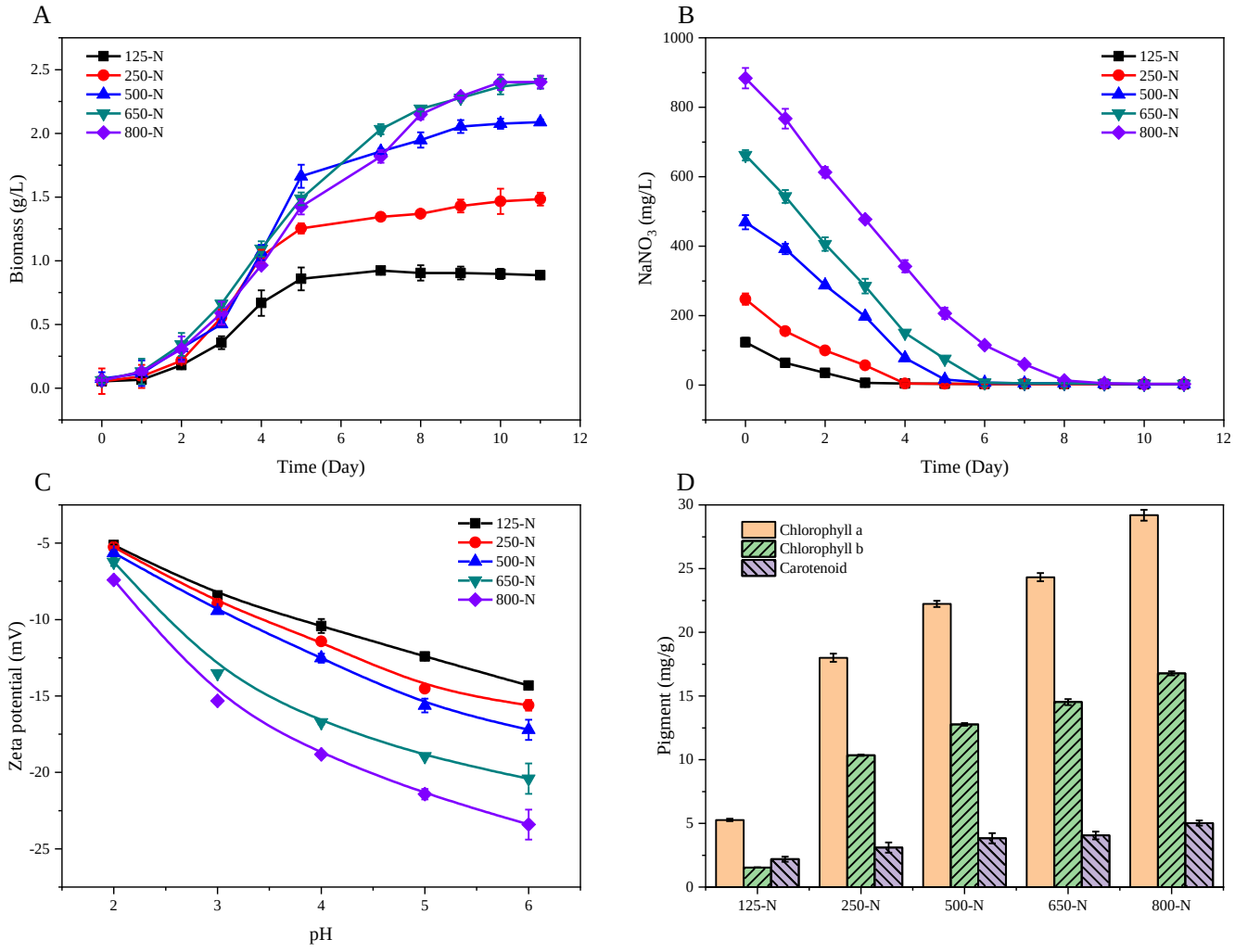

Figure 4-23 Growth of microalgal *N. oleoabundans* under different concentration of NaNO3 (125-800 mg/L): A) Effect of NaNO3 on microalgal biomass, B) NaNO3 consumption, C) Biomass zeta potential from pH 2.0 to 6.0 at day 11, and D) photosynthesis pigments.

Table 4-16 Effect of sodium nitrate on convert factor (g/L*OD), biomass(g/L), doubling time (day), cellular nitrate content (mg/g) and pigment concentration (mg/g) by microalgal *N. oleoabundans* harvested at 11 day.

$NaNO_3$ (mg/L)	N/P ratio (g/g)	Convert factor (g/L*OD)	Biomass (g/L)	μ (day^{-1})	τ_d (day)	C_N (mg/g)	*Chlorophyll a* (mg/g)	*Chlorophyll b* (mg/g)	*Carotenoid* (mg/g)
125	0.21	0.55	0.88	0.76	1.31	22.59	5.27	1.54	2.19
250	0.42	0.63	1.48	0.73	1.37	27.39	18.00	10.35	3.10
500	0.84	0.63	2.09	0.81	1.23	39.16	22.22	12.77	3.82
650	1.09	0.66	2.40	0.84	1.19	44.33	24.32	14.52	4.05
800	1.35	0.70	2.41	0.90	1.11	54.59	29.19	16.78	5.02

The availability of essential micronutrients, such as nitrate, is critical for the optimal growth and cellular metabolism of microalgae. This study investigated the effect of nitrate on the growth of *Neochloris oleoabundans* by varying the concentrations of $NaNO_3$ (125, 250, 500, 650, and 800 mg/L). Throughout microalgal cultivation, four distinct growth phases were observed: log phase, exponential phase, linear phase, and stationary phase. However, distinguishing between the different growth phases was challenging due to the rapid depletion of $NaNO_3$. The cultures with lower concentrations of $NaNO_3$ reached the stable phase more quickly. Figure 4-23A illustrates the exponential growth period for the five cultures between day 2 and day 5. The time-course profiles of $NaNO_3$ concentrations for the cultures of 125, 250, 500, 650, and 800 mg/L are shown in Figure 1B. It is worth noting that cell growth continued even after the nitrate concentration in the culture reached zero, likely due to the utilization of nitrogenous biochemicals, such as pigments, within the cells [243]. The conversion factor for biomass slightly increased with increasing $NaNO_3$ concentration, resulting in varying biomass results for the same strain. The highest biomass concentration of *N. oleoabundans* was achieved with 800 mg/L $NaNO_3$, reaching 2.41 g/L DCW on the 11^{th} day, while the lowest biomass concentration was obtained with 150 mg/L $NaNO_3$, yielding only 0.88 g/L DCW on the 11^{th} day. The culture with 800 mg/L $NaNO_3$

also exhibited the highest specific growth rate of 0.90 day^{-1}, corresponding to the shortest doubling time of 1.11 days.

Nitrogen is a critical element in the molecules of chlorophyll a, b and carotenoids, which are essential for efficient light absorption during photosynthesis. In this study, pigment concentrations were measured in microalgae cultures at day 11, as presented in Figure 4-23D. The results showed that the pigment concentrations (mg/g) for chlorophyll a, chlorophyll b, and carotenoids increased from 5.27 to 29.19, 1.54 to 16.78, and 2.19 to 5.02, respectively, with an increase in $NaNO_3$ concentration from 125 to 800 mg/L. It is important to note that the pigment concentrations were measured in mg/g rather than mg/L, and if converted to mg/L, the differences in pigment content production would have been even greater due to the biomass concentration (g/L). Previous research has confirmed that the efficiency of microalgal photosynthesis can be affected by nitrate concentration due to the biochemical role of pigment synthesis. For example, Song et al. [198] studied the effect of sodium nitrate on the photosynthesis of the microalga *Dunaliella tertiolecta* and found that as the nitrate concentration increased from 63.74 to 2039.87 mg $NaNO_3$/L, the total chlorophyll content increased from 20 to 29 mg/g. Liao et al. [243] reported a direct relationship between chlorophyll content and residual nitrate concentration. When external nitrogen sources are exhausted, the chlorophyll content decreases as microalgae cells utilize chlorophylls as an intracellular nitrogen source to support their continued growth. Moreover, Li's study [128] indicated that the highest biosorption capacity of Pb(II) can be achieved by biomass harvested in the stable phase (day 11) compared to the exponential and death phases. To simplify the naming of the biomass cultures cultivated with different nitrate concentrations (ranging from 125 to 800 mg $NaNO_3$/L) and harvested on day 11, they were referred to as 125-N, 250-N, 500-N, 650-N, and 800-N.

Zeta potential is a useful parameter for evaluating the biosorption capacity of HMIs. It is widely accepted that a lower zeta potential value (mV) corresponds to a higher biosorption capacity for HMIs [244]. The relationship between the zeta potential and biomass at different pH values (ranging from 2.0 to 6.0) is shown in Figure 4-23C. The results revealed that the zeta potential of the biomass decreased as the concentration of $NaNO_3$ increased from 125 to 800 mg/L at all pH values. Additionally, the negative zeta potential of 800-N decreased from -14.31 mV to -23.41 mV as the pH increased from 2.0 to 6.0. The lowest zeta potential value (-5.12 mV) was obtained by 125-N at pH 2.0. Due to the different zeta potential values obtained with different cultures, it is reasonable to assume that the biosorption capacity of Pb(II) may vary. Specifically, the highest biosorption capacity of Pb(II) is expected to be obtained by 800-N biomass at pH 6.0, which is characterized by the most negative zeta potential value (-23.41 mV). Numerous studies have established a positive correlation between increased zeta potential and greater biosorption of HMIs [94,237]. For example, Xia et al. reported that the zeta potential of *Chlorella sorokiniana* cultures cultivated with different phosphate concentrations differed, and biomass cultivated with 160 mg/L phosphate had a higher net negative zeta potential than P-20 within pH ranges from 2.0 to 8.0, resulting in a greater capacity to adsorb Cd(II) [237]. Our hypothesis should be interpreted clearly, as the nitrate content has a major influence on cell metabolism, especially on the cell wall, as the composition of the cell wall plays a vital role in the biosorption capacity of HMIs.

It has been confirmed that various nitrate concentration in medium that results difference of dried cell weight, lipid and carbohydrate content [198,245,246]. For instance, Araujo et al. investigated the effect of sodium nitrate on four microalgal species cultivation (*Chlorella vulgaris, Nannochloropsis oculata, Tetraselmis chui*, and *Tetraselmis tetrathele*), reporting that when increasing $NaNO_3$ form 25 to 75 mg/L, the cell number and cell weight were increasing sharply

[239]. And the highest biomass for *Chlorella vulgaris*, *Nannochloropsis oculata*, *Tetraselmis chui*, and *Tetraselmis tetrathele* were 1.9, 1.1, 2.2 and 3.4 g/L, respectively. Sun et al. also studied the effect of nitrate on microalgal *Chlorella sorokiniana* cultivation, when nitrate concentration used from 60.71- 971.43 mg $NaNO_3$/L, the biomass increases and achieved the highest value of 2.3 g/L at 485.71 mg $NaNO_3$/L, then biomass became decreasing, which means higher nitrate concentration pose a negative effect on microalgal growth [247]. They explained this maybe due to the effect of pH drop to pH 3.0 for microalgal cultivation. Another investigation found that higher concentration of sodium nitrate (measuring 1821 mg $NaNO_3$/L) will reduce microalga *Microcystis aeruginosa* cellular density [248]. Our research demonstrates a positive correlation between nitrate concentration and biomass concentration, ranging from 150 to 800 mg $NaNO_3$/L.

4.4.4.2 SEM-EDS

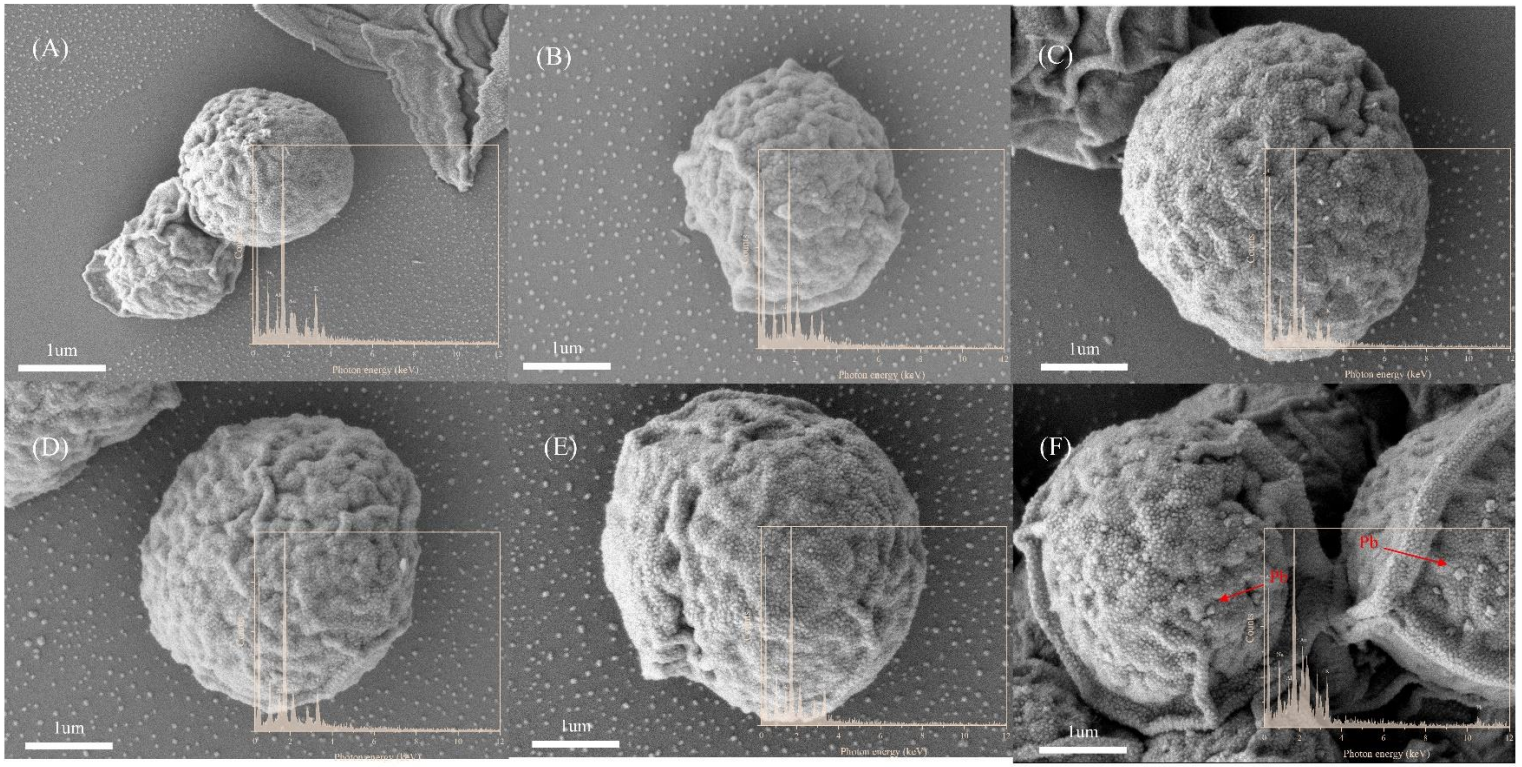

Figure 4-24 SEM-EDS of *N. oleoabundans* cultivated in various NaNO3 concentration (125 (A), 250 (B), 500 (C), 650 (D) and 800 (E) mg/L) and 800-N biomass loading 200 mg/L Pb(II) (F).

The impact of varying concentrations of sodium nitrate ($NaNO_3$) on the morphology of *N. oleoabundans* microalgae and its biomass loaded with 200 mg/L Pb(II) was investigated using scanning electron microscopy (SEM) and energy-dispersive X-ray spectroscopy (EDS). SEM analysis revealed that the cell surface of *N. oleoabundans* biomass remained consistent with increasing $NaNO_3$ concentration, but distinct changes in morphological diameter size (ranging from 1.5 to 3 um) were observed. At low $NaNO_3$ concentrations (125-250 mg/L), the cells appeared small and round with a smooth surface. However, at higher concentrations (500-800 mg/L), the cells became larger with an increasingly rough surface. Figure 2F illustrates the presence of large particles adsorbed on the cell surface. This observation suggests that these particles may result from the conversion of Pb(II) into Pb-containing particles, leading to a reduction in the concentration of HMIs in the solution.

EDS analysis of the microalgae biomass revealed the presence of carbon, oxygen, nitrogen, and phosphate, which are typical elements found in microalgae cells. Additionally, the analysis detected the presence of other elements, such as magnesium, calcium, and potassium, which are likely derived from the growth medium. Interestingly, the EDS analysis also confirmed the presence of Pb(II) on the surface of the microalgae biomass when loaded with Pb(II), as shown in Figure 2F. This finding supports the ability of *N. oleoabundans* to adsorb HMIs and has significant implications for the bioremediation of wastewater contaminated with HMIs.

4.4.4.3 XRD

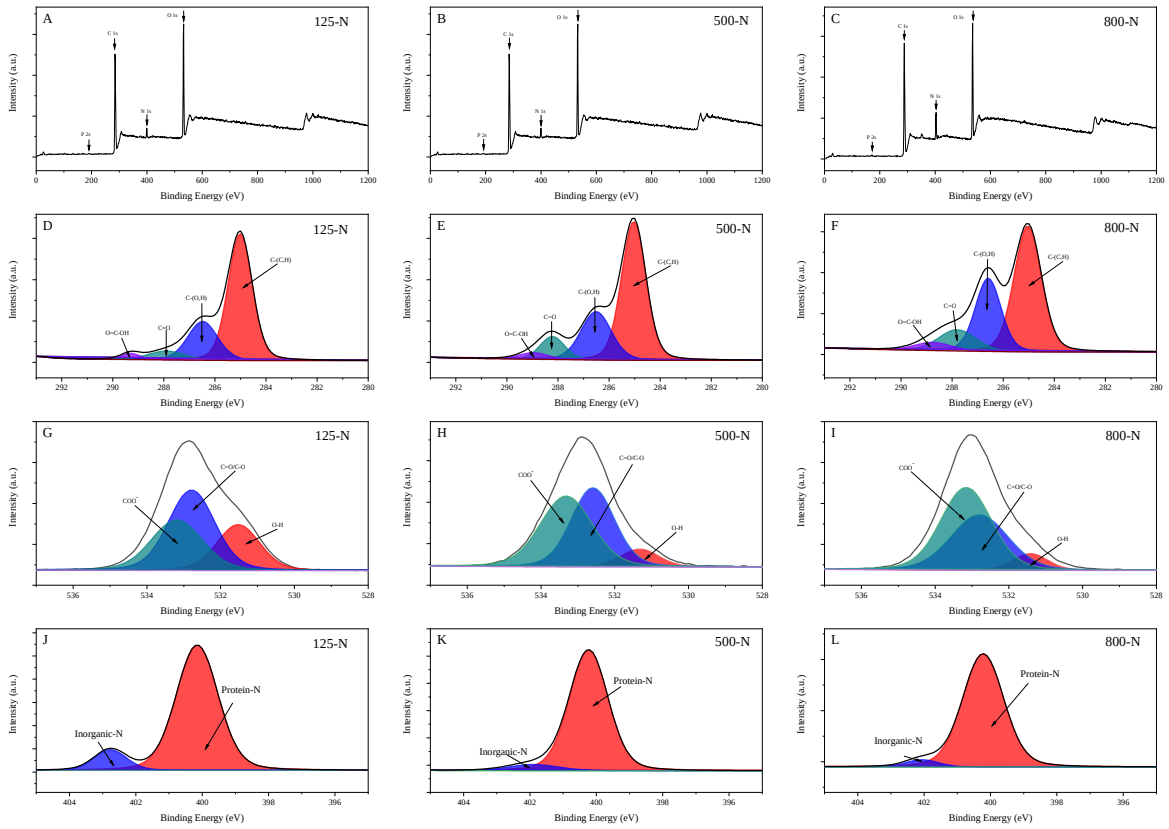

Figure 4-25 XPS survey spectra of frozen-dried *N. oleoabundans* algae cultures after 11 days of growth: A, B, C, full-range spectra; D, E, F region of C 1s; G, H, I, region of O 1s.

Table 4-17 Characterization of microalgal cell surface chemical composition through XPS: elemental composition, surface chemical composition, carbon functional groups and oxygen functional groups.

Biomass	Elemental composition (a.t.%)					Surface chemical composition (a.t.%)			Carbon functional groups (weight%)				Oxygen functional groups (weight%)			Nitrogen functional groups	
	C 1s	N 1s	O 1s	P 2s	S 2p	Polysaccharide	Protein	Lipid	C-(C,H)	C-O,C-N	O-C-O	COOH,R	O-H	C=O/C-O	COO-	Protein-N	Inorganic-N
125-N	79.04	0.80	19.17	0.84	0.15	27.70	3.63	68.67	65.72	24.91	6.87	2.51	23.77	45.07	31.16	88.70	11.30
500-N	75.75	1.87	21.41	0.67	0.29	30.48	8.85	60.67	60.27	26.21	10.11	3.41	8.67	44.00	47.33	93.93	6.06
800-N	72.80	2.39	23.97	0.15	0.69	34.94	11.77	53.30	53.57	29.44	12.35	4.65	7.37	39.75	52.88	95.26	4.74

Fig. 4-25 presents the XPS survey spectra of frozen-dried *N. oleoabundans* algae cultures after 11 days of growth in three different media: 125-N, 500-N, and 800-N. The results showed that an

increase in nitrate concentration from 125 to 800 mg $NaNO_3$/L led to changes in the cell surface composition of *N. oleoabundans.* Specifically, the N content increased from 0.80 to 2.39%, while the O and S contents increased from 19.17 to 23.97% and 0.15 to 0.69%, respectively. Meanwhile, the C and P contents decreased from 79.04 to 72.80% and 0.84 to 0.15%, respectively. Further analysis revealed that the major compositions present on the microalgal cell surface were polysaccharide, protein, and lipid. With an increase in nitrate concentration, the concentration of polysaccharide and protein on the cell surface increased from 27.70 to 34.95% and 3.63 to 11.77%, respectively. The functional groups on the cell surface were determined through C1s and O1s analysis. The C1s analysis revealed four major functional groups: C-(C,H), C-O/C-N, O-C-O, and COO-(H,R). The highest concentration of carboxylic acid (4.65%) was observed in cultures with 800 mg/L $NaNO_3$. Similarly, the O1s analysis revealed three main oxygen-related functional groups: O-H, C-O/C=O, and COOH. The highest concentration of COOH (52.88%) was obtained in cultures with 800 mg/L $NaNO_3$. These findings indicate that the nitrate concentration in the medium can significantly influence the composition of elements, biochemicals, and functional groups on the microalgal cell surface, which in turn can affect the biosorption capacity of HMIs. For instance, the high fraction of -COOH groups, which are negatively charged when protonated, could be directly responsible for the large biosorption capacity of Pb(II) by 800-N biomass.

The nitrogen functional groups on the microalgal cell surface include protein-N and inorganic-N [249]. As shown in Fig. 4-25 J-L, the raw algae N1s spectra exhibited two peaks: protein-N (399.8 ± 0.3 eV) and inorganic-N (402.5 ± 0.3 eV, ammonia-N [NH_4^+] and nitrate-N [NO_3^-]). Protein-N, which consists of nitrogen-containing organic compounds such as urea, amino acids, proteins, nucleic acids, and alkaloids, was the major N-containing functional group in all three

cultures, accounting for approximately 88-96%. With an increase in sodium nitrate concentration, higher protein-N content and lower inorganic-N content were observed. Due to the peptide structure of proteins (O=C-C-N), they can chelate HMIs, thereby increasing the biosorption capacity.

4.4.4.4 Effect of pH on biosorption of Pb(II)

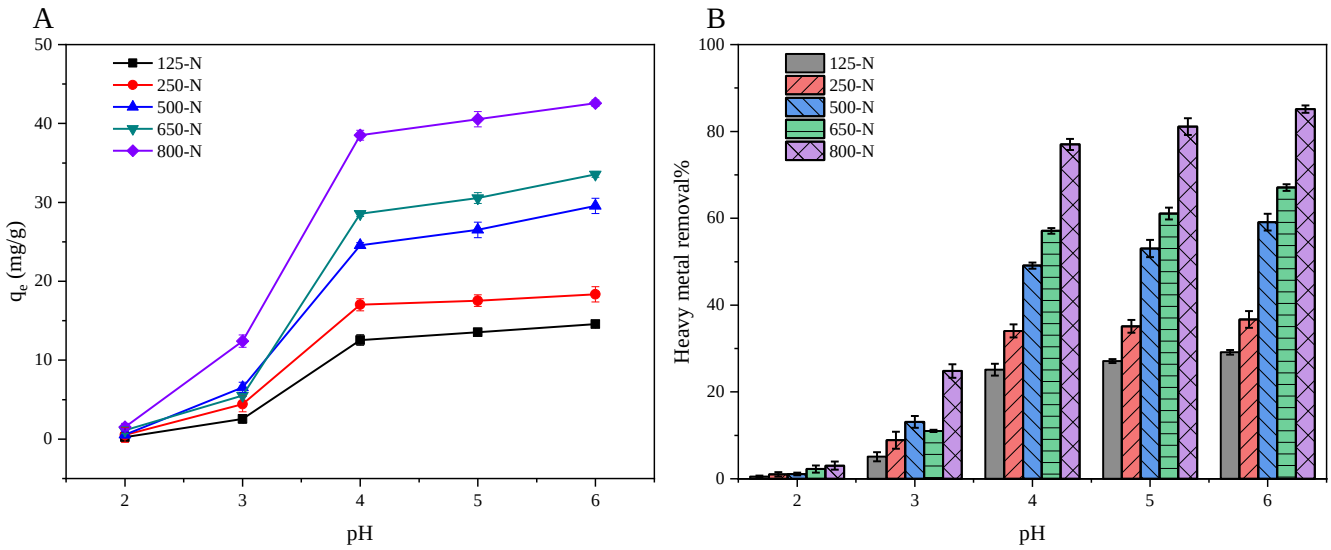

Figure 4-26 Effect of pH (A) and HMIs removal% (B) on biosorption of Pb(II), 50 mg/L Pb(II), 0.5 g/L biomass, 10 min contact time, 25 ℃. The dataset comprises triplets of values, with their corresponding standard deviations provided (n = 3).

The biosorption of Pb(II) by microalgal biomass is influenced by pH, as it affects the interaction between negative functional groups and positive HMIs. In this section, the effect of pH on the biosorption of Pb(II) by wet microalgal biomass (125-N, 250-N, 500-N, 650-N, and 800-N) under different nitrate concentration cultures was evaluated. The experiments were conducted at an initial Pb(II) concentration of 50 mg/L, a biomass dosage of 0.5 g/L, a contact time of 10 min, and a temperature of 25 ℃. It is important to note that the contact time was determined based on previous studies, which indicated that equilibrium could be reached within 10 min, simulating the

real process of wastewater treatment at room temperature and the similar test was carried [14]. To prevent HMIs precipitation, all pH values were kept below 7.0, as alkaline pH can lead to the formation of $Pb(OH)_2$ and subsequent precipitation of HMIs. The biosorption of Pb(II) exhibited an increasing trend as the pH increased from 2.0 to 6.0 (acidic to neutral), with 800-N biomass demonstrating the highest equilibrium biosorption capacity compared to the other cultures. The highest equilibrium biosorption of Pb(II) by 800-N was achieved at pH 6.0, with a value of 42.57 mg Pb(II)/g biomass. The removal efficiency of heavy metal ions varied with pH, following the order: 85.13% (pH 6.0) > 81.10% (pH 5.0) > 77% (pH 4.0) > 24.82% (pH 3.0) > 3.02% (pH 2.0), as shown in Fig. 4-26B.

The primary mechanism for HMIs removal by microalgae involves ion exchange, chelation, complexation, and absorption, with bio-adsorption being the initial step. Among these mechanisms, ion exchange is the dominant process and is pH-dependent. When the pH is below 7.0, there is competition between the positive HMIs (Pb(II)) and hydrogen ions (H^+) for the limited positive functional groups. The highest equilibrium biosorption of Pb(II) at pH 6.0 is mainly attributed to the strong electrostatic force of attraction between the cationic species (Pb(II)) and the anionic ligands present on the microalgal cell surface [250]. Several studies have reported that higher biosorption capacity can be achieved by microalgal biomass as the pH increases from acidic to neutral conditions [128,237,251]. Our previous study also found that the optimal pH for different heavy metal ions was below 6.0. This consistency among various reported works highlights the dependence of the optimum biosorption pH on the functional groups present in microalgae. For the subsequent biosorption tests, a pH of 6.0 will be maintained as the optimal pH value.

4.4.4.5 Isotherm

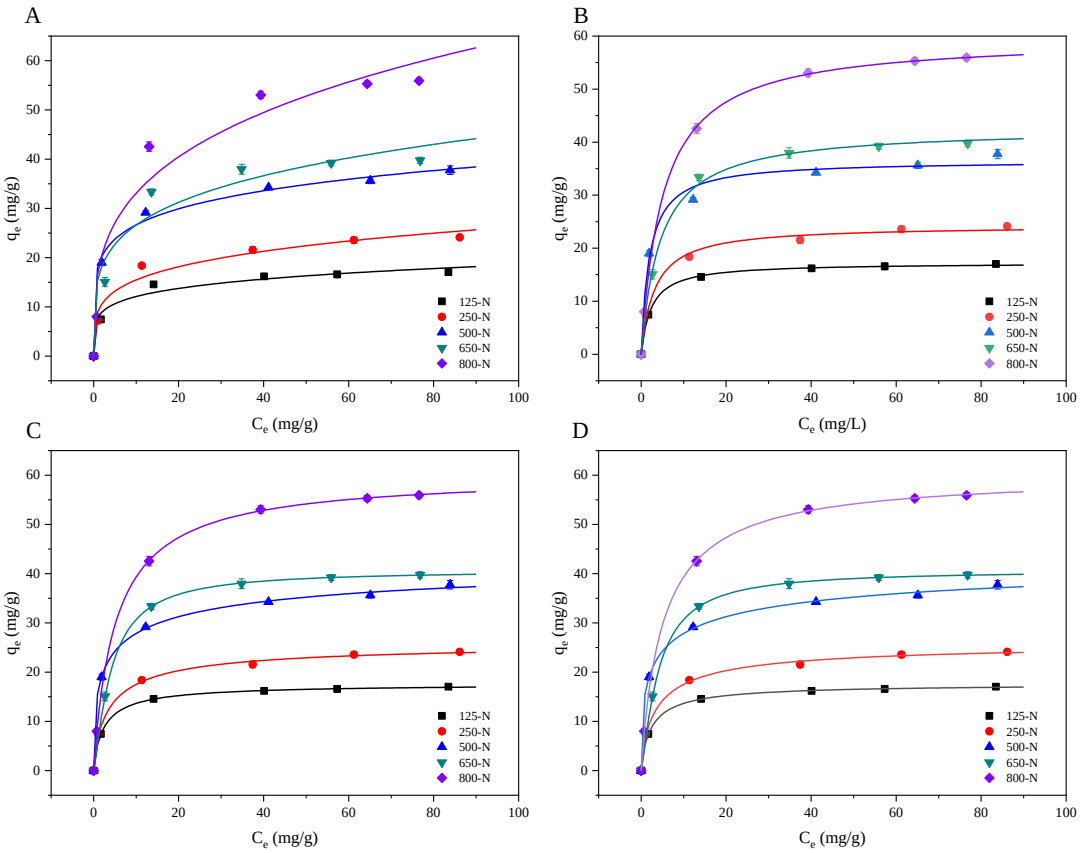

Figure 4-27 Biosorption isotherm of Pb(II) by microalgal with fitting Freundlich (A), Langmuir (B), Sips (C) and BET (D) model under 0.5 g/L biomass, pH 6.0, 10 min contact time, 25 ℃.

Table 4-18 Biosorption isotherm constants of Freundlich, Langmuir, Sips and BET model obtained for biosorption of Pb(II) on microalgal *N. oleoabundans*.

Biosorbent	Freundlich			Langmuir			Sips				BET			
	K_F ($L^{1/n}\cdot mg^{1-1/n}\cdot g^{-1}$)	n	R^2	q_L (mg/g)	K_L (L/mg)	R^2	q_S (mg/g)	K_S ($L^{ns}\cdot mg^{-ns}$)	*NS*	R^2	q_B (mg/g)	K_{B1} (L/mg)	K_{B2} (L/mg)	R^2
125-N	7.89	0.18	0.9122	17.24	0.43	0.9977	17.72	0.45	0.87	0.9996	16.62	0.47	5.65E-04	0.9997
250-N	9.11	0.23	0.9339	24.28	0.32	0.9882	26.22	0.34	0.77	0.9969	21.85	0.42	1.43E-03	0.9994
500-N	18.16	0.17	0.9486	36.52	0.52	0.9791	40.40	0.52	0.45	0.9961	31.75	0.78	2.02E-03	0.9994
650-N	15.65	0.23	0.8651	42.67	0.22	0.9935	46.67	0.17	1.25	0.9999	46.66	0.19	1.28E-03	0.9993
800-N	16.95	0.29	0.9181	59.67	0.20	0.9997	60.26	0.20	0.96	0.9999	58.93	0.20	1.51E-04	0.9999

For the removal of HMIs, the isotherm of biosorption of Pb(II) is crucial to investigate. This can help to predict biosorption capacity (mg/g) and determine equilibrium biosorption (mg/g) under different concentration of HMIs (mg/L) and biomass dosage (g/L). Four biosorption isotherm models were employed to investigate biosorption capacity, which included two-parameter models: Freundlich, Langmuir models, and the three-parameter models: Sips, BET models. Among these four models, Langmuir and Sips model assumes monolayer biosorption, while Freundlich and BET model assumes multilayer biosorption [252]. These equations (4.46-4.49) are shown below:

$$q_e = K_F(C_e)^{\frac{1}{n}} \quad 4.46$$

$$q_e = \frac{q_L K_L C_e}{1 + K_L C_e} \quad 4.47$$

$$q_e = \frac{q_S K_S C_e^{NS}}{1 + K_S C_e^{NS}} \quad 4.48$$

$$q_e = \frac{q_B K_{B1} C_e}{(1 - K_{B2} C_e)(1 - K_{B2} C_e + K_{B1} C_e)} \quad 4.49$$

where q_e is presented as equilibrium biosorption and, q_L, q_S and q_B (mg/g) are presented as biosorption capacity, and C_e (mg/L) the equilibrium HMIs concentration. *NS* and *n* are the equilibrium constant for Sips and Freundlich model. K_F ($L^{1/n} \cdot mg^{1-1/n} \cdot g^{-1}$), K_L (L/mg), K_S ($L^{ns} \cdot mg^{-ns}$), K_{B1}(L/mg) and K_{B2} (L/mg) are the equilibrium constant for Freundlich, Langmuir, Sips and BET models, respectively.

Figure 4-27 presents the experimental results of Pb(II) biosorption on different biomass cultures (125-N, 250-N, 500-N, 650-N, and 800-N) and their fitting to four isotherm models: Freundlich, Langmuir, Sips, and BET. Table 4-18 summarizes the results, indicating that the Sips and BET

isotherm models exhibit a better fit (R^2>0.99) compared to the Freundlich and Langmuir models (R^2>0.86). Among the two parameters of the BET model, K_{B1} represents the adsorbates' first layer on the adsorbents, while K_{B2} corresponds to the upper layer. In most cases, K_{B2} was negligible compared to K_{B1}, indicating that monolayer biosorption was the primary mechanism. The Sips model suggests that, except for 650-N, the biomass exhibits NS values in the range of 0-1, implying that one adsorbate molecule (HMIs) can occupy more than one biosorption site [253]. The value of N in the range of 0.1-0.5 obtained from the Freundlich model suggests an easily occurring biosorption process [254]. Due to its physical significance, the Sips model was selected to compare the maximum biosorption capacity.

Figure 4-27 depicts the biosorption results of Pb(II) by microalgal cultures grown under varying nitrate concentrations. The data shows a positive correlation between the biosorption capacity and the nitrate concentration of the culture medium, with a noticeable increase in biosorption capacity as the nitrate concentration increases from 150 to 800 mg $NaNO_3$/L. According to the Sips model, the order of Pb(II) biosorption capacity by different biomass cultures is as follows: 125-N (17.72 mg/g) < 250-N (26.22 mg/g) < 500-N (40.40 mg/g) < 650-N (46.67 mg/g) < 800-N (60.26 mg/g). It is worth mentioning that a prior study utilizing the same cultivation medium (500-N) reported a biosorption capacity of *N. oleoabundans* as 207.87 mg/g [14]. However, in our current study, the biosorption capacity was only 36.52 mg/g. This discrepancy can be attributed to the difference in medium pH, with our study maintaining a pH of 7.5 compared to the pH of 9.5 in the prior study. These findings underscore the significance of medium pH in determining the biosorption capacity. The increased biosorption capacity of Pb(II) resulting from changes in nitrate concentration in the medium may be attributed to the higher protein content associated with nitrate on the cell wall, as

indicated by the XPS results showing an increase in amine and amide groups, which are negative functional groups related to protein on the cell cytomembrane.

The biosorption capacity of Pb(II) observed in our study is comparable to or higher than values reported in other studies. For instance, the biosorption capacity of Pb(II) by *Chlorella vulgaris* was reported as 6.58 mg/g [255], which is considerably lower than the value reported by Edris et al. [256] for the same species (149.9 mg/g). Similarly, the biosorption capacity of Pb(II) by *Scenedesmus obliquus* was reported as 19.74 mg/g [257]. The mechanisms involved in the biosorption of Pb(II) by microalgae include ion exchange, biosorption, and chelation. Studies by Zhou et al. [233] and Alam et al. [234] suggest that the extracellular process primarily contributes to the removal of HMIs. Considering the significant impact of pH on the biosorption of Pb(II), it can be inferred that the primary mechanism involved is ion exchange occurring on the surface of the microalgal cells.

4.4.4.6 Binary system

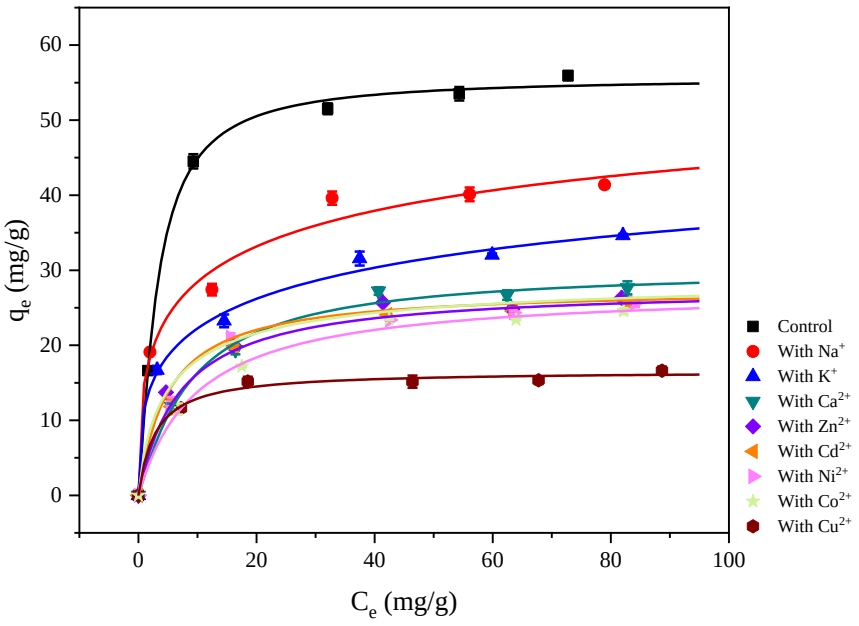

Figure 4-28 Isotherm of Pb(II) by competition ions in binary system, 0.5 g/L 800-N biomass, 1 mmol/L competition metal ions, pH 6.0, 10 min contact time, 25℃.

Table 4-19 Metal properties and effect of competition ion on biosorption of Pb(II), the impact factor (=Electronegativity/Ionic radius) [14].

					Sips model				
Competition ion	Lewis bases	Electronegativity	Ionic radius (pm)	Impact factor (pm^{-1})	q_s (mg/g)	K_S ($L^{ns}\cdot mg^{-ns}$)	*NS*	R^2	Inhibition %
None	\	\	\	\	55.70	0.24	1.24	0.9964	\
Na^+	Hard	0.93	102	0.0091	41.60	0.28	0.41	0.9559	25.31
K^+	Hard	0.82	138	0.0059	34.66	0.22	0.38	0.9802	37.77
Ca^{2+}	Hard	1.00	100	0.0100	30.33	0.09	1.11	0.9806	45.55
Zn^{2+}	Intermediate	1.65	74	0.0223	29.26	0.25	0.81	0.9766	47.47
Cd^{2+}	Soft	1.69	95	0.0178	27.53	0.10	1.00	0.9858	50.58
Ni^{2+}	Intermediate	1.91	70	0.0273	26.57	0.10	1.21	0.9983	52.29
Co^{2+}	Intermediate	1.88	70	0.0269	25.32	0.08	1.47	0.9888	54.54
Cu^{2+}	Intermediate	1.90	73	0.0260	15.83	0.54	1.99	0.9153	71.59

The inhibition% was determined using the following Equation:

$$Inhibition\% = \frac{q_s - q_{sn}}{q_{sn}} * 100\% \quad 4.50$$

where q_s and q_{sn} present the biosorption capacity of Pb(II) without competition ion and biosorption capacity of Pb(II) with 1 mmol/L competition ion, respectively.

In binary system, the presence of two different metal ions creates a competition for binding sites on the microalgal cell surface, thereby impacting the biosorption capacity of HMIs. In this study, we investigated the influence of several metal ions, including Na(I), K(I), Ca(II), Zn(II), Cd(II), Ni(II), Co(II), and Cu(II), on the biosorption isotherm of Pb(II) in binary systems. Each competition ion was maintained at a constant concentration of 1 mmol/L. The results were fitted with the Sips model, and the isotherm parameters are summarized in Table 3, with the corresponding plot shown in Figure 4-28.

All competition ions exhibited an inhibitory effect on the biosorption capacity of Pb(II), with the degree of inhibition following the order: Cu(II)>Co(II)>Ni(II)>Cd(II)>Zn(II)>Ca(II)>K(I)>Na(I). Among the competition ions, Na(I) showed the lowest inhibition, reducing the Pb(II) biosorption capacity of the 800-N biomass to 41.60 mg/g (25.31% inhibition), while Cu(II) exhibited the highest inhibition, reducing the biosorption capacity to 16.58 mg/g (71.59% inhibition). These results clearly demonstrate that monovalent heavy metal ions have a smaller inhibitory effect compared to divalent heavy metal ions. Moreover, among the divalent metal ions, Lewis hard bases such as Na(I) and Ca(II) had a smaller effect compared to Lewis intermediate bases like Zn(II) and Ni(II), as well as Lewis soft bases like Cd(II). It is important to note that Cu(II) exhibited the highest inhibition percentage (71.59%) among all the competition ions, which can be partially attributed to cell aggregation caused by copper ions, as observed at concentrations of 50 mg/L or higher, which has been reported in previous studies [126]. Cell aggregation reduces the specific surface area available for biosorption, thereby decreasing the biosorption capacity.

4.4.4.7 Effect of microalgal cultivation conditions for HMIs biosorption

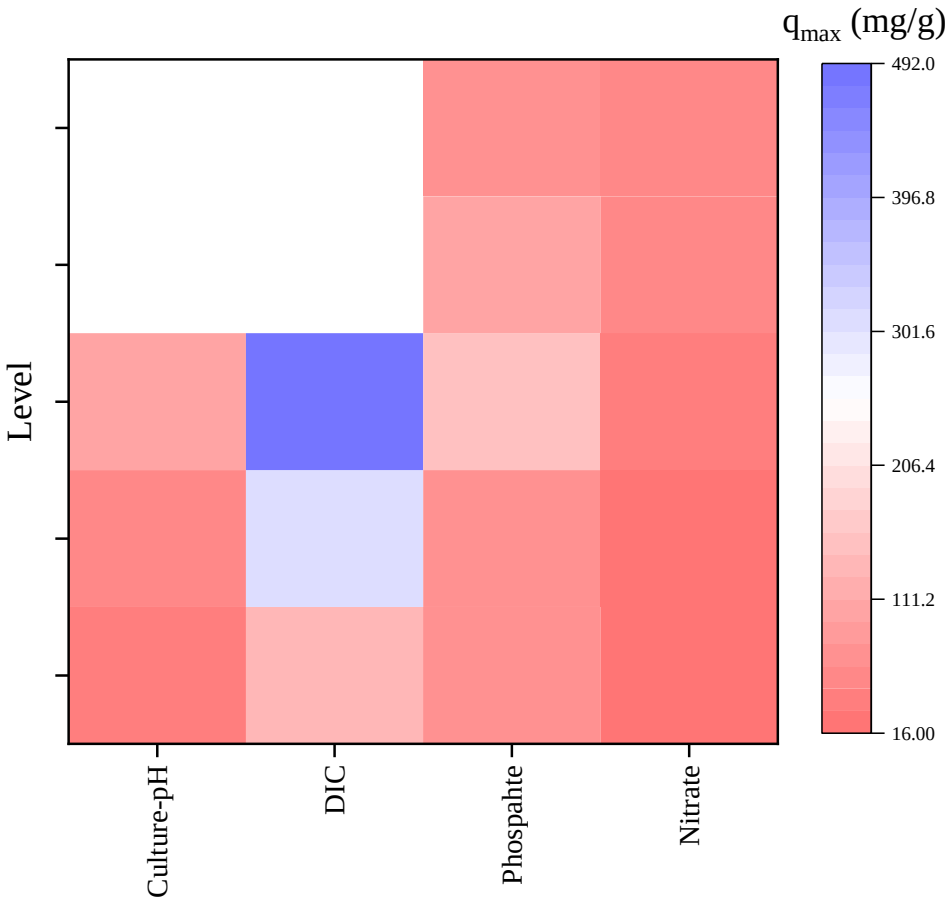

Figure 4-29 Heat map of biosorption capacity of HMIs by *N. oleoabundans* biomass cultivated under different medium parameters, including culture pH, dissolved inorganic carbon (DIC), phosphate concentration and nitrate concentration.

Table 4-20 Effect of medium parameters (culture pH, DIC, phosphate and nitrate) on HMIs biosorption capacity by *N. oleoabundans*.

Parameter	Level (/)	q_{max} (mg Pb(II)/g)	Ref.
pH	7.5	32.85	[238]
	8.5	40.47	
	9.5	100.01	
DIC ($NaHCO_3$)	Level (mmol/L)	q_{max} (mg Pb(II)/g)	[43]
	0	142.52	
	160	317.36	
	320	491.54	
Phosphate	Level (mg/L)	q_{max} (mg Cu(II)/g)	[126]
	100	69.91	
	200	78.68	
	300	150.66	
	400	98.88	
	500	65.55	
Nitrate	Level (mg/L)	q_{max} (mg Pb(II)/g)	This study
	125	17.72	
	250	26.22	
	500	40.40	
	650	46.67	
	800	60.26	

In this study, we integrated the influence of various medium parameters on the biosorption capacity of HMIs, specifically Pb(II) and Cu(II), using microalgae *Neochloris oleoabundans* as efficient biosorbents. Figure 4-29 presents a comprehensive heat map illustrating the biosorption capacity of HMIs under the influence of distinct medium parameters, including culture pH, dissolved inorganic carbon (DIC) concentration, phosphate, and nitrate concentrations. The results clearly demonstrate that elevated culture pH, increased nitrate concentration, appropriate phosphate concentration, and heightened dissolved inorganic carbon (DIC) level positively correlate with enhanced HMIs biosorption capacities. Notably, Pb(II) and Cu(II) exhibit

amplified affinity for the microalgae or biosorbents under these cultivation conditions, underscoring the pivotal roles played by these variables in optimizing the efficiency of the biosorption process.

A comprehensive analysis of the biosorption capacities achieved under different conditions, as presented in Table 4-20. It is noteworthy that higher cultivation pH, DIC concentration, and nitrate levels lead to increased biosorption capacities of HMIs. The maximum biosorption capacities recorded are 100.01 mg Pb(II)/g for culture pH, 491.54 mg Pb(II)/g for DIC, 150.66 mg Cu(II)/g for phosphate concentration, and 60.26 mg Pb(II)/g for nitrate concentration, respectively. Interestingly, the data also highlights the pronounced influence of dissolved inorganic carbon (DIC) on biosorption capacity, surpassing the significance of other studied parameters, i.e., culture pH, nitrate and phosphate. This observation underscores the crucial role that dissolved inorganic carbon, as a key medium constituent, plays in shaping the biosorption mechanism. Its substantial impact on the biosorption process, particularly in relation to its ability to significantly modulate the potential of microalgae or biosorbents to capture Pb(II), is a noteworthy finding. The concentration of functional groups attached to the cell surface is identified as a fundamental factor contributing to the biosorption capacity of HMIs. Changes in the medium conditions result in variations in the types of functional groups present, such as COOH, OH, C-O-C, and PO_4. For instance, modulating the cultivation nitrate levels has the potential to elevate the concentration of carboxyl groups, consequently leading to a higher biosorption capacity. These insights collectively emphasize the critical importance of precise medium parameter optimization to unlock the maximum biosorption capacity for efficient removal of HMIs. The intricate interplay between pH, nitrate concentrations, dissolved inorganic carbon, and phosphate levels unveils a spectrum of optimization opportunities. These

opportunities can be strategically harnessed to achieve highly effective sequestration of HMIs from aqueous solutions.

4.4.5 Conclusion

This study is the first time to investigate the influence of nitrate concentration ($NaNO_3$) on the culture of *N. oleoabundans* for Pb(II) biosorption, signifying the originality and significance of the research outcomes. The findings conclusively demonstrate that the biosorption capacity of Pb(II) exhibits a direct correlation with increasing sodium nitrate concentration. Isotherm experiments provide strong evidence that the binding of Pb(II) occurs predominantly on the surface of microalgal cells, consistent with the Langmuir, Sips, and BET models. Notably, XPS analysis elucidates the impact of cultivating microalgae in a higher pH medium, which triggers an augmentation in the presence of protein and carboxylic groups on the cell wall. This phenomenon ultimately leads to a marked improvement in Pb(II) removal efficiency. These pivotal findings shed light on the complex mechanisms underlying microalgal biosorption and offer valuable insights for the development of sustainable and efficient strategies for HMIs removal utilizing microalgal biomass.

4.4.6 Acknowledgment

Financial support of the Natural Science and Engineering Research Council of Canada (NSERC) in a Discovery Grant RGPIN-2022–05242 is gratefully acknowledged.

Chapter 5 Lipid-extraction algal biomass for biosorption of bivalent lead and cadmium ions: kinetics and isotherm[1]

Siwei Gu & Christopher Q. Lan*

Department of Chemical and Biological Engineering

University of Ottawa

* Chrisotpher.Lan@Uottawa.ca

[1] The content of this chapter was published and the detail: Gu, S., Lan, C. Q. (2023). Lipid-extraction algal biomass for biosorption of bivalent lead and cadmium ions: kinetics and isotherm. Chemical Engineering Science, 118778.

Highlights

- Residual biomass has the highest adsorption capacities on both Pb(II) and Cd(II) compared with wet and dried biomass.
- Exposure of inner cell wall surface likely the primary reason for enhanced adsorption of residual biomass.
- Larger impactor factor of metal ion had larger adsorption capacity of on wet, dried, and residual biomass.
- Biosorption by microalgal biomass is a monolayer adsorption.
- Negative functional groups e.g., P=O, C-O-C, O-H, C-N as the binding sites adsorb heavy metal ions.

5.1 Abstract

Residual algal biomass, which is the by-product of the extraction value-added products such as lipids, proteins, pigments and antioxidants, from algal biomass, represent a potentially massive and inexpensive source of biosorbents. The biosorption of heavy metal Pb(II) and Cd(II) by the residual biomass of *Chlorella vulgaris* after lipid extraction was investigated under varied conditions including pH, contact time and initial heavy metal concentration. That of the wet and dried biomasses of *C. vulgaris* were also studied for comparison. Biosorption plateaus were achieved within 10 minutes for Pb(II) and 30 minutes for Cd(II). The Pb(II) biosorption capacity by residual, wet, and dried biomass were 194.79, 106.25 and 68.69 mg/g, respectively, and that of Cd(II) were 54.98, 30.47 and 21.44 mg/g, respectively. The biosorption capacities of residual biomass of Pb(II) and Cd(II) were 2.83 and 2.56-fold higher than dried biomass, which can be explained by increasing surface area after lipid extraction process.

Key words: Biosorption, Lead, Cadmium, *Chlorella vulgaris*, residual biomass

5.2 Introduction

Heavy metal contamination of the aquatic ecosystem has attracted tremendous interests as it has become a severe and fast growing a global environmental problem. Heavy metals are non-biodegradable, toxic, and bio-accumulative, which pose serious risks to the ecosystem and human health [258]. Among various heavy metal ions, lead (Pb(II)) and cadmium (Cd(II)) are highly toxic to humans as they may cause severe damages the nervous system, kidneys, and digestive systems [223,259]. Consequently, the drinking water standards for Pb(II) and Cd(II) have been set to be 10 and 3 ppb by the WHO regulations and 15 and 5 ppb by the USEPA regulations, respectively [5,6]. Herein, many methods have been developed to remove Pb(II) and Cd(II) from contaminated waters, such as chemical precipitation [260], ion exchange [261], reverse osmosis [262], chemical precipitation enabled UF/MF membrane filtration [13] and biosorption [126]. Of particular relevance, it has been found that microalgae might be an economically viable and environmentally friendly alternative due to their vast genetic diversity that allows them to thrive in almost any aquatic ecosystems, self-propagative nature, the ability to remove a large variety of different heavy metals even from dilute influents [36]. In addition, the heavy metal loaded biomass could be conveniently combusted to generate heat while dramatically reducing the volume of waste disposal or recovering heavy metals when applicable.

Microalgae of different forms, e.g., wet, dried, and residual biomasses, can be utilized for heavy metal removal. For instance, wet biomass of green alga *Neochloris oleoabundans* has been shown to have high biosorption capacities for Pb(II) and Cd(II) of 213.42 mg/g and 73.07 mg/g, respectively [14] while that of *Chlorella minutissima* was demonstrated of high adsorption capacity for Pb(II) (303.03 mg/g) [263]. Furthermore, it was shown that manipulating the concentration of dissolved inorganic carbon in medium could significantly increase the Pb(II)

adsorption by *N. oleoabundans* [67]. Due to the fact that dried biomass is easy to store and transport, various dried microalgae have been reported for Pb(II) removal, e.g., *Aphanothece sp.* (185.64 mg/g) [54], *Chaetoceros Sp*. (0.95 mg/g) [264], *Chlorella Sp*. (9.78 mg/g) [264], and Cd(II), *Parachlorella sp*. (96.20 mg/g) [45], *Scenedesmus-24* (50.00 mg/g) [265]. While in general wet algal biomass showed better biosorption capacity, dried biomasses are more economical considering the costs of storage and transportation [266].

Microalgal biomasses have high commercial values as feedstock for the production of human nutrients, animal feeds, biofuels, and biofertilizers [267,268]. They could also be used for production of novel products such as cosmetics, antioxidants, pigments, stable isotope biochemicals, antimicrobials, antivirals, and anticancer drugs [269,270]. The massive and rapidly increasing quantities of microalgal residues as by-products of the extraction of target products at commercial scale has created another category of microalgal biosorbents, i.e., residual algal biomasses [271]. In addition to their low costs, residual algal biomass shares the same advantages of dried biomasses in terms of easy storage, transportation, and good stability. Nevertheless, comparing the vast number of literatures on biosorption using wet or dried algal biomass as biosorbents, studies on the utilization of residual algal biomass for heavy metal removal is still in its embryo. Indeed, the only paper on this topic we have managed to extract from the literature is that of Zheng et al. (2016), which reported the adsorption of Cd(II) by the lipid-extraction residual biomasses three lipid-rich algal species, i.e., *Chlorella sp.* CHA-01, *Chlamydomonas sp.* TAI-03, and *Coelastrum sp.* PTE-15 after lipid extraction.

In this study, we systematically investigated the biosorption of two toxic heavy metal ions, i.e., Pb(II) and Cd(II), using the residue of green alga *C. vulgaris* after a simulated lipid-extraction

process. The effects of biosorption time, initial metal concentration and pH were tested in terms of kinetics and isotherms. The functional groups responsible for adsorbing heavy metals were analyzed using Fourier transform infrared spectroscopy (FTIR). Studies were also carried out on wet and dried biomass of the same microalgae for the purpose of comparison, based on which a hypothesis explaining the doubled adsorption capacity of the residual biomass in comparison to that of the dried biomass was proposed.

5.3 Materials and methods

5.3.1 Microalgal cultivation

Chlorella vulgaris, UTEX 2714 was collected from the microalgal culture collection at the University of Texas in Austin. The alga was maintained in autoclaved Bold Basal Medium (BBM) [133], which is suitable for freshwater algae. Bold Basal Medium contains chemicals, per liter of distilled water, which has 0.25 g $NaNO_3$, 0.025 g $CaCl_2 \cdot 2H_2O$, 0.75 g $MgSO_4 \cdot 7H_2O$, 0.075 g K_2HPO_4, 0.175 g KH_2PO_4, 0.025 g NaCl, 0.00498 g $FeSO_4 \cdot 7H_2O$, 0.01 g $Na_2EDTA \cdot 2H_2O$, 0.00805 g H_3BO_3, 1 mL trace elements solution, which was composed of (analytical grade, per liter) 2.86 g $H_3BO_3 \cdot 2H_2O$, 1.81 g $MnCl_2 \cdot 4H_2O$, 0.222 g $ZnSO_4$, 0.0494 g $Co(NO_3)_2 \cdot 6H_2O$, 0.39 g $NaMoO_4 \cdot 5H_2O$, 0.079 g $CuSO_4 \cdot 5H_2O$. For microalgal cultivation, 3-L photobioreactor was used. The lamps were arranged evenly around the bioreactor chamber and were programmed to be 12 hours light on, and 12 hours light off. The photobioreactor containing 2 liters of fresh medium was sterilized for 20 minutes at 121℃ before inoculation. For inoculation, 50 mL of inoculant microalgal seeds (1.0 g/L) were transferred to bioreactor after it was cooled to room temperature in sterilization chamber. During cultivation, constant air flow of 0.5 vvm (i.e., 1 LPM) was applied at 25°C, 180 RPM, with a constant air speed of 180 RPM. By mixing pure CO_2 into the air stream, the pH of the culture was kept at 9.5. This was achieved by passing the airstream

through distilled water before passing it through a microfilter before being sprayed into the culture at the bottom of the bioreactor. After two-week cultivation, the microalgae reached stable phase (10^7 cells/ml), and biomass was harvested and stored for future usage under -80°C freezer.

5.3.2 Biosorbent preparation

The wet biomass was obtained by washing three times with deionized water. 40 mL of sample in 50 mL centrifugal tube was centrifuged at 6000 rpm in 10 min for three times to remove chemicals and fragments remaining in medium. After that, wet sample was resuspended in deionized water for biosorption test.

The dried biomass, when applicable, is produced by drying the afore prepared wet biomass at 60°C overnight. Afterwards, for ensuring that the microalgae cells do not adhere to each other, the dried biomass was resuspended in deionized water and sonicated with a supersonic probe under ice-bath (QSonica LLC, Newtown, USA) under 50 HZ (3s on and 3s off) for 10 minutes.

The lipid extract biomass, a.k.a. residual biomass, is prepared by drying the aforesaid wet biomass at 60°C overnight and adding 15 mL of solvent (chloroform: methanol: 2:1) to dried pellet biomass, sonicating with a supersonic probe under ice-bath (QSonica LLC., Newtown, USA) under 50 HZ (3s on and 3s off) for 10 minutes, then washing twice by deionized water to remove solvent. Then, residual biomass was resuspended by deionized water for biosorption tests. An illustration of the sample preparation procedure is shown in Figure 5-1.

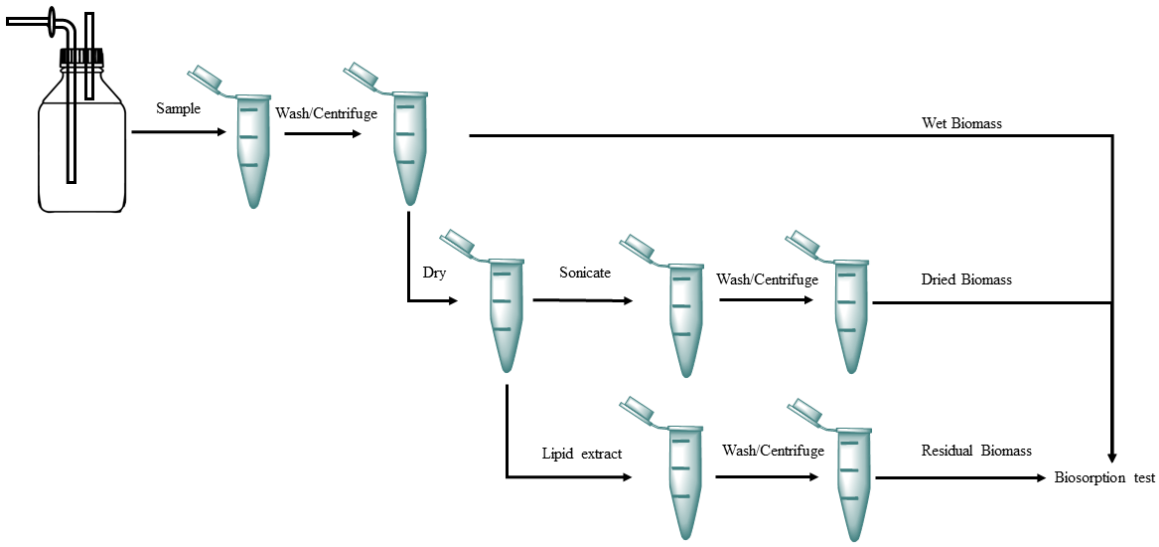

Figure 5-1 Preparation of wet, dried, and residual biomasses of *C. vulgaris*.

5.3.3 Heavy metal stock solution

Heavy metal stock solution was prepared by dissolving appropriate amount of $Pb(NO_3)_2$ (Strem Chemicals Inc., USA) and $Cd(NO_3)_2$ (Fisher Scientific, USA) into deionized water using volumetric flask to obtain 1000 mg/L lead and cadmium ions. Then, the stock solution was store in 100 mL white plastic bottle under room temperature. In this study, all of the chemical reagents used were analytical grade reagents.

5.3.4 Biosorption test

5.3.4.1 Effect of pH

For pH adjustment, suitable acids, bases, or buffers should be chosen based on metal ion solubility. It is not recommended to use H_2SO_4 in the biosorption of lead and cadmium due to the formation of the $PbSO_4$ and $CdSO_4$ precipitates. In addition, $Pb(NO_3)_2$ and $Cd(NO_3)_2$ are soluble in aqueous solution. Therefore, in this study, pH was adjusted by HNO_3 and NaOH. Batch biosorption experiment was carried out in a 2 mL graduated microcentrifuge tube using 1.5 mL wet, dried and residual biomass, and Pb(II), Cd(II) stock solution were added into tube to ensure

50 mg/L Pb(II), Cd(II) and 0.5 g/L biomass under 25℃. The initial pH of the mixture was adjusted to 6.0 by adding 0.1 N HNO_3 after mixing. After that, the mixture was shaken at 200 RPM shaker for 30 mins contact time as specified in the text at room temperature (25 ℃). Afterwards, the sample was centrifuged for 1.5 minutes at 13000 rpm (18500 rcf). The concentration of residual Pb(II) or Cd(II) in the supernatant were extracted and determined using FAAS. The detail is shown in previous paper [14].

5.3.4.2 Effect of contact time

To study the effect of important parameters like contact time on the biosorption removal of Pb(II) and Cd(II), experiments were conducted under room temperature (25℃). The experiments of biosorption kinetics were carried out in a 15 mL glass tube. For each experiment, 10 mL of three types of 0.5 g/L concentrations algal biomass solution were continuously stirred at 200 rpm with 50 mg/L heavy metal ion. 1 mL sample was withdrawn at appropriate time intervals (1, 3, 5, 10, 30, 45, 60 mins) and then centrifuged under 13000 rpm (18500 rcf) for 1.5 min. Then, 0.5 mL of solution at supernatant was determined using FAAS.

5.3.4.3 Effect of initial heavy metal concentration

Biosorption of Pb(II) and Cd(II) on algal biomass were carried out in a single-metal-batch system. Several factors contributed to the selection of the batch technique, including its simplicity and reliability. 1.5 mL algal solution (0.5 g/L) in 2 mL centrifugal tube was agitated in a rotary shaker at 200 rpm and 25℃ and 30-mins incubation time with various initial heavy metal concentration (Pb(II): 10-200, Cd(II): 10-100 mg/L). Then, samples were then centrifuged under 13000 rpm (18500 rcf) for 1.5 min to separate the remaining heavy metal ions from biomass. 0.5 mL of solution at supernatant was determined using FAAS. Moreover, experiment without algal biomass was included in the experiment using the same procedure as control group.

Overall, there is an evaluation of the effect of initial pH (2-6), initial heavy metal concentration (10-200 mg/L), contact times (1, 3, 5, 10, 30, 45, 60 minutes) on biosorption of Pb(II) and Cd(II).

Experimental results are reported as arithmetic means with standard deviations (as error bars in graphs).

The equilibrium biosorption capacity and heavy metal removal% by algae were calculated by using Eq.5.1 and 5.2, which shows below:

$$q = \frac{C_0 - C}{x} \quad 5.1$$

$$Heavy\ metal\ removal\% = \frac{C_0 - C}{C_0} \times 100\% \quad 5.2$$

where C_0 (mg/L) is presented as the initial concentration of heavy metal solution, C (mg/L) the final heavy metal concentration in supernatant, x (g DCW/L) the concentration of algal biomass, q (mg/g DCW), the mass of heavy metal adsorbed by unit mass of biosorbents, and %removal efficiency of Pb(II) or Cd(II).

5.3.5 Analyses and characterization

5.3.5.1 Microalgal biomass

In general, at a certain wavelength in the range from 450 to 700 nm, the dry biomass concentration of microalgae has a linear relationship with optical density (OD) [128]. However, the photosynthetic pigments of microalgae, including chlorophyll a and b, carotenoid (e.g., β-carotene), and phycocyanin, have absorption peaks within wavelength from 400 to 680 nm. Of particular relevance, chlorophyll a has an absorption peak at 660 nm [134]. Avoiding the interference of pigments, the wavelength of 700 nm was selected for spectrometric measurement

of biomass concentration in this study. The optical density was determined by a GENESYS^{TM} 10S UV-VIS spectrophotometer (Thermo Fisher Scientific Inc., USA). There is a linear relationship between OD_{700} and *C. vulgaris* biomass concentration, which showing in following Eq. 5.3.

$$X_b = 0.4813 \times OD_{700} \quad 5.3$$

where OD_{700} is the optical density at wavelength under 700 nm and X_b (g/L) refers to the dried cell weight (DCW) concentration of algal.

The residual biomass was determined by drying 40 mL residual samples overnight under the same dried biomass optical density, and weighting the biomass using the following equation:

$$X_r = 0.1816 \times OD_{700} \quad 5.4$$

where OD_{700} is the optical density at wavelength under 700 nm and X_r (g/L) refers to the residual cell weight (RCW) concentration of algal.

5.3.5.2 Heavy metal concentration

Flame Atomic Absorption Spectrophotometers (Thermo Fisher Scientific, USA) were used to determine lead and cadmium concentrations in solution. Due to the fact that spectrophotometers cannot measure high lead and cadmium concentrations (more than 10 mg/L), it is necessary to dilute the solution to a certain concentration using deionized water. In order to determine heavy metal, i.e., Pb(II), Cd(II) concentration (0.1-10 mg/L), the supernatant solution containing heavy metal ions was diluted with deionized water to ensure the concentration is within signal scale, and then FAAS was applied to determine the diluted concentration.

5.3.5.3 Zeta potential and cell size distribution

To measure the zeta potential and cell size distribution of cells, Zetasizer nanometers (Malvern Panalytical, UK) were used. Samples were diluted to 0.1 OD_{700} using deionized water. Then 1 mL sample was ejected into DTS1070 cuvette for analysis.

5.3.5.4 FTIR

FTIR spectra of dried and residue biomass with or without biosorption of Pb(II) and Cd(II) were obtained using an Angel Technology Cary 630 spectrophotometer. The dried and residue microalgal samples were prepared by filtering the culture through a 0.45um membrane filter, drying them in an oven at 60°C overnight, and then analyzing them.

5.3.5.5 SEM

The morphology of dried microalgae and residual microalgae was examined using scanning electron microscope. The microalgal samples were mixed with glutaraldehyde fixative for 2 hours, then soaked in 0.1 M PBS for 48 hours. Afterward, the sample was rinsed in 0.1M PBS three times for 20 minutes each time. Following that, the sample was dehydrated in an increasing concentration of ethanol solution for a duration of 10 minutes (30, 50, 70, 90, 95%, 100%). After drying at room temperature, samples were coated with gold (882, Gatan, USA) and analyzed with JSM-7500F FESEM (JEOL, USA).

5.3.5.6 Lipid extraction

Lipids were extracted by 1.0 g dried biomass with 30 mL chloroform-methanol in a ratio(volume) of 2:1 [272]. The sample was shaken overnight under 180 rpm shaker. To obtain soluble solution, a separatory funnel was used. After the lipid fraction was separated from the separatory funnel, the solvent was evaporated from it using an evaporator. In the following step, an electronic scale was used to measure the lipid weight.

5.4 Result and discussion

5.4.1 Microalgal morphology

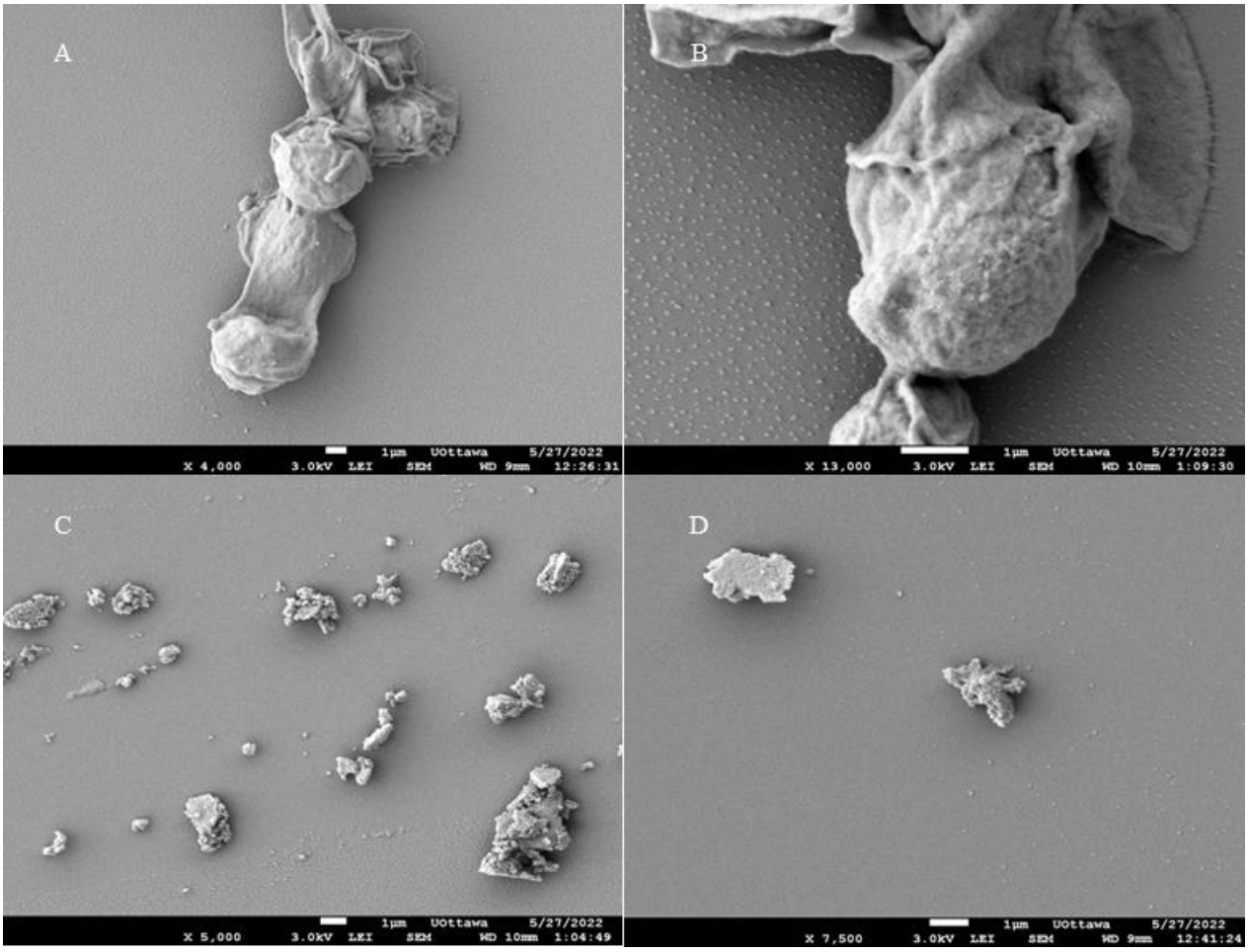

Figure 5-2 SEM images of dried (A&B) and residual (C&D) *C. vulgaris* biomass.

The SEM images of dried cells and cell debris in the residual biomass of *C. vulgaris*, a unicellular green alga, are shown in Figure 5-2. While the morphology of *C. vulgaris* cells are typical near-spheric unicellular [49], that of the cells in the dry biomass as shown in Figure 5-2 (A&B) were deformed with several cells sticking to each other, apparently because of heating and dehydrating in the drying process. As also shown in Figure 5-2 (C&D), after lipid extraction process, the microalgal cells were broken into cell debris of irregular morphology. While the

average diameter of the cells in the wet and dried microalgae was approximately 3.0 μm, that of the residual biomass (cell debris) was about 1.0 um with a very large size distribution measured by Zetasizer nanometers. In the extraction process, the lipids were extracted from microalgae using a mixture of chloroform and methanol (2:1) assisted by ultrasonication, obtaining approximately 18 wt% lipids. As the residual biomass after lipid extraction reveals a larger inner surface area than whole cells, it potentially has a higher biosorption capacity than both dried and wet biomass.

Ultrasonication has been frequently used for the disruption of microalgal cells [273,274]. According to current research, acoustic cavitation is the most popular theory of ultrasonic cell disruption, which is based on the fact that ultrasonic waves cause molecular motions via rarefaction and compression. It was reported the bulk sample temperature reached 85°C within 15 min when 100.7 MJ/kg of energy was supplied by ultrasound in the cell disruption of *Scenedesmus* cells [275]. Of particular relevance, it was shown that the local temperature and pressure could rise up to 5,000 K and 100 MPa, respectively in sonication for the disruption of *Microcystis aeruginosa* cells [276]. Such high temperature and pressure could cause complex physical and chemical effects to cells in the proximity, which, in combination, with the effects of negative pressure at the rarefaction cycle, may cause cells to be porated, torn apart, or even defragmented. As a result of cell disruption, ultrasonication of microalgae may result in more hydroxyl and carbohydrate functional groups on the inside and outside of the cell [277]. Therefore, the inner cell wall of cells in residual biomass would be available for heavy metal adsorption, roughly doubling the adsorption surface in comparison to that of wet and dried biomass.

5.4.2 FTIR

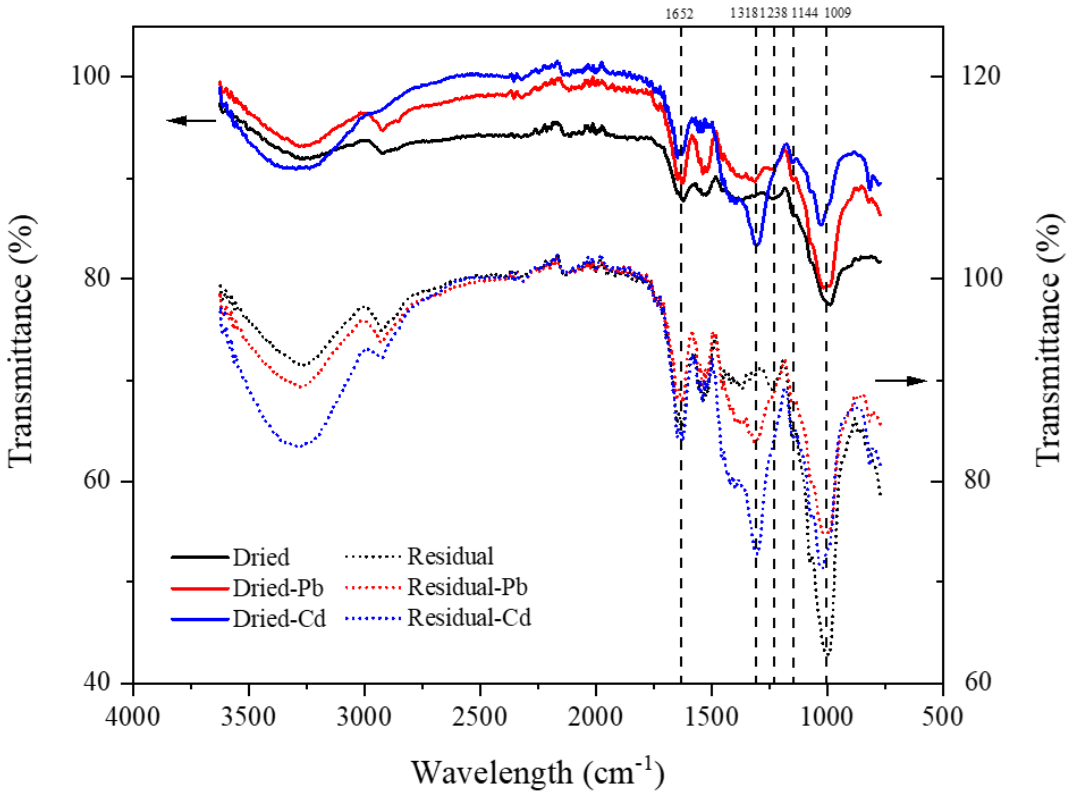

Figure 5-3 FTIR of dried or residual *C. vulgaris* biomass with or without loading Pb(II) or Cd(II) (200 mg/L heavy metal ion and 0.5 g/L biomass).

FTIR spectra of *C. vulgaris*, as well as those loaded with Pb(II) and Cd(II), were obtained in the range of 4000–400 $cm^{-1,}$ showing in Figure 5-3. Based on FTIR analysis, the functional groups for biosorption of Pb(II) and Cd(II) are confirmed. The dried and residual biomass are characterized by: the peak occurs around 1652 cm^{-1}, which corresponds to the vibrations of C=N of peptides on cell wall [167]; the peak occurs at 1318 cm^{-1} corresponding to C-H bending of aromatic hydrocarbon [278]; the peak at 1238 cm^{-1}, which is attributed to asymmetric and symmetric stretching of P=O in the phosphodiester backbone of the nucleic acid [236]; the

strong and broad band around 1147 cm^{-1} was attributed to the stretching vibration of the C-OH group from polysaccharide, the peaks at 1073 and 1013 cm^{-1} are corresponding to the C-O-C in the glycosidic linkage of polysaccharide [279].

After biosorption of Pb(II) and Cd(II), peak at 1652 cm^{-1} redshifted to 1650 and 1651 cm^{-1}, respectively. This indicates that the amine groups on the cell wall surfaces contributed to the biosorption. FTIR spectra of biomass has a peak at 1318 cm^{-1}, which redshifted to 1313 and 1304 cm^{-1} when loaded with Pb(II) and Cd(II), respectively. This peak is usually attributed to C-H of aromatic hydrocarbon related with chitin and other polysaccharides, which widely exits on cell wall. Furthermore, the peak at 1238 cm^{-1} blueshifted to 1249 and 1244 cm^{-1} after loading Pb(II) and Cd(II), respectively. As a result of the peak at 1238 cm^{-1} being P=O bound, it has been involved in the biosorption of Pb(II) and Cd(II), which has also been confirmed in previous study [126]. Additionally, the peak around 1144 cm^{-1} blueshifted to 1147 and 1150 cm^{-1} after loading with Pb(II) and Cd(II), respectively, which indicates the participation of the C-OH in the biosorption. It is also of interest to note that the peak at 1073 cm^{-1} redshifted to 1071 cm^{-1} after heavy metal biosorption as well as the peak at 1013 cm^{-1} blueshifted to 1016 and 1023 cm^{-1} after loading with Pb(II) and Cd(II), indicating the carboxyl group involvement in biosorption. The aforementioned evidence suggests that partial negative charge of P=O, C-O-C, C-OH and C-N bonds contributed to biosorption of positive charge heavy metal ions. Moreover, those chelate compounds like P=O, C-O, O-H, C-N are organic groups that form two or more bonds, chelating toxic metal ions, resulting in the formation of metalled-organic molecules, thereby preventing their interaction with biological macromolecules [280]. Overall, functional groups on the surface of cells such as phosphate, carboxyl and amino groups, play important roles in the biosorption of

Pb(II) and Cd(II), which is consistent to the results of our previous studies on a different green alga, i.e., *N. oleoabundans* [14].

5.4.3 Biosorption

5.4.3.1 Effect of pH

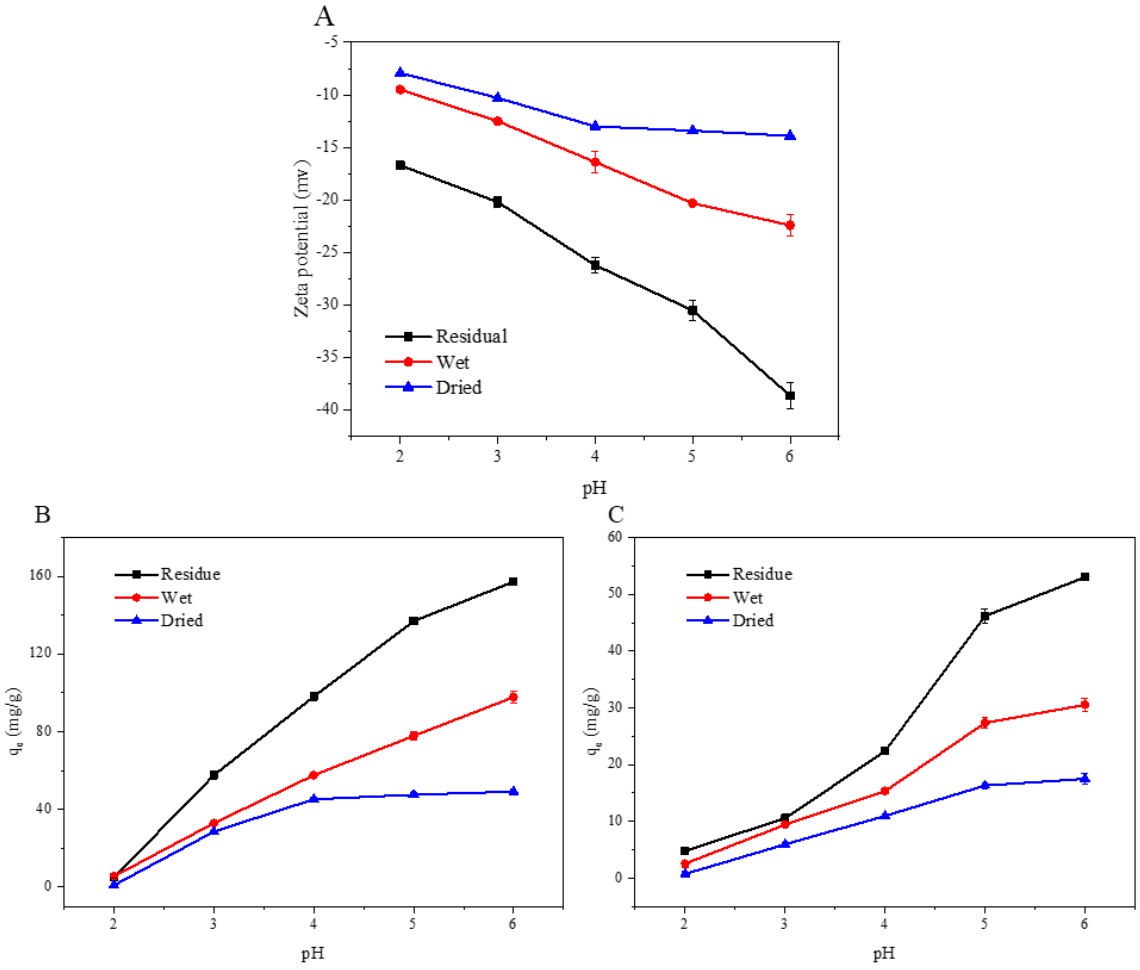

Figure 5-4 Effect of pH on equilibrium biosorption of Pb(II)(B) and Cd(II)(C) and zeta potential (A) of *C. vulgaris* biomass, initial 50 mg/L heavy metal concentration, 0.5 g/L biomass dosage, 30 mins contact time, 25 ℃.

The influence of pH value on biosorption for Pb(II) and Cd(II) was studied within a range from pH 2 to 6 and the results are depicted in Figure 5-4. The equilibrium biosorption (i.e., q_e)

increased with increasing pH value in the entire range from 2 to 6 for all the three types of biomasses. The highest equilibrium biosorption of Pb(II) were 157.29 mg/g, 97.84 mg/g and 41.37 mg/g for residual, wet, and dried biomass under pH 6, respectively. And the highest equilibrium biosorption of Cd(II) were 52.99 mg/g, 30.51 mg/g and 17.49 mg/g for residual, wet, and dried biomass under pH 6 as well. A comparison of equilibrium biosorption of Pb(II) and Cd(II) at the same pH revealed residual biomass followed by wet biomass followed by dried biomass throughout the entire pH range. Microalgal cell wall abundant negative charged functional groups including amino, carboxyl, thiol, sulfhydryl, and phosphate groups. Depending on the pH, these functional groups are protonated or unprotonated. It was observed that all metal ions at pH 2.0 showed a lowest equilibrium biosorption value due to their ionic forms and electric charges. Due to a low pH, functional groups on algal cells are protonated, which results in the absence of binding sites for positive heavy metal ions. Under different pH values (2-6), the ionic states of functional groups in algal cells have a significant effect on the level of biosorption on their cell walls, which obtaining different equilibrium biosorption. Using different types of biomass, researchers have investigated the effects of pH on biosorption of heavy metals, finding that higher pH results in higher equilibrium biosorption [94,108]. For microalgal biochemical content, Mathys et al. reported that major components of *C. vulgaris* were carbohydrates (44.5%), proteins (11.6%), lipids (6.9%), minerals (0.9%) etc. [281]. And cell wall composition of *C. vulgaris* were glucuronic acid (pka=3.21), galacturonic acid (pka=3.47), palmitic acid (pka=4.75), stearic acid (pka=4.95) and chitin (pka= 6.1) [281,282]. When pH increases from 4 to 6, these binding sites were deprotonation, which leading higher equilibrium biosorption. Considering that the drying process at 60 ℃ can cause irreversible chemical reactions on the surface of cells, this may result in the destruction of functional groups, leading a reduced capacity for biosorption. In

combination with FTIR data, it demonstrates that the mechanism of biosorption occurs through ion exchange, which involve negative functional groups, e.g., hydroxyl, carboxyl, phosphate etc.

In Figure 5-4 C, the zeta potentials of residual, wet, and dried biosorbents are shown as a function of pH. In the pH range of 2 to 6, the zeta potential was negative for all biosorbents tested, and the absolute value of zeta potential increased with increasing pH. Since the biomass has a negative zeta potential, positively charged metals can be removed from an aqueous solution more readily. The results are consistent with equilibrium biosorption. Accordingly, the biosorption experiments below were carried out at pH 6, which achieved the highest equilibrium biosorption of Pb(II) and Cd(II).

5.4.3.2 Biosorption kinetics

A series of experiments were carried out to study the kinetics of the biosorption at initial heavy metal concentration 50 mg/L, pH6, biosorbent dose=0.5 g/L, and various contact times (0-60 mins). Data were evaluated using a pseudo-first-order (Eq. 5.5) and pseudo-second-order (Eq. 5.6) model [32].

$$q(t) = q_e[1 - \exp(-k_1 t)] \quad 5.5$$

$$q(t) = q_e \frac{k_2 t}{1 + k_2 t} \quad 5.6$$

where q(t) (mg/g) and q_e (mg/g) are the biosorption at a certain time (min) and the equilibrium biosorption, respectively. K_1 (min^{-1}) and K_2 (g/min^{-2}) are the pseudo-first-order and pseudo-second-order model constants, respectively.

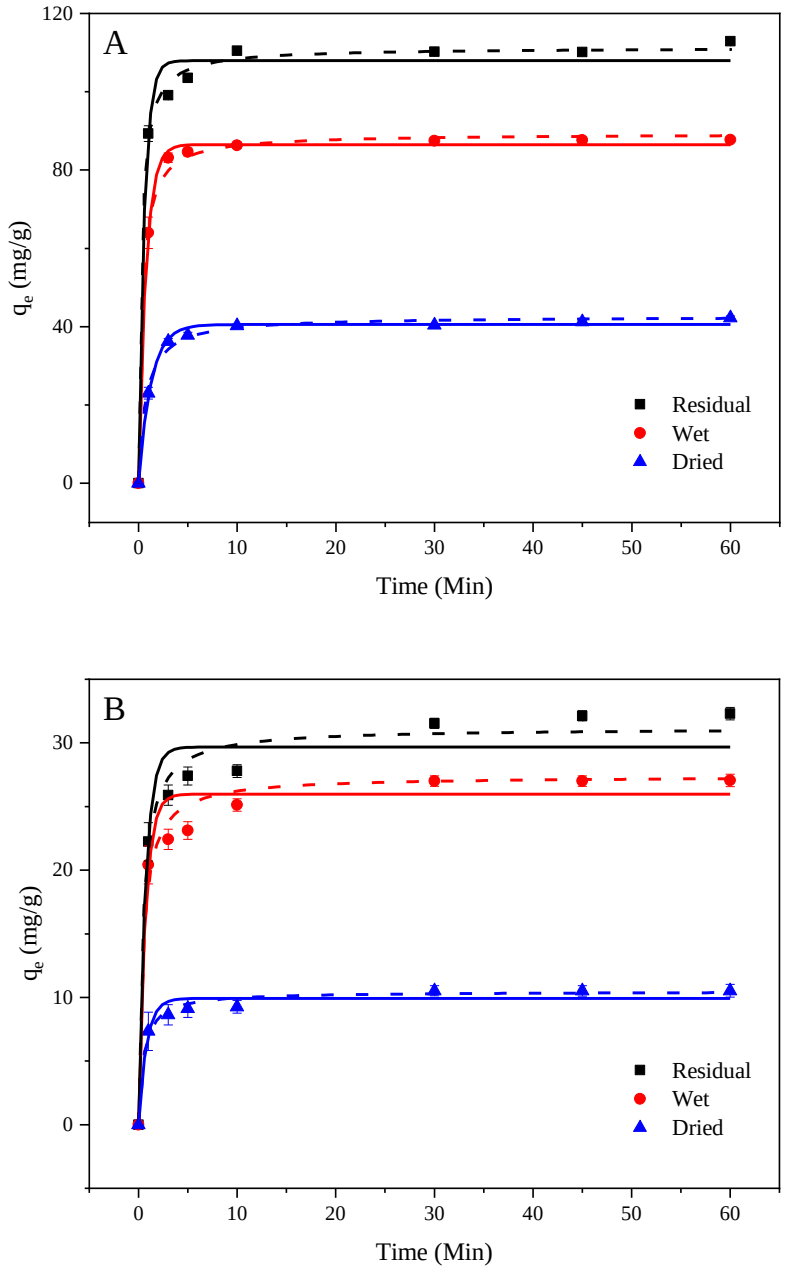

Figure 5-5 Kinetics of Pb(II) (A) and Cd(II) adsorption by residual, wet, and dried cells fitting with two kinetic models: pseudo-first (solid) and pseudo-second order (dash); at pH 6, 0.5 g/L biomass, and 50 mg/L heavy metal ion concentration. A mean value of triplets along with a standard deviation is reported (n = 3).

Table 5-1 Kinetics model parameters for Pb(II) and Cd(II) biosorption by microalgae *C. vulgaris*.

Kinetic model	Parameters	Pb(II)			Cd(II)		
		Residual	Wet	Dried	Residual	Wet	Dried
Pseudo-first	$K_1(min^{-1})$	1.719	1.328	0.795	1.421	1.440	1.243
	$q_{e,cal}$ (mg/g)	107.94	86.5	40.55	29.67	25.98	9.92
	R^2	0.9872	0.9971	0.9938	0.9536	0.9436	0.9560
	SSE	21.45	18.72	9.14	6.1	34.44	3.88
Pseudo-second	$K_2(g/min^{-2})$	3.729	2.816	1.358	2.309	2.219	1.976
	$q_{e,cal}$(mg/g)	111.29	89.31	42.65	31.17	27.39	10.46
	R^2	0.9975	0.9984	0.9944	0.9826	0.9778	0.9863
	SSE	6.70	10.07	8.24	2.29	13.56	1.21

Figure 5-5 presents the kinetics of biosorption of Pb(II) and Cd(II) by residual, wet, and dried *C. vulgaris* biomass. It was observed that Pb(II) and Cd(II) biosorption increased rapidly and >95% was completed within 5 mins for all biosorbents. Plateau were established within 10 mins for the biosorption of Pb(II) for all biomasses. However, the plateaus of the biosorption of Cd(II) were established in 30 mins with wet and dried biomasses while slight increase was observed from 30 to 60 minutes. When compared to residual, wet and dried biomass, the equilibrium biosorption of Pb(II) and Cd(II) by residual biomass were the highest at any point during the sorption process comparing with wet and dried biomass. In addition, the kinetic data were fitted with pseudo-first order and pseudo-second order models in Table 5-1. According to the pseudo-first order and pseudo-second order model, adsorption rate is proportional to vacant sites for adsorption and square of the number of vacant adsorption sites, respectively [283]. A summary of the modelling parameters is presented in Table 5-1. It shows that experimental data for all biosorbents were better fitted by the pseudo-second-order model based on R^2 or SSE, indicating that the biosorption rate was proportional to the square of the concentration of heavy metal ion and

biomass. For the following experiments, the biosorption of Pb(II) and Cd(II) was conducted for 30 minutes to ensure adequate contact time.

5.4.3.3 Isotherm

In isotherm study, biosorption equilibrium experiments (pH 6, biosorbent dose = 0.5 g/L, contact time: 30 min) were carried out with different metal concentrations (Pb(II) 10-200 mg/L Cd(II) 10-100 mg/L). Two parametric models were applied, including Langmuir's (Eq. 5.7) and Freundlich's (Eq. 5.7) isotherm models [50].

$$q_e = \frac{q_m K_L C_e}{1 + K_L C_e} \tag{5.7}$$

where C_e is the equilibrium concentration of the heavy metal ions in the solution (mg/L), q_e the equilibrium biosorption (mg/g), q_m the biosorption capacity (i.e., maximum equilibrium biosorption) of the biosorbent (mg/g), and K_L the Langmuir model constant, which is related to the energy of biosorption (L/mg).

The Langmuir model assumes monolayer adsorption of absorbates on homogeneous the sorbent surfaces and constant adsorption energy. As an alternative to a dimensionless separation factor, the Langmuir equation can be expressed by a dynamic equilibrium parameter, R_L, which is defined as follows (Eq. 5.8).

$$R_L = \frac{1}{1 + K_L C_0} \tag{5.8}$$

In this case, C_0 indicates the initial metal concentration in the solution (mg/L). The R_L value can be used to classify biosorption based on its irreversibility ($R_L = 0$), favorable ($0 < R_L < 1$), linear ($R_L = 1$), and unfavorable ($R_L > 1$).

A Freundlich isotherm model is used to assess multilayer sorption on heterogeneous surfaces. An appropriate sorption process usually involves 1/n between 0 and 1.

$$q_e = K_F C_e^{\frac{1}{n}} \qquad 5.9$$

where K_F ($mg^{(1-1/n)}g^{-1}L^{1/n}$) and n are empirical constants of the Freundlich model. $1/n$ represents the biosorption intensity, and K_F represents the relative biosorption capacity.

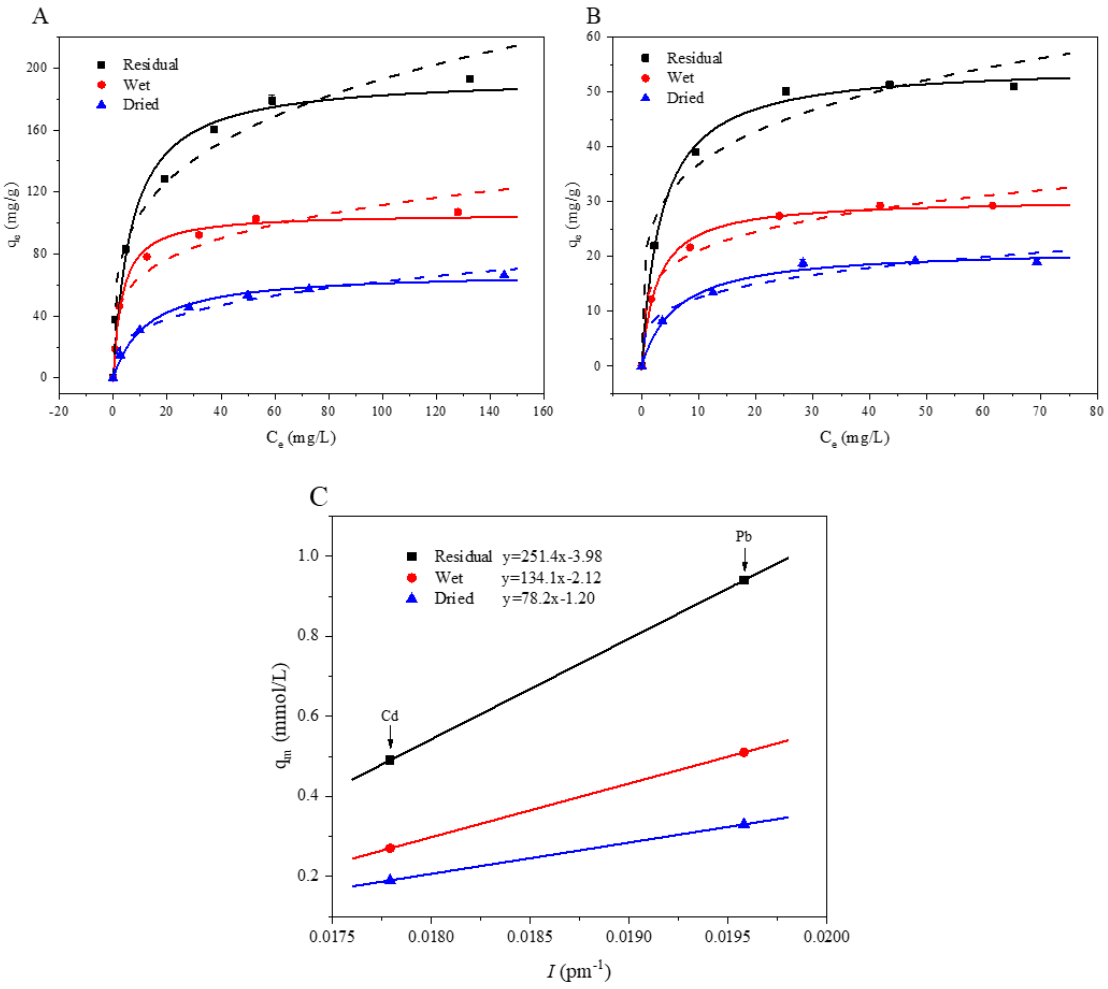

Figure 5-6 Isotherm of Pb(II) (A) and Cd(II) (B) fitted by Langmuir model (solid) and Friedrich model (dash) under pH 6, 0.5 g/L biomass, 30 mins incubation, 25℃, and dependence of biosorption capacity (mmol/L) of metal ions by biomasses on the impactor factor of metal ions (I = Electronegativity/Radius) (C).

Table 5-2 Isotherm parameters for Pb(II) and Cd(II) biosorption by microalgae *C. vulgaris*.

		Langmuir				Freundlich		
	Biosorbents	q_{max} (mg/g)	K_L (L/mg)	R_L	R^2	K_F ($mg^{(1-1/n)}g^{-1}L^{1/n}$)	1/n	R^2
Pb	Residual	194.79	0.1476	0.005-0.404	0.9755	58.01	0.2610	0.9548
	Wet	106.25	0.2982	0.005-0.251	0.9871	38.15	0.2331	0.9081
	Dried	68.69	0.0803	0.005-0.555	0.9852	15.26	0.3054	0.9636
Cd	Residual	54.98	0.2887	0.005-0.709	0.9904	22.34	0.2169	0.8866
	Wet	30.47	0.3647	0.005-0.657	0.9855	12.82	0.2160	0.9369
	Dried	21.44	0.1618	0.005-0.770	0.9684	6.91	0.2585	0.8848

Experimental isotherms were fitted with the Langmuir and Freundlich isotherm models as shown in Figure 5-6. A summary of the isotherm parameters and R^2 obtained from the two isotherm models are shown in Table 5-2. According to the results, the R^2 values obtained from Langmuir model (>0.96) were consistently higher than those obtained from Freundlich's model for both the metal ions, i.e, Pb(II) and Cd(II), and all the three biosorbents, i.e., residual, wet and dried biomasses. Langmuir isotherm implies monolayer adsorption of the metal ions on the surface of biosorbents, i.e., microalgal cells. Furthermore, wet biomass produced the highest K_L values, suggesting that it was a stable biosorption product with a high affinity for Pb(II) and Cd(II). Additionally, all R_L are between 0 and 1, which indicates favorable biosorption.

The adsorption capacities of Pb(II) and Cd(II) by different biomasses as calculated according to the Langmuir isotherm model, i.e., q_{max}, are summarized in Table 5-3. For the same metal ion, either Pb(II) or Cd(II), the q_{max} by different biomasses follow the order of residual> wet> dried. Wet biomass has a higher adsorption capacity for Pb(II) and Cd(II) than the corresponding dried

biomass by two close ratios, i.e., 1.55 and 1.42, respectively, suggesting that the difference was cause primarily by the different properties of the wet and dried biomasses. These differences between the dried biomass and the wet biomass might be caused by the physical and chemical changes occurred to the biomacromolecules on the surface of the cells and the functional groups on them during the high temperature dehydrating process.

Table 5-3 Relationship between biosorption capacity (mmol/g) and metal properties.

Metal ion properties				q_{max} (mmol/g)		
Metal	Electronegativity	Radius (pm)	I (pm^{-1})	Residual	Wet	Dried
Pb	2.33	119	0.0196	0.94	0.51	0.33
Cd	1.69	95	0.0178	0.49	0.27	0.19

It is worth noting that the residual biomass underwent the same drying process as the dried biomass. However, its biosorption capacities for Pb(II) and Cd(II) were 1.84 and 1.81 times that of the wet biomass, respectively. Furthermore, the biosorption capacities for Pb(II) and Cd(II) by the residual biomass were 2.85 and 2.58 times of that of the dried biomass, respectively. The remarkable increase of the adsorption capacity of the residual biomass in comparison to both the wet and the dried biomass could be mainly attributed to the increase of the surfaces available for heavy metal adsorption. The cells in the residual biomass were broken up into cell debris in the sonication process in preparation for lipid extraction, which exposed the inner surface of cell wall that was not accessible to metal ions in the dried biomass. Indeed, Jung et al. (2011) reported in their study on the utilization of the residual biomass of another green alga, *Nannochloris oculate*, after lipid extraction for Cr(III)/Cr(VI) biosorption that the residual *N. oculate* biomass had a BET surface area of 1.87 m^2/g, which was 2.1 times that of the original biomass (0.89 m^2/g). It is therefore reasonable to assume that the surface area of the residual biomass of *C. vulgaris* after

lipid extraction would also be slightly larger than twofold of the dried biomass. The other factors that might also have contributed to the large capacity of the residual biomass include: 1). the inner surface of cell wall may harbor metal-binding functional groups not available on the outer cell wall surface; and 2). lipid extraction might have removed most lipids from the cell wall surfaces, both inner and outer, which may expose more functional groups for metal ion adsorption. Hypothetically, the vastly enhanced biosorption capacity of residual biomass in comparison to both wet and dried biomass is attributed primarily to the exposure of the inner cell wall surface of cell debris in residual biomass. Therefore, the biosorption capacity of residual biomass for both Pb(II) and Cd(II) were 2.83 and 2.56-fold than dried biomass, which can be hypothetically explained by its doubled surfaces for heavy metal adsorption in comparison to that of intact cells in wet and dried biomasses.

In a previous research on the biosorption of five strategically selected heavy metal ions by wet *N. oleoabundans* biomass [14], we found that there was a linear relationship between the impact factor (*I*), which was defined by the electronegativity of an ion by the radius of the ion, and its adsorption capacity (q_{max}). It was further found several data found in the literature also showed linear relationship with different slope when different biomasses were involved as the biosorbents. Biosorption of two different heavy metal ions was investigated, i.e., Pb(II) and Cd(II), which do not give us enough data points to judge if such a linear relationship exists. Nevertheless, the general trend, that is, the q_{max} increases with the impact factor of a given heavy metal ion when the same biomass is used as the biosorbent. Furthermore, when the q_{max} of Pb(II) and Cd(II) on different biomasses, i.e., residual, wet, and dried, are plotted in pairs as shown in Figure 5-6 C, the slopes were 251.4, 134.1, and 78.2 mmol $g^{-1}p^{-1}$, in a range the same magnitude as reported in the aforementioned previous research (26.6-117.51 mmol $g^{-1}p^{-1}$). It can be concluded according

to the data of both this study and that reported before that the slope of the q_{max} vs I linear curve depends on the properties of the biomass as biosorbents. In this study, it is further observed that the order of the slope values, i.e., residual> wet> dried, was the same as that when the q_{max} of the adsorption of the same metal ion, i.e., either Pb(II) or Cd(II), by different biomasses were compared.

Table 5-4 Biosorption capacities of Pb(II) and Cd(II) by different microalgal biomasses.

Heavy metal	Biosorbents	Form	Biosorption capacity(mg/g)	pH	Equilibrium time (min)	Reference
Pb(II)	*N. oleoabundans*	Wet	213.42	7	5	[14]
	Chlorococcum aquaticum	Wet	500.00	7	720	[149]
	Aphanothece sp.	Dried	185.64	6	120	[54]
	Gelidiella acerosa	Dried	74.00	5	120	[285]
	Ochrobactrum cicero	Dried	87.71	6	30	[286]
		Residual	194.79	6	10	
	C. vulgaris	Wet	106.25	6	10	This study
		Dried	68.69	6	10	
Cd(II)	*Ochrobactrum cicero*	Dried	67.84	6	30	[286]
	C. vulgaris	Dried	97.43	4.5	120	[108]
	N. oleoabundans	Wet	73.07	7	5	[14]
	C. vulgaris (13- 1)	Wet	59.50	5.5	1440	
	Coelastrella sp. (3-4)	Wet	83.00	5.5	1440	[287]
	Scenedesmus obliquus (13-8)	Wet	28.00	5.5	1440	
	Coelastrum sp.	Residual	32.80	7.5	2	[46]
		Residual	54.98	6	30	
	C. vulgaris	Wet	30.47	6	30	This study
		Dried	21.44	6	30	

Table 5-4 compares the biosorption capacities of Pb(II) and Cd(II) by different microalgal biomasses. The highest capacity for Pb(II) was reported with wet *Chlorococcum aquaticum* at 500 mg/g at an incubation time of 720 min [149] and that for Cd(II) was with dried biomass of *C. vulgaris* at 97.43 mg/g with a 120 min incubation time [108]. It should be pointed out that the Cd(II) adsorption capacity by dried *C. vulgaris* biomass was only 21.44 mg/g in this study, which

is only 22% of the aforementioned literature value. This vast different adsorption capacities to the same heavy metal ion by the same green alga species are compatible with a commonly observed phenomenon, i.e., the adsorption capacity of algal biomass is dependent on many parameters, including the medium and condition of algal cultivation, physiological state when algae were harvested, condition of the drying process, as well as the adsorption conditions such as the buffer pH, metal ion concentration in feed, incubation time, and dosage of biomass [20].

5.5 Conclusion

Results indicate that residual biomass of *C. vulgaris* is potentially an effective biosorbent with a high biosorption capacity, when comparing based on same dry mass, vastly larger than that of both wet and dried biomasses. It seems quite conclusive that the adsorption capacity of residual biomass was primarily due to the exposure of the inner cell wall surface for heavy metal adsorption, which doubles the adsorption surface. Other factors such as the exposure of functional groups that are unique to the inner cell wall surface and the removal of lipid from cell wall surfaces might also have contributed to the improvement of biosorption of heavy metal ions with residual algal biomass. This cheap residual biomass after lipid extraction exhibits fast kinetics and a high biosorption capacity for Pb(II) and Cd(II), making it suitable for industrial plants.

5.6 Acknowledgment

This work was supported by NSERC Discovery Grant RGPIN-2022–05242 from the Natural Sciences and Engineering Research Council of Canada (NSERC).

Chapter 6 Mechanism of heavy metal ion biosorption by microalgal cells, a mathematic approach[1]

Siwei Gu & Christopher Q. Lan*

Department of Chemical and Biological Engineering

University of Ottawa

* Chrisotpher.Lan@Uottawa.ca

[1] This paper is publicised on journal of hazardous materials: Gu, S., Lan, C.Q., 2024. Mechanism of heavy metal ion biosorption by microalgal cells : A mathematic approach. J. Hazard. Mater. 463, 132875. https://doi.org/10.1016/j.jhazmat.2023.132875

Highlights

- Biosorption of six heavy metals by microalgae *Chlorella vulgaris* were systematically investigated.
- Langmuir model based on isotherm data suggests monolayer adsorption.
- A mathematical model is proposed and verified for predicting biosorption capacity.
- Microalgal surface structure, metal ion electronegativity, and operational pH influence the model's reliability.

6.1 Abstract

Microalgal biomasses have been established as promising biosorbents for biosorption to remove heavy metal ions (HMIs) from wastewaters and contaminated natural waterbodies. Understanding the mechanism is important for the development of cost-effective processes for large scale applications. In this paper, a simple mathematical model was proposed for the predication of biosorption capacity of HMI by microalgal cells based on microalgal cell weight, cell size, and HMI radius. The model was validated using experimental and literature data and was demonstrated to be good for rough estimation. The validation of the model, in combination of kinetic, isotherm, and FTIR data generated in this study and in literature, affirmed one fundamental assumption based on which this model was developed, i.e., the biosorption of HMI by microalgal cells is predominantly monolayer bioadsorption. The maximum biosorption capacities of HMIs (mmol/g) by *Chlorella vulgaris* were determined to be in the following order: Pb(II)(0.360)>Zn(II)(0.325)>Cu(II)(0.254)>Ni(II)(0.249)>Cd(II)(0.235)>Co(II)(0.182). We also systematically investigated the variations in predicted biosorption capacities in term discrepancies caused by a few important parameters that were unaccounted for by the model, including the nanostructures on cell surface, HMI electronegativity, and biosorption buffer pH. Results suggest that the nanostructures on cell wall, most likely the hairlike fibers, might be where the binding sites for HMI located.

Key words: Biosorption, theoretical modeling, heavy metal ion, *Chlorella vulgaris*

6.2 Introduction

The utilization of microalgae as a biosorption material has garnered significant attention for heavy metal ion (HMI) removal from contaminated water sources, owing to its environmental compatibility, promising cost-effectiveness, straightforward operational procedures, and adaptability for large-scale industrial applications as biosorbent [36,288,289]. Microalgae can grow in extreme environmental conditions, including low nutrients (phosphate and nitrate), extreme pH (~10.5) and high temperature (35 ℃) [232,290]. Furthermore, microalgae possess the capability of self-propagate and have high efficiency in HMI removal from contaminated waters even at low concentration (<1.5 mg/L) [235]. Additionally, the biomass containing HMIs could be conveniently combusted to reduce the volume of waste disposal or to recover HMIs, as appropriate, while generating heat or for other applications [291,292].

The biosorption of HMIs by microalgae may occur in two steps: bioadsorption and bioabsorption [20]. Firstly, the cell wall of microalgae provides a large surface area due to the presence of negative functional groups in biochemicals such as polysaccharides, lipids, and proteins. Positively charged HMIs can be adsorbed onto the cell wall via electrostatic interaction with these negative functional groups. This is bioadsorption. Secondly, the HMIs adsorbed onto cell surface in bioadsorption could be transported to inside the microalgal cells through specialized ion channels, which is an active transportation process that is highly selective, ATP-consuming, and slow in comparison to bioadsorption [293,294].

Numerous studies have reported on the biosorption of HMIs by microalgae, and it is evident that the biosorption capacity of HMIs varies considerably due to three primary factors: the properties of microalgae, the properties of HMIs, and the biosorption conditions [14,70,71,292,295]. The

variations in biosorption capacity of HMIs observed among different microalgal biomass can often be attributed to differences in microalgal properties such as cell weight, cell size and the nanostructures on cell surface. For instance, unicellular microalgal biomass, such as *Chlorella vulgaris*, *Chlorella minutissima* and *Parachlorella sp*., exhibit higher biosorption capacities than multicellular microalgal biomass, like *Scenedesmus-24* and *Spirulina platensis* [70,71]. Moreover, it's worth noting that variations in biosorption capacity for different HMIs can be remarkable with the same microalgal biomass. These discrepancies are often associated with the properties of the HMIs themselves, particularly ionic radius and electronegativity [14].

In this study, we systematically studied the FTIR spectra, isotherm, and kinetics of HMIs biosorption by green microalga *C. vulgaris* for six selected HMIs, i.e., Pb(II), Zn(II), Cu(II), Ni(II), Cd(II), and Co(II). Furthermore, the distribution of Pb(II) on cell surface and inside cell were studied at different initial Pb(II) concentration. These data, in combination with numerous literature data, all support the notion that the biosorption of HMIs by *C. vulgaris* is predominantly monolayer surface bioadsorption. Based on this understanding, we proposed a novel model for the prediction of biosorption of HMIs based on cell weight, cell size and HMI ionic radius. This model was then validated with experimental data of the biosorption of six HMIs on *C. vulgaris* and literature data on the biosorption of various HMIs using three microalgal species, i.e., *C. vulgaris*, *Neochloris oleoabundans*, and *Scenedesmus quadricauda*. The deviations of the biosorption capacities predicted by this rather rigid model from experimental and literature data were also discussed in the context of how different factors, including ionic electronegativity, nanostructures on cell surface, and biosorption buffer pH, affecting biosorption and therefore causing deviation in the predictions.

6.3 Materials and methods

All experiments were conducted in triplicate with mean values and error bars reported.

6.3.1 Microalgal cultivation

The microalgae strain *C. vulgaris*, UTEX 2714, was obtained from the University of Texas in Austin. The cultivation of the microalga was carried out using autoclaved Bold Basal medium (BBM) [133], specifically designed for freshwater microalgae. The composition of one liter of distilled water used in the medium was as follows: 0.25 g $NaNO_3$, 0.025 g $CaCl_2 \cdot 2H_2O$, 0.75 g $MgSO_4 \cdot 7H_2O$, 0.075 g K_2HPO_4, 0.175 g KH_2PO_4, 0.025 g NaCl, 0.00498 g $FeSO_4 \cdot 7H_2O$, 0.01 g $Na_2EDTA \cdot 2H_2O$, 0.00805 g H_3BO_3. Additionally, 1 mL of trace elements solution was added to the medium. The trace elements solution was prepared by dissolving the following chemicals in one liter of water: 2.86 g $H_3BO_3 \cdot 2H_2O$, 1.81 g $MnCl_2 \cdot 4H_2O$, 0.222 g $ZnSO_4$, 0.0494 g $Co(NO_3)_2 \cdot 6H_2O$, 0.39 g $NaMoO_4 \cdot 5H_2O$, 0.079 g $CuSO_4 \cdot 5H_2O$. The cultivation of the green microalga *C. vulgaris* was carried out in a 3-L photobioreactor vessel suitable for autotrophic cell growth. The photobioreactor was equipped with vertical lamps arranged evenly around the chamber, programmed to operate in 12/12 hours on/off cycles. Before inoculation, cultivation bottles containing 2.0 liters of fresh medium each were sterilized by autoclaving at 121 ℃ for 20 mins. Once the sterilized medium reached room temperature, 40 mL of microalgal seed culture was inoculated into the bioreactor. During cultivation, a constant airflow of 0.5 vvm (i.e., 1 LPM) was maintained, along with continuous agitation at 200 rpm, at 25 ℃. To control the pH of the culture at 9.5, pure CO_2 was continuously mixed into the air stream. This was achieved by passing the airstream through distilled water and a microfilter before it was sprayed into the culture at the bottom of the bioreactor. After a two-week cultivation period, the microalgae reached a stable phase with a cell density of 10^7 cells/ml. The biomass was then harvested and

stored for future use at -80 ℃ freezer. Wet microalgal was obtained to be used as a biosorbent for the following biosorption test. In order to remove remaining chemical residues and fragments in solution, 40 mL of sample was centrifuged three times using deionized water 5 mins under 6000 rpm (8500 rcf). Then wet biomass samples were then resuspended in deionized water by vortexes prior biosorption tests.

6.3.2 HMI stock solution

Heavy metal ion stock solutions, i.e., 1000 mg/L Pb(II), Zn(II), Cu(II), Ni(II), Cd(II), Co(II), were prepared by $Pb(NO_3)_2$, $Zn(NO_3)_2 \cdot 6H_2O$, $Cd(NO_3)_2$, (Strem Chemicals Inc., USA), $Cu(NO_3)_2 \cdot 2.5H_2O$ (Alfa Aesar, USA), $Ni(NO_3)_2 \cdot 6H_2O$ (Thermo Fisher Scientific, UK), and $Co(NO_3)_2 \cdot 6H_2O$ (Thermo Fisher Scientific, USA), which were dissolved in deionized water, respectively. The stock solution was stored in plugged bottle at room temperature.

6.3.3 Biosorption test

6.3.3.1 Effect of contact time

Batch biosorption experiment was conducted in a 2.0 mL graduated microcentrifuge tube using 1.5 mL microalgal biomass. Lead(II), Cadmium(II), Zinc(II), Copper(II), Nickel(II), and Cobalt(II) stock solutions were added into the tube to achieve an initial 0.3 mmol/L HMI concentration. The biomass employed had 0.5 g/L dried cell weight (DCW). Before biosorption incubation, the pH of the mixture was adjusted to 6.0 by adding 0.1 N HNO_3 by Corning pH/ion meter (Model 350). Then, the mixture was shaken under 200 rpm (r/min), continually for a period of time specified in the text (5, 10, 15, 20, 25, 30 mins) at room temperature (25 ℃). Finally, the supernatant solution was extracted by centrifuging the sample for 5 mins at 13000 rpm (18500 rcf). Flame absorption atomic spectrometer (FAAS) was used to determine the

concentration of residual HMI in the supernatant. More the details can be found in previous paper [14].

6.3.3.2 Effect of pH

Effect of pH (2.0-6.0) was carried out under 0.3 mmol/L HMI concentration and 0.5 g DCW/L dosage, 10 mins contact time. Prior to incubation, the pH was adjusted to the desired value by adding amount of 0.1 N HNO_3 to 1.5 mL of biomass solution in a 2.0 mL microcentrifuge tube. Supernatant solution was extracted by centrifugation for 5 mins at 13000 rpm (18500 rcf). Then the HMIs in supernatant was determined using flame absorption atomic spectrometer (FAAS).

6.3.3.3 Effect of HMI concentration

Batch experiment was carried out at various HMI concentration (0.01-1 mmoL/L) under 0.5 g DCW/L, pH 6.0, 10 mins incubation, 25 ℃. Same procedure was followed in previous procedure (Section 2.3.2 under constant operation pH 6.0).

The equilibrium HMI biosorption (q_e, mmol/g DCW) and HMI removal% by microalga were calculated by using the following equations:

$$q_e = \frac{C_0 - C_e}{x} \tag{6.1}$$

$$HMI\ removal\% = \frac{C_0 - C_e}{C_0} \times 100\% \tag{6.2}$$

where C_0 (mmol/L) and C_e (mmol/L) are the initial and equilibrium HMI concentration, respectively, and x (g DCW/L) refers to the microalgal biomass concentration in the biosorption mixture.

6.3.4 Intracellular and extracellular Pb(II)

The determination of intracellular and extracellular Pb(II) concentration followed the methodology described by Zhou et al. [233] with minor modifications.

6.3.4.1 Equilibrium Pb(II) concentration in supernatant:

Batch biosorption experiment was conducted in a 2.0 mL graduated microcentrifuge tube using 1.0 mL microalgal suspension with initial Pb(II) concentration from 5-100 mg/L, pH 6.0, 10 mins contact time and 25 ℃. The sample was then centrifuged at 13000 rpm (18500 rcf) for 5 mins. The supernatant was subjected to flame absorption atomic spectrometer (FAAS) analysis for determination of residual Pb(II) in supernatant. The biomass pellets were subjected to analysis of extracellular and intracellular Pb(II) when applicable.

6.3.4.2 Equilibrium bioadsorption and equilibrium bioabsorption:

The microalgal biomass separated from Pb(II) biosorption sample by separation described in Section 2.4.1 was re-suspended by adding 0.02 M EDTA solution to 1.0 mL. This suspension was gently agitated for approximately 30 seconds with the aim of removing Pb(II) that had adhered to the cell surfaces. Subsequently, the suspended sample underwent an additional round of centrifugation at 13000 rpm (18500 rcf) for 5 mins. The supernatant containing EDTA-bound Pb(II) was then subjected for the purpose of quantifying the Pb(II) concentration by FAAS. The equilibrium bioadsorption ($q_{e,ad}$), i.e., the Pb(II) adsorbed on cell surface per unit mass of cells, and the equilibrium bioabsorption ($q_{e,ab}$), i.e., the Pb(II) absorbed into the cells per unit mass of cells, were determined by the following equations:

$$q_{e,ad} = \frac{C_s}{x} \tag{6.3}$$

$$q_{e,ab} = \frac{C_o - C_e - C_s}{x} \tag{6.4}$$

Furthermore, the Pb(II) contents% on cell surface, i.e., bioadsorption, and in cell body, i.e., bioabsorption, were calculated by the following equations:

$$Pb\ bioadsorption\% = \frac{C_S}{C_o - C_e} * 100\% \quad 6.5$$

$$Pb\ bioabsorption\% = \frac{(C_0 - C_e) - C_s}{C_0 - C_e} * 100\% \quad 6.6$$

where C_0 (mmol/L), C_e (mmol/L) and C_s (mmol/L) are the initial Pb(II) concentration in biosorption mixture, equilibrium residual HMI concentration in supernatant, and HMI concentration in EDTA extract, respectively. And x (g DCW/L) refers to the microalgal biomass concentration. $q_{e,ad}$ (mmol/g) and $q_{e,ab}$ (mmol/g) refer to the equilibrium bioadsorption and equilibrium bioabsorption. *Pb bioadsorption%* and *Pb bioabsorption%* refer to percentage of Pb(II) adsorbed onto cell surface, and the percentage of Pb(II) absorbed into the cells, respectively, based on the total Pb(II) removed from the supernatant by biosorption.

6.3.5 Analyses and characterization

6.3.5.1 Microalgal biomass

In general, within the specified wavelength range of 450 to 700 nm, the quantification of microalgal dry biomass concentration correlates linearly with its optical density (OD) [128]. The wavelength of 700 nm was deliberately chosen for spectrometric analysis of *C. vulgaris* biomass concentration to avoid the interference of photosynthetic pigments, including chlorophylls a, b, c, and carotenoids. The determination of optical density was executed using the GENESYS™ 10S UV-VIS spectrophotometer (Thermo Fisher Scientific Inc., USA). This relationship is expressed in Eq. 6.7 [296].

$$x = 0.4332 \times OD_{700} \quad 6.7$$

where OD_{700} is the optical density at 700 nm, *x* (g/L) the dried cell weight (DCW) concentration of algae, and 0.4332 the empirically determined conversion factor.

6.3.5.2 Heavy metal ion concentration

Flame atomic absorption spectrophotometer (Thermo Fisher Scientific, USA) were used to determine HMI concentrations in solution. For HMI measurement, a specific hollow cation lamp with 1.2 L/min mixing air made up of acetylene and air (pressure ratio is 10 psig: 50 psig) were used. Then, HMI standards (Sigma-Aldrich, Canada) with 0.1 M HNO_3 were utilized for establishment of standard curves. 1 mL sample solution containing HMIs was diluted with deionized water (if applicable) to ensure the concentration was in the range of (1-100 umol/L), and then subjected to FAAS analysis. The wavelength were 217, 228.8, 213.9, 324.8, 232 and 240.7 nm for Pb(II), Cd(II), Zn(II), Cu(II), Ni(II) and Co(II), respectively.

6.3.5.3 Zeta potential

Zetasizer nanometers (Malvern Panalytical, UK) were used to measure the zeta potential of *C. vulgaris*. The microalgal biomass samples were adjusted to 0.1 g/L biomass by deionized water prior to analysis. Then, 1 mL sample was ejected into a DTS1070 cuvette (Malvern Panalytical, UK) for zeta potential analysis.

6.3.5.4 FTIR

FTIR spectrophotometer (Cary 630 Angellent technology, USA) was used to analyze the infrared spectra of biomass. 0.5 g DCW/L algal biomass with or without 0.5 mmol/L HMIs loaded pellet were obtained by centrifugation for 5 mins at 13000 rpm (18500 rcf), dried at 60 ℃ overnight in oven, and subjected for analyses.

6.4 Result and discussion

6.4.1 HMI biosorption by microalgal cells: monolayer surface bioadsorption

6.4.1.1 FTIR evidence of surface biosorption

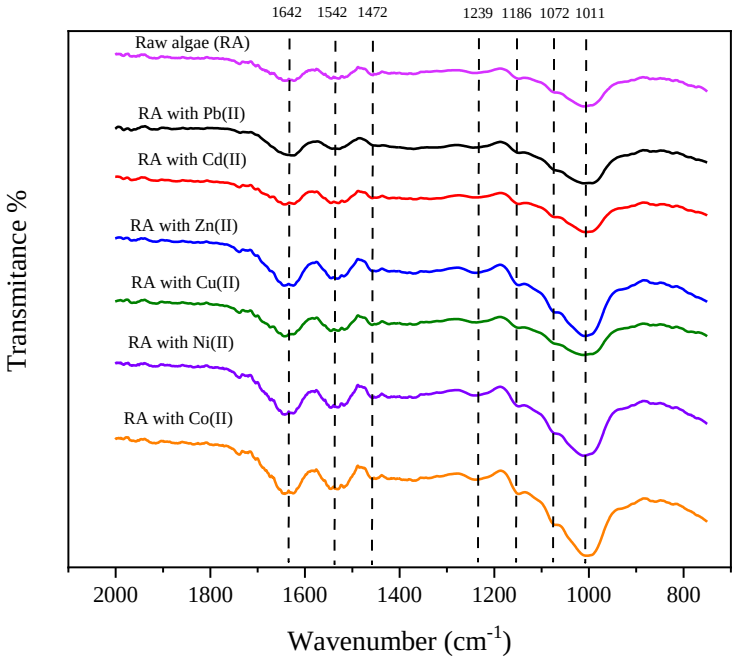

Figure 6-1 FTIR spectra of C. vulgaris cells before and after adsorbing Pb(II), Cd(II), Zn(II), Cu(II), Ni(II), or Co(II), 0.5 g/L DCW, 50 mg/L initial metal concentration 50 mg/L 10 mins contact time.

Table 6-1 FTIR spectrum of *C. vulgaris* before and after HMI biosorption.

Biosorbent	Raw	Pb	Cd	Zn	Cu	Ni	Co	Functional group	Ref.*
Wavenumber (cm^{-1})	1011	1005	1012	1003	1002	1006	1010	C-O-C	[297]
	1072	1083	1050	1069	1051	1072	1087	C-O-C	
	1186	1188	1187	1188	1191	1186	1188	C-OH	[298]
	1239	1269	1228	1294	1240	1277	1289	P=O	[299]
	1472	1477	1474	1477	1484	1445	1471	C-H	[300]
	1542	1543	1543	1542	1543	1544	1535	C-N (amide I)	[141]
	1642	1623	1651	1645	1644	1675	1643	C-N (amide II)	[74]

* References in which the corresponding functional group/absorbance wavenumber pairing are reported.

Table 6-1 displays the FTIR spectra (ranging from 2000 to 750 cm^{-1}) of *C. vulgaris* cells, along with the cells loaded with 0.5 mmol/L Pb(II), Zn(II), Cu(II), Ni(II), or Cd(II) Co(II) aqueous solutions. Additionally, the FTIR wavenumber curve is depicted in Figure 6-1. The FTIR spectra provide evidence of various functional groups on the surface of *C. vulgaris* cells, including C-O-C, C-OH, P=O, C-H, and C-N, which likely played a role in facilitating the biosorption of HMIs. Specifically, the peaks at 1642 and 1542 cm^{-1} correspond to the C=N bonds in the amide II and amide I groups, respectively, indicating the presence of peptide bonds and, consequently, proteins on the cell surface. This observation aligns with previous findings [74,141]. The absorption peak at 1472 cm^{-1} results from bending vibrations in aliphatic C-H bonds, which are abundant in various biochemical compounds [300]. Furthermore, the peak at 1239 cm^{-1} corresponds to phosphate, a common component of cytomembranes [299], while the peak at 1186 cm^{-1} is attributed to the stretching vibrations in C-OH bonds present in carboxyl groups, found in carbohydrates, lipids, proteins, and amino acids [298]. The peaks at 1072 and 1011 cm^{-1} represent asymmetric C-O-C stretching vibrations characteristic of ester bonds in proteins, such as PHA [297].

After being loaded with six different HMIs (Pb(II), Zn(II), Cu(II), Ni(II), Cd(II), Co(II)), the biomass exhibited notable shifts in the peaks observed in its FTIR spectrum. Noticeably, shifts were observed at 1642, 1542, 1472, 1239, 1186, 1072, and 1011 cm^{-1}, which can be attributed to changes in the C=N, C-H, P=O, C-O-C, and C-OH bonds, respectively. These shifts strongly suggest that the HMIs bind to functional groups containing these bonds, leading to alterations in

the energy states of the involved electrons and subsequent absorption of photons to excite the electrons. The functional groups linked to these bonds encompass a diverse array of elements, such as carbon (2.55), hydrogen (2.2), nitrogen (3.04), and phosphate (2.19). Among these elements, oxygen, with a relatively high electronegativity (3.44) is likely to exert a stronger attractive force while interacting with positively charged HMIs. Moreover, certain functional groups, including C=N, P=O, and O-H, may form double-toothed structures that could facilitate chelation with HMIs [301].

6.4.1.2 Kinetic evidence of surface bioadsorption

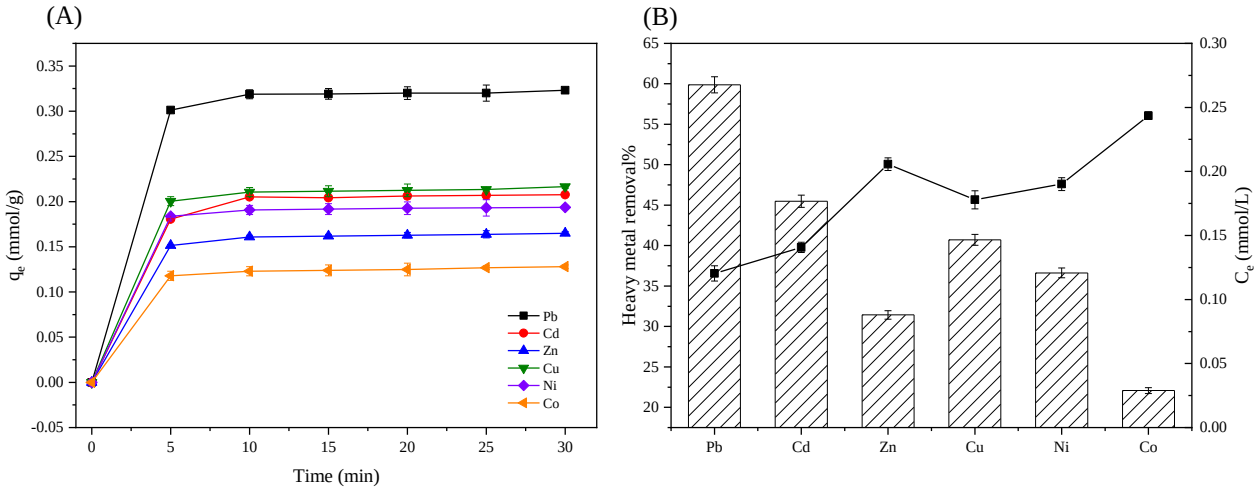

Figure 6-2 Kinetics of HMIs (A) and HMIs removal% with equilibrium HMIs concentration (B) by C. vulgaris at pH 6.0, 0.3 mmol/L HMIs, 0.5 g DCW/L, 25 ℃. Mean values with error bars (n = 3) are provided.

In this study, we investigated the kinetics of HMIs biosorption onto microalgal biomass and the experiment was conducted in the presence of 0.3 mmol/L of Pb(II), Cd(II), Zn(II), Cu(II), Ni(II), and Co(II) at 0.5 biomass dosage, pH 6.0 and 25 ℃, as illustrated in Figure 6-2. Notably, rapid biosorption of HMIs was observed with equilibrium achieved within 10 mins. Following 30 mins contact period, the equilibrium biosorption (mmol/g) for Pb(II), Cd(II), Zn(II), Cu(II), Ni(II), and

Co(II) were determined to be 0.32, 0.21, 0.16, 0.22, 0.19, and 0.13, respectively. The removal percentages of HMIs (Pb(II), Cd(II), Zn(II), Cu(II), Ni(II), and Co(II)) were found to be 59.88%, 45.48%, 31.43%, 40.72%, 36.52%, and 22.08%, respectively, when exposed to a 0.3 mmol/L HMIs solution at 30 mins. Furthermore, the equilibrium HMIs concentration in the supernatant were measured at 0.12 mmol/L, 0.14 mmol/L, 0.20 mmol/L, 0.18 mmol/L, 0.19 mmol/L, and 0.24 mmol/L for Pb(II), Cd(II), Zn(II), Cu(II), Ni(II), and Co(II), respectively. While the equilibrium HMIs concentration did not meet drinking water standards, it is important to note that by employing higher biomass dosages, reducing the initial HMI concentration, and implementing multiple-stage treatment, it is possible to achieve drinking water standards at the parts per billion (ppb) level, as established by the US Environmental Protection Agency (USEPA) and the World Health Organization (WHO) [5,6]. Many publications in the literature have reported fast HMIs biosorption kinetics by different microalgal species [237,302]. For instance, Lekshmi R et al.[302] investigated the biosorption of *Ulva flexuosa* for three HMIs, i.e., Cd(II), Co(II), and Zn(II), where biosorption reached plateau rapidly within 30 mins. Pham et al. [60] reported the biosorption of Cd(II), Cu(II), Ni(II), Pb(II) by *Hizikia fusiformis*, finding that biosorption can take up 90–95% HMIs removal% within the first 15 mins. Furthermore, Hockaday et al. [127] declared that the equilibrium-reaching time were as short as 10 seconds for the biosorption of Cu(II) and Cd(II) by microalgae *C. vulgaris* and *S. obliquus*. In one of our earlier experiments, we observed quick biosorption of several HMIs on green alga *N. oleoabundans* [14]. The consistent observation of kinetic behavior of the biosorption of a large variety of different HMIs onto various microalgal species indicates a similarity in the underlying biosorption mechanisms. It is important to highlight that the kinetics of HMIs removal by microalgae may involve both bioadsorption, which is a rapid process, and bioabsorption process,

which is a much slower process, as discussed in the introduction. Therefore, the rapid kinetics of HMI biosorption onto microalgal biomass serves as another evidence that it is predominantly surface bioadsorption rather than bioabsorption.

6.4.1.3 Isothermal evidence of monolayer surface bioadsorption

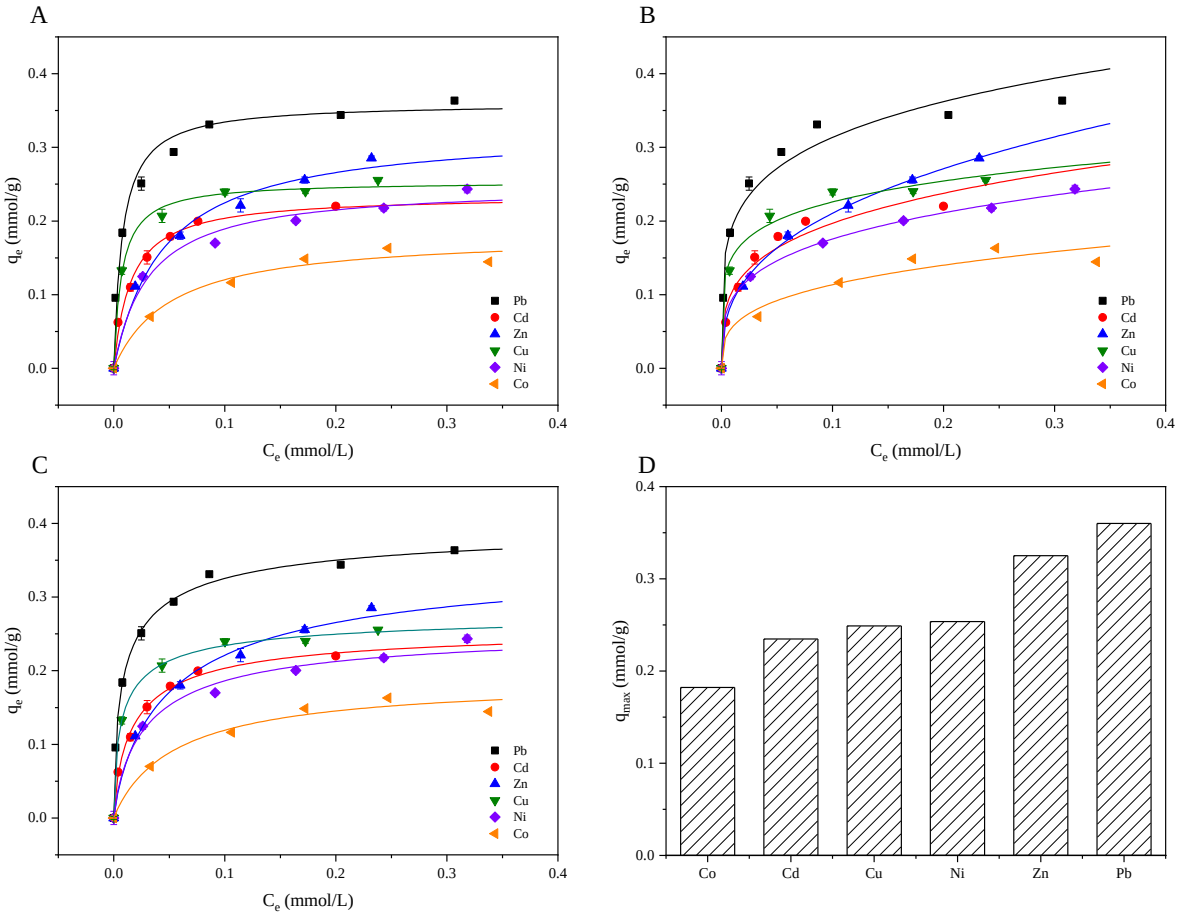

Figure 6-3 Isotherms of Pb(II), Cd(II), Zn(II), Cu(II), Ni(II) and Co(II) biosorption by C. vulgaris biomass fitted to the Langmuir (A), Freundlich (B) and Sips (C) model and the biosorption capacity (D) of HMIs. (0.5 g DCW/L, 10 mins, pH 6.0). Mean values with error bars (n = 3) are provided.

Table 6-2 Isotherm constants of Pb(II), Zn(II), Cu(II), Ni(II), Cd(II), Co(II) biosorption by C. vulgaris biomass using Langmuir and Freundlich models.

		Langmuir				Freundlich			Sips			
Metal	Mw (g/mol)	q_m (mmol/g)	K_L (L/mmol)	R_L	R^2	K_F($mg^{(1-1/n)}g^{-1}L^{1/n}$)	N	R^2	q_m (mmol/g)	K_L (L/mmol)	*ns*	R^2
Pb^{2+}	207.2	0.36	129.24	0.02-0.07	0.9459	0.50	4.76	0.9369	0.41	16.23	0.62	0.9961
Cd^{2+}	112.4	0.23	65.52	0.03-0.13	0.9803	0.37	3.70	0.9250	0.26	20.38	0.77	0.9916
Zn^{2+}	65.38	0.32	22.40	0.08-0.31	0.9920	0.49	2.78	0.9370	0.36	10.48	0.82	0.9985
Cu^{2+}	63.54	0.25	142.98	0.01-0.07	0.9740	0.33	5.88	0.9450	0.28	21.48	0.65	0.9917
Ni^{2+}	58.69	0.25	31.84	0.06-0.24	0.9933	0.32	3.70	0.9143	0.30	7.24	0.66	0.9628
Co^{2+}	58.93	0.18	19.41	0.09-0.34	0.9178	0.23	3.33	0.8308	0.17	45.45	1.23	0.9231

The Langmuir (Eq. 7), Freundlich (Eq. 8), and Sips (Eq. 9) are three commonly used isotherm models in the field. Both the Langmuir isotherm and Sips model assume that the adsorbates evenly occupy binding sites distributed throughout the adsorbent once all sites are filled. Furthermore, these models consider all biosorption sites as independent and possessing identical energetic characteristics. The following equations are frequently employed to describe bellow:

$$q_e = \frac{q_m K_L C_e}{1 + K_L C_e} \quad 6.8$$

$$q_e = K_F (C_e)^{1/n} \quad 6.9$$

$$q_e = \frac{q_{mS} K_S C_e^{n_S}}{1 + K_S C_e^{n_S}} \quad 6.10$$

where there are four factors to consider when dealing with HMIs adsorbed in the solution: q_e the HMIs content adsorbed per gram of adsorbent (mmol/g), C_e the equilibrium HMIs concentration in supernatant (mmol/L), K_L, K_F and K_S the model constants in the Langmuir, Freundlich, and Sips model, respectively (which are related to the affinity of biosorption), q_m the maximum

equilibrium biosorption (mmol/g), i.e., the biosorption capacity, and *n* and *ns* the empirical constants of Freundlich and Sips models, respectively.

Isotherms of the biosorption of six HMIs, i.e., Pb(II), Cd(II), Zn(II), Cu(II), Ni(II), and Co(II), onto green microalga *C. vulgaris* were carried out at pH 6.0 to prevent the precipitation of HMIs with 10 mins contact time. The isothermal data obtained from these experiments were fitted to the Langmuir, Freundlich, and Sips equations using the software Origin. The results are depicted in Figure 6-3 and the corresponding isothermal parameters and correlation coefficients (R^2) are presented in Table 6-2. Notably, as shown in Table 6-2, the Langmuir model fits better than the Freud model since the R^2 values of the former are better than that of the latter in all cases. Furthermore, the Sips model exhibited superior fitting to the HMIs compared to the Langmuir and Freundlich models, as evidenced by the high R^2 values, which were in most cases larger than 0.99.

The Sips model represents the monolayer adsorption of one adsorbate molecule onto 1/*ns* adsorption sites [253]. As shown in Table 6-4, the *ns* values of all scenarios were smaller than 1 except for Co^{2+} biosorption, which had an *ns* value that was slightly larger than 1 (1.23). Similar observations were reported with the biosorption of Pb(II), Cd(II), Zn(II) by *N. oleoabundans* [238]. Therefore, the biosorption of these HMI by microalgae was monolayer surface bioadsorption with more than one binding site for one HMI.

While Sips model gives slightly different biosorption capacities than the Langmuir model, we will use Langmuir values in discussions from this point on to allow comparison with most literature data. As listed in Table 6-2, the biosorption capacities (mmol/g) of the six HMIs obtained by fitting Langmuir model are in the order of: Pb(II)(0.360)> Zn(II)(0.325)>

Cu(II)(0.254)> Ni(II)(0.249)> Cd(II)(0.235)> Co(II)(0.182). Apparently, the HMI properties had had significant effects on the biosorption capacity of HMIs.

Extensive studies have been carried on the effects of HMI properties on their affinity with cellular ligands [14,70,292,303] and electronegativity and ionic radius have been generally recognized as the parameters that play important roles in biosorption. Nonetheless, the literature data on the effects of these two HMI properties had been unconclusive and in many cases contradictory to each other. As a most recent development in this field, we established in a previous study using experimental and literature data that the biosorption capacity would increase with the ratio of HMI electronegativity and radius, which is in many cases linear increase [14].

6.4.1.4 Intracellular and extracellular Pb(II) content

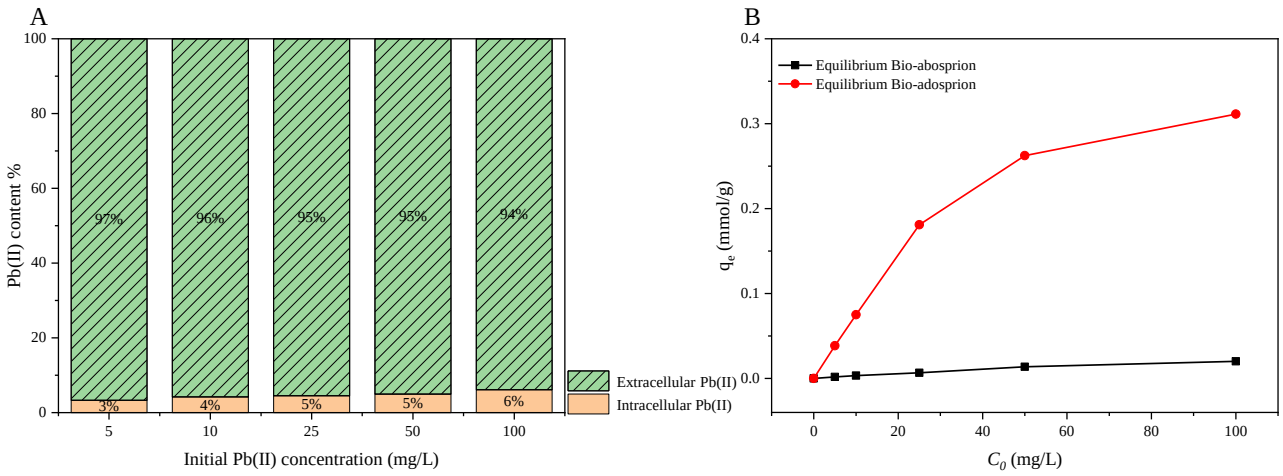

Figure 6-4 (A) Pb(II) content% on cell surface (Extracellular), and inside cells (Intracellular); and (B) equilibrium bioabsorption and equilibrium bioadsorption (mg/g) at different initial Pb(II) concentration (5-100 mg/L) by C. vulgaris. Experiment carried out at 0.5 g DCW/L, 10 mins, and pH 6.0.

To assess the distribution of intracellular and extracellular HMIs, we conducted Pb(II) biosorption experiments as a representation. These experiments involved varying initial Pb(II) concentrations from 5 to 100 mg/L, with a fixed biomass concentration of 0.5 g DCW/L, contact time of 10 mins, and pH 6.0 shown in Figure 6-4. Figure 6-4A reveals that, regardless of the initial Pb(II) concentration, the bioadsorption of Pb(II) consistently dominated the total Pb(II) removal, constituting a significant portion of 94% to 96%. In Figure 6-4B, we observe that both the equilibrium bioadsorption and equilibrium bioabsorption of Pb(II) increased with increasing initial Pb(II) concentration from 10 to 100 mg/L. The highest equilibrium biosorption, 0.31 mmol/g and 0.02 mmol/g, were achieved at an initial Pb(II) concentration of 100 mg/L, for bioadsorption and bioabsorption, respectively. This indicates that the removal of HMIs by microalgal cells is primarily achieved through bioadsorption, which occurred on the cell surface. It is worthy to note that the predominance of bioadsorption in biosorption of HMI by microalgae was also reported in the literature [233,234].

6.4.2 Mathematical model for HMIs biosorption based on ideal surface bio-adsorption

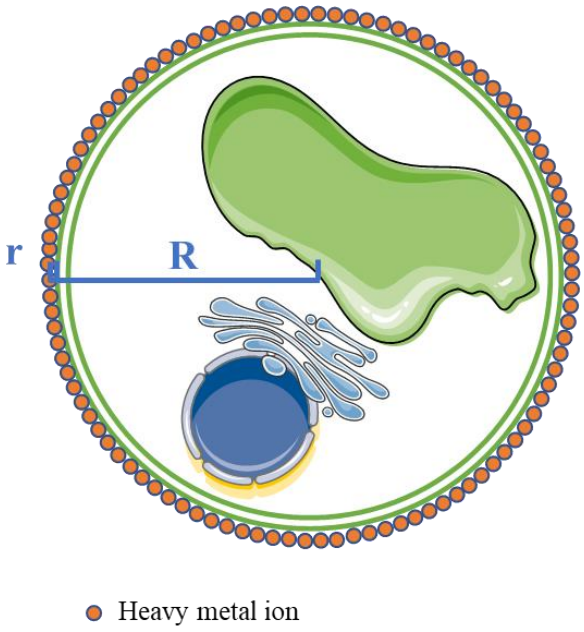

Figure 6-5 Biosorption of HMI model assuming: 1) microalgal cell has smooth surface (R and r present radius of biosorbent and HMI, respectively); 2) monolayer bioadsorption; and 3) complete occupation of cell surface by HMI; 4) Functional site is scattered uniformly across the cell surface; 5) Microalgal cells present in low concentrations with no agglomeration**.**

As discussed above, there are abundant and multifaceted evidence supporting the hypothesis that biosorption of HMIs by microalgal biomass is predominantly bioadsorption that occurs at cell surface. Based on this understanding, we propose here a mathematical model for prediction of biosorption capacity based on cell size, morphology, weight, and HMI radius as follows.

Figure 6-5 describes an idealized biosorption process on a single microalgal cell with the following assumptions: 1) microalgal biomass consisting of only unicellular cells of smooth surface; 2) the biosorption is monolayer bioadsorption; 3) HMIs fully occupy the entire cell surface; 4) Functional site is scattered uniformly across the cell surface; 5) Microalgal cells are present in low concentrations with no agglomeration. These assumptions allow the estimation of

the HMIs biosorption capacity of a given microalga of known properties including cell size and cell weight on a particular multivalent HMIs of known ionic radius.

Assume the surface of a spheric cell of radius R (μm) is fully occupied by ionic radius r (pm), then surface area of the sphere ($A_{S,S}$, μm^2) passing the central points of all the occupying ions is given by Eq. 6.11. For cylindrical cell of diameter (d, μm) and heigh (h, μm) is fully occupied by ionic radius r (pm), the surface area of cylinder ($A_{S,C}$, μm^2) is given by Eq 6.12:

$$A_{s,s} = 4\pi(R + r \times 10^{-6})^2 \quad 6.11$$

$$A_{s,c} = \pi(d + r \times 10^{-6})[(h + r \times 10^{-6}) + \frac{(d + r \times 10^{-6})}{2}] \quad 6.12$$

The area of the plane intersecting the central point of each ionic sphere (A_I, μm^2) is given by Eq. 6.13:

$$A_I = \pi(r \times 10^{-6})^2 \quad 6.13$$

The number of HMIs to occupy the surface of a cell fully (n, ions/cell) can be obtained by dividing A_S (using sphere ($A_{S,S}$, μm^2) as representative) with A_I, i.e.,

$$n = \frac{A_S}{A_I} = 4(\frac{R + r \times 10^{-6}}{r \times 10^{-6}})^2 \quad 6.14$$

N (ions/g), the number of HMIs on all the cells in a unit mass of sample with a cell weight of C_w (g/cell) can be obtained by:

$$N = \frac{n}{C_w} \quad 6.15$$

For unit conversion, the predicted biosorption capacity (q_p, mmol/g) of HMIs on microalgal biomass can therefore be determined through the following mathematical model:

$$q_p = \frac{N}{6.022 \times 10^{26}} \quad (6.16)$$

6.4.3 Validation of model

Table 6-3 Experimental and predicted biosorption capacity of different HMIs by different microalgal species.

Biosorbent	Cell (μm)	Cell weight (g/cell)	Ion	Electronegativity	Ionic radius (pm)	q_m (mmol/g)	q_p (mmol/g)	*qm/qp*	Ref.
C. vulgaris	2.20 (Radius)	2.78E-11	Pb^{2+}	2.33	119	0.360	0.081	4.44	This study
			Cd^{2+}	1.69	95	0.235	0.128	1.84	
			Zn^{2+}	1.65	74	0.325	0.210	1.55	
			Cu^{2+}	1.95	73	0.254	0.216	1.18	
			Ni^{2+}	1.91	70	0.249	0.235	1.06	
			Co^{2+}	1.88	70	0.182	0.235	0.77	
N. oleoabundans	2.25 (Radius)	1.33E-11	Pb^{2+}	2.33	119	1.030	0.170	6.06	[14]
			Cd^{2+}	1.69	95	0.650	0.266	2.44	
			Zn^{2+}	1.65	74	1.200	0.438	2.74	
			Cu^{2+}	1.95	73	1.230	0.450	2.73	
S. quadricauda	11.50×5.90 (Lenth*Diameter)	1.55E-11	Pb^{2+}	2.33	119	1.185	0.645	1.84	[55]
			Cd^{2+}	1.69	95	1.609	1.012	1.59	

q_m: Experimental biosorption capacity (mmol/g) from Langmuir model

q_p: Predicted biosorption capacity (mmol/g) from Mathematical model

To validate the model, we compared the model predictions and the experimentally determined biosorption capacities and the results are summarized in Table 6-3. In addition, we cited the experimental results from two well-executed studies in the literature for comparison as well [14,55]. Three distinct microalgal species, i.e., *C. vulgaris, N. oleoabundans*, and *S. quadricauda* are involved. These three microalgae exhibit varying morphologies, with *C. vulgaris* and *N.*

oleoabundans being unicellular having radii of ~2.20 and ~2.25 μm, respectively, and *S. quadricauda* consisting of multicellular cells resembling a four-rod configuration with dimensions of 11.50*5.90 (Length*Diameter). The cell weight (expressed in g/cell) is another critical parameter used in our calculations, typically determined through weighting biomass by freeze-drying process and cell numbers counting using hematocytometer. Each of these three microalgal species demonstrates distinct biosorption capacities for different HMIs. In the experimental dataset, the biosorption capacities for *C. vulgaris* towards Pb(II), Cd(II), Zn(II), Cu(II), Ni(II), and Co(II) were found to be 0.360, 0.235, 0.325, 0.254, 0.249, and 0.182 mmol/g, respectively. *N. oleoabundans* exhibited biosorption capacities for Pb(II), Cd(II), Zn(II), and Cu(II) of 1.030, 0.650, 1.200, and 1.230 mmol/g, respectively. Meanwhile, *S. quadricauda* displayed biosorption capacities of 1.185 and 1.609 mmol/g for Pb(II) and Cd(II), respectively. While the predicted biosorption capacities derived from the mathematical model closely align with some of the experimentally observed values, the deviation from others is quite remarkable, exhibiting q_m/q_p ratios ranging from 0.77 to 6.06. As to be discussed later, these discrepancies are reasonable. In fact, detailed analyses on them may lead to some very intriguing findings.

6.4.4 Deviations of model

As shown in Table 6-3, all the q_m/q_p ratios were larger than 1, except for Co^{2+} biosorption onto *C. vulgaris*¸ which had a q_m/q_p of 0.77. In the case of biosorption of Pb(II) on to *C. vulgaris* cells, the predicted capacity was 6.06 times of the experimentally determined capacity, i.e., the q_m/q_p ratio was 6.06. This needs explanation since one of the model assumptions is the full occupancy of cell surface by HMIs and there are isothermal evidences of monolayer biosorption. This incongruity between model predictions and experimental outcomes beckons attention to other pivotal parameters that wield the potential to exert tremendous influence upon the biosorption

capacity. Three such parameters are microalgal surface nanostructures, HMIs electronegativity and biosorption buffer pH. Each of these factors bears significance in the intricate biosorption process. The microalgal surface nanostructures are a critical determinant in biosorption, dictating the availability of binding sites and the extent of surface contact, which ultimately impacts the biosorption capacity. The electronegativity of HMIs, on the other hand, inherently affects their affinity to the functional group of the macromolecules on microalgal cell surface, thereby influence the biosorption interactions. Moreover, the operational pH plays a crucial role in shaping the net charge of both the microalgal biomass and the HMIs, thereby influence their attraction to each other and therefore binding. Delving into the interplay of these factors, their nuanced examination offers a promising avenue to enrich our understanding of the mechanisms of biosorption. In the following sections, the impacts of each parameter on biosorption capacity are systematically discussed.

6.4.4.1 Deviation caused by cell surface properties: nanostructures

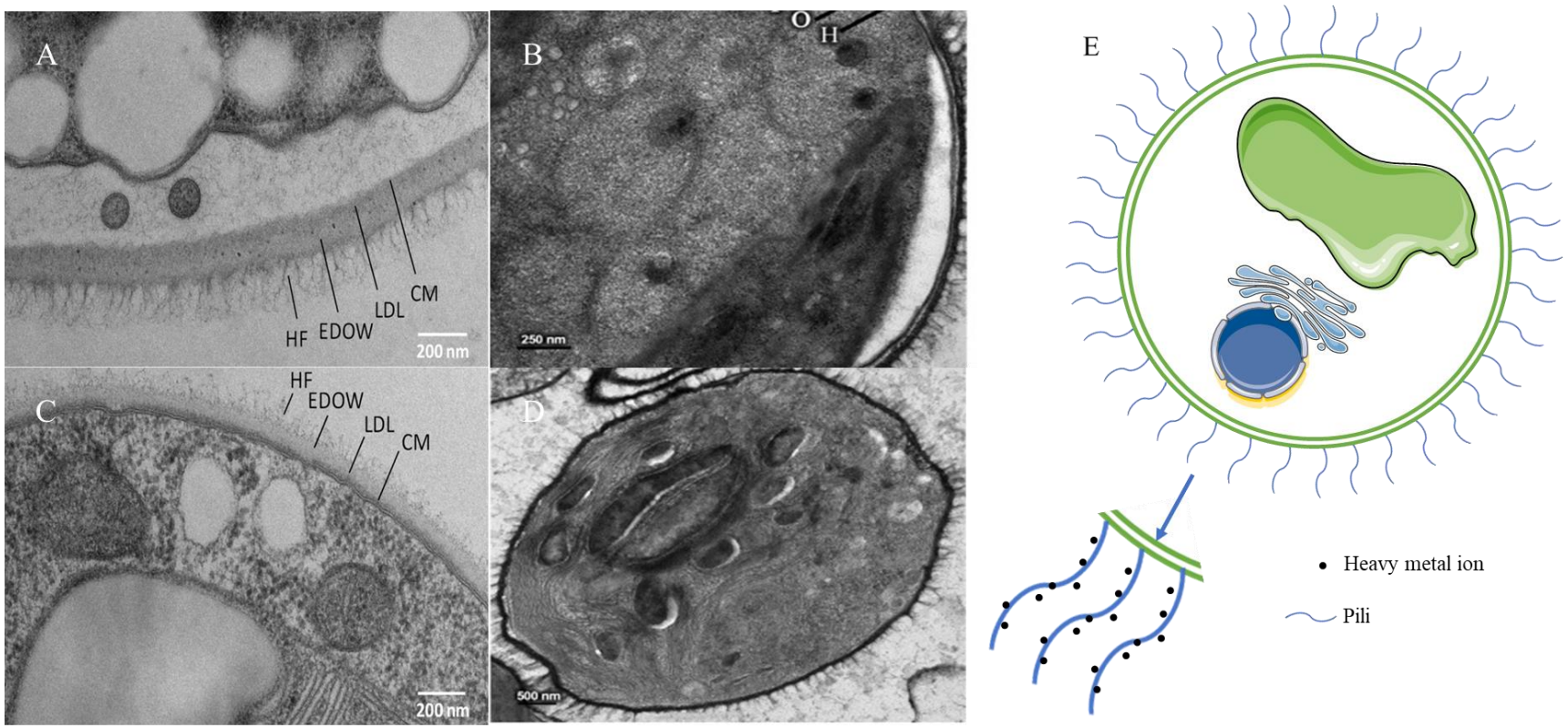

Figure 6-6 Representative transmission electron micrographs of *C. vulgaris* (A, C) and *N. oleoabundans* (B, D). Hairlike fiber (HF), electron-dense outer wall (EDOW), LDL (low density layer), CM (cytoplasmic membrane). Revised with permission from authors [110,281]. Copyright 2021 American Chemical Society & 2018 Elsevier.

Figure 6-6A,C and 6-6B,D are the transmission electron microscopy (TEM) images of *C. vulgaris* and *N. oleoabundans*, respectively, unveiling the presence of nanostructures, i.e., the hairlike fibers (HF), on the cellular surfaces. Pili, slender protein filaments with a diameter of around 2-12 nm are likely the major members of these HF extending from the outer membrane of cells [304]. The existence of HF in microalgal cells has also been reported in studies involving other species such as *Scenedesmus sp.*, *Haematococcus pluvialis*, and *Coelastrella sp.* [305]. Researchers have affirmed that extracellular polymeric substances (EPS), which could be the major components of the HF, comprise negatively charged functional groups like $-COO^-$ and $-PO_4^-$ that exhibit a propensity for adsorbing HMIs [306,307]. As illustrated in Figure 6-6E, the surfaces of the HF would house the binding sites for HMI, lending an effective surface area far beyond that is calculated by Eq. 6.10 or Eq. 6.11.

6.4.4.2 Deviation due to HMI properties: electronegativity

As shown in Table 6-3, the q_m/q_p ratios Pb(II) biosorption onto *C. vulgaris* and *N. oleoabundans* were 4.44 and 6.06, respectively. These are several times of other HMI/microalga pairs listed in Table 6-3, that were in the range of 0.77-2.73. These remarkable differences seem to be at least partially related to the large electronegativity of Pb(II) in comparison with that of all the other HMIs involved. While the impacts or at least the spacious impact of ionic radius have been factored into the mathematic model, the impacts of electronegativity are not accounted for. Large electronegativity of Pb(II) would hypothetically lend it large affinity with the negative functional groups and/or chelating groups on the surfaces of cells. In other words, some functional groups on the surface of the nanostructures, e.g., the HF, on cell surface might be too weak to bind to other HMIs but Pb(II), which has the largest electronegativity with a large margin in comparison to that of the second largest, i.e., that of Cu(II), which is 1.95. Nonetheless, this explanation is far

from perfection since the q_m/q_p ratios of other HMIs do not necessarily increase with their electronegativity when compared with each other. Apparently, this simplistic model cannot fully capture the intricate relationships between HMI and ligands on cell surfaces.

6.4.4.3 Deviation due to biosorption condition: pH

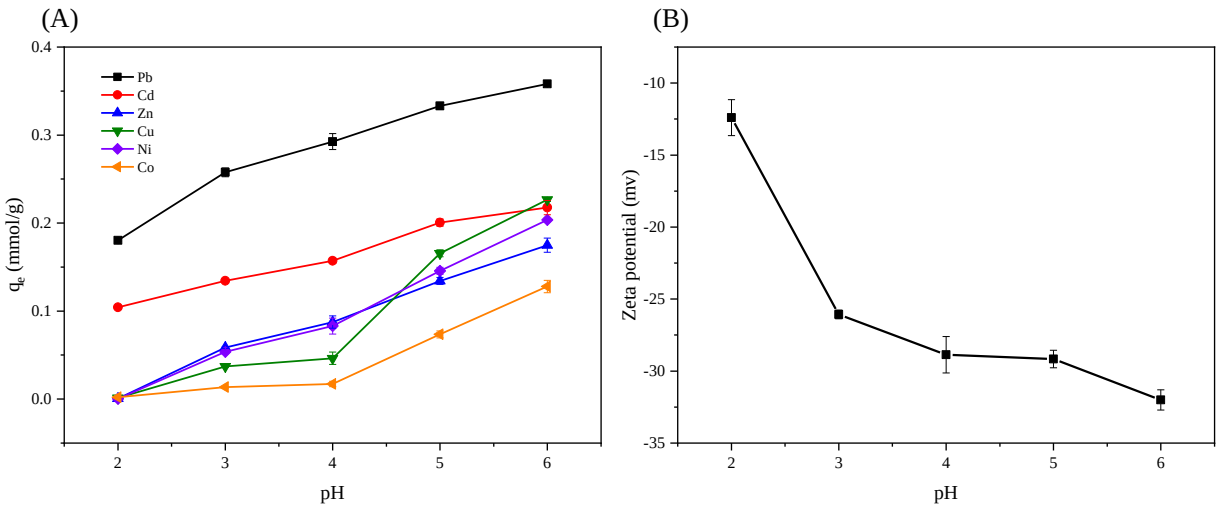

Figure 6-7 The equilibrium biosorption (A) of Pb(II), Zn(II), Cu(II), Ni(II), Cd(II), Co(II) by *C. vulgaris* and Zeta potential (B) of biomass in pH range 2.0–6.0, 0.3 mmol/L initial HMIs concentration, 0.5 g DCW/L, 10 mins contact time, and 25 ℃. Mean values with error bars (n = 3) are provided.

Table 6-4 Summary of microalgal cell wall biochemical composition and related functional groups for HMI biosorption [110,305,308].

Macromolecule	Biochemical	pKa_1	Functional groups
Monosaccharide	D-Arabinopyranose	11.30	C-O-C, C-OH
	6-Deoxy-D-mannopyranose	11.30	C-O-C, C-OH
	6-Deoxy-D-galactopyranose	11.30	C-O-C, C-OH
	D-Xylopyranose	11.31	C-O-C, C-OH
	D-Mannopyranose	12.08	C-O-C, C-OH
	D-Galactopyranose	12.35	C-O-C, C-OH
	D-Galactopyranuronic acid	3.51	C-O-C, COOH, C-OH
	D-Glucopyranose	11.30	C-O-C, C-OH
	D-Glucopyranuronic acid	3.21	C-O-C, COOH, C-OH

Amino acid	Histidine	1.80	C=N, COOH
	Arginine	12.48	C=N, COOH
	Serine	2.19	C-N, COOH, C-OH
	Glycine	2.35	C-N, COOH
	Glutamic acid	2.10	C-N, COOH
	Aspartic acid	3.90	C-N, COOH
	Threonine	2.09	C-N, COOH, C-OH
	Alanine	9.87	C-N, COOH
	Proline	1.97	C-N, COOH
	Lysine	10.40	C-N, COOH
	Tyrosine	10.46	C-N, COOH, C-OH
	Valine	2.29	C-N, COOH
	Leucine	9.74	C-N, COOH
	Phenylalanine	2.20	C-N, COOH
	Isoleucine	2.32	C-N, COOH
Lipid	Palmitic acid	4.95	COOH
	Stearic acid	4.75	COOH
	Cis-10-Nonadecenoic acid	5.02	-COO-
Protein	Hydroxyproline	10.62	C-N, COOH, C-OH
	Hydroxylysine	2.45	C-N, COOH, C-OH
	Glycine	2.35	C-N, COOH
	Thiols	6.40	C-S
	Tryptophan	9.39	C-N, COOH

The effect of pH on the biosorption of Pb(II), Cd(II), Zn(II), Cu(II), Ni(II), and Co(II) by *C. vulgaris* was investigated across a pH range of 2.0-6.0 in this study. Figure 6-7 illustrates the strong dependence of the equilibrium biosorption of different HMIs on biosorption pH. In general, the equilibrium biosorption of all HMI increased with pH and highest were observed at pH6.0.

As shown in Figure 6-7B, the zeta potential of cells was -12.4 mV at pH 2.0, which decreased as the pH increased (the absolute value increased with pH). The most negative zeta potential value of cells was -32.0 mV at pH 6.0, indicating that *C. vulgaris* surfaces under higher pH conditions possess more negative functional groups capable of adsorbing positive HMIs.

Studies revealed that the major constituents of the cell wall were carbohydrates (29.7%), proteins (14.6%), lipids (13.1%), minerals (1.5%), and other molecules (41.1%) [281]. The macromolecules contain abundant carboxyl groups (-COOH), phosphate groups (-PO_4), amino groups (-C=N), and hydroxyl groups (-OH) that have been identified using FTIR spectra as the primary functional groups contributing to the negative charge on the cell surfaces. As summarized in Table 6-4, the pKa values of functional groups carrying constituent monomers of cell wall range from 1.97 of proline to 12.35 for D-galactopyranose and the monomeric constituents of carbohydrates, peptidoglycans, and lipoglycans possess abundant functional groups of small pKa, e.g., D-glucopyranuronic acid (pKa = 3.21) and D-galactopyranuronic acid (pKa = 3.51) [110,305,308]. The functional group would be deprotonated to acquire negative charges when buffer pH is above their pKa values and therefore creating biting sites for HMI in bioadsorption.

The current model, however, it too rigid to accommodate the capacity change caused by biosorption conditions, e.g., pH.

6.5 Conclusions

A simplistic model was proposed for predicting HMI biosorption capacity by leveraging insights from microalgal cell geometry and ionic radius. The model was validated using experimental and literature data to be able to provide reasonably good estimation in most cases. The deviations of the model were explained in the context of the influence of other important parameters, including nanostructures on cell surface, HMI electronegativity, and biosorption buffer pH, that are not accounted for in the model. The validation of the model support one of the key assumptions based on which the model was developed, i.e., biosorption of HMI by microalgal cells is

predominantly monolayer surface bioadsorption other than bioabsorption that involves the entire cell volume. Furthermore, the fact that the experimental biosorption capacities were larger than the predicted values in most cases, in combination with the monolayer biosorption isotherm, suggest that the surfaces of nanostructures on cell wall, most likely the HF, might be where the binding sites are located. Different deviations among different HMI suggest HMI properties other than ionic radius, e.g., electronegativity, have important influence on biosorption.

6.6 Acknowledgment

It is gratefully acknowledged that the Natural Sciences and Engineering Research Council of Canada (NSERC) provided financial support in the form of a Discovery Grant RGPIN-2022–05242.

Chapter 7 Conclusions and recommendations

7.1 Conclusions

This research was focused on biosorption of heavy metal ions (HMIs) by microalgae: mechanisms and conditioning. The overarching goals of this work included to:

1. Establishing the correlation between biosorption capacity and HMIs properties.
2. Enhancing HMIs biosorption capacity through diverse microalgae cultivation conditions: nitrate, phosphate, dissolved inorganic carbon, and culture-pH.
3. Employing cost-efficient lipid-extracted microalgal biomass by-products for practical biosorption applications.
4. Developing and validating a mathematical model utilizing three microalgal species.

In Chapter 3, our research delved comprehensively into various facets of HMIs biosorption using microalgae, with a particular focus on *Neochloris oleoabundans*. The following provides a more logical and detailed account of our key findings. Our initial investigation aimed to understand the interplay between HMIs biosorption capacity and the properties of HMIs themselves, using *N. oleoabundans* as biosorbent. We examined the biosorption capacity (measured in mmol/g) across a range of HMIs, including Pb(II), Hg(II), Zn(II), Cd(II), and Cu(II). Our findings unveiled an intriguing linear relationship between biosorption capacity and an impact factor, which we defined as "*I*" equal to the electronegativity derived from ionic radius. This relationship sheds light on the underlying mechanisms of HMI biosorption and provides a valuable foundation for further investigations. Additionally, we conducted competition tests, revealing that the biosorption capacity of HMIs decreased as the concentration of competing ions increased. This

underscores the importance of considering competitive effects when designing HMI biosorption strategies.

In Chapter 4.1-4.4, we dedicated a substantial portion of our research to examining the impact of various cultivation conditions on the biosorption of Pb(II) by *N. oleoabundans*. The following key points emerged: 1) Our original research demonstrated a direct and significant correlation between sodium nitrate ($NaNO_3$) concentration and Pb(II) biosorption capacity. This discovery was substantiated by isotherm experiments that provided insights into the binding of Pb(II) to the microalgal cell surface, ultimately enhancing biosorption capacity (60.26 mg/g) of Pb(II) with 800 mg/L $NaNO_3$. 2) Under specific conditions, notably with of 300 mg/L KH_2PO_4, we achieved the highest biosorption capacity (180.19 mg/g) for Cu(II), providing valuable insights into optimizing biosorption for this particular HMI. 3) The most noteworthy result was the exceptional biosorption capacity (100.01 mg/g) of Pb(II) achieved under a culture pH of 9.5. This finding suggests novel possibilities for enhancing the removal efficiency of Pb(II) from contaminated water sources. 4) We also observed a remarkable biosorption capacity (490.47 mg/g) for Pb(II) when exposed to 320 mmol/L $NaHCO_3$, further expanding the toolkit of sustainable strategies for HMI removal.

In Chapter 5, our study ventured into the practical application of residual biomass excrete lipids from *Chlorella vulgaris* as an exceptionally effective biosorbent for HMIs. The distinct advantages of this approach were apparent when compared to the use of wet and dried biomass. Factors such as enhanced exposure of the inner cell wall surface, the presence of unique functional groups, and the removal of lipids all contributed to the notable enhancement of biosorption capacity. This low-cost residual biomass exhibited rapid kinetics and remarkable

biosorption capacity, particularly for Pb(II) and Cd(II), positioning it as a promising candidate for various industrial applications, thereby contributing to sustainable HMIs removal practices.

In Chapter 6, to further our understanding of HMI biosorption by microalgal biomass, we embarked on the development of a mathematical model. This model primarily focused on establishing correlations between HMI ionic radius and biomass properties. Rigorously validated across six HMIs and various microalgal species, the model serves as a foundational tool for comprehending and predicting HMIs biosorption behavior. Future enhancements to the model are under consideration, including the incorporation of HMIs electronegativity, specific surface area calculations, and the inclusion of pili structures on cell walls to enhance its accuracy and applicability. In summary, our study contributes significantly to the understanding of microalgal-based HMI removal strategies and offers valuable insights that pave the way for further research in this burgeoning field. The comprehensive exploration of biosorption mechanisms, cultivation conditions, low-cost biosorbents, and the development of predictive models collectively positions this work as a vital contribution to sustainable and effective HMI remediation practices.

7.2 Future works

Building upon the findings and insights gained from this study, there are several promising avenues for future research in the field of HMIs removal using microalgae. Here are some potential directions for future work:

Delve deeper into the mechanisms of HMIs biosorption by microalgae. Investigate the specific molecular interactions and binding sites involved in the biosorption process to gain a more comprehensive understanding of how different HMIs interact with microalgal biomass. Explore novel cultivation strategies to further optimize microalgal growth and biosorption performance.

Investigate the use of controlled environmental factors, such as light intensity, temperature, and nutrient ratios, to enhance biosorption capacity of HMIs. Conduct in-depth studies on the competitive biosorption of HMIs in mixed-metal systems. Examine how different HMIs interact with one another and microalgal biomass under varying conditions, mirroring real-world scenarios.

Investigate the modification of microalgal biomass to enhance its biosorption capabilities. This could include genetic engineering or the introduction of specific functional groups to increase its affinity for targeted HMIs. Focus on scaling up microalgal-based HMIs removal processes for practical industrial applications. Explore cost-effective and efficient ways to implement microalgal biosorption on a larger scale, considering factors such as reactor design and biomass harvesting techniques. Develop methods for the regeneration and reusability of microalgal biomass as biosorbents. Investigate techniques for desorbing and recovering HMIs from loaded biomass, making the process more sustainable and economically viable. Conduct field studies and pilot projects to evaluate the feasibility of applying microalgal-based HMIs removal in real-world scenarios, such as wastewater treatment plants, industrial effluent treatment, and contaminated water bodies.

Continue to refine and expand mathematical models for predicting HMIs biosorption by microalgal biomass. Incorporate additional factors, such as HMIs electronegativity, specific surface area calculations, and the influence of environmental parameters, to improve model accuracy. Encourage collaboration between researchers from various disciplines, including biology, chemistry, engineering, and environmental science, to approach HMIs removal and other organic pollutant from a holistic perspective. Interdisciplinary efforts can lead to innovative

solutions and a more comprehensive understanding of the challenges involved. By pursuing these future research directions, we can further advance the field of microalgal-based HMIs removal, making it a more practical, efficient, and environmentally sustainable solution for addressing heavy metal contamination in water sources.

References

[1] S. Ahuja, Water quality worldwide, 2021. https://doi.org/10.1016/B978-0-12-821057-4.00003-3.

[2] F. Edition, I. The, F. Addendum, Guidlines for Drinking-water Quality, n.d.

[3] Z. Zhang, Y. Lu, H. Li, Y. Tu, B. Liu, Z. Yang, Science of the Total Environment Assessment of heavy metal contamination , distribution and source identi fi cation in the sediments from the Zijiang River , China, 645 (2018) 235–243. https://doi.org/10.1016/j.scitotenv.2018.07.026.

[4] A. Nargis, A. Habib, Harun-Or-Rashid, H.B. Harun, M.S. Islam Sarker, R. Jin, G. Liu, W. Liu, A.N.M. Al-Razee, K. Chen, M. Cai, Status of multielement in water of the river Buriganga, Bangladesh: Aquatic chemistry of metal ions in polluted river water, Emerg. Contam. 7 (2021) 99–115. https://doi.org/10.1016/j.emcon.2021.03.001.

[5] WHO, Guidelines for Drinking-water Quality, (2017). https://www.who.int/publications/i/item/9789241549950.

[6] USEPA, National Primary Drinking Water Regulations, U. S. Environ. Prot. Agency Washington, DC. (2022). https://www.epa.gov/ground-water-and-drinking-water/national-primary-drinking-water-regulations#Inorganic.

[7] R. Saavedra, R. Muñoz, M. Elisa, M. Vega, S. Bolado, Bioresource Technology Comparative uptake study of arsenic , boron , copper , manganese and zinc from water by di ff erent green microalgae, Bioresour. Technol. 263 (2018) 49–57. https://doi.org/10.1016/j.biortech.2018.04.101.

[8] O. Gyam, P. Borgen, G. Darko, E. Ansah, Chemosphere Human health risk assessment of exposure to indoor mercury vapour in a Ghanaian artisanal small-scale gold mining community, 241 (2020). https://doi.org/10.1016/j.chemosphere.2019.125014.

[9] A. Bakshi, A.K. Panigrahi, A comprehensive review on chromium induced alterations in fresh water fi shes, Toxicol. Reports. 5 (2018) 440–447. https://doi.org/10.1016/j.toxrep.2018.03.007.

[10] H. Peng, J. Guo, Removal of chromium from wastewater by membrane filtration , chemical precipitation , ion exchange , adsorption electrocoagulation , electrochemical reduction , electrodialysis , electrodeionization , photocatalysis and nanotechnology : a review, Environ. Chem. Lett. 18 (2020) 2055–2068. https://doi.org/10.1007/s10311-020-01058-x.

[11] Y. Ibrahim, V. Naddeo, F. Banat, S.W. Hasan, Preparation of novel polyvinylidene fluoride (PVDF) -Tin (IV) oxide (SnO 2) ion exchange mixed matrix membranes for the removal of heavy metals from aqueous solutions, Sep. Purif. Technol. 250 (2020) 117250. https://doi.org/10.1016/j.seppur.2020.117250.

[12] Y. Wang, A. Li, C. Cui, Chemosphere Remediation of heavy metal-contaminated soils by

electrokinetic technology : Mechanisms and applicability, Chemosphere. 265 (2021) 129071. https://doi.org/10.1016/j.chemosphere.2020.129071.

[13] Z. Xu, S. Gu, D. Rana, T. Matsuura, C.Q. Lan, Chemical precipitation enabled UF and MF filtration for lead removal, J. Water Process Eng. 41 (2021) 101987. https://doi.org/10.1016/j.jwpe.2021.101987.

[14] S. Gu, C.Q. Lan, Biosorption of heavy metal ions by green alga Neochloris oleoabundans: Effects of metal ion properties and cell wall structure, J. Hazard. Mater. 418 (2021) 126336. https://doi.org/10.1016/j.jhazmat.2021.126336.

[15] O. Spain, M. Plöhn, C. Funk, The cell wall of green microalgae and its role in heavy metal removal, Physiol. Plant. 173 (2021) 526–535. https://doi.org/10.1111/ppl.13405.

[16] M.L. Thi Nguyen, C.Y. Lin, C.H. Lay, Microalgae cultivation using biogas and digestate carbon sources, Biomass and Bioenergy. 122 (2019) 426–432. https://doi.org/10.1016/j.biombioe.2019.01.050.

[17] G. Bayramo, I. Tuzun, G. Celik, M. Yilmaz, M.Y. Arica, Biosorption of mercury (II), cadmium (II) and lead (II) ions from aqueous system by microalgae Chlamydomonas reinhardtii immobilized in alginate beads, 81 (2006) 35–43. https://doi.org/10.1016/j.minpro.2006.06.002.

[18] G. Joo, W. Lee, Y. Choi, Heavy metal adsorption capacity of powdered Chlorella vulgaris biosorbent: effect of chemical modification and growth media, Environ. Sci. Pollut. Res. 28 (2021) 25390–25399. https://doi.org/10.1007/s11356-021-12396-w.

[19] M.Y. Arıca, Bioresource Technology Construction a hybrid biosorbent using Scenedesmus quadricauda and Ca-alginate for biosorption of Cu (II), Zn (II) and Ni (II): Kinetics and equilibrium studies, 100 (2009) 186–193. https://doi.org/10.1016/j.biortech.2008.05.050.

[20] C. Yan, Z. Qu, J. Wang, L. Cao, Q. Han, Chemosphere Microalgal bioremediation of heavy metal pollution in water : Recent advances , challenges , and prospects, Chemosphere. 286 (2022) 131870. https://doi.org/10.1016/j.chemosphere.2021.131870.

[21] J. He, J.P. Chen, A comprehensive review on biosorption of heavy metals by algal biomass: Materials, performances, chemistry, and modeling simulation tools, Bioresour. Technol. 160 (2014) 67–78. https://doi.org/10.1016/j.biortech.2014.01.068.

[22] E. Rita, S. Dewi, R. Nuravivah, Potential Of Microalgae Chlorella vulgaris As Bioremediation Agents of Heavy Metal Pb (Lead) On Culture Media, 05010 (2018) 3–6.

[23] A. Mantzorou, F. Ververidis, Science of the Total Environment Microalgal bio fi lms : A further step over current microalgal cultivation techniques, Sci. Total Environ. 651 (2019) 3187–3201. https://doi.org/10.1016/j.scitotenv.2018.09.355.

[24] M. Abdelrazek, S. Abdelrazek, A.M. Abozeid, M. Eltholth, F. Abouelenien, BIOREMEDIATION OF A PESTICIDE AND SELECTED HEAVY METALS IN WASTEWATER FROM VARIOUS SOURCES USING A CONSORTIUM, (2019). https://doi.org/10.26873/SVR-744-2019.

[25] E. Daneshvar, C. Santhosh, E. Antikainen, A. Bhatnagar, Microalgal growth and nitrate removal efficiency in different cultivation conditions: Effect of macro and micronutrients and salinity, J. Environ. Chem. Eng. 6 (2018) 1848–1854. https://doi.org/10.1016/j.jece.2018.02.033.

[26] D.Y. Cho, S.T. Lee, S.W. Park, A.S. Chung, Studies on the biosorption of heavy metals onto Chlorella vulgaris, 1204 (2008). https://doi.org/10.1080/10934529409376043.

[27] P. Spolaore, C. Joannis-Cassan, E. Duran, A. Isambert, Commercial applications of microalgae, J. Biosci. Bioeng. 101 (2006) 87–96. https://doi.org/10.1263/jbb.101.87.

[28] N. Abdel-Raouf, A.A. Al-Homaidan, I.B.M. Ibraheem, Microalgae and wastewater treatment, Saudi J. Biol. Sci. 19 (2012) 257–275. https://doi.org/10.1016/j.sjbs.2012.04.005.

[29] V.K. Gupta, A. Rastogi, Biosorption of lead (II) from aqueous solutions by non-living algal biomass Oedogonium sp . and Nostoc sp .— A comparative study, 64 (2008) 170–178. https://doi.org/10.1016/j.colsurfb.2008.01.019.

[30] A. Sarı, Ö. Do, M. Tüzen, Equilibrium , thermodynamic and kinetic investigations on biosorption of arsenic from aqueous solution by algae (Maugeotia genuflexa) biomass, 167 (2011) 155–161. https://doi.org/10.1016/j.cej.2010.12.014.

[31] M. Kumar, A. Kumar, M. Sikandar, Biosorption of Hg (II) from aqueous solution using algal biomass : kinetics and isotherm studies, Heliyon. 6 (2020) e03321. https://doi.org/10.1016/j.heliyon.2020.e03321.

[32] C. Escudero-o, Biosorption of Cd (II) by Nordic microalgae : Tolerance , kinetics and equilibrium studies, 59 (2021). https://doi.org/10.1016/j.algal.2021.102471.

[33] H. Qin, T. Hu, Y. Zhai, N. Lu, J. Aliyeva, The improved methods of heavy metals removal by biosorbents: A review, Environ. Pollut. 258 (2020) 113777. https://doi.org/10.1016/j.envpol.2019.113777.

[34] C. Wang, C.Q. Lan, Effects of shear stress on microalgae – A review, Biotechnol. Adv. 36 (2018) 986–1002. https://doi.org/10.1016/j.biotechadv.2018.03.001.

[35] P.X. Sheng, Y.P. Ting, J.P. Chen, L. Hong, Sorption of lead, copper, cadmium, zinc, and nickel by marine algal biomass: Characterization of biosorptive capacity and investigation of mechanisms, J. Colloid Interface Sci. 275 (2004) 131–141. https://doi.org/10.1016/j.jcis.2004.01.036.

[36] Y.K. Leong, J.S. Chang, Bioremediation of heavy metals using microalgae: Recent advances and mechanisms, Bioresour. Technol. 303 (2020) 122886. https://doi.org/10.1016/j.biortech.2020.122886.

[37] S. Priatni, D. Ratnaningrum, S. Warya, E. Audina, Phycobiliproteins production and heavy metals reduction ability of Porphyridium sp, IOP Conf. Ser. Earth Environ. Sci. 160 (2018). https://doi.org/10.1088/1755-1315/160/1/012006.

[38] D. Pradhan, L.B. Sukla, B.B. Mishra, N. Devi, Biosorption for removal of hexavalent

chromium using microalgae, J. Clean. Prod. 209 (2019) 617–629. https://doi.org/10.1016/j.jclepro.2018.10.288.

[39] A.K. Zeraatkar, H. Ahmadzadeh, A.F. Talebi, N.R. Moheimani, M.P. McHenry, A. Keyvan, H. Ahmadzadeh, A. Farhad, N.R. Moheimani, M.P. McHenry, Potential use of algae for heavy metal bioremediation, a critical review, J. Environ. Manage. 181 (2016) 817–831. https://doi.org/10.1016/j.jenvman.2016.06.059.

[40] Z. Lou, J. Wang, X. Jin, L. Wan, Y. Wang, H. Chen, W. Shan, Y. Xiong, Brown algae based new sorption material for fractional recovery of molybdenum and rhenium from wastewater, Chem. Eng. J. 273 (2015) 231–239. https://doi.org/10.1016/j.cej.2015.03.054.

[41] E. Son, K. Poo, J. Chang, K. Chae, Science of the Total Environment Heavy metal removal from aqueous solutions using engineered magnetic biochars derived from waste marine macro-algal biomass, Sci. Total Environ. 615 (2018) 161–168. https://doi.org/10.1016/j.scitotenv.2017.09.171.

[42] Y. Li, S. Song, L. Xia, H. Yin, J.V. García Meza, W. Ju, A modified single solution method for the determ, Chem. Eng. J. 361 (2019) 167–179. https://doi.org/10.1016/j.cej.2018.12.070.

[43] S. Gu, E.M. Boase, C.Q. Lan, Enhanced Pb(II) removal by green alga Neochloris oleoabundans cultivated in high dissolved inorganic carbon cultures, Chem. Eng. J. 416 (2021) 128983. https://doi.org/10.1016/j.cej.2021.128983.

[44] M.A. Fawzy, A.F. Hifney, M.S. Adam, A.A. Al-badaani, Environmental Technology & Innovation Biosorption of cobalt and its effect on growth and metabolites of Synechocystis pevalekii and Scenedesmus bernardii : Isothermal analysis, Environ. Technol. Innov. 19 (2020) 100953. https://doi.org/10.1016/j.eti.2020.100953.

[45] M. Dirbaz, A. Roosta, Journal of Environmental Chemical Engineering Adsorption , kinetic and thermodynamic studies for the biosorption of cadmium onto microalgae Parachlorella sp ., J. Environ. Chem. Eng. 6 (2018) 2302–2309. https://doi.org/10.1016/j.jece.2018.03.039.

[46] H. Zheng, W. Guo, S. Li, Q. Wu, R. Yin, X. Feng, J. Du, N. Ren, J.S. Chang, Biosorption of cadmium by a lipid extraction residue of lipid-rich microalgae, RSC Adv. 6 (2016) 20051–20057. https://doi.org/10.1039/c5ra27264e.

[47] V.K. Gupta, A. Rastogi, Equilibrium and kinetic modelling of cadmium (II) biosorption by nonliving algal biomass Oedogonium sp . from aqueous phase, 153 (2008) 759–766. https://doi.org/10.1016/j.jhazmat.2007.09.021.

[48] Y.N. Mata, M.L. Bl, A. Ballester, F. Gonz, J.A. Mu, Characterization of the biosorption of cadmium , lead and copper with the brown alga Fucus vesiculosus, 158 (2008) 316–323. https://doi.org/10.1016/j.jhazmat.2008.01.084.

[49] N. Abdel-raouf, E. Nageh, N. Bukhari, N.M. Al-enazi, K. Ibrahim, S.H.A. Al-khiat, I. Borie, M. Ibraheem, Bioremoval capacity of Co + 2 using Phormidium tenue and Chlorella vulgaris as biosorbents, Environ. Res. 204 (2022) 111630.

https://doi.org/10.1016/j.envres.2021.111630.

[50] N. Bordoloi, R. Goswami, M. Kumar, R. Kataki, Biosorption of Co (II) from aqueous solution using algal biochar: Kinetics and isotherm studies, Bioresour. Technol. 244 (2017) 1465–1469. https://doi.org/10.1016/j.biortech.2017.05.139.

[51] B. Kızılkaya, G. Türker, R. Akgül, F. Doğan, Comparative Study of Biosorption of Heavy Metals Using Living Green Algae Scenedesmus quadricauda and Neochloris pseudoalveolaris : Equilibrium and Kinetics Comparative Study of Biosorption of Heavy Metals Using Living Green Algae Scenedesmus quadricauda , 2691 (2012). https://doi.org/10.1080/01932691.2011.567181.

[52] F.A.A. Al-rub, I. Ashour, Biosorption of copper on Chlorella vulgaris from single , binary and ternary metal aqueous solutions, 41 (2006) 457–464. https://doi.org/10.1016/j.procbio.2005.07.018.

[53] I. Tu, Equilibrium and kinetic studies on biosorption of Hg (II), Cd (II) and Pb (II) ions onto microalgae Chlamydomonas reinhardtii, 77 (2005) 85–92. https://doi.org/10.1016/j.jenvman.2005.01.028.

[54] K. Keryanti, E. Wahyu, S. Mulyono, Determination of Optimum Condition of Lead (Pb) Biosorption Using Dried Biomass Microalgae Aphanothece sp ., 65 (2021) 116–123. https://doi.org/10.3311/PPch.15773.

[55] N. Mirghaffari, E. Moeini, O. Farhadian, Biosorption of Cd and Pb ions from aqueous solutions by biomass of the green microalga, Scenedesmus quadricauda, J. Appl. Phycol. 27 (2015) 311–320. https://doi.org/10.1007/s10811-014-0345-z.

[56] A.M. Abdel, N.S. Ammar, H.H.A. Ghafar, R.K. Ali, Biosorption of cadmium and lead from aqueous solution by fresh water alga Anabaena sphaerica biomass, J. Adv. Res. 4 (2013) 367–374. https://doi.org/10.1016/j.jare.2012.07.004.

[57] C.M. Monteiro, P.M.L. Castro, F.X. Malcata, Biosorption of zinc ions from aqueous solution by the microalga Scenedesmus obliquus, (2011) 169–176. https://doi.org/10.1007/s10311-009-0258-2.

[58] Y. Kit, J. Chang, Bioresource Technology Bioremediation of heavy metals using microalgae : Recent advances and mechanisms, Bioresour. Technol. 303 (2020) 122886. https://doi.org/10.1016/j.biortech.2020.122886.

[59] S. Tripathi, K.M. Poluri, Heavy metal detoxification mechanisms by microalgae: Insights from transcriptomics analysis, Environ. Pollut. 285 (2021) 117443. https://doi.org/10.1016/j.envpol.2021.117443.

[60] B.N. Pham, J.K. Kang, C.G. Lee, S.J. Park, Removal of heavy metals (Cd2+, cu2+, ni2+, pb2+) from aqueous solution using hizikia fusiformis as an algae-based bioadsorbent, Appl. Sci. 11 (2021). https://doi.org/10.3390/app11188604.

[61] A.H. Sulaymon, A.A. Mohammed, T.J. Al-Musawi, Competitive biosorption of lead, cadmium, copper, and arsenic ions using algae, Environ. Sci. Pollut. Res. 20 (2013) 3011–

3023. https://doi.org/10.1007/s11356-012-1208-2.

[62] E. Romera, F. González, A. Ballester, M.L. Blázquez, J.A. Muñoz, Comparative study of biosorption of heavy metals using different types of algae, Bioresour. Technol. 98 (2007) 3344–3353. https://doi.org/10.1016/j.biortech.2006.09.026.

[63] M. Mar, S. Hanela, J. Duran, S. Afonso, Biosorption of Cu (II), Zn (II), Cd (II) and Pb (II) by dead biomasses of green alga Ulva lactuca and the development of a sustainable matrix for adsorption implementation, J. Hazard. Mater. 213–214 (2012) 123–132. https://doi.org/10.1016/j.jhazmat.2012.01.073.

[64] J.M. Tobin, D.G. Cooper, R.J. Neufeld, Uptake of metal ions by Rhizopus arrhizus biomass, Appl. Environ. Microbiol. 47 (1984) 821–824. https://doi.org/10.1128/aem.47.4.821-824.1984.

[65] P.X. Sheng, Y.-P.P. Ting, J.P. Chen, Biosorption of heavy metal ions (Pb, Cu, and Cd) from aqueous solutions by the Marine Alga Sargassum sp. in single- And multiple-metal systems, Ind. Eng. Chem. Res. 46 (2007) 2438–2444. https://doi.org/10.1021/ie0615786.

[66] M.S. Rahman, K. V. Sathasivam, Heavy metal adsorption onto kappaphycus sp. from aqueous solutions: The use of error functions for validation of isotherm and kinetics models, Biomed Res. Int. 2015 (2015). https://doi.org/10.1155/2015/126298.

[67] Siwei, C. Gu, Emma Boase, Q.Lan, Enhanced Pb(II) removal by green algae Neochloris oleoabundans cultivated in high-dissolved inorganic carbon bicarbonate cultures, Chem. Eng. J. (2021) 128983. https://doi.org/doi.org/10.1016/j.cej.2021.128983.

[68] U. Farooq, J.A. Kozinski, M. Ain, M. Athar, Bioresource Technology Biosorption of heavy metal ions using wheat based biosorbents – A review of the recent literature, Bioresour. Technol. 101 (2010) 5043–5053. https://doi.org/10.1016/j.biortech.2010.02.030.

[69] S. Rangabhashiyam, P. Balasubramanian, Characteristics, performances, equilibrium and kinetic modeling aspects of heavy metal removal using algae, Bioresour. Technol. Reports. 5 (2019) 261–279. https://doi.org/10.1016/j.biteb.2018.07.009.

[70] A.K. Zeraatkar, H. Ahmadzadeh, A.F. Talebi, N.R. Moheimani, M.P. McHenry, Potential use of algae for heavy metal bioremediation, a critical review, J. Environ. Manage. 181 (2016) 817–831. https://doi.org/10.1016/j.jenvman.2016.06.059.

[71] A.T. Ubando, A. Don, M. Africa, M.C. Maniquiz-redillas, A.B. Culaba, W. Chen, J. Chang, Microalgal biosorption of heavy metals : A comprehensive bibliometric review, J. Hazard. Mater. 402 (2021) 123431. https://doi.org/10.1016/j.jhazmat.2020.123431.

[72] R. Dineshkumar, M. Sowndariya, S. Kalaiselvi, G. Israth Rehana, M. Durai Murugan, Marykutty Abraham, Meivelu Moovendhan, M. Kavisri, Effective removal of lead (Pb) by natural biosorbent marine microalgae (Dunaliella salina) through batch experiment, Biomass Convers. Biorefinery. (2022). https://doi.org/10.1007/s13399-021-02260-9.

[73] A. Fraile, S. Penche, F. González, M.L. Blázquez, J.A. Muñoz, A. Ballester, S. Penche, F. González, M.L. Blázquez, J.A. Muñoz, Biosorption of copper , zinc , cadmium and nickel

by Chlorella vulgaris, 7540 (2006). https://doi.org/10.1080/02757540512331334933.

[74] M. Tunali, O. Yenigun, Biosorption of - Ag + and - Nd 3 + from single - and multi - metal solutions - (Ag + , - Nd 3 + , and - Au 3 +) by using living and dried microalgae, J. Mater. Cycles Waste Manag. 23 (2021) 764–777. https://doi.org/10.1007/s10163-020-01168-2.

[75] J. Cheng, Biosorption capacity and kinetics of cadmium (II) on live and dead Chlorella vulgaris, (2017) 211–221. https://doi.org/10.1007/s10811-016-0916-2.

[76] R. Li, T. Zhang, H. Zhong, W. Song, Y. Zhou, X. Yin, Bioadsorbents from algae residues for heavy metal ions adsorption: chemical modification, adsorption behaviour and mechanism, Environ. Technol. (United Kingdom). 42 (2021) 3132–3143. https://doi.org/10.1080/09593330.2020.1723711.

[77] E. Yalçin, K. Çavuşoğlu, M. Maraş, M. Biyikoğlu, Biosorption of lead (II) and copper (II) metal ions on Cladophora glomerata (L.) Kütz. (Chlorophyta) algae: Effect of algal surface modification, Acta Chim. Slov. 55 (2008) 228–232.

[78] D. Kaplan, Absorption and Adsorption of Heavy Metals by Microalgae, (2013) 602–611.

[79] A. Rinanti, M.F. Fachrul, R. Hadisoebroto, M. Silalahi, Improving biosorption of Cu(II)-ion on artificial wastewater by immobilized biosorbent of tropical microalgae, Int. J. GEOMATE. 13 (2017) 6–10. https://doi.org/10.21660/2017.36.2744.

[80] V.J.P. Vilar, C.M.S. Botelho, R.A.R. Boaventura, Influence of pH, ionic strength and temperature on lead biosorption by Gelidium and agar extraction algal waste, Process Biochem. 40 (2005) 3267–3275. https://doi.org/10.1016/j.procbio.2005.03.023.

[81] Z. Aksu, Determination of the equilibrium , kinetic and thermodynamic parameters of the batch biosorption of nickel (II) ions onto Chlorella v ulgaris, 38 (2002) 89–99.

[82] K. Kumar, K. Krishna, P. Mondithoka, Entrapment of marine microalga , Isochrysis galbana , for biosorption of Cr (III) from aqueous solution : isotherms and spectroscopic characterization, (2013) 85–92. https://doi.org/10.1007/s13201-012-0062-1.

[83] Q. Yang, Z. Li, X. Lu, Q. Duan, L. Huang, J. Bi, Science of the Total Environment A review of soil heavy metal pollution from industrial and agricultural regions in China : Pollution and risk assessment, Sci. Total Environ. 642 (2018) 690–700. https://doi.org/10.1016/j.scitotenv.2018.06.068.

[84] A. Bano, J. Hussain, A. Akbar, K. Mehmood, M. Anwar, M.S. Hasni, S. Ullah, S. Sajid, I. Ali, Biosorption of heavy metals by obligate halophilic fungi, Chemosphere. 199 (2018) 218–222. https://doi.org/10.1016/j.chemosphere.2018.02.043.

[85] J.H. Duffus, Metales pesados: ¿Un plazo significativo?, Pure Appl. Chem. 74 (2002) 793–807. http://www.degruyter.com/view/j/pac.2002.74.issue-5/pac200274050793/pac200274050793.xml.

[86] N. Vanhoudt, H. Vandenhove, N. Leys, P. Janssen, Potential of higher plants, algae, and cyanobacteria for remediation of radioactively contaminated waters, Chemosphere. 207 (2018) 239–254. https://doi.org/10.1016/j.chemosphere.2018.05.034.

[87] H. Demey, T. Vincent, E. Guibal, A novel algal - based sorbent for heavy metal removal, Chem. Eng. J. 332 (2018) 582–595. https://doi.org/10.1016/j.cej.2017.09.083.

[88] M. Bilal, J.A. Shah, T. Ashfaq, S. Mubashar, H. Gardazi, A.A. Tahir, A. Pervez, H. Haroon, Q. Mahmood, Waste biomass adsorbents for copper removal from industrial wastewater–A review, J. Hazard. Mater. (2013). https://doi.org/10.1016/j.jhazmat.2013.07.071.

[89] Z. Lin, J. Li, Y. Luan, W. Dai, Ecotoxicology and Environmental Safety Application of algae for heavy metal adsorption : A 20-year meta-analysis, Ecotoxicol. Environ. Saf. 190 (2020) 110089. https://doi.org/10.1016/j.ecoenv.2019.110089.

[90] Z.S. Birungi, E.M.N. Chirwa, The adsorption potential and recovery of thallium using green micro-algae from eutrophic water sources, J. Hazard. Mater. 299 (2015) 67–77. https://doi.org/10.1016/j.jhazmat.2015.06.011.

[91] T. Li, G. Lin, B. Podola, M. Melkonian, Continuous removal of zinc from wastewater and mine dump leachate by a microalgal biofilm PSBR, Elsevier B.V. (2015). https://doi.org/10.1016/j.jhazmat.2015.04.080.

[92] J.A. Cotruvo, 2017 Who guidelines for drinking water quality: first addendum to the fourth edition, 2017. https://doi.org/10.5942/jawwa.2017.109.0087.

[93] R. Huang, G. Huo, S. Song, Y. Li, L. Xia, J.F. Gaillard, Immobilization of mercury using high-phosphate culture-modified microalgae, Environ. Pollut. 254 (2019) 112966. https://doi.org/10.1016/j.envpol.2019.112966.

[94] Y. Li, S. Song, L. Xia, H. Yin, J. Viridiana, G. Meza, Enhanced Pb (II) removal by algal-based biosorbent cultivated in high- phosphorus cultures, Chem. Eng. J. 361 (2019) 167–179. https://doi.org/10.1016/j.cej.2018.12.070.

[95] E.B. Son, K.M. Poo, H.O. Mohamed, Y.J. Choi, W.C. Cho, K.J. Chae, A novel approach to developing a reusable marine macro-algae adsorbent with chitosan and ferric oxide for simultaneous efficient heavy metal removal and easy magnetic separation, Bioresour. Technol. 259 (2018) 381–387. https://doi.org/10.1016/j.biortech.2018.03.077.

[96] L. Peng, C.Q. Lan, Z. Zhang, C. Sarch, M. Laporte, Control of protozoa contamination and lipid accumulation in Neochloris oleoabundans culture: Effects of pH and dissolved inorganic carbon, Bioresour. Technol. 197 (2015) 143–151. https://doi.org/10.1016/j.biortech.2015.07.101.

[97] S. Husien, A. Labena, E.F. El-belely, H.M. Mahmoud, A.S. Hamouda, Journal of Environmental Chemical Engineering Adsorption studies of hexavalent chromium [Cr (VI)] on micro-scale biomass of Sargassum dentifolium , Sea weed, J. Environ. Chem. Eng. 7 (2019) 103444. https://doi.org/10.1016/j.jece.2019.103444.

[98] S. Xu, Y. Xing, S. Liu, X. Hao, W. Chen, Q. Huang, Characterization of Cd2+ biosorption by Pseudomonas sp. strain 375, a novel biosorbent isolated from soil polluted with heavy metals in Southern China, Chemosphere. 240 (2020) 124893. https://doi.org/10.1016/j.chemosphere.2019.124893.

[99] M. Tavana, H. Pahlavanzadeh, M.J. Zarei, The novel usage of dead biomass of green algae of Schizomeris leibleinii for biosorption of copper(II) from aqueous solutions: Equilibrium, kinetics and thermodynamics, J. Environ. Chem. Eng. 8 (2020) 104272. https://doi.org/10.1016/j.jece.2020.104272.

[100] M. Kajeiou, A. Alem, S. Mezghich, N.D. Ahfir, M. Mignot, C. Devouge-Boyer, A. Pantet, Competitive and non-competitive zinc, copper and lead biosorption from aqueous solutions onto flax fibers, Chemosphere. 260 (2020) 127505. https://doi.org/10.1016/j.chemosphere.2020.127505.

[101] M. Amin, P. Chetpattananondh, Biochar from extracted marine Chlorella sp. residue for high efficiency adsorption with ultrasonication to remove Cr(VI), Zn(II) and Ni(II), Bioresour. Technol. 289 (2019) 121578. https://doi.org/10.1016/j.biortech.2019.121578.

[102] A. De Rossi, C.V.T. Rigueto, A. Dettmer, L.M. Colla, J.S. Piccin, Synthesis, characterization, and application of Saccharomyces cerevisiae/alginate composites beads for adsorption of heavy metals, J. Environ. Chem. Eng. 8 (2020) 104009. https://doi.org/10.1016/j.jece.2020.104009.

[103] H.A. Cid, M.I. Flores, J.F. Pizarro, X.A. Castillo, D.E. Barros, J.C. Moreno-Piraján, C.A. Ortiz, Mechanisms of Cu2+ biosorption on Lessonia nigrescens dead biomass: Functional groups interactions and morphological characterization, J. Environ. Chem. Eng. 6 (2018) 2696–2704. https://doi.org/10.1016/j.jece.2018.03.034.

[104] M. Tavana, H. Pahlavanzadeh, M. Javad, Journal of Environmental Chemical Engineering The novel usage of dead biomass of green algae of Schizomeris leibleinii for biosorption of copper (II) from aqueous solutions : Equilibrium , kinetics and thermodynamics, J. Environ. Chem. Eng. 8 (2020) 104272. https://doi.org/10.1016/j.jece.2020.104272.

[105] I. Persson, Hydrated metal ions in aqueous solution : How regular are their structures ?, 82 (2010) 1901–1917. https://doi.org/10.1351/PAC-CON-09-10-22.

[106] G. Quijano, J.S. Arcila, G. Buitrón, Microalgal-bacterial aggregates: Applications and perspectives for wastewater treatment, Biotechnol. Adv. 35 (2017) 772–781. https://doi.org/10.1016/j.biotechadv.2017.07.003.

[107] J. Li, C. Li, C.Q. Lan, D. Liao, Effects of sodium bicarbonate on cell growth, lipid accumulation, and morphology of Chlorella vulgaris, Microb. Cell Fact. 17 (2018) 1–10. https://doi.org/10.1186/s12934-018-0953-4.

[108] M. Kumar, A. Kumar, S. Mohd, Study of sorption and desorption of Cd (II) from aqueous solution using isolated green algae Chlorella vulgaris, Appl. Water Sci. 8 (2018) 1–11. https://doi.org/10.1007/s13201-018-0871-y.

[109] T. Kiran Marella, A. Saxena, A. Tiwari, Diatom mediated heavy metal remediation: A review, Bioresour. Technol. 305 (2020) 123068. https://doi.org/10.1016/j.biortech.2020.123068.

[110] B. Rashidi, L.M. Trindade, Detailed biochemical and morphologic characteristics of the green microalga Neochloris oleoabundans cell wall, Algal Res. 35 (2018) 152–159.

https://doi.org/10.1016/j.algal.2018.08.033.

[111] T. Alam, K. Amer, A. Mukhlif, E.A. Khan, D.K. Sharma, Isotherm and kinetics modeling of Pb (II) and Cd (II) adsorptive uptake from aqueous solution by chemically modified green algal biomass, Model. Earth Syst. Environ. 2 (2016) 1–13. https://doi.org/10.1007/s40808-016-0157-z.

[112] M. Akbari, A. Hallajisani, A.R. Keshtkar, H. Shahbeig, S. Ali Ghorbanian, Equilibrium and kinetic study and modeling of Cu(II) and Co(II) synergistic biosorption from Cu(II)-Co(II) single and binary mixtures on brown algae C. indica, J. Environ. Chem. Eng. 3 (2015) 140–149. https://doi.org/10.1016/j.jece.2014.11.004.

[113] R. Foroutan, H. Esmaeili, M. Abbasi, M. Rezakazemi, Adsorption behavior of Cu (II) and Co (II) using chemically modified marine algae, 3330 (2018). https://doi.org/10.1080/09593330.2017.1365946.

[114] X. Sun, H. Huang, Y. Zhu, Y. Du, L. Yao, X. Jiang, P. Gao, Adsorption of Pb2+ and Cd2+ onto Spirulina platensis harvested by polyacrylamide in single and binary solution systems, Colloids Surfaces A Physicochem. Eng. Asp. 583 (2019) 123926. https://doi.org/10.1016/j.colsurfa.2019.123926.

[115] G. Lin, B. Zeng, J. Li, Z. Wang, S. Wang, T. Hu, L. Zhang, A systematic review of metal organic frameworks materials for heavy metal removal: Synthesis, applications and mechanism, Chem. Eng. J. 460 (2023). https://doi.org/10.1016/j.cej.2023.141710.

[116] T. He, Q. Li, T. Lin, J. Li, S. Bai, S. An, X. Kong, Y. Song, Recent progress on highly efficient removal of heavy metals by layered double hydroxides, Chem. Eng. J. 462 (2023) 142041. https://doi.org/10.1016/j.cej.2023.142041.

[117] J. Luo, W. Xing, J.A. Ippolito, L. Zhao, K. Han, Y. Wang, K. Qiu, L. Li, Bioaccessibility, source and human health risk of Pb, Cd, Cu and Zn in windowsill dusts from an area affected by long-term Pb smelting, Sci. Total Environ. 842 (2022) 156707. https://doi.org/10.1016/j.scitotenv.2022.156707.

[118] H.X. Zhao, Y. Wang, J.J. Yang, J.G. Zhang, Y.R. Guo, S. Li, Q.J. Pan, Treatment of heavy metal ions-polluted water into drinkable water: Capture and recovery of Pb2+ by cellulose@CaCO3 bio-composite filter via spatial confinement effect, Chem. Eng. J. 454 (2023) 140297. https://doi.org/10.1016/j.cej.2022.140297.

[119] M.E. Hong, B.S. Yu, A.K. Patel, H. Il Choi, S. Song, Y.J. Sung, W.S. Chang, S.J. Sim, M. Eui, B. Sun, A. Kumar, H. Il, S. Song, Enhanced biomass and lipid production of Neochloris oleoabundans under high light conditions by anisotropic nature of light-splitting CaCO3 crystal, Bioresour. Technol. 287 (2019) 121483. https://doi.org/10.1016/j.biortech.2019.121483.

[120] Y. Du, B. Schuur, S.R.A. Kersten, D.W.F. (Wim. Brilman, Multistage wet lipid extraction from fresh water stressed Neochloris oleoabundans slurry – Experiments and modelling, Algal Res. 31 (2018) 21–30. https://doi.org/10.1016/j.algal.2018.01.001.

[121] C.A. Popovich, C. Damiani, D. Constenla, A.M. Martínez, H. Freije, M. Giovanardi, S.

Pancaldi, P.I. Leonardi, Neochloris oleoabundans grown in enriched natural seawater for biodiesel feedstock: Evaluation of its growth and biochemical composition, Bioresour. Technol. 114 (2012) 287–293. https://doi.org/10.1016/j.biortech.2012.02.121.

[122] B. Wang, C.Q. Lan, Biomass production and nitrogen and phosphorus removal by the green alga Neochloris oleoabundans in simulated wastewater and secondary municipal wastewater effluent, Bioresour. Technol. 102 (2011) 5639–5644. https://doi.org/10.1016/j.biortech.2011.02.054.

[123] D.T. Molina-Aulestia, C.R. Soccol, A.I.M. Júnior, O.I. González-Marín, C.G. de Souza, A.B.P. Medeiros, E. Klein, J.C. de Carvalho, Resistance of Neochloris oleoabundans to six terpenes applicable as green contamination control agents, J. Appl. Phycol. 34 (2022) 261–267. https://doi.org/10.1007/s10811-021-02612-y.

[124] T.G. Tornabene, G. Holzer, S. Lien, N. Burris, Lipid composition of the nitrogen starved green alga Neochloris oleoabundans, Enzyme Microb. Technol. 5 (1983) 435–440. https://doi.org/10.1016/0141-0229(83)90026-1.

[125] A.K. Priya, L. Gnanasekaran, K. Dutta, S. Rajendran, D. Balakrishnan, M. Soto-Moscoso, Biosorption of heavy metals by microorganisms: Evaluation of different underlying mechanisms, Chemosphere. 307 (2022) 135957. https://doi.org/10.1016/j.chemosphere.2022.135957.

[126] S. Gu, Y. Su, C.Q. Lan, Effect of phosphate in medium on cell growth and Cu(II) biosorption by green alga Neochloris oleoabundans, Chem. Eng. Res. Des. 185 (2022) 186–197. https://doi.org/10.1016/j.cherd.2022.07.004.

[127] J. Hockaday, A. Harvey, S. Velasquez-orta, A comparative analysis of the adsorption kinetics of Cu 2 + and Cd 2 + by the microalgae Chlorella vulgaris and Scenedesmus obliquus, Algal Res. 64 (2022) 102710. https://doi.org/10.1016/j.algal.2022.102710.

[128] Y. Li, Algal biomass from the stable growth phase as a potential biosorbent for Pb (II) removal from water, (2017) 34600–34608. https://doi.org/10.1039/c7ra06749f.

[129] R. Jiang, L. Qin, S. Feng, D. Huang, Z. Wang, S. Zhu, The joint effect of ammonium and pH on the growth of Chlorella vulgaris and ammonium removal in artificial liquid digestate, Bioresour. Technol. 325 (2021) 124690. https://doi.org/10.1016/j.biortech.2021.124690.

[130] R. Qiu, S. Gao, P.A. Lopez, K.L. Ogden, Effects of pH on cell growth, lipid production and CO2 addition of microalgae Chlorella sorokiniana, Algal Res. 28 (2017) 192–199. https://doi.org/10.1016/j.algal.2017.11.004.

[131] H. Yuan, X. Zhang, Z. Jiang, X. Wang, X. Chen, L. Cao, X. Zhang, Analyzing the effect of pH on microalgae adhesion by identifying the dominant interaction between cell and surface, Colloids Surfaces B Biointerfaces. 177 (2019) 479–486. https://doi.org/10.1016/j.colsurfb.2019.02.023.

[132] G.Y. Kim, J. Heo, K. Kim, J. Chung, J.I. Han, Electrochemical pH control and carbon supply for microalgae cultivation, Chem. Eng. J. 426 (2021) 131796.

https://doi.org/10.1016/j.cej.2021.131796.

[133] P. Matos, W.B. Ferreira, L.R.I. Morioka, E.H.S. Moecke, K.B. França, E.S. Sant'Anna, Cultivation of Chlorella vulgaris in medium supplemented with desalination concentrate grown in a pilot-scale open raceway, Brazilian J. Chem. Eng. 35 (2018) 1183–1192. https://doi.org/10.1590/0104-6632.20180354s20170338.

[134] L. De Boni, D.S. Correa, F.J. Pavinatto, D.S. Dos Santos, C.R. Mendoņa, Excited state absorption spectrum of chlorophyll a obtained with white-light continuum, J. Chem. Phys. 126 (2007). https://doi.org/10.1063/1.2722755.

[135] P.G. Rouxhet, N. Mozes, P.B. Dengis, Y.F. Dufrêne, P.A. Gerin, M.J. Genet, Application of X-ray photoelectron spectroscopy to microorganisms, Colloids Surfaces B Biointerfaces. 2 (1994) 347–369. https://doi.org/10.1016/0927-7765(94)80049-9.

[136] R. Lakshmidevi, N. Nagendra Gandhi, K. Muthukumar, Bioelectricity and bioactive compound productionin an algal-assisted microbial fuel cell with immobilized bioanode, Biomass Convers. Biorefinery. 12 (2022) 3457–3473. https://doi.org/10.1007/s13399-020-00916-6.

[137] S. Das, V. Thiagarajan, N. Chandrasekaran, B. Ravindran, A. Mukherjee, Nanoplastics enhance the toxic effects of titanium dioxide nanoparticle in freshwater algae Scenedesmus obliquus, Comp. Biochem. Physiol. Part - C Toxicol. Pharmacol. 256 (2022) 109305. https://doi.org/10.1016/j.cbpc.2022.109305.

[138] P. Deore, J. Beardall, Y.M. Palacios, S. Noronha, P. Heraud, FTIR combined with chemometric tools — a potential approach for early screening of grazers in microalgal cultures, J. Appl. Phycol. 33 (2021) 2709–2722. https://doi.org/10.1007/s10811-021-02543-8.

[139] C. Prieto, J.M. Lagaron, Nanodroplets of docosahexaenoic acid-enriched algae oil encapsulated within microparticles of hydrocolloids by emulsion electrospraying assisted by pressurized gas, Nanomaterials. 10 (2020). https://doi.org/10.3390/nano10020270.

[140] R.M. Moghazy, A. Labena, S. Husien, E.S. Mansor, A.E. Abdelhamid, Neoteric approach for efficient eco-friendly dye removal and recovery using algal-polymer biosorbent sheets: Characterization, factorial design, equilibrium and kinetics, Int. J. Biol. Macromol. 157 (2020) 494–509. https://doi.org/10.1016/j.ijbiomac.2020.04.165.

[141] A. Kose, S.S. Oncel, Properties of microalgal enzymatic protein hydrolysates: Biochemical composition, protein distribution and FTIR characteristics, Biotechnol. Reports. 6 (2015) 137–143. https://doi.org/10.1016/j.btre.2015.02.005.

[142] K. Wang, S. Wang, K. Gu, W. Yan, Y. Zhou, C. Gao, Ultra-low pressure PES ultrafiltration membrane with high-flux and enhanced anti-oil-fouling properties prepared via in-situ polycondensation of polyamic acid, Sci. Total Environ. 842 (2022) 156661. https://doi.org/10.1016/j.scitotenv.2022.156661.

[143] Y. Chau, G. Kwan, G. Meng, C. Hon, A. Huan, Identification of functional groups and determination of carboxyl formation temperature in graphene oxide using the XPS O 1s

spectrum, Thin Solid Films. 590 (2015) 40–48. https://doi.org/10.1016/j.tsf.2015.07.051.

[144] Q. yu Chen, L. Yang, L. Liu, X. xuan Li, H. dong Li, Q. Zhang, D. ju Cao, XPS and NMR analyze the combined forms of Pb in Cladophora rupestris subcells and its detoxification, Environ. Sci. Pollut. Res. 29 (2022) 57490–57501. https://doi.org/10.1007/s11356-022-19880-x.

[145] R.C. Oliveira, P. Hammer, E. Guibal, J.M. Taulemesse, O. Garcia, Characterization of metal-biomass interactions in the lanthanum(III) biosorption on Sargassum sp. using SEM/EDX, FTIR, and XPS: Preliminary studies, Chem. Eng. J. 239 (2014) 381–391. https://doi.org/10.1016/j.cej.2013.11.042.

[146] D.N.G. Krishna, J. Philip, Review on surface-characterization applications of X-ray photoelectron spectroscopy (XPS): Recent developments and challenges, Appl. Surf. Sci. Adv. 12 (2022) 100332. https://doi.org/10.1016/j.apsadv.2022.100332.

[147] W. Huang, J. Deng, J. Liang, X. Xia, Comparison of lead adsorption on the aged conventional microplastics , biodegradable microplastics and environmentally-relevant tire wear particles, Chem. Eng. J. 460 (2023) 141838. https://doi.org/10.1016/j.cej.2023.141838.

[148] Z. Yin, S. Li, D. Hu, Z. Li, R. Chu, C. Liu, X. Li, J. Hu, L. Zhu, Performance evaluation of different chitosan-clay composite materials for efficient harvesting of Chlorella vulgaris and impacts on downstream bioproduct processing and water reusability, Chem. Eng. J. 430 (2022) 132892. https://doi.org/10.1016/j.cej.2021.132892.

[149] L.M.M. Liyanage, W.G.M. Lakmali, S.N.P. Athukorala, K.B. Jayasundera, Application of live Chlorococcum aquaticum biomass for the removal of Pb(II) from aqueous solutions, J. Appl. Phycol. 32 (2020) 4069–4080. https://doi.org/10.1007/s10811-020-02242-w.

[150] X. Zhang, X. Zhao, C. Wan, B. Chen, F. Bai, Efficient biosorption of cadmium by the self-flocculating microalga Scenedesmus obliquus AS-6-1, Algal Res. 16 (2016) 427–433. https://doi.org/10.1016/j.algal.2016.04.002.

[151] M. Hu, L. Liu, N. Hou, X. Li, D. Zeng, H. Tan, Insight into the adsorption mechanisms of ionizable imidazolinone herbicides in sediments: Kinetics, adsorption model, and influencing factors, Chemosphere. 274 (2021) 129655. https://doi.org/10.1016/j.chemosphere.2021.129655.

[152] R. Ezzati, Derivation of Pseudo-First-Order , Pseudo-Second-Order and Modified Pseudo-First-Order rate equations from Langmuir and Freundlich isotherms for adsorption, Chem. Eng. J. 392 (2020) 123705. https://doi.org/10.1016/j.cej.2019.123705.

[153] G.K. Rajahmundry, C. Garlapati, P.S. Kumar, R.S. Alwi, D.V.N. Vo, Statistical analysis of adsorption isotherm models and its appropriate selection, Chemosphere. 276 (2021) 130176. https://doi.org/10.1016/j.chemosphere.2021.130176.

[154] E. Wi, S. Go, S.Y. Shin, H.J. Cheon, G. Jeong, H. Cheon, J. Kim, H.R. Jung, H. Kim, M. Chang, Highly efficient and selective removal of anionic dyes from aqueous solutions using magneto-responsive Fe-aminoclay/Fe2O3/polyvinyl alcohol composite microgels,

Chem. Eng. J. 454 (2023) 140309. https://doi.org/10.1016/j.cej.2022.140309.

[155] Z. Wang, H. Wang, Q. Nie, Y. Ding, Z. Lei, Z. Zhang, K. Shimizu, T. Yuan, Pb(II) bioremediation using fresh algal-bacterial aerobic granular sludge and its underlying mechanisms highlighting the role of extracellular polymeric substances, J. Hazard. Mater. 444 (2023) 130452. https://doi.org/10.1016/j.jhazmat.2022.130452.

[156] K. Suresh Kumar, H.-U. Dahms, E.-J. Won, J.-S. Lee, K.-H. Shin, Microalgae – A promising tool for heavy metal remediation, Ecotoxicol. Environ. Saf. 113 (2015) 329–352. https://doi.org/10.1016/j.ecoenv.2014.12.019.

[157] S.Y. Cheng, P. Show, F. Lau, J. Chang, T.C. Ling, Review New Prospects for Modified Algae in Heavy Metal Adsorption, Trends Biotechnol. 37 (2019) 1255–1268. https://doi.org/10.1016/j.tibtech.2019.04.007.

[158] Y. Liu, Q. Gao, C. Li, S. Liu, K. Xia, B. Han, C. Zhou, Effective coating of crosslinked polyethyleneimine on elastic spongy monolith for highly efficient batch and continuous flow adsorption of Pb(II) and acidic red 18, Chem. Eng. J. 391 (2020). https://doi.org/10.1016/j.cej.2019.123610.

[159] Q. Chen, Y. Yao, X. Li, J. Lu, J. Zhou, Z. Huang, Journal of Water Process Engineering Comparison of heavy metal removals from aqueous solutions by chemical precipitation and characteristics of precipitates, J. Water Process Eng. 26 (2018) 289–300. https://doi.org/10.1016/j.jwpe.2018.11.003.

[160] Q. Dong, X. Guo, X. Huang, L. Liu, R. Tallon, B. Taylor, J. Chen, Selective removal of lead ions through capacitive deionization: Role of ion-exchange membrane, Chem. Eng. J. 361 (2019) 1535–1542. https://doi.org/10.1016/j.cej.2018.10.208.

[161] N. Abdullah, N. Yusof, W.J. Lau, J. Jaafar, A.F. Ismail, Journal of Industrial and Engineering Chemistry Recent trends of heavy metal removal from water / wastewater by membrane technologies, J. Ind. Eng. Chem. 76 (2019) 17–38. https://doi.org/10.1016/j.jiec.2019.03.029.

[162] M.A. Barakat, New trends in removing heavy metals from industrial wastewater, Arab. J. Chem. 4 (2011) 361–377. https://doi.org/10.1016/j.arabjc.2010.07.019.

[163] S.K. Gunatilake, Methods of Removing Heavy Metals from Industrial Wastewater, 1 (2015) 12–18.

[164] A. Dąbrowski, Z. Hubicki, P. Podkościelny, E. Robens, Selective removal of the heavy metal ions from waters and industrial wastewaters by ion-exchange method, Chemosphere. 56 (2004) 91–106. https://doi.org/10.1016/j.chemosphere.2004.03.006.

[165] M. Shi, Z. Wang, S. Zhao, J. Wang, P. Zhang, X. Cao, A novel pathway for high performance RO membrane: Preparing active layer with decreased thickness and enhanced compactness by incorporating tannic acid into the support, J. Memb. Sci. 555 (2018) 157–168. https://doi.org/10.1016/j.memsci.2018.03.025.

[166] S.S. Yoo, K.H. Chu, I.H. Choi, J.S. Mang, K.B. Ko, Operating cost reduction of UF

membrane filtration process for drinking water treatment attributed to chemical cleaning optimization, J. Environ. Manage. 206 (2018) 1126–1134. https://doi.org/10.1016/j.jenvman.2017.02.072.

[167] V.K. Gupta, A. Rastogi, Biosorption of lead from aqueous solutions by green algae Spirogyra species: Kinetics and equilibrium studies, J. Hazard. Mater. 152 (2008) 407–414. https://doi.org/10.1016/j.jhazmat.2007.07.028.

[168] Z. Wang, G. Xu, L. Zhao, Y. Gao, M.A. Al, H. Xu, A new method for evaluating defense of microalgae against protozoan grazing, Ecol. Indic. 77 (2017) 261–266. https://doi.org/10.1016/j.ecolind.2017.02.026.

[169] C. Zhu, R. Zhang, L. Cheng, Z. Chi, A recycling culture of Neochloris oleoabundans in a bicarbonate-based integrated carbon capture and algae production system with harvesting by auto-flocculation, Biotechnol. Biofuels. 11 (2018) 1–11. https://doi.org/10.1186/s13068-018-1197-6.

[170] K. Mokashi, V. Shetty, S.A. George, G. Sibi, Sodium Bicarbonate as Inorganic Carbon Source for Higher Biomass and Lipid Production Integrated Carbon Capture in Chlorella vulgaris, Achiev. Life Sci. 10 (2016) 111–117. https://doi.org/10.1016/j.als.2016.05.011.

[171] S. Joseph, L. Fernando, D.S. Lima, N. Della, S. Mohallem, Enhancement of adsorption capacity of clay through spray drying and surface modi fi cation process for wastewater treatment, Chem. Eng. J. 334 (2018) 1719–1728. https://doi.org/10.1016/j.cej.2017.11.084.

[172] N. Mohammad, B. Hayati, M. Arami, C. Lan, Adsorption of textile dyes on Pine Cone from colored wastewater : Kinetic , equilibrium and thermodynamic studies, DES. 268 (2011) 117–125. https://doi.org/10.1016/j.desal.2010.10.007.

[173] Dilek (Yalcin) Duygu, Fourier transform infrared (FTIR) spectroscopy for identification of Chlorella vulgaris Beijerinck 1890 and Scenedesmus obliquus (Turpin) Kützing 1833, AFRICAN J. Biotechnol. 11 (2012). https://doi.org/10.5897/AJB11.1863.

[174] M. Mecozzi, M. Pietroletti, A. Tornambè, Molecular and structural characteristics in toxic algae cultures of Ostreopsis ovata and Ostreopsis spp. evidenced by FTIR and FTNIR spectroscopy, Spectrochim. Acta Part A Mol. Biomol. Spectrosc. 78 (2011) 1572–1580. https://doi.org/10.1016/j.saa.2011.02.002.

[175] L. Dao, J. Beardall, P. Heraud, Characterisation of Pb-induced changes and prediction of Pb exposure in microalgae using infrared spectroscopy, Aquat. Toxicol. 188 (2017) 33–42. https://doi.org/10.1016/j.aquatox.2017.04.006.

[176] L. Liu, G. Pohnert, D. Wei, Extracellular Metabolites from Industrial Microalgae and Their Biotechnological Potential., Mar. Drugs. 14 (2016). https://doi.org/10.3390/md14100191.

[177] I.M. Id, M.M. Id, K. Marycz, A comprehensive analysis of biosorption of metal ions by macroalgae using ICP-OES , SEM- EDX and FTIR techniques, (2018) 1–20.

[178] B. Rashidi, A. Dechesne, M.G. Rydahl, B. Jørgensen, L.M. Trindade, Neochloris

oleoabundans cell walls have an altered composition when cultivated under different growing conditions, Algal Res. 40 (2019) 101482. https://doi.org/10.1016/j.algal.2019.101482.

[179] D. Roy, P.N. Greenlaw, B.S. Shane, D. Roy, P.N. Greenlaw, B.S. Shane, A. Hall, Adsorption of heavy metals by green algae and ground rice hulls, 1204 (2008). https://doi.org/10.1080/10934529309375861.

[180] N.A. Negm, M.G. Abd El Wahed, A.R.A. Hassan, M.T.H. Abou Kana, Feasibility of metal adsorption using brown algae and fungi: Effect of biosorbents structure on adsorption isotherm and kinetics, J. Mol. Liq. 264 (2018) 292–305. https://doi.org/10.1016/j.molliq.2018.05.027.

[181] J.A. Dean, Lange's Handbook of Chemistry, 15th ed., McGraw-Hill, New York, 1999.

[182] Nornickel, Navigating the Transition to a Net Zero World, (2021) 68. https://www.nornickel.com/upload/iblock/27f/strategy_day_presentation_2021.pdf.

[183] L. Trotochaud, A.R. Head, S. Pletincx, O. Karslloğlu, Y. Yu, A. Waldner, L. Kyhl, T. Hauffman, H. Terryn, B. Eichhorn, H. Bluhm, Water Adsorption and Dissociation on Polycrystalline Copper Oxides: Effects of Environmental Contamination and Experimental Protocol, J. Phys. Chem. B. 122 (2018) 1000–1008. https://doi.org/10.1021/acs.jpcb.7b10732.

[184] J. López, O. Gibert, J.L. Cortina, Evaluation of an extreme acid-resistant sulphonamide based nanofiltration membrane for the valorisation of copper acidic effluents, Chem. Eng. J. 405 (2021). https://doi.org/10.1016/j.cej.2020.127015.

[185] X. Wei, D. Liu, W. Huang, W. Huang, Z. Lei, Simultaneously enhanced Cu bioleaching from E-wastes and recovered Cu ions by direct current electric field in a bioelectrical reactor, Bioresour. Technol. 298 (2019) 122566. https://doi.org/10.1016/j.biortech.2019.122566.

[186] H. Wang, H. Wang, C. Gao, L. Liu, Enhanced removal of copper by electroflocculation and electroreduction in a novel bioelectrochemical system assisted microelectrolysis, Bioresour. Technol. 297 (2020) 122507. https://doi.org/10.1016/j.biortech.2019.122507.

[187] S. Vinardell, S. Astals, J. Mata-Alvarez, J. Dosta, Techno-economic analysis of combining forward osmosis-reverse osmosis and anaerobic membrane bioreactor technologies for municipal wastewater treatment and water production, Bioresour. Technol. 297 (2020) 122395. https://doi.org/10.1016/j.biortech.2019.122395.

[188] R. Katiyar, A.K. Patel, T.B. Nguyen, R.R. Singhania, C.W. Chen, C. Di Dong, Adsorption of copper (II) in aqueous solution using biochars derived from Ascophyllum nodosum seaweed, Bioresour. Technol. 328 (2021) 124829. https://doi.org/10.1016/j.biortech.2021.124829.

[189] A. Bashir, L. Ahmad, M. Sozia, A. Taniya, M. Mudasir, A. Bhat, Abiotic ge and biosorption methods, Environ. Chem. Lett. 17 (2019) 729–754. https://doi.org/10.1007/s10311-018-00828-y.

[190] A.R. Lucaci, D. Bulgariu, M. Popescu, L. Bulgariu, Adsorption of Cu (II) Ions on Adsorbent Materials Obtained from Marine Red Algae, (2020). https://doi.org/doi.org/10.3390/w12020372.

[191] M. Priyadarshanee, S. Das, Biosorption and removal of toxic heavy metals by metal tolerating bacteria for bioremediation of metal contamination: A comprehensive review, J. Environ. Chem. Eng. (2020) 104686. https://doi.org/10.1016/j.jece.2020.104686.

[192] S. Satyro, M. Race, F. Di Natale, A. Erto, M. Guida, R. Marotta, Simultaneous removal of heavy metals from field-polluted soils and treatment of soil washing effluents through combined adsorption and artificial sunlight-driven photocatalytic processes, Chem. Eng. J. 283 (2016) 1484–1493. https://doi.org/10.1016/j.cej.2015.08.039.

[193] Y. Li, M. Horsman, B. Wang, N. Wu, C.Q. Lan, Effects of nitrogen sources on cell growth and lipid accumulation of green alga Neochloris oleoabundans, Appl. Microbiol. Biotechnol. 81 (2008) 629–636. https://doi.org/10.1007/s00253-008-1681-1.

[194] A.N. Sadovski, Study on ph in water and potassium chloride for bulgarian soils, Eurasian J. Soil Sci. 8 (2019) 11–16. https://doi.org/10.18393/ejss.477560.

[195] W. Kim, J.M. Park, G.H. Gim, S.H. Jeong, C.M. Kang, D.J. Kim, S.W. Kim, Optimization of culture conditions and comparison of biomass productivity of three green algae, Bioprocess Biosyst. Eng. 35 (2012) 19–27. https://doi.org/10.1007/s00449-011-0612-1.

[196] P. Feng, Z. Deng, L. Fan, Z. Hu, Lipid accumulation and growth characteristics of Chlorella zo fi ngiensis under different nitrate and phosphate concentrations, J. Biosci. Bioeng. 114 (2012) 405–410. https://doi.org/10.1016/j.jbiosc.2012.05.007.

[197] V. da Silva Ferreira, C. Sant'Anna, Impact of culture conditions on the chlorophyll content of microalgae for biotechnological applications, World J. Microbiol. Biotechnol. 33 (2017) 1–8. https://doi.org/10.1007/s11274-016-2181-6.

[198] D. Song, B. Xi, J. Sun, Characterization of the growth, chlorophyll content and lipid accumulation in a marine microalgae Dunaliella tertiolecta under different nitrogen to phosphorus ratios, J. Ocean Univ. China. 15 (2016) 124–130. https://doi.org/10.1007/s11802-016-2797-z.

[199] M. Zhang, K.T. Leung, H. Lin, B. Liao, The biological performance of a novel microalgal-bacterial membrane photobioreactor: Effects of HRT and N/P ratio, Chemosphere. 261 (2020) 128199. https://doi.org/10.1016/j.chemosphere.2020.128199.

[200] F.A. AlMomani, B. Örmeci, Performance Of Chlorella Vulgaris, Neochloris Oleoabundans, and mixed indigenous microalgae for treatment of primary effluent, secondary effluent and centrate, Ecol. Eng. 95 (2016) 280–289. https://doi.org/10.1016/j.ecoleng.2016.06.038.

[201] M. Franchino, E. Comino, F. Bona, V.A. Riggio, Growth of three microalgae strains and nutrient removal from an agro-zootechnical digestate, Chemosphere. 92 (2013) 738–744. https://doi.org/10.1016/j.chemosphere.2013.04.023.

[202] A.B.D. Nandiyanto, R. Oktiani, R. Ragadhita, How to read and interpret ftir spectroscope of organic material, Indones. J. Sci. Technol. 4 (2019) 97–118. https://doi.org/10.17509/ijost.v4i1.15806.

[203] A.M. Turner, M.J. Abplanalp, T.J. Blair, R. Dayuha, R.I. Kaiser, An Infrared Spectroscopic Study Toward the Formation of Alkylphosphonic Acids and Their Precursors in Extraterrestrial Environments, Astrophys. J. Suppl. Ser. 234 (2018) 6. https://doi.org/10.3847/1538-4365/aa9183.

[204] O. Derkacheva, D. Sukhov, Investigation of lignins by FTIR spectroscopy, Macromol. Symp. 265 (2008) 61–68. https://doi.org/10.1002/masy.200850507.

[205] R. Norman Jones, D.A. Ramsay, D.S. Keir, The Intensities of Carbonyl Bands in the Infrared Spectra of Steroids, J. Am. Chem. Soc. 74 (1952) 80–88. https://doi.org/10.1021/ja01121a019.

[206] K. Cacua, F. Ordoñez, C. Zapata, B. Herrera, E. Pabón, Surfactant concentration and pH e ff ects on the zeta potential values of alumina nano fl uids to inspect stability, 583 (2019). https://doi.org/10.1016/j.colsurfa.2019.123960.

[207] Y. Huang, C. Wei, Q. Liao, A. Xia, X. Zhu, X. Zhu, Bioresource Technology Biodegradable branched cationic starch with high C / N ratio for Chlorella vulgaris cells concentration : Regulating microalgae flocculation performance by pH, Bioresour. Technol. 276 (2019) 133–139. https://doi.org/10.1016/j.biortech.2018.12.072.

[208] R.A. Rahardini, S. Helmiati, B. Triyatmo, W.P. Siwi, A. Rinanti, A. Rinanti, D. Jonathan, Biosorption of Copper (II) Ions using Living Chlorella sp . from Aqueous Solution Biosorption of Copper (II) Ions using Living Chlorella sp . from Aqueous Solution, (2020). https://doi.org/10.1088/1757-899X/742/1/012026.

[209] Z. Chen, W. Ma, M. Han, Biosorption of nickel and copper onto treated alga (Undaria pinnatifida): Application of isotherm and kinetic models, J. Hazard. Mater. 155 (2008) 327–333. https://doi.org/10.1016/j.jhazmat.2007.11.064.

[210] R. Li, T. Zhang, H. Zhong, W. Song, Y. Zhou, X. Yin, Bioadsorbents from algae residues for heavy metal ions adsorption: chemical modification, adsorption behaviour and mechanism, Environ. Technol. (United Kingdom). 0 (2020) 1–44. https://doi.org/10.1080/09593330.2020.1723711.

[211] H. Wang, H. Wang, H. Zhao, Q. Yan, Adsorption and Fenton-like removal of chelated nickel from Zn-Ni alloy electroplating wastewater using activated biochar composite derived from Taihu blue algae, Chem. Eng. J. 379 (2020) 122372. https://doi.org/10.1016/j.cej.2019.122372.

[212] X. Chen, M. Zheng, G. Zhang, F. Li, H. Chen, Y. Leng, The nature of dissolved organic matter determines the biosorption capacity of Cu by algae, Chemosphere. 252 (2020) 126465. https://doi.org/10.1016/j.chemosphere.2020.126465.

[213] L. Shen, J. Wang, Z. Li, L. Fan, R. Chen, X. Wu, J. Li, W. Zeng, A high-efficiency Fe2O3@Microalgae composite for heavy metal removal from aqueous solution, J. Water

Process Eng. 33 (2020) 101026. https://doi.org/10.1016/j.jwpe.2019.101026.

[214] L. Zhu, Z. Li, E. Hiltunen, Microalgae Chlorella vulgaris biomass harvesting by natural flocculant: Effects on biomass sedimentation, spent medium recycling and lipid extraction, Biotechnol. Biofuels. 11 (2018) 1–10. https://doi.org/10.1186/s13068-018-1183-z.

[215] J.F. Reyes, C. Labra, Biomass harvesting and cscenedesmus sp.oncentration of microalgae cultivated in a pilot phobioreactor, Biomass and Bioenergy. 87 (2016) 78–83. https://doi.org/10.1016/j.biombioe.2016.02.014.

[216] N.B. Wyatt, L.M. Gloe, P. V. Brady, J.C. Hewson, A.M. Grillet, M.G. Hankins, P.I. Pohl, Critical conditions for ferric chloride-induced flocculation of freshwater algae, Biotechnol. Bioeng. 109 (2012) 493–501. https://doi.org/10.1002/bit.23319.

[217] A. Papazi, P. Makridis, P. Divanach, Harvesting Chlorella minutissima using cell coagulants, J. Appl. Phycol. 22 (2010) 349–355. https://doi.org/10.1007/s10811-009-9465-2.

[218] E. Gunasundari, S.K. P., Adsorption isotherm, kinetics and thermodynamic analysis of Cu(II) ions onto the dried algal biomass (Spirulina platensis), J. Ind. Eng. Chem. 56 (2017) 129–144. https://doi.org/10.1016/j.jiec.2017.07.005.

[219] G. Markou, D. Mitrogiannis, A. Çelekli, H. Bozkurt, D. Georgakakis, C. V. Chrysikopoulos, Biosorption of Cu2+ and Ni2+ by Arthrospira platensis with different biochemical compositions, Chem. Eng. J. 259 (2015) 806–813. https://doi.org/10.1016/j.cej.2014.08.037.

[220] H. Cid, C. Ortiz, J. Pizarro, D. Barros, X. Castillo, L. Giraldo, J.C. Moreno-Piraján, Characterization of copper (II) biosorption by brown algae Durvillaea antarctica dead biomass, Adsorption. 21 (2015) 645–658. https://doi.org/10.1007/s10450-015-9715-3.

[221] J. Lee, Y. Ko, S. Kim, H.G. Hur, Highly effective biosorption capacity of Cladosporium sp. strain F1 to lead phosphate mineral and perovskite solar cell Pb(II), J. Hazard. Mater. 442 (2023) 130106. https://doi.org/10.1016/j.jhazmat.2022.130106.

[222] R.Z. Xia, X. Cai, B. Liang, H.H. Dai, Y.Z. Liu, M. Yang, S.H. Chen, P.H. Li, X.J. Huang, Bimodal interferences of Pb(II) induced by parallel deposition in Pb(II)-Cu(II) electrochemical detections: Voltammetric signals analysis combined with numerical simulations on transient interfacial phenomena, J. Hazard. Mater. 459 (2023). https://doi.org/10.1016/j.jhazmat.2023.132104.

[223] A. Kumar, A. Kumar, M. Cabral-Pinto, A.K. Chaturvedi, A.A. Shabnam, G. Subrahmanyam, R. Mondal, D.K. Gupta, S.K. Malyan, S.S. Kumar, S.A. Khan, K.K. Yadav, Lead toxicity: Health hazards, influence on food Chain, and sustainable remediation approaches, Int. J. Environ. Res. Public Health. 17 (2020). https://doi.org/10.3390/ijerph17072179.

[224] J. Briffa, E. Sinagra, R. Blundell, Heavy metal pollution in the environment and their toxicological effects on humans, Heliyon. 6 (2020) e04691. https://doi.org/10.1016/j.heliyon.2020.e04691.

[225] Q. Wang, Y. Zhang, H. Chen, S. Chen, Y. Wang, Effects of humic acids on the adsorption of Pb(II) ions onto biofilm-developed microplastics in aqueous ecosystems, Sci. Total Environ. 882 (2023) 163466. https://doi.org/10.1016/j.scitotenv.2023.163466.

[226] V. Paul, M.S. Sankar, S. Vattikuti, P. Dash, Z. Arslan, Pollution assessment and land use land cover influence on trace metal distribution in sediments from five aquatic systems in southern USA, Chemosphere. 263 (2021) 128243. https://doi.org/10.1016/j.chemosphere.2020.128243.

[227] H. Zhang, T.R. Walker, E. Davis, G. Ma, Ecological risk assessment of metals in small craft harbour sediments in Nova Scotia, Canada, Mar. Pollut. Bull. 146 (2019) 466–475. https://doi.org/10.1016/j.marpolbul.2019.06.068.

[228] Z. Zhang, Y. Lu, H. Li, Y. Tu, B. Liu, Z. Yang, Assessment of heavy metal contamination, distribution and source identification in the sediments from the Zijiang River, China, Sci. Total Environ. 645 (2018) 235–243. https://doi.org/10.1016/j.scitotenv.2018.07.026.

[229] H. Ucun Ozel, B.T. Gemici, E. Gemici, H.B. Ozel, M. Cetin, H. Sevik, Application of artificial neural networks to predict the heavy metal contamination in the Bartin River, Environ. Sci. Pollut. Res. 27 (2020) 42495–42512. https://doi.org/10.1007/s11356-020-10156-w.

[230] B. Qiu, X. Tao, H. Wang, W. Li, X. Ding, H. Chu, Biochar as a low-cost adsorbent for aqueous heavy metal removal: A review, J. Anal. Appl. Pyrolysis. 155 (2021) 105081. https://doi.org/10.1016/j.jaap.2021.105081.

[231] G. Crini, E. Lichtfouse, Advantages and disadvantages of techniques used for wastewater treatment, Environ. Chem. Lett. 17 (2020) 145–155. https://doi.org/10.1007/s10311-018-0785-9.

[232] W. Siong, W. Gee, H. Siti, H. Munawaroh, V. Kumar, S. Ho, P. Loke, Multifaceted roles of microalgae in the application of wastewater biotreatment : A review *, Environ. Pollut. 269 (2021) 116236. https://doi.org/10.1016/j.envpol.2020.116236.

[233] G.J. Zhou, F.Q. Peng, L.J. Zhang, G.G. Ying, Biosorption of zinc and copper from aqueous solutions by two freshwater green microalgae Chlorella pyrenoidosa and Scenedesmus obliquus, Environ. Sci. Pollut. Res. 19 (2012) 2918–2929. https://doi.org/10.1007/s11356-012-0800-9.

[234] M.A. Alam, C. Wan, X.Q. Zhao, L.J. Chen, J.S. Chang, F.W. Bai, Enhanced removal of Zn2+ or Cd2+ by the flocculating Chlorella vulgaris JSC-7, J. Hazard. Mater. 289 (2015) 38–45. https://doi.org/10.1016/j.jhazmat.2015.02.012.

[235] C. Li, C. Zheng, H. Fu, S. Zhai, F. Hu, S. Naveed, C. Zhang, Y. Ge, Contrasting detoxification mechanisms of Chlamydomonas reinhardtii under Cd and Pb stress, Chemosphere. 274 (2021) 129771. https://doi.org/10.1016/j.chemosphere.2021.129771.

[236] S. Zheng, Q. Zhou, C. Chen, F. Yang, Z. Cai, D. Li, Q. Geng, Y. Feng, H. Wang, Role of extracellular polymeric substances on the behavior and toxicity of silver nanoparticles and ions to green algae Chlorella vulgaris, Sci. Total Environ. 660 (2019) 1182–1190.

https://doi.org/10.1016/j.scitotenv.2019.01.067.

[237] L. Xia, J. Tan, R. Huang, Z. Zhang, K. Zhou, Y. Hu, S. Song, L. Xu, M.E. Farías, R.M.T. Sánchez, Enhanced Cd(II) biomineralization induced by microalgae after cultivating modification in high-phosphorus culture, J. Hazard. Mater. 443 (2023). https://doi.org/10.1016/j.jhazmat.2022.130243.

[238] S. Gu, C.Q. Lan, Effects of culture pH on cell surface properties and biosorption of Pb(II), Cd(II), Zn(II) of green alga Neochloris oleoabundans, Chem. Eng. J. 468 (2023) 143579. https://doi.org/10.1016/j.cej.2023.143579.

[239] G.S. Araujo, J.W.A. Silva, C.A.S. Viana, F.A.N. Fernandes, Effect of sodium nitrate concentration on biomass and oil production of four microalgae species, Int. J. Sustain. Energy. 39 (2020) 41–50. https://doi.org/10.1080/14786451.2019.1634568.

[240] H. Wu, X. Miao, Biodiesel quality and biochemical changes of microalgae Chlorella pyrenoidosa and Scenedesmus obliquus in response to nitrate levels, Bioresour. Technol. 170 (2014) 421–427. https://doi.org/10.1016/j.biortech.2014.08.017.

[241] H. Zhou, Z. Xu, L. Zhou, Z. Zhang, J. Wang, C.Q. Lan, High cell density culture of Neochloris oleoabundans in novel horizontal thin-layer algal reactor: Effects of localized aeration, nitrate concentration and mixing frequency, Biochem. Eng. J. 192 (2023) 108839. https://doi.org/10.1016/j.bej.2023.108839.

[242] A.R. Wellburn, The spectral determination of chlorophylls a and b, as well as total carotenoids, using various solvents with spectrophotometers of different resolution, J. Plant Physiol. 144 (1994) 307–313.

[243] Q. Liao, Y. Sun, Y. Huang, A. Xia, Q. Fu, X. Zhu, Simultaneous enhancement of Chlorella vulgaris growth and lipid accumulation through the synergy effect between light and nitrate in a planar waveguide flat-plate photobioreactor, Bioresour. Technol. 243 (2017) 528–538. https://doi.org/10.1016/j.biortech.2017.06.091.

[244] T. Akar, S. Celik, S.T. Akar, Biosorption performance of surface modified biomass obtained from Pyracantha coccinea for the decolorization of dye contaminated solutions, Chem. Eng. J. 160 (2010) 466–472. https://doi.org/10.1016/j.cej.2010.03.047.

[245] L. Zhu, S. Li, T. Hu, Y.K. Nugroho, Z. Yin, D. Hu, R. Chu, F. Mo, C. Liu, E. Hiltunen, Effects of nitrogen source heterogeneity on nutrient removal and biodiesel production of mono- and mix-cultured microalgae, Energy Convers. Manag. 201 (2019) 112144. https://doi.org/10.1016/j.enconman.2019.112144.

[246] A. Khalili, G.D. Najafpour, G. Amini, F. Samkhaniyani, Influence of nutrients and LED light intensities on biomass production of microalgae Chlorella vulgaris, Biotechnol. Bioprocess Eng. 20 (2015) 284–290. https://doi.org/10.1007/s12257-013-0845-8.

[247] S. Kim, Y. Lee, S.J. Hwang, Removal of nitrogen and phosphorus by Chlorella sorokiniana cultured heterotrophically in ammonia and nitrate, Int. Biodeterior. Biodegrad. 85 (2013) 511–516. https://doi.org/10.1016/j.ibiod.2013.05.025.

[248] W. Chen, Q. Zhang, S. Dai, Effects of nitrate on intracellular nitrite and growth of Microcystis aeruginosa, J. Appl. Phycol. 21 (2009) 701–706. https://doi.org/10.1007/s10811-009-9405-1.

[249] T. Wang, Y. Zhai, Y. Zhu, C. Peng, B. Xu, T. Wang, C. Li, G. Zeng, Influence of temperature on nitrogen fate during hydrothermal carbonization of food waste, Bioresour. Technol. 247 (2018) 182–189. https://doi.org/10.1016/j.biortech.2017.09.076.

[250] R.K. Mohapatra, P.K. Parhi, S. Pandey, B.K. Bindhani, Active and passive biosorption of Pb(II)using live and dead biomass of marine bacterium Bacillus xiamenensis PbRPSD202: Kinetics and isotherm studies, (2019). https://doi.org/10.1016/j.jenvman.2019.06.073.

[251] J. Wang, Q. Tian, L. Cui, J. Cheng, H. Zhou, Y. Zhang, A. Peng, L. Shen, Bioimmobilization and transformation of chromium and cadmium in the fungi-microalgae symbiotic system, J. Hazard. Mater. 445 (2023) 130507. https://doi.org/10.1016/j.jhazmat.2022.130507.

[252] H. Zhang, J. Wang, Y. Teng, S. Jia, H. Huang, Y. Li, C. Wang, Ce-MOF composite electrospinning as antibacterial adsorbent for the removal of 2,4-dichlorophenoxyacetic acid, Chem. Eng. J. 462 (2023) 142195. https://doi.org/10.1016/j.cej.2023.142195.

[253] J. Wang, X. Guo, Adsorption isotherm models: Classification, physical meaning, application and solving method, Chemosphere. 258 (2020) 127279. https://doi.org/10.1016/j.chemosphere.2020.127279.

[254] S. Zhao, M. Zhao, X. Fan, Z. Meng, Q. Zhang, F. Lv, MoS42- intercalated magnetic layered double hydroxides for effective removal and expedient recovery of heavy metals from soil, Chem. Eng. J. 454 (2023) 139965. https://doi.org/10.1016/j.cej.2022.139965.

[255] G.A. Dakroury, E.A.A. El-Shazly, H.S. Hassan, Sorption of lead (II) and strontium (II) ions from aqueous solutions onto non-living Chlorella Vulgaris Alga/ Date pit activated carbon composite, Carbon Lett. 32 (2022) 495–512. https://doi.org/10.1007/s42823-021-00280-z.

[256] G. Edris, Y. Alhamed, A. Alzahrani, Biosorption of Cadmium and Lead from Aqueous Solutions by Chlorella vulgaris Biomass: Equilibrium and Kinetic Study, Arab. J. Sci. Eng. 39 (2014) 87–93. https://doi.org/10.1007/s13369-013-0820-x.

[257] X. Ma, Y. Guan, R. Mao, S. Zheng, Q. Wei, Modeling of lead removal by living Scenedesmus obliquus using backpropagation (BP) neural network algorithm, Environ. Technol. Innov. 22 (2021) 101410. https://doi.org/10.1016/j.eti.2021.101410.

[258] C. Zamora-Ledezma, D. Negrete-Bolagay, F. Figueroa, E. Zamora-Ledezma, M. Ni, F. Alexis, V.H. Guerrero, Heavy metal water pollution: A fresh look about hazards, novel and conventional remediation methods, Environ. Technol. Innov. 22 (2021) 101504. https://doi.org/10.1016/j.eti.2021.101504.

[259] I. Zwolak, The Role of Selenium in Arsenic and Cadmium Toxicity: an Updated Review of Scientific Literature, Biol. Trace Elem. Res. 193 (2020) 44–63. https://doi.org/10.1007/s12011-019-01691-w.

[260] J. Wu, T. Wang, J. Wang, Y. Zhang, W.P. Pan, A novel modified method for the efficient removal of Pb and Cd from wastewater by biochar: Enhanced the ion exchange and precipitation capacity, Sci. Total Environ. 754 (2021) 142150. https://doi.org/10.1016/j.scitotenv.2020.142150.

[261] S.S. Elanchezhiyan, P. Karthikeyan, K. Rathinam, M. Hasmath Farzana, C.M. Park, Magnetic kaolinite immobilized chitosan beads for the removal of Pb(II) and Cd(II) ions from an aqueous environment, Carbohydr. Polym. 261 (2021) 117892. https://doi.org/10.1016/j.carbpol.2021.117892.

[262] Y.J. Lim, K. Goh, M. Kurihara, R. Wang, Seawater desalination by reverse osmosis: Current development and future challenges in membrane fabrication – A review, J. Memb. Sci. 629 (2021) 119292. https://doi.org/10.1016/j.memsci.2021.119292.

[263] J.S. Yang, J. Cao, G.L. Xing, H.L. Yuan, Lipid production combined with biosorption and bioaccumulation of cadmium, copper, manganese and zinc by oleaginous microalgae Chlorella minutissima UTEX2341, Bioresour. Technol. 175 (2015) 537–544. https://doi.org/10.1016/j.biortech.2014.10.124.

[264] P. Molazadeh, N. Khanjani, M.R. Rahimi, A. Nasiri, Adsorption of Lead by Microalgae Chaetoceros Sp. and Chlorella Sp. from Aqueous Solution, J. Community Heal. Res. 4 (2015) 114–127. http://jhr.ssu.ac.ir/article-1-248-en.html.

[265] J. Jena, N. Pradhan, V. Aishvarya, R.R. Nayak, B.P. Dash, L.B. Sukla, P.K. Panda, B.K. Mishra, Biological sequestration and retention of cadmium as CdS nanoparticles by the microalga Scenedesmus-24, J. Appl. Phycol. 27 (2015) 2251–2260. https://doi.org/10.1007/s10811-014-0499-8.

[266] X.J. Lee, H.C. Ong, J. Ooi, K.L. Yu, T.C. Tham, W.H. Chen, Y.S. Ok, Engineered macroalgal and microalgal adsorbents: Synthesis routes and adsorptive performance on hazardous water contaminants, J. Hazard. Mater. 423 (2022) 126921. https://doi.org/10.1016/j.jhazmat.2021.126921.

[267] V.C. Liyanaarachchi, M. Premaratne, T.U. Ariyadasa, P.H.V. Nimarshana, A. Malik, Two-stage cultivation of microalgae for production of high-value compounds and biofuels: A review, Algal Res. 57 (2021) 102353. https://doi.org/10.1016/j.algal.2021.102353.

[268] W. Meng, T. Mu, H. Sun, M. Garcia-Vaquero, Evaluation of the chemical composition and nutritional potential of brown macroalgae commercialised in China, Algal Res. 64 (2022) 102683. https://doi.org/10.1016/j.algal.2022.102683.

[269] F. Hussain, S.Z. Shah, H. Ahmad, S.A. Abubshait, H.A. Abubshait, A. Laref, A. Manikandan, H.S. Kusuma, M. Iqbal, Microalgae an ecofriendly and sustainable wastewater treatment option: Biomass application in biofuel and bio-fertilizer production. A review, Renew. Sustain. Energy Rev. 137 (2021) 110603. https://doi.org/10.1016/j.rser.2020.110603.

[270] K.A. Martínez Andrade, C. Lauritano, G. Romano, A. Ianora, Marine microalgae with anti-cancer properties, Mar. Drugs. 16 (2018). https://doi.org/10.3390/md16050165.

[271] E.A. Ehimen, Z.F. Sun, C.G. Carrington, E.J. Birch, J.J. Eaton-Rye, Anaerobic digestion of microalgae residues resulting from the biodiesel production process, Appl. Energy. 88 (2011) 3454–3463. https://doi.org/10.1016/j.apenergy.2010.10.020.

[272] R.R. Kumar, P.H. Rao, M. Arumugam, Lipid extraction methods from microalgae: A comprehensive review, Front. Energy Res. 3 (2015) 1–9. https://doi.org/10.3389/fenrg.2014.00061.

[273] J.A. Gerde, M. Montalbo-Lomboy, L. Yao, D. Grewell, T. Wang, Evaluation of microalgae cell disruption by ultrasonic treatment, Bioresour. Technol. 125 (2012) 175–181. https://doi.org/10.1016/j.biortech.2012.08.110.

[274] Y. Liu, X. Liu, Y. Cui, W. Yuan, Ultrasound for microalgal cell disruption and product extraction: A review, Ultrason. Sonochem. 87 (2022) 106054. https://doi.org/10.1016/j.ultsonch.2022.106054.

[275] C. González-Fernández, B. Sialve, N. Bernet, J.P. Steyer, Comparison of ultrasound and thermal pretreatment of Scenedesmus biomass on methane production, Bioresour. Technol. 110 (2012) 610–616. https://doi.org/10.1016/j.biortech.2012.01.043.

[276] Y. Peng, Z. Zhang, Y. Kong, Y. Li, Y. Zhou, X. Shi, X. Shi, Effects of ultrasound on Microcystis aeruginosa cell destruction and release of intracellular organic matter, Ultrason. Sonochem. 63 (2020) 104909. https://doi.org/10.1016/j.ultsonch.2019.104909.

[277] B.H. Jeon, J.A. Choi, H.C. Kim, J.H. Hwang, R.A.I. Abou-Shanab, B.A. Dempsey, J.M. Regan, J.R. Kim, Ultrasonic disintegration of microalgal biomass and consequent improvement of bioaccessibility/bioavailability in microbial fermentation, New Microb. Technol. Adv. Biofuels Towar. More Sustain. Prod. Methods. (2015) 197–214. https://doi.org/10.1201/b18525-16.

[278] Y. Wei, H. Voon, J. Ching, S. Phang, Production of new cellulose nanomaterial from red algae marine biomass Gelidium elegans, Carbohydr. Polym. 151 (2016) 1210–1219. https://doi.org/10.1016/j.carbpol.2016.06.083.

[279] Q. Wang, J. Bin Ye, H.Y. Yang, Q. Liu, Chemical Composition and Structural Characteristics of Oil Shales and Their Kerogens Using Fourier Transform Infrared (FTIR) Spectroscopy and Solid-State 13C Nuclear Magnetic Resonance (NMR), Energy and Fuels. 30 (2016) 6271–6280. https://doi.org/10.1021/acs.energyfuels.6b00770.

[280] K. Miazek, W. Iwanek, C. Remacle, A. Richel, D. Goffin, Effect of metals, metalloids and metallic nanoparticles on microalgae growth and industrial product biosynthesis: A review, Int. J. Mol. Sci. 16 (2015) 23929–23969. https://doi.org/10.3390/ijms161023929.

[281] A. Mathys, G. Canelli, P.M. Martínez, S. Austin, M.E. Ambühl, F. Dionisi, C.J. Bolten, R. Carpine, L. Neutsch, Biochemical and morphological characterization of heterotrophic crypthecodinium cohnii and chlorella vulgaris cell walls, J. Agric. Food Chem. 69 (2021) 2226–2235. https://doi.org/10.1021/acs.jafc.0c05032.

[282] P. Poirrier, R. Soto-ramírez, M. Lobos, C. Olivia, R. Chamy, Effect of growth conditions on cell wall composition and cadmium adsorption in Chlorella vulgaris : A new approach

to biosorption research, 411 (2021). https://doi.org/10.1016/j.jhazmat.2021.125059.

[283] G. Song, X. Zhu, R. Chen, Q. Liao, Y.D. Ding, L. Chen, An investigation of CO2 adsorption kinetics on porous magnesium oxide, Chem. Eng. J. 283 (2016) 175–183. https://doi.org/10.1016/j.cej.2015.07.055.

[284] E. Jung, S. Park, H. Hong, Y. Choi, J. Yang, Bioresource Technology Biosorption of chromium (Cr (III)/ Cr (VI)) on the residual microalga Nannochloris oculata after lipid extraction for biodiesel production, Bioresour. Technol. 102 (2011) 11155–11160. https://doi.org/10.1016/j.biortech.2011.09.107.

[285] J. Vijayaraghavan, D. Zunaithur Rahman, J. Thivya, Comparative assessment and optimization of Pb(II), Ni(II), and Zn(II) biosorption onto gelidiella acerosa in single systems: Equilibrium and kinetic modeling, Desalin. Water Treat. 209 (2021) 254–266. https://doi.org/10.5004/dwt.2021.26487.

[286] Q. Li, L. Wang, R. Xu, Y. Yang, H. Yin, S. Jin, T. Jiang, Chemosphere Potentiality of phosphorus − accumulating organisms biomasses in biosorption of Cd (II), Pb (II), Cu (II) and Zn (II) from aqueous solutions : Behaviors and mechanisms, 303 (2022). https://doi.org/10.1016/j.chemosphere.2022.135095.

[287] C. Escudero-o, M. Plöhn, C. Escudero-Oñate, C. Funk, Biosorption of Cd(II) by Nordic microalgae: Tolerance, kinetics and equilibrium studies, Algal Res. 59 (2021). https://doi.org/10.1016/j.algal.2021.102471.

[288] H. Li, J. Watson, Y. Zhang, H. Lu, Z. Liu, Bioresource Technology Environment-enhancing process for algal wastewater treatment , heavy metal control and hydrothermal biofuel production : A critical review, Bioresour. Technol. 298 (2020) 122421. https://doi.org/10.1016/j.biortech.2019.122421.

[289] M. Mohammadi, B. Reinicke, K. Wawrousek, Biosorption and biomagnetic recovery of La3+ by Magnetospirillum magneticum AMB-1 biomass, Sep. Purif. Technol. 303 (2022) 122140. https://doi.org/10.1016/j.seppur.2022.122140.

[290] M.Y.D. Alazaiza, A. Albahnasawi, Z. Ahmad, M.J.K. Bashir, T. Al-wahaibi, M. Shadi, S. Abujazar, S.S. Abu, D. Eddin, Potential use of algae for the bioremediation of different types of wastewater and contaminants : Production of bioproducts and biofuel for green circular economy, J. Environ. Manage. 324 (2022) 116415. https://doi.org/10.1016/j.jenvman.2022.116415.

[291] K. Poo, E. Son, J. Chang, X. Ren, Y. Choi, K. Chae, Biochars derived from wasted marine macro-algae (Saccharina japonica and Sargassum fusiforme) and their potential for heavy metal removal in aqueous solution, J. Environ. Manage. 206 (2018) 364–372. https://doi.org/10.1016/j.jenvman.2017.10.056.

[292] I.S. Bădescu, D. Bulgariu, I. Ahmad, L. Bulgariu, Valorisation possibilities of exhausted biosorbents loaded with metal ions – A review, J. Environ. Manage. 224 (2018) 288–297. https://doi.org/10.1016/j.jenvman.2018.07.066.

[293] C. Zheng, M. Aslam, X. Liu, H. Du, X. Xie, H. Jia, N. Huang, K. Tang, Y. Yang, P. Li,

Impact of Pb on Chlamydomonas reinhardtii at Physiological and Transcriptional Levels, Front. Microbiol. 11 (2020) 1–14. https://doi.org/10.3389/fmicb.2020.01443.

[294] M. Nanda, V. Kumar, D.K. Sharma, Multimetal tolerance mechanisms in bacteria: The resistance strategies acquired by bacteria that can be exploited to 'clean-up' heavy metal contaminants from water, Aquat. Toxicol. 212 (2019) 1–10. https://doi.org/10.1016/j.aquatox.2019.04.011.

[295] S. Gu, C.Q. Lan, Lipid-extraction algal biomass for biosorption of bivalent lead and cadmium ions: kinetics and isotherm, Chem. Eng. Sci. (2023) 118778. https://doi.org/https://doi.org/10.1016/j.ces.2023.118778.

[296] L.A. Castillo, P.J. Valadés-Pelayo, H.J. Avila-Paredes, J.J. Cabello, A. Balbuena, Methodology for the fast direct estimation of spectral radiative transport properties in microalgae photobioreactors, Chem. Eng. J. 458 (2023) 141462. https://doi.org/10.1016/j.cej.2023.141462.

[297] N. Zhang, X. Guo, T. Han, L. Tan, Q. Xue, J. Wang, Isolation and identification of allelochemicals produced by Phaeodactylum tricornutum for Prorocentrum donghaiense, Algal Res. 66 (2022) 102808. https://doi.org/10.1016/j.algal.2022.102808.

[298] C. Khomlaem, H. Aloui, A.R. Deshmukh, J.H. Yun, H.S. Kim, S.C. Napathorn, B.S. Kim, Defatted Chlorella biomass as a renewable carbon source for polyhydroxyalkanoates and carotenoids co-production, Algal Res. 51 (2020) 102068. https://doi.org/10.1016/j.algal.2020.102068.

[299] C. Fuentes-Grünewald, C. Bayliss, M. Zanain, C. Pooley, M. Scolamacchia, A. Silkina, Evaluation of batch and semi-continuous culture of Porphyridium purpureum in a photobioreactor in high latitudes using Fourier Transform Infrared spectroscopy for monitoring biomass composition and metabolites production, Bioresour. Technol. 189 (2015) 357–363. https://doi.org/10.1016/j.biortech.2015.04.042.

[300] A. Kumar, B. Yan, J. Tao, J. Li, L. Kumari, B. Tafa Oba, M. Akintayo Aborisade, I. Ali Jamro, G. Chen, Co-pyrolysis of de-oiled microalgal biomass residue and waste tires: Deeper insights from thermal kinetics, behaviors, drivers, bio-oils, bio-chars, and in-situ evolved gases analyses, Chem. Eng. J. 446 (2022) 137160. https://doi.org/10.1016/j.cej.2022.137160.

[301] X. Gao, C. Guo, J. Hao, Z. Zhao, H. Long, M. Li, Adsorption of heavy metal ions by sodium alginate based adsorbent-a review and new perspectives, Int. J. Biol. Macromol. 164 (2020) 4423–4434. https://doi.org/10.1016/j.ijbiomac.2020.09.046.

[302] L. Lekshmi R., T.S. Rejiniemon, R. Sathya, P. Kuppusamy, F.A. AL-mekhlafi, M.A. Wadaan, P. Rajendran, Adsorption of heavy metals from the aqueous solution using activated biomass from Ulva flexuosa, Chemosphere. 306 (2022) 135479. https://doi.org/10.1016/j.chemosphere.2022.135479.

[303] A.R. Lucaci, D. Bulgariu, L. Bulgariu, In situ functionalization of iron oxide particles with alginate: A promising biosorbent for retention of metal ions, Polymers (Basel). 13 (2021)

1–19. https://doi.org/10.3390/polym13203554.

[304] R.J. Auchus, The Physiology and Biochemistry of Pili, Endocr. Dev. 20 (1998) 20–27. https://doi.org/10.1159/000321209.

[305] C. Funk, Detailed Characterization of the Cell Wall Structure and Composition of Nordic Green Microalgae, (2022). https://doi.org/10.1021/acs.jafc.2c02783.

[306] S. Naveed, C. Li, X. Lu, S. Chen, B. Yin, C. Zhang, Y. Ge, Microalgal extracellular polymeric substances and their interactions with metal(loid)s: A review, Crit. Rev. Environ. Sci. Technol. 49 (2019) 1769–1802. https://doi.org/10.1080/10643389.2019.1583052.

[307] C. Li, P. Li, H. Fu, J. Chen, M. Ye, S. Zhai, F. Hu, C. Zhang, A comparative study of the accumulation and detoxi fi cation of copper and zinc in Chlamydomonas reinhardtii : The role of extracellular polymeric substances, Sci. Total Environ. 871 (2023) 161995. https://doi.org/10.1016/j.scitotenv.2023.161995.

[308] B.Z. Siegel, S.M. Siegel, CRC Critical Reviews in Microbiology The Chemical Composition of Algal Cell Walls, 6454 (2008). https://doi.org/10.3109/10408417309108743.

Appendix Biosorption of Pb (II) by free and alginate-immobilized *Chlorella vulgaris* and *Neochloris oleoabundans*

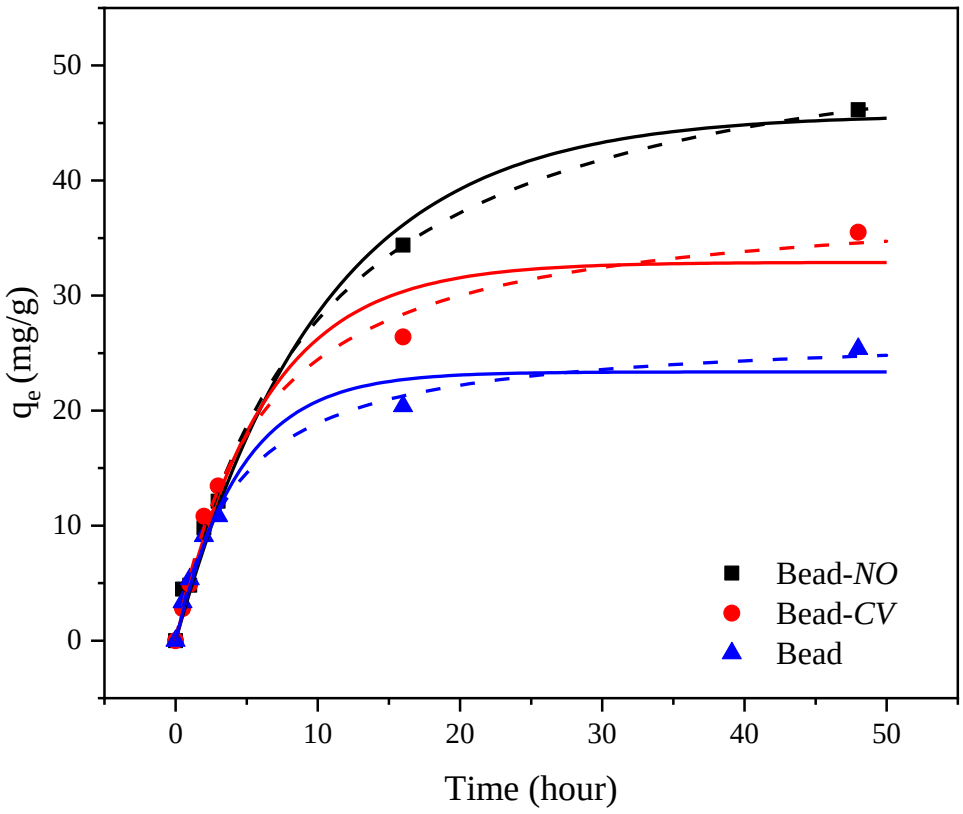

Figure A-1 Kinetics of Pb(II) biosorption by alginate-immobilized *Chlorella vulgaris* and *Neochloris oleoabundans*, under 25 °C, 50 mg/L Pb(II), pH 6, 0.5 g/L biomass dosage.

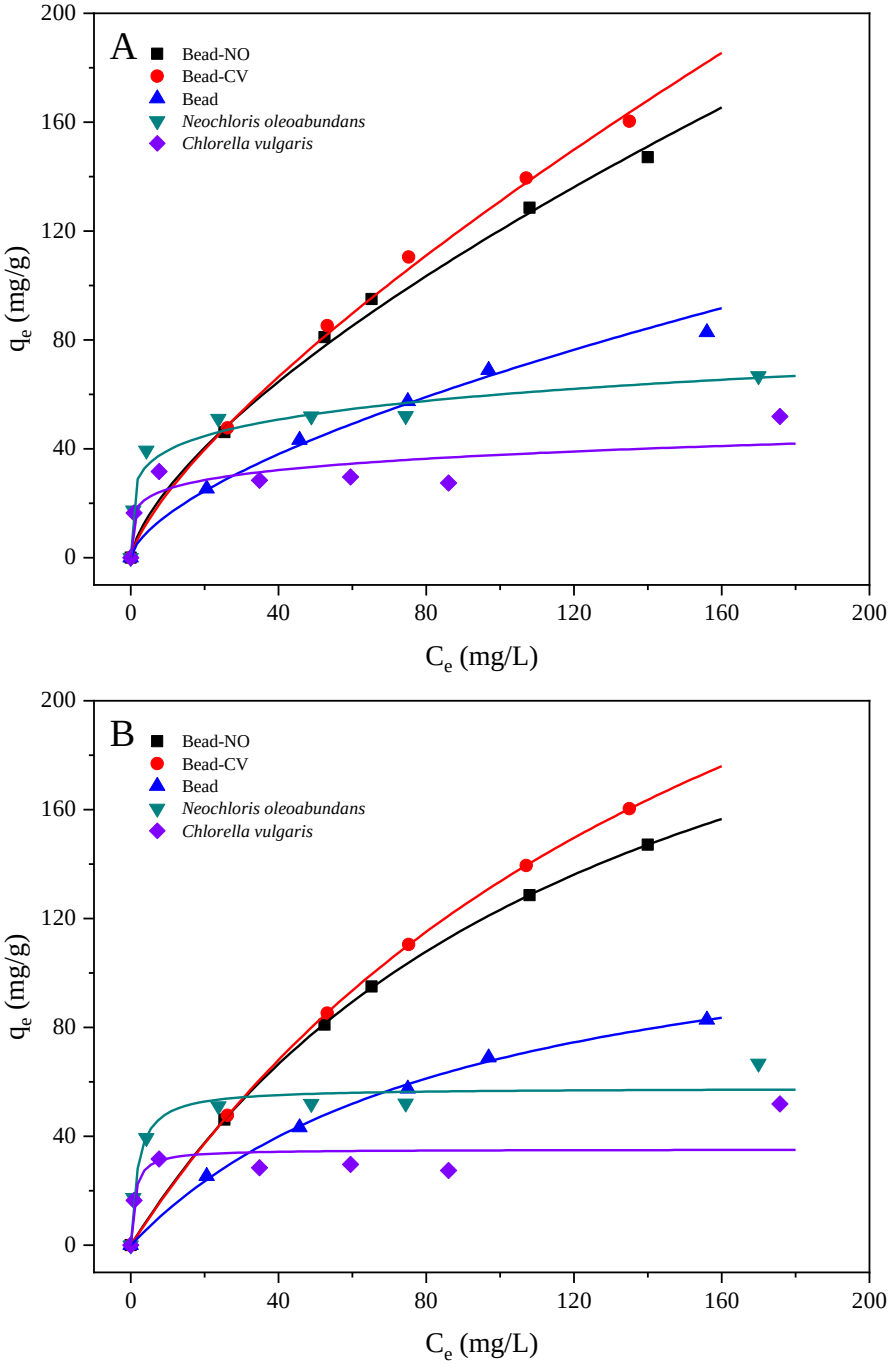

Figure A-2 Isotherm of Pb(II) by alginate-immobilized *Chlorella vulgaris* and *Neochloris oleoabundans* and wet biomass, fitting with Freundlich (A) and Langmuir model (B), under 25 ℃, pH 6.0, 0.5 g/L biomass dosage, 48 hours contact time.